



**HAL**  
open science

# Shape and anisotropy optimization by an isogeometric-polar method

Félix D. Kpadonou

► **To cite this version:**

Félix D. Kpadonou. Shape and anisotropy optimization by an isogeometric-polar method. Optimization and Control [math.OA]. Université Paris Saclay (COMUE), 2017. English. NNT: 2017SACLV048. tel-01693872

**HAL Id: tel-01693872**

**<https://theses.hal.science/tel-01693872>**

Submitted on 26 Jan 2018

**HAL** is a multi-disciplinary open access archive for the deposit and dissemination of scientific research documents, whether they are published or not. The documents may come from teaching and research institutions in France or abroad, or from public or private research centers.

L'archive ouverte pluridisciplinaire **HAL**, est destinée au dépôt et à la diffusion de documents scientifiques de niveau recherche, publiés ou non, émanant des établissements d'enseignement et de recherche français ou étrangers, des laboratoires publics ou privés.

NNT : 2017SACLV048

PHD THESIS  
OF PARIS-SACLAY UNIVERSITY  
PREPARED AT LABORATOIRE DE MATHÉMATIQUES DE  
VERSAILLES, UMR 8100 CNRS

École doctorale n°574  
École Doctorale de Mathématiques Hadamard  
Speciality: Applied Mathematics

by

**MR. DOSSOU FÉLIX KPADONOU**

Shape and anisotropy optimization by an isogeometric-polar method

Thesis defended at Université de Versailles, 31 August 2017.

**Jury members:**

Mr.	A. HABBAL	MdC HDR Univ. de Nice Sophia-Antipolis	(Reviewer)
Mr.	L. GALLIMARD	Pr. Univ. Paris Nanterre	(Reviewer)
Mrs.	E. JAMELOT	Dr. CEA Gif-sur-Yvette	(Examiner)
Mr.	M. MONTEMURRO	MdC ENSAM Bordeaux	(Examiner)
Mr.	L. DUMAS	Pr. Univ. de Versailles Saint-Quentin	(Jury president)
Mr.	F. JOUVE	Pr. Univ. de Paris Diderot	(Examiner)
Mr.	CHR. FOURCADE	MdC Renault SA	(Thesis Co-advisor)
Mr.	P. VANNUCCI	Pr. Univ. de Versailles Saint-Quentin	(Thesis advisor)
Mr.	P. DE NAZELLE	Dr. IRT-SystemX	(Guest)



**Titre :** Optimisation de forme et anisotropie par une méthode isogéométrique-polaire

**Mots clefs :** Optimisation, forme & anisotropie, isogéométrie, formalisme polaire, modèle de Naghdi, jonction de coques.

**Résumé :** Nous nous intéressons dans cette thèse à l'optimisation conjointe de forme et d'anisotropie pour les structures surfaciques. Nous nous focalisons dans un premier temps sur l'analyse de ces structures minces modélisées par des coques. Le modèle utilisé pour décrire le comportement mécanique est celui de Naghdi communément utilisé pour les coques modérément épaisses et qui permet de prendre en compte l'effet transverse de déformation. La discrétisation par méthode éléments finis est réalisée avec des éléments Lagrange standards de classe  $C^0$ . Nous considérons la simulation d'assemblage de coques en utilisant la méthode des éléments finis avec joint (mortier). Cette méthode est flexible, elle est adaptée à l'utilisation de maillages localement raffinés et/ou non-conformes, c-

à-d non coïncidents. La deuxième partie se consacre à la définition d'un paramétrage pour la conception optimale de champ d'anisotropie. Notre approche se base sur l'utilisation conjointe du formalisme polaire pour représenter le tenseur d'élasticité et le principe isogéométrique permettant de paramétrer les champs d'anisotropie par des fonctions de type B-splines. La dernière partie est dédiée à l'optimisation conjointe de forme et de propriétés matériaux. Le nombre de paramètres d'optimisation dans l'approche proposée est maîtrisé puisque les paramètres d'optimisation sont les coordonnées des points de contrôle. Nous considérons principalement pour l'optimisation un critère de type compliance.

**Title :** Shape and anisotropy optimization by an isogeometric-polar method

**Keywords :** Optimization, shape & anisotropy, isogeometry, polar formalism, Naghdi's shell, junction of shells.

**Abstract :** This thesis tackles the problem of the shape and anisotropy optimization of shell structures. The first part of this work focuses on the analysis of the shell model. The mechanical behavior of the structure is described using the Naghdi's shell model which allows to take into account the transverse shear deformation. This model is typically used for shallow shells. We use a standard Lagrange  $C^0$  finite elements discretization and we numerically simulate the shell assemblings by means of the mortar technique. This approach enables the application of local refinements and the use of nonconforming mesh discretizations. The second part of

this thesis aims at defining an effective parameterization for the optimal design of the shell's distributed elastic properties. The method adopted is based on the joint use of a polar formalism to represent the elastic tensor and an isogeometric technique for the parameterization of the elastic tensor fields by CAD-based functions such as B-splines. The number of design variables thus only depends on the control points coordinates making the approach numerically manageable. The last part is devoted to the joint optimization of both the material properties and shape of the shell using the structure compliance as objective function.





# Remerciements

---

Je suis reconnaissant pour ces dernières années et je ne saurais commencer ni terminer ce manuscrit sans dire MERCI à celles et ceux qui ont fait partie de ces quelques lignes écrites.

Mes premiers remerciements vont à l'endroit de M. Paolo Vannucci pour m'avoir donné l'opportunité de réaliser cette thèse et pour son encadrement. Je remercie aussi MM. Christian Fourcade et Paul de Nazelle pour la part qu'ils ont pris dans ce parcours de recherche. Merci Paul pour la nuance que tu as apporté lors de cette aventure, et pour tous les extras.

Je remercie les membres du jury qui ont donné de leurs précieux temps pour juger ce travail. Je veux, en particulier, remercier M. François Jouve qui a présidé ce jury, MM. Laurent Gallimard et Abderrahmane Habbal pour leurs temps et l'attention que leurs aura demandé le rapport de ce manuscrit, vu ma familiarité avec Shakespeare.

Je remercie Renault pour le financement de cette thèse, les différentes institutions qui m'ont accueilli et m'ont offert le cadre le plus idéal possible pour réaliser ces travaux : principalement, l'IRT SystemX qui a été le cadre prépondérant où s'est déroulée la plupart de la thèse -au sein du projet ROM, les personnes extra-ordinaires que j'y ai rencontrées, les camarades de thèse Sarah J., Timothée L., François G., mes collègues de bureau par intermittence Ming C. et Gabriel D. Je remercie aussi le Laboratoire de Mathématiques de Versailles, qui m'a accueilli les derniers mois de thèse, et les personnes qui le constituent, en particulier les camarades doctorants (sacrée coordination pour le partage de bureau), le directeur M. Christophe Chalons, l'ancienne directrice de labo Mme Cathérine Donati-Martin. Merci pour les nombreuses attestations lors des démarches administratives. Je remercie bien évidemment les secrétaires Mmes Nadège Arnaud, Laure Frerejean et Liliane Roger, pour les nombreuses assistances, leurs gentillesse et leurs disponibilités.


Dans cette toile de fond professionnelle, il y a des relations plus personnelles qui se créent, par simple ouverture et disponibilité : Merci aux Mangeant que j'ai eu le privilège de connaître plus personnellement après une coïncidence de séjour de vacances au Bénin, d'un certain mois d'octobre 2014.

Je remercie aussi mes amis, Hermann F., Djime M., Salomon N., Ronel T., avec qui je partage beaucoup depuis tant d'années et notre rencontre sur les côtes d'Agadir au Maroc. Bien plus que des amis, ils font partie de la "bro-corp" (brothers corporation) -qui aiment *Les P'tis Gars*. Je remercie également Franck H. et Eloi L., depuis le bâtiment 76 sur le "platal", toujours au top pour les sessions de "boeuf" avec Laura P. aux maracas ou à la batterie. À toi aussi Laure P., toujours au top chef(fe), *Thanks you (for) so much*. Il fallait bien retrouver le sud dans un coin du platal.

Je pense fortement à deux personnes que j'ai tant de privilèges à cotoyer depuis quelques années : M. Patrick Ciarlet que j'ai eu la chance inespérée d'avoir comme professeur en analyse numérique et ensuite avec Mme Erell Jamelot comme encadrants pour mon projet de fin d'études de Master. Je ne saurais assez vous remercier.

Mes pensées vont naturellement à ma famille pour leur soutien. Merci maman pour votre générosité infinie, Merci papa pour l'exemple et le modèle que vous représentez sur bien de plans. Merci Socrate. Tu es la passerelle vers bien de choses insoupçonnées.

À vous tous que je n'ai pu citer mais qui avez fait parti de ce tableau, qui avez été -et êtes- importants par votre amitié, tout quelconque geste d'amitié à un certain moment, des moments partagés, vos sourires ou simplement votre cordialité, je vous remercie.

“A te ... ”

L. JOVANNOTTI - A. BOCELLI





# Contents

---

<b>Remerciements</b>	<b>v</b>
<b>Introduction</b>	<b>1</b>
<b>1 Position of the structural optimization</b>	<b>5</b>
1.1 Optimization issues . . . . .	5
1.2 Structural optimization classification . . . . .	6
1.3 General formulation of an optimization problem . . . . .	7
1.4 Classical analysis and optimization approach . . . . .	8
1.5 The Isogeometric method . . . . .	11
1.6 Synthesis . . . . .	11
<b>I Analysis of shell assemblings</b>	<b>13</b>
<b>2 Naghdi Shell Model</b>	<b>15</b>
2.1 Differential geometry . . . . .	16
2.1.1 Differential geometry of surface . . . . .	16
2.1.2 Differential geometry for curvilinear 3D body . . . . .	19
2.2 Mechanical model . . . . .	20
2.2.1 Kinematic assumptions . . . . .	20
2.2.2 Constitutive equations . . . . .	21
2.2.3 Strain, stress and energies . . . . .	23
2.2.4 Naghdi's equation . . . . .	25
2.3 On the existence results . . . . .	26
2.4 Synthesis . . . . .	29

<b>3</b>	<b>Naghdi shell junctions with Nonconforming Discretization</b>	<b>31</b>
3.1	General equations for an assembling of shells . . . . .	32
3.1.1	Geometric decomposition aspects . . . . .	32
3.1.2	Junction conditions . . . . .	35
3.1.3	General mechanical problem . . . . .	36
3.2	Finite element space - Mortar method for shell . . . . .	39
3.2.1	Discrete problem . . . . .	39
3.2.2	Mortar principle on an abstract problem . . . . .	42
3.2.3	Mortar method implementation for shell junction . . . . .	46
3.2.4	Finite elements implementation . . . . .	48
3.3	Numerical results . . . . .	52
3.3.1	Vibration frequencies of a plate . . . . .	53
3.3.2	Vibration frequencies of a 3D L-plate . . . . .	57
3.3.3	Frequency analysis of a cylindrical shell . . . . .	60
3.3.4	Rectangular plate under pointwise load . . . . .	61
3.4	Synthesis . . . . .	66
<b>II</b>	<b>Anisotropy and shape optimal design</b>	<b>67</b>
<b>4</b>	<b>Anisotropy properties and material optimization</b>	<b>69</b>
4.1	Introduction . . . . .	69
4.2	The polar formalism . . . . .	71
4.2.1	Polar formalism representation . . . . .	71
4.2.2	Constraints on the parameters . . . . .	73
4.3	Parametrization tailored to the polar formalism . . . . .	74
4.3.1	Conformal parameterization . . . . .	77
4.3.2	Direct parameterization . . . . .	78
4.4	Formulation of the optimization problem . . . . .	81
4.4.1	Design parameters . . . . .	82
4.4.2	Derivatives with respect to the polar parameters . . . . .	82
4.5	Numerical Results . . . . .	84
4.5.1	Plate under two in-plane concentrated loads . . . . .	86
4.5.2	Anisotropy design of a cantilever . . . . .	90
4.5.3	Cylinder shell under torsional load . . . . .	94
4.5.4	Anisotropy design of a plate submitted to torsion . . . . .	97
4.6	Synthesis . . . . .	99

<b>5</b>	<b>Simultaneous optimization of shape and anisotropy</b>	<b>101</b>
5.1	Introduction . . . . .	102
5.2	Isogeometric shape parameterization . . . . .	103
5.2.1	Multiple patches . . . . .	105
5.3	Anisotropy and shape optimization . . . . .	110
5.3.1	Derivatives with respect to the shape . . . . .	112
5.3.2	Derivatives of the strain bilinear form . . . . .	113
5.3.3	Derivatives of the linear form . . . . .	115
5.4	Sensitivity for an assembling of shells . . . . .	116
5.4.1	Problem setting . . . . .	116
5.4.2	Gradient for an assembling of shells . . . . .	117
5.4.3	Constraints on the design's geometry . . . . .	117
5.4.4	General overview on the derivative of the junction . . . . .	119
5.4.5	Sensitivity of the shells junction . . . . .	121
5.5	Numerical results . . . . .	127
5.5.1	Optimal design of a circular plate . . . . .	127
5.5.2	Optimization of a holed circular plate . . . . .	136
5.5.3	Plate submitted to torsional load . . . . .	146
5.5.4	Optimal design of a square plate under weight-load . . . . .	149
5.6	Synthesis . . . . .	152
	<b>Conclusion and Perspectives</b>	<b>153</b>
<b>A</b>	<b>Résumé de thèse</b>	<b>157</b>
A.1	Motivations . . . . .	157
A.2	Modèle de coques de Naghdi . . . . .	160
A.3	Jonction de coques de Naghdi et discrétisation non-conformes . . . . .	163
A.3.1	Considérations géométriques . . . . .	163
A.3.2	Raccordement entre coques . . . . .	164
A.3.3	Méthode mortier . . . . .	166
A.4	Optimisation d'anisotropie et propriétés matériaux . . . . .	169
A.4.1	Formalisme polaire . . . . .	169
A.4.2	Discrétisation des paramètres polaires . . . . .	172
A.4.3	Prise en compte de contraintes . . . . .	173
A.5	Optimisation conjointe de formes et propriétés matériaux . . . . .	173
A.5.1	Géométrie et paramétrage de la forme . . . . .	173
A.5.2	Optimisation . . . . .	176
	<b>Bibliography</b>	<b>184</b>



# List of Figures

Structural assemblage of a car (Source [35]) . . . . .	6
Standard optimization process of shape design . . . . .	9
Definition of a three-dimensional surface $\Omega$ . . . . .	17
Illustration of an assembling of two shells . . . . .	34
$P_2$ -finite element . . . . .	51
Trace functions of the Lagrange $P_2$ basis functions . . . . .	52
Example of middle-surface defined through a Bézier function and the associated parametric interfaces with their associated mappings . . . . .	53
Representation of the vibration modes 7 to 12 for the free plate . . . . .	54
Illustration of the convergence of the 7th eigenvalue as the meshing step diminishes. $Np$ represents the number of degrees of freedom. . . . .	55
7th frequency corresponding to the nonconforming discretization of the $2 \times 2$ -plate. . . . .	57
Representation of the first six eigenmodes of deformation of the L-plate. . . . .	58
Representation of the first six eigenvectors of deformation corresponding to the free L-plate. . . . .	59
Representation of the first four non rigid body modes. . . . .	61
Geometric and material characteristics of the plate . . . . .	61
Displacement field corresponding to the plate under concentrated load and the control polygon associated to the shape mapping . . . . .	62
Convergence of the displacement vertical component. The reference value $u_G$ is plotted in green and the values $u_G^1$ in blue . . . . .	63
Displacement field with local refinement with a fixed finest mesh for the sub-plate supporting the concentrated load. The total number of DOFs is 9780 . . . . .	64
Global discretization error . . . . .	66
Example of clamped B-spline . . . . .	76
Illustration of subdivision on a B-spline curve . . . . .	81
Boundary and loading conditions of the plate. . . . .	86
Optimal orthotropy direction distribution and the corresponding displacement field . . . . .	87

From left to the right the optimal distribution of $R_0^K$ and $R_1$ . . . . .	88
Optimal distribution of the polar parameters $R_0^K$ and $R_1$ corresponding to the plate under two concentrated loads. . . . .	88
Optimal orthotropy direction orientation: the fibers are locally in the loading directions and anywhere else in the 1 axis direction. . . . .	89
Comparison of the deformations corresponding to the different cases of optimization	90
Boundary and loading conditions of the plate with tangential load. . . . .	90
Optimal distribution of the orthotropy direction. . . . .	91
Optimal distribution of the polar modulus $R_0^K$ . . . . .	91
Optimal distribution of the polar modulus $R_1^K$ . . . . .	92
Optimal distribution of the orthotropy . . . . .	92
Optimal distribution of the parameter $R_0^K$ . . . . .	93
Optimal distribution of the parameter $R_1$ . . . . .	93
Deformation corresponding to the different case of design of the plate subjected to vertical edge force, with an amplification factor $\times 200$ . . . . .	94
Initial displacement field induced by the torsional load on the cylindrical shell. . .	95
The optimal orthotropy direction. . . . .	95
$R_0^K$ and $R_1$ optimal distributions . . . . .	96
The distributions of the polar parameters . . . . .	96
Optimal orthotropy direction corresponding to the optimal material on the cylinder under torsion. . . . .	97
Optimal orthotropy direction corresponding to the optimal design. . . . .	98
The optimal polar parameters $R_0^K$ and $R_1$ for a plate submitted to torsional load	98
Illustration of the deformed configurations for the anisotropy design of the plate under torsional load . . . . .	99
Illustration of a B-spline basis functions . . . . .	104
Illustration of a $C^1$ -regularity on the junction of two B-splines curves of order 4 and of knot vector $\Sigma^{(k)} = \{0, 0, 0, 0, 1, 1, 1, 1\}$ , $k \in \{n, m\}$ . . . . .	106
Illustration of the junction between the patches $\Omega_n$ and $\Omega_m$ . . . . .	108
Circular plate geometry and boundary condition. . . . .	127
Optimal shape corresponding to the circular plate with isotropic material . . . .	128
History of the compliance for the shape optimal design of the circular plate with isotropic material . . . . .	129
History of the variations of the different internal energies to the total strain energy (compliance) for the optimal design of the isotropic circular plate. . . . .	129
Shape design: Variation of the area of the shell during optimization. $\mathcal{A}_u$ is the upper bound of the area variation and $\mathcal{A}$ is the area of the design. . . . .	130

Orthotropy and shape design: Illustration of the optimal shape corresponding to the circular plate under weight-load. . . . .	130
Orthotropy direction for the joint design of orthotropy and angle. . . . .	131
Orthotropy and shape optimization: History of the objective function throughout optimization. . . . .	131
History of the contribution the different internal energies to the total strain energy (compliance) throughout optimization. . . . .	132
Orthotropy and shape design: Variation of the area of the shell during optimization. $\mathcal{A}_u$ is the upper bound of the area variation and $\mathcal{A}$ is the area of the design. . . . .	133
anisotropy and shape design: Optimal shape corresponding to the circular plate under weight-load. . . . .	133
Anisotropy and shape design: Optimal orthotropy direction field of the optimal design corresponding to the circular plate under weight-load. . . . .	134
Anisotropy and shape design: Optimal polar moduli fields of the optimal design corresponding to the circular plate under weight-load. . . . .	134
Anisotropy and shape optimization: History of the objective function throughout optimization. . . . .	135
Anisotropy and shape design: History of the contribution the different internal energies to the total strain energy (compliance) throughout optimization. . . . .	135
Anisotropy and shape design: Variation of the area of the shell during optimization. . . . .	136
Geometric and boundary conditions of the circular holed plate . . . . .	137
Shape design: Optimal shape corresponding to the holed circular plate under edge load. . . . .	138
Circular holed plate: History of the objective function throughout shape optimization for the isotropic case. . . . .	138
Contribution of the different internal energies to the total strain energy (compliance) throughout the optimization of the holed circular plate with isotropic material. . . . .	139
Variation of the area of the shell during shape optimization of the holed circular plate with isotropic material. . . . .	139
Shape design with anisotropy material with an orthotropy angle $\Phi_1 = \frac{\pi}{4}$ : Optimal shape corresponding to the holed circular plate under edge load. . . . .	140
Orthotropy direction on the optimal shape design . . . . .	140
Circular holed plate: History of the objective function throughout shape optimization for the anisotropic material case. . . . .	141
Shape design of anisotropic holed circular plate: History of the contribution of the different internal energies to the total strain energy (compliance) throughout optimization. . . . .	141
Shape design of holed circular plate: Variation of the area of the shell during optimization. . . . .	142



Optimal shape for the joint anisotropy and shape design of the holed circular plate.	142
Optimal orthotropy direction corresponding to the joint anisotropy and shape design of the holed circular plate. . . . .	143
Distribution of the optimal polar moduli $R_0^K$ and $R_1$ . . . . .	143
Contribution of the different internal energies to the total strain energy (compliance) throughout optimization. . . . .	144
History of the objective function . . . . .	145
Variation of the area of the shell during optimization corresponding to the joint shape and anisotropy design of the holed circular plate . . . . .	145
Geometric description of the plate under torsion . . . . .	146
Plate under torsion: optimal design corresponding to the shape optimizations with isotropic and anisotropic material . . . . .	147
Plate under torsion: optimal shape corresponding to the joint orthotropy/shape design and global anisotropy/shape design . . . . .	147
Plate under torsion: Optimal orthotropy direction corresponding to the joint orthotropy/shape design and global anisotropy/shape design . . . . .	148
Plate under torsion: Optimal polar moduli corresponding to the joint design of the global anisotropy and the shape . . . . .	148
Optimal shape for the joint anisotropy and shape design of the plate under weight-load . . . . .	150
Distribution of the optimal polar moduli $R_0^K$ and $R_1$ of the joint shape and material design of the plate under weight-load . . . . .	150
History of the objective function and area . . . . .	151
History corresponding to the internal energies. . . . .	152

# List of Tables

---

Barycentric coordinates of a $P_2$ interpolation. . . . .	51
Comparison of the computed eigenvalues corresponding to free-plate with the theoretical ones . . . . .	55
Comparison of the computed eigenvalues corresponding to free-plate decomposed into $2 \times 2$ patches . . . . .	56
Eigenvalues and errors corresponding to the nonconforming meshing of the $2 \times 2$ decomposition of the plate. . . . .	57
Comparison of the computed eigenvalues corresponding to free-L-plate with the reference eigenvalues computed with the Code-Aster software. . . . .	60
Eigenvalues corresponding to a free cylindrical shell . . . . .	60
Relative errors on the third component of displacement . . . . .	62
Relative errors on the vertical component of displacement . . . . .	63
Discretization errors local to each patch . . . . .	65
Global discretization error . . . . .	65
Table of polar parameters corresponding to the different part of the elastic tensor.	85
Information related to the different cases of optimization ( <i>plate under point-wise loads</i> ) . . . . .	89
Informations relative to the different cases of design ( <i>plate with tangential edge load</i> )	93
Informations related to the different cases of optimization ( <i>cylindrical shell under torsional load</i> ) . . . . .	97
Summary of the different optimizations concerning the holed circular plate. . . .	146
Summary of the different optimizations concerning the plate under torsional load.	149
Summary of the different optimizations concerning the plate under weight-load. .	151



# Introduction

---

Optimal design is a natural concern in many daily tasks. This issue is of particular interest in several fields of application such as civil engineering, automotive and aerospace where the challenge of construction of lightweight structures, which are environmentally friendly and consume less fuel, is of major importance. Such a task is very challenging because the optimal design is subjected to a lot of constraints; basically the optimal design, for instance the lightweight design, must keep ensuring good functionalities or performances. Different types of structures are concerned, namely the surface structures such as plates and shells which represent a preponderant part of the construction; for instance surface structures represent more than 70% of an automobile.

Since many decades, composite structures are intensively used thanks to their mechanical behaviour and their high stiffness-to-weight ratio. The perpetual advances in composite material technology favour their fabrication through different techniques such as additive manufacturing (3D printing) and reduce the barriers to their intensive use and integration in construction, in order to take benefit of the flexibilities. These structures offer many flexibilities from a standpoint of geometry and elastic properties fine-tuning in comparison to standard material such as steel. In order to exploit those flexibilities the use of optimization and mathematical programming techniques is necessary.

Structural optimization can be performed at various scales of a design, namely the shape and the material. The admissible design depends on the kind of optimization which usually is classified into three classes: shape optimization, sizing and topological optimization. The first involves the shape as design variables and the topology is not changed in its frame, i.e, roughly, no appearance or disappearance of holes with respect to the initial design. In the second type of optimization the variables are the geometrical parameters such as length (beam cross-section), width or thickness and also material elastic properties coefficients such as Young modulus and Poisson's ratio. The last type of optimization mentioned is the most complex one which allows to handle complex geometries. Roughly speaking, in this kind of optimization, the topology can change and the design parameter is commonly a density function which defines the distribution of the material. This class of optimization mainly concerns mass reducing problems. Among this common classification, sizing at a first appearance seems the most "simple" due to the fact that topology is commonly fixed within this frame (length, cross-beam sizing). But this class of optimization encompasses various optimizations and hide complexity. For instance topological optimization can also be viewed as sizing of material properties constituted of two phases (one strong and the other weak defining void-hole-), so that material optimization can also be considered as a full-blown structural optimization type at the same title as the topological one.

In this thesis, we consider a mixture of both the shape and material optimization of shell struc-

tures, which are part of the most predominant basic components encountered in automotive. The standard optimization process in industry is complex and heterogeneous. Indeed, optimization is quite interdisciplinary, it combines many counterparts such as modelling, design, and computer science techniques namely simulation and mathematical programming. All these components do not coexist naturally and homogeneously. Basically, the structure designed using the Computational Aided Design (CAD) software must be supplied to a structural analysis in a Computer Aided Engineering (CAE) environment, in order to compute the structural response using numerical methods such as Finite Element Analysis (FEA) which further allows to compute the performance (objective function) to be optimized or the constraints. The FEA analysis being made on a mesh of the structure, the transit from the CAD to CAE is done at a price of an expensive meshing step. Moreover, the optimization, in this classical manner, is performed on the same structural analysis mesh and the shape design variables are the mesh points coordinates. On another hand, when a material design is tackled, the material properties design variables are usually set discrete per finite element. This approach has several drawbacks. First, the time-consuming CAD-mesh conversion deteriorates the initial design and thus the structural response; and consequently the optimization performed does not correspond exactly to the one of the original design. This procedure is also intrusive. In fact, due to the lack of optimal and efficient mesh generator, the meshing step must be controlled and adjusted by a specialist. Secondly, the computational complexity of the optimization problem is very important and requires huge numerical resources. It has been shown in [4] that for complex engineering structures the conversion between the original geometry and the mesh takes up to almost 80% of the total analysis time. Also, the optimal design is subject to many constraints relative to the regularity of the shape which cannot be taken into account easily. Basically, the material properties are desired to be continuous, with continuous fibre orientation to be manufactured by numerically controlled devices. To summarize, the meshing conversion of the original CAD geometry affects the quality of the numerical solution. This conversion step deteriorates harshly the optimal solution. The resulting design from the optimization process is no longer a CAD object but a mesh. One thus needs a costly step of mesh-to-CAD conversion. To tackle this, a new technique called isogeometric has recently emerged. It allows to reduce the gap between the CAD and CAE environments. Isogeometric analysis, pioneered by R.T Hughes [28], offers the possibility of integrating the NURBS-based CAD design tools into the (FEA) CAE environment. In fact, within this framework, the classical interpolation basis functions in FEA model are replaced by the CAD-basis functions, i.e the Bézier, Splines and NURBS. The isogeometric designation was later widened to a set of techniques which use the design basis functions to define a given quantity of interest.

This thesis stems from the desire of Renault to dispose of efficient and accurate tools capable to help the optimal design of surface structures and is in the continuation of research done this recent past with the thesis of P. de Nazelle [35] and in parallel to the work of S. Julisson [39] which was concerned with shape optimization under acoustic criterion. In this thesis, we are more specifically interested in shape and material design for anisotropic shells. The manuscript is organised as follows:

- **Chapter 1:** we briefly present a state of the art and introduce the general issue concerning the shape and material design problem.

- **Chapter 2:** the chapter recalls the derivation of the Naghdi equations for anisotropic shells used in this thesis. Shells structures are bi-dimensional structures slender through one dimension (the thickness), so that they are commonly identified by their middle-surfaces. Thus defining their middle-surfaces by an injective regular mappings (to be precise), one can derive from the classical three-dimensional mechanical equations the specific equations of shell structures. The advantages of this model are several: the mechanical problem is defined on the parametric bi-dimensional domain associated to the mapping of the middle-surface, the problem is intrinsically parameterized by the mapping and finally from a numerical point of view the reduction of the analysis complexity.
- **Chapter 3:** this chapter is devoted to the generalization of the Naghdi shell model to assembled structures. From the standard model valid for regular shells defined by mean of one mapping, we derive the variational problem for structures made of an assembling of shells. The matching conditions at the interfaces are consequences of the efforts and moments transmission at the interfaces. We further describe the practical implementation aspects and the discretization of the problem using a mortar method which is a commonly used technique in domain decomposition problem. It allows to handle and enforce weakly the matching conditions, in an integral sense, in the variational space. The interest of this approach is that it allows to use non-conforming discretizations. The non-conformity can occur at two levels: the functional one, that is the finite elements used can be different, while the other is relative to the meshing and allows many flexibilities such as local refinements and independent mesh generations. We conclude the chapter with relevant numerical results which validate the implementations. Illustrations involving nonconforming meshes are also given.
- **Chapter 4:** this chapter deals with the discretization of the elastic properties. We develop an approach based on the polar formalism and isogeometric techniques. The polar technique allows to represent the elastic tensor through its invariants and angles; so doing, it exhibits the main characteristic feature of anisotropy, i.e property dependence to direction, which turns to be interesting for the design problem in comparison to Cartesian representation. With an isogeometric approach, these invariants are parameterized using B-splines polynomial functions. This yields to a drastic reduction of the number of design variables and constraints of the optimization problem allowing to envisage the treatment of material properties design of more complex geometries. In this chapter, we discuss two choices for the parameterization of the design variables. The chapter is concluded by some relevant numerical results which prove the capability of the proposed isogeometric-polar method.
- **Chapter 5:** in this chapter, we focus on shape and material design problem. Shell model naturally favours the use of isogeometric techniques. In fact the mechanical problem is already parameterized by the shape through the metric and curvature tensors, and the Christoffel symbols. The shape and elastic parameters are both parameterized using CAD-basis functions and particularly in this work with B-spline functions, conversely to the standard way of setting the elastic material properties (constant per element). In order to envisage a possible use of gradient-based algorithm for the optimization, we compute the derivative of the mechanical problem and of the criterion with respect to the design control parameters. A particular attention is devoted to the derivative of the matching matrix

## Introduction

---

involved in the definition of the mechanical problem for assembling of shells structures. The objective function considered is notably the compliance. We conclude the chapter with some numerical results.

- The manuscript ends with a conclusion and perspectives for future developments.

# Position of the structural optimization

---

## Contents

<b>1.1 Optimization issues</b> . . . . .	<b>5</b>
<b>1.2 Structural optimization classification</b> . . . . .	<b>6</b>
<b>1.3 General formulation of an optimization problem</b> . . . . .	<b>7</b>
<b>1.4 Classical analysis and optimization approach</b> . . . . .	<b>8</b>
<b>1.5 The Isogeometric method</b> . . . . .	<b>11</b>
<b>1.6 Synthesis</b> . . . . .	<b>11</b>

---

## 1.1 Optimization issues

Structural optimization is of crucial importance in industry and engineering where the challenge of construction of lightweight and optimally designed structures with respect to specific criteria is of paramount importance. The reduction and the scarcity of the natural resources create the need of optimization techniques in order to rationalize the use of the available resources. This question is intimately linked to the reduction of the cost of conception, indeed proportional to the weight and quantity of material used. To that accomplishment the constructor can work on different features or parameters such as the geometry (shape), the constituent material and the size of different structural elements. In this quest of lightness, the shell structures occupy an important part. In fact, they are very attractive thanks to their excellent mechanical properties and aesthetic advantages; for instance they count for almost 70% of the total constituents of a car, see Fig. 1.1.



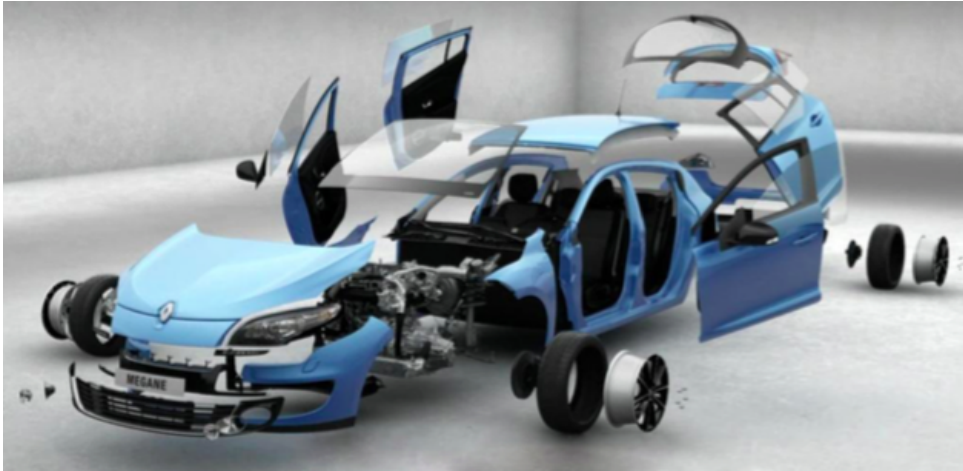


Figure 1.1 Structural assemblage of a car (Source de Nazelle [35])

Many efforts are devoted to the development of practical numerical methods and tools for designers. Fortunately, the growth of the numerical and computer resources has favored the development of various types of structural optimization and at the same time create the need of their tight integration in the optimal design process (in many areas such as automotive, aeronautic, civil engineering etc).

## 1.2 Structural optimization classification

In optimization, the design variables are the set of chosen design parameters in regards to which the objective function and structural response can be sensitive. The goal of the optimization strategy and the relative mathematical programming tools is then to, based on the sensitivity, set them properly; in order to find a set of optimal parameters, defining an optimal design, which minimize a given objective function over an admissible space. The admissible space depends on the type of the design variables and on the constraints to which they are subjected. These design parameters and their corresponding structural optimization can be classified in three mains classes, namely topology, sizing and shape.

- o Topology optimization searches for the best material distribution within a prescribed domain [5]. In this type of optimization the topology is not fixed a priori. There exists several methods for topology optimization. In the homogenization method, introduced by [54], further popularized by Bendsoe and Kikuchi[7], the shape is defined through density distribution taking the value 0 for void (where the matter can be saved) and 1 for full presence of material. The main drawback of this method is the introduction of composite materials, corresponding to intermediate distributions, which induces that a shape with clear boundaries is rarely obtained. One of the most used techniques to address this is the Solid Isotropic Material with Penalization (SIMP) method [6]. Another method of topological optimization without introducing intermediate material densities is through boundary variation techniques. In that class of methods, the interface boundaries are explicitly optimized.

### 1.3. General formulation of an optimization problem

---

The most well-known is the level-set method [1]. This technique has been applied in many references such as, shortly, Delgado [33] and Dapogny [29].

- In sizing optimization, the design variables are some geometric parameters such as some characteristic dimensions: length, height, thickness, cross-sectional area of a bar or parameter such as elastic constants. Regarding the material optimization, one is looking for the best elastic properties, i.e the elastic coefficients, and more generally, in order to enjoy more flexibility, the optimal distribution of the elastic material properties. This type of structure can nowadays be conceived thanks to the development of digital and manufacturing 3D printing. This type of optimization concerns anisotropic or laminated structures, mainly in the form of plate and shells composite.
- In shape optimization, the design variables are generally some control points describing the geometry. The topology is fixed; indeed, the connectivity between geometric element could not be modified and if a shape with single connectivity is initially chosen the optimal solution belong to the same class of domain. There is no insertion or deletion of hole.

Each of the cited structural optimization has its advantages and shortcomings. An undeniable advantage of topology optimization in regards to the two other types of structural optimization is that no restriction is placed on the topology thus the space of admissible design is enlarged. However, the drawback is the presence of composite, intermediate densities, which make the resulting design, even the best one, hardly manufacturable in practice, unless a specific post-processing is performed. Regarding the shape optimization, the advantage basically is that the topology is fix and already interesting variation of the shape can be obtained comparatively to some shape sizing structural. However, the drawback can be the possible use of unsuitable geometric representation, as will be highlighted subsequently. These optimizations are generally performed separately. Usually topology optimization is used as a tool for finding new design concepts at the early stage of a design, whereas sizing and shape optimizations are used at a later stage for detailed design. Several approaches aim at combining both structural optimizations in order to take advantage of the both; we can mention the following references [12] and [77].

### 1.3 General formulation of an optimization problem

A structural optimization problem, independently to the type, is composed of three main constituents. A given model which governs the behaviour of the design, the admissible design space with its induced design parameters space and, finally, the objective function associated to the criterion which is to be minimized or maximized. Since maximization is equivalent to minimize the negative of the gain, one just focuses on minimization problem.

Given a three-dimensional structure  $\Omega$ , consider a static problem defined as:

$$\left\{ \begin{array}{l} -div(\boldsymbol{\sigma}) = \mathbf{f}, \text{ on } \Omega \\ \boldsymbol{\sigma} \cdot \mathbf{n} = \mathbf{g}, \text{ on } \Gamma_1 \\ \mathbf{u} = \tilde{\mathbf{u}}_0, \text{ on } \Gamma_0. \end{array} \right. \quad (1.1)$$

where  $\mathbf{u}$  is the displacement of the structure,  $\Gamma_0$  and  $\Gamma_1$  are two non-intersecting parts of the boundary  $\partial\Omega$ . On the boundary  $\Gamma_0$ , the displacement  $\mathbf{u}$  is assigned to be equal to  $\tilde{\mathbf{u}}_0$ , while on  $\Gamma_1$  some natural conditions prescribing the value of the traction are given.  $\mathbf{n}$  is the outer unit

normal vector,  $\mathbf{g}$  the traction force and  $\mathbf{f}$  is the body force.

We suppose that  $\Omega$  is made of homogeneous elastic material thus the stress  $\sigma$  and the strain  $\epsilon$  second rank tensors are related through the elasticity tensor  $\mathbb{E}$ , as stated by the Hooke's law:

$$\boldsymbol{\sigma} = \mathbb{E} : \boldsymbol{\epsilon} \quad \text{and componentwise } \sigma^{ij} = E^{ijkl} \epsilon_{kl}.$$

$\epsilon$  is the small strain tensor, defined as a symmetrized displacement gradient:

$$\epsilon = \frac{1}{2}(\nabla \mathbf{u} + \nabla^T \mathbf{u}).$$

The elastic tensor  $\mathbb{E}$  satisfies the classical minor and major symmetries, respectively read as

$$E^{ijkl} = E^{ijlk}, \quad \text{and } E^{ijkl} = E^{klij}.$$

Let us denote by  $\mathbf{d}$  the vector collecting the design variables which define the design and let  $\mathcal{E}_{ad}$  be the space of admissible design which encompasses some inequality constraints, bound constraints. These constraints involve for instance bounded mass, maximum stress, maximum compliance, maximum displacement, etc. When the design involves the material optimization, the material properties design parameters must satisfy at least some constraints resulting from the positive-definiteness constraint on the elastic tensor.

Given an objective function  $J : \mathcal{E}_{ad} \rightarrow \mathbb{R}$ , the optimization problem is stated as follows: find the optimal design variables  $\mathbf{d}^*$  associated to the optimal design  $\Omega^*$  such that

$$J(\mathbf{d}^*) = \min J(\mathbf{d}), \quad \text{such that (1.1) and } \mathbf{d} \in \mathcal{E}_{ad}. \quad (1.2)$$

$J(\mathbf{d})$  is for instance the total mass or eigenfrequency of vibration, the compliance etc. Usually,  $J(\mathbf{d})$  depends on the state variables which in turn depend implicitly on the design variables. We then denote the objective function by  $J(\mathbf{d}, \mathbf{u}(\mathbf{d}))$ .

## 1.4 Classical analysis and optimization approach

Solving problem (1.1) involves the resolution of problem 1.1 for each design candidate in order to compute the corresponding objective function. The mechanical problem cannot be solved analytically, unless for trivial geometry, loads and boundary conditions. In practice, an approximated solution is generally computed using the finite element analysis (FEA). FEA is based on a variational approach whose problem is further discretized using, e.g., a Galerkin method. The variational formulation allows to obtain a weak formulation of (1.1) and is equivalent to the principle of virtual work in mechanics. Basically, the generic form of the variational problem associated to (1.1) is:

$$\begin{aligned} \text{Find } & u \in \mathcal{V} \text{ such that} \\ & \int_{\Omega} \mathbb{E} : \epsilon(\mathbf{u}) \epsilon(\mathbf{v}) d\Omega = \int_{\Omega} \mathbf{f} \mathbf{v} d\Omega + \int_{\Gamma_1} \mathbf{g} \mathbf{v} d\Gamma_1, \quad \text{for all } \mathbf{v} \in \mathcal{V}. \end{aligned} \quad (1.3)$$

In the above equation,  $d\Omega$  and  $d\Gamma_1$  are respectively volume and surface elements, and  $\mathcal{V}$  is an appropriated variational space with the boundary condition on  $\Gamma_0$ .

The objective function corresponding to the compliance, i.e the work of applied loads, is basically defined as

$$J(\mathbf{d}, \mathbf{u}(\mathbf{d})) = \frac{1}{2} \int_{\Omega} \boldsymbol{\sigma} : \boldsymbol{\epsilon}(\mathbf{u}) d\Omega = \int_{\Omega} \mathbf{f} \cdot \mathbf{u} d\Omega + \int_{\Gamma_1} \mathbf{g} \cdot \mathbf{u} d\Gamma_1.$$

The variational problem is solved on a mesh of the design. Based on this mesh, one also constructs a discrete space  $\mathcal{V}_h$  associated to  $\mathcal{V}$ . Using the geometric discretization, one approximates the continuous integral over  $\Omega$  as a sum of elementary integrals over the elements constituting discretizing mesh often called finite elements mesh (FEM). The discrete space and its interpolation polynomial basis functions depend on the regularity of the solution. Considering, for instance, the case of problem with  $C^0$  continuity, the most widespread used in most CAE software are Lagrange and Hermite polynomials.

On the other hand, the optimization is generally performed based on the FEA mesh. The geometry control variables are usually the nodal points coordinates of the mesh and the elastic properties are basically discretized as constant per element.

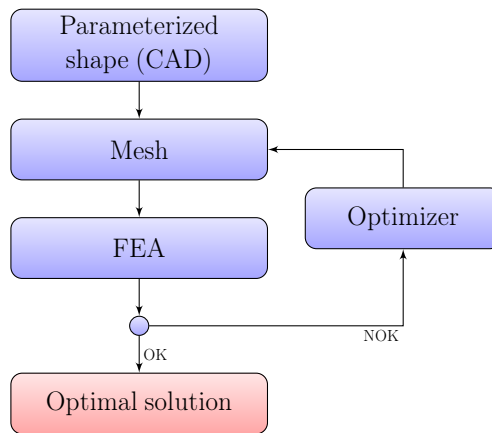


Figure 1.2 Standard optimization process of shape design. The process is constituted of three main blocks: a meshing conversion step which deteriorates the geometry which is further submitted to the FEA software and finally the optimizer.

The drawback of this traditional approach is that it yields to severe inaccuracies at both the analysis and optimization steps. First, the geometric representation on which the FEA is performed is not the exact one and hence the structural response does not correspond to that of the exact structure. Furthermore, the optimization also is performed on an approximated geometry. Because of the continuous change of the finite element mesh through the optimization process it is difficult to ensure that the accuracy of the FEA remains preserved. The meshing suitability and the regularity constraints on the shape occupies a preponderant place in such an approach. Different works focus on this point. In fact, one must avoid distortions of the FEM grid and remeshing must be performed at each iteration in order to maintain the regularity of the FE

near the boundary [36]. In [57] the authors have worked on optimal design processes where the computer program combines automatic remeshing, mesh adaptation and design change. As a last step, once the optimal geometry mesh is found, a time consuming step of conversion from the resulting optimal “mesh” to an exact geometry (CAD) object must be performed. For material properties design, the complexity and the size of problem with this kind of standard process is huge. The complexity is of the order of the number of elements and highly dependent on the refinement of the FEM needed for analysis convergence.

In the framework of topology optimization problems, we emphasize that the formulation is similar but the design is now the density function. Roughly speaking, one searches for the optimal material properties distribution in a given bounded domain. In the original approach, described in the pioneering work of Bendsoe [7]: the topology optimization consists in finding the optimal distribution of material. The elastic tensor is set of the form

$$E^{ijkl} = \chi_{\Omega_m} A^{ijkl}$$

where the constants  $A^{ijkl}$  are the elastic constants of the material employed for the design,  $\Omega_m$  a subset of  $\Omega$  with material and  $\chi_{\Omega_m}$  represents the indicator function on  $\Omega_m$

$$\chi_{\Omega_m}(x) = \begin{cases} 1 & \text{if } x \in \Omega_m \\ 0 & \text{otherwise.} \end{cases}$$

The void material is to be understood in the sense of matter with weak material properties have “weak elastic properties”. The design space constraint usually involves fix volume constraint on the amount of (strong) material used which, indeed, is commonly expensive. The volume is typically defined as

$$\text{Vol}(\Omega) = \int_{\Omega} \chi_{\Omega_m} dx.$$

During the past few years the isogeometric method allows to abort the time consuming and quality degrading meshing step and intends to unify the geometry representation on CAD and CAE environment. The isogeometric concept is based on geometric representation. Thus a brief historic on geometric representation in CAD environment is subsequently reviewed.

It appears so far that a crucial point for the optimization is the parameterization of the design and the associated design parameters which have to be driven through the design process. A huge number of design parameters as in the case of FEA-based optimization allows to explore widely the design space but present the shortcoming of yielding to non smooth design, with singularity which therefore are not manufacturable, in addition to the complexity of their corresponding problem. Other approach exists and attenuate these shortcomings. We can cite the morphing. Roughly speaking, within this approach, the design is separated in some groups or components and the element belonging to the same component are moved jointly. Here the design variables are the position coordinates associated to the blocks. By doing so, the initial connectivity within each component is preserved and the resulting design is smooth. However, the price to paid is that the design space exploration is reduced and also a priori suitable decomposition is required. The mesh-CAD conversion is commonly made through filtering techniques but the post-processing result is highly sensitive to the filtering parameters. This step deteriorates the optimal solutions which present few reliability.

## 1.5 The Isogeometric method

The standard FEA-based shape optimization involves different representations of the design, namely the CAD design and its mesh approximation. The isogeometric method [28],[37] developed these few past years aim at the reduction of this heterogeneity due to the presence of many representations of the same geometry. This method encompasses isoparametric technique which consists on the approximation of the solution of a given problem or a quantity of interest by using the same parameterization in regards to the object to which they are associated. This is transcribed in the partial differential equation solving framework by the substituting of the classical finite element basis functions with those associated to the design geometric representation. The trial functions used are then NURBS, B-Spline or Bezier functions. Such a kind of choice is possible since these functions satisfy the requisites of the classical FEA trial functions, commonly the linear independence and the unit partition property. The concept has been widened to optimization problem within which the design variables are some CAD parameters, i.e the control points coordinates. Among the amount of references we can cite non exhaustively [40, 23], and specially mentioned [56] which is concerned with both shape and material optimal design.

## 1.6 Synthesis

We have recalled in this introductory chapter the different ingredients of structural optimization and have highlighted the particular role play the the parameterization. Our approach throughout this manuscript falls within the isogeometric method regarding the optimal design. We emphasize that the analysis, i.e solving of the mechanical problem, will be performed using classical finite element method, since the concern in the ideal design process is that one mainly needs a resulting optimal design which is already a CAD object. A special representation of the elastic properties is discussed in chapter 4.



## Part I

# Analysis of shell assemblings





# Naghdi Shell Model

---

## Contents

---

<b>2.1</b>	<b>Differential geometry</b>	<b>16</b>
2.1.1	Differential geometry of surface	16
2.1.2	Differential geometry for curvilinear 3D body	19
<b>2.2</b>	<b>Mechanical model</b>	<b>20</b>
2.2.1	Kinematic assumptions	20
2.2.2	Constitutive equations	21
2.2.3	Strain, stress and energies	23
2.2.4	Naghdi's equation	25
<b>2.3</b>	<b>On the existence results</b>	<b>26</b>
<b>2.4</b>	<b>Synthesis</b>	<b>29</b>

---

## Introduction

Among the different approaches to justify shell models we can cite the asymptotic development approach and the direct:

- Asymptotic methods are generally used to describe a limit behavior of a model or equation when a given parameter tends to zero. In the case of shell model this approach is used to derive the bi-dimensional mechanical model from three-dimensional equations when the thickness goes to zero. The model is derived, as shown in [27], [34], after a proper expansion of the three-dimensional elasticity equations in term of the thickness parameter. The asymptotic method is commonly used to justify the model for *thin shell structures*: the well-known Koiter's model [41] similar to the Kirchoff-Love model for plate structures.
- In the direct approach, the bi-dimensional model is derived with the help of assumption on the displacement field and a direct use of three-dimensional Hooke's law as firstly introduced by Naghdi [55]. An integration over the thickness is then made to derived the bi-dimensional model, [64], [9].

We describe in this chapter the second approach leading to the well-known model of Naghdi corresponding to the Reissner-Mindlin plate model. The Naghdi shell model is valid for moderately thick structure and allows to mechanically take into account for the shear deformation. In fact, unlike the Kirchoff-Love model, which assumes that the normal fiber to the middle-surface of

the shell remains an orthogonal straight line to the middle-surface after deformation, the Naghdi shell model assume that the normal fiber, which remains a straight line after deformation can rotate.

A practical interest of bi-dimensional models is that analytically and numerically they reduce the complexity of the mechanical problem comparatively to the three-dimensional one. In fact, analytically the problem is defined on a parametric bi-dimensional domain of curvilinear coordinates instead of the three-dimensional body. However, an inherent drawback to such a kind of model is the spurious phenomenon of numerical locking [22]. This phenomenon is due to the approximation of the three-dimensional model by a bi-dimensional one and is not investigated in this thesis.

## 2.1 Differential geometry

Let  $\mathcal{E}^3$  be the three-dimensional Euclidean space, equipped with the standard orthonormal basis  $(O, \mathbf{e}_1, \mathbf{e}_2, \mathbf{e}_3)$ . The dot symbol “.” denotes the standard Euclidean scalar product,  $\| \cdot \|$  the associated norm and  $\wedge$  the wedge product.

Throughout the sequel; a bold character denotes a tensor or a vector. Given  $x$  a generic point in  $\mathcal{E}^3$ , we will denote  $\mathbf{x}$  its position vector with respect to the origin in the Cartesian frame,  $\mathbf{x} := Ox$ .

The subscript comma stands for differentiation; for instance “, $j$ ” stand for the derivative with respect to the  $j$ -th coordinate. Latin indexes range in the set  $\{1, 2, 3\}$ , except when they are used to index sequences. Greek indexes range in  $\{1, 2\}$  excepted when they are underlined. For compactness and simplicity reasons, we use the Einstein summation convention over repeated subscript or superscript index, otherwise explicitly stated. For instance

$$G^{ij}e_j = \sum_{j=1}^3 G^{ij}e_j = G^{i\alpha}e_\alpha + G^{i3}e_3 = G^{i1}e_1 + G^{i2}e_2 + G^{i3}e_3.$$

Now, we introduce the element of differential geometry which held to define locally quantities parameterized by the mapping of the shell’s middle-surface and to derive the shell equations. The following synthesis of different geometry used can be found in Ciarlet [25].

### 2.1.1 Differential geometry of surface

Let  $\omega$  be an open bounded set of  $\mathbb{R}^2$ , and consider an immersion  $\Phi \in C^2(\omega, \mathcal{E}^3)$ ; suppose that the surface  $\Omega$  is defined as the image of the domain  $\omega$  through the mapping or chart  $\Phi$ , i.e  $\Omega := \Phi(\bar{\omega})$ . The surface  $\Omega$  is defined as

$$\Omega = \{m \in \mathcal{E}^3 \text{ such that } \mathbf{m} = \Phi(\boldsymbol{\xi}), \boldsymbol{\xi} \in \bar{\omega}\}. \tag{2.1}$$

An illustration of such a definition is provided in Figure 2.1.

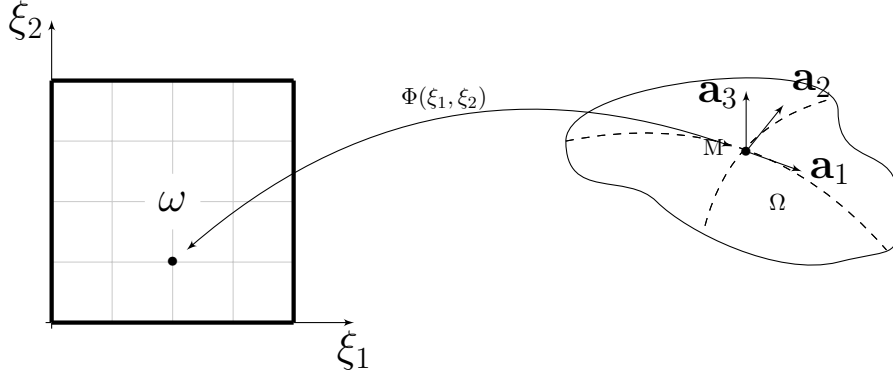


Figure 2.1 Definition of a three-dimensional surface  $\Omega$ , as image of the domain  $\bar{\omega}$  through the mapping  $\Phi$ . In the further applications, see chapter 3 and 5, we will assume that the surface are defined by CAD patches so that the reference domain is the dimensionless unique square,  $\omega = [0, 1]^2$ .

Let  $\mathbf{a}_\alpha = \Phi_{,\alpha}$  be the covariant vector which, see Figure 2.1, is tangent to the coordinate line of the surface with constant curvilinear coordinate  $\xi^\alpha$ . The vectors  $\mathbf{a}_1$  and  $\mathbf{a}_2$  span the tangent plane to  $\Omega$  at  $\Phi(\xi^1, \xi^2)$ . The surface  $\Omega$  is regular in the sense that the covariant vectors  $\mathbf{a}_\alpha$  are linearly independent, so we can define the normal vector  $\mathbf{a}_3$  by

$$\mathbf{a}_3 = \frac{\mathbf{a}_1 \wedge \mathbf{a}_2}{\|\mathbf{a}_1 \wedge \mathbf{a}_2\|}. \quad (2.2)$$

### Metric and curvature tensors

We define the metric tensor (resp. the curvature tensor)  $\mathbf{a} = (a_{\alpha\beta})$  (resp.  $\mathbf{b} = (b_{\alpha\beta})$ ) whose covariant components are:

$$a_{\alpha\beta} = \mathbf{a}_\alpha \cdot \mathbf{a}_\beta, \text{ and } b_{\alpha\beta} := \mathbf{a}_{\alpha,\beta} \cdot \mathbf{a}_3 = -\mathbf{a}_{3,\beta} \cdot \mathbf{a}_\alpha. \quad (2.3)$$

The former allows to compute the elements of length, area and to measure angles on the surface  $\Omega$  while the latter allows to measure the curvature of the surface.

Let  $d\Omega$  be the element of area on the middle-surface

$$d\Omega = \sqrt{a} dS, \text{ where } a = \det((a_{\alpha\beta})) = a_{11}a_{22} - a_{12}a_{12}.$$

$dS$  is the element of area on the parametric domain  $\omega$ . In the case where  $\omega$  is a unit square  $dS = d\xi^1 d\xi^2$ .

Given a parametric curve  $\eta \in I \mapsto (\xi^\alpha) = (\varphi^\alpha(\eta)) \in \bar{\omega}$ , with  $I$  a bounded interval of  $\mathbb{R}$ , the element of length  $ds$  is defined as

$$ds = s(\eta) d\eta; \text{ where } s^2(\eta) = a_{\alpha\beta}(\varphi(\eta)) \frac{\partial \varphi^\alpha}{\partial \eta}(\eta) \frac{\partial \varphi^\beta}{\partial \eta}(\eta). \quad (2.4)$$

We associate to the vectors  $\mathbf{a}_\alpha$ , their dual vectors  $\mathbf{a}^\alpha$  called contravariant vectors defined by

$$\mathbf{a}^\beta \cdot \mathbf{a}_\alpha = \delta_{\alpha}^{\beta}, \text{ with } \delta_{\alpha}^{\beta} = \delta_{\alpha\beta} \text{ the Kronecker delta symbol.} \quad (2.5)$$

The third contravariant vector is  $\mathbf{a}^3 = \mathbf{a}_3$ . The contravariant components of the metric tensor are  $a^{\alpha\beta} := \mathbf{a}^\alpha \cdot \mathbf{a}^\beta$  and with the help of (2.5)

$$(\mathbf{a}^{\alpha\beta}) = (\mathbf{a}_{\alpha\beta})^{-1}.$$

Considering the definition of the covariant and contravariant basis, we have

$$a^{\alpha 3} = a_{\alpha 3} = 0, \text{ and } \mathbf{a}_{33} = 1.$$

These different forms of the metric tensor allow to perform a change between covariant and contravariant tensor quantities defined on the surface  $\Omega$ ; for instance we define the mixt components of the curvature tensor  $\mathbf{b}$  as follows

$$b_{\alpha}^{\beta} := a^{\beta\sigma} b_{\sigma\alpha} = \mathbf{a}_{,\alpha}^{\beta} \cdot \mathbf{a}_3 = -\mathbf{a}_{3,\alpha} \cdot \mathbf{a}^{\beta}.$$

### Levi-Cevita symbols

Let  $\hat{\mathbf{e}} = (\hat{e}_{\alpha\beta}) = (\hat{e}^{\alpha\beta})$  be the permutation symbols  $\hat{e}_{\alpha\alpha} = 0$ , and  $\hat{e}_{12} = -\hat{e}_{21} = 1$ . The Levi-Cevita symbols  $e_{\alpha\beta}$  and  $e^{\alpha\beta}$  are defined as follows

$$\mathbf{a}_3 \wedge \mathbf{a}_\alpha = e_{\alpha\beta} \mathbf{a}^\beta, \quad \mathbf{a}_3 \wedge \mathbf{a}^\alpha = e^{\alpha\beta} \mathbf{a}_\beta \text{ and } \mathbf{a}_\alpha \wedge \mathbf{a}_\beta = e_{\alpha\beta} \mathbf{a}_3, \quad (2.6)$$

where  $e_{\alpha\beta} := \sqrt{a} \hat{e}_{\alpha\beta}$  and  $e^{\alpha\beta} := \frac{1}{\sqrt{a}} \hat{e}_{\alpha\beta}$  are the permutation tensor on the middle-surface.

### Covariant derivatives

Let  $\Gamma_{\alpha\beta}^{\sigma}$  be the Christoffel symbols of the first kind, i.e the contravariant components of the covariant basis vector derivative written in the covariant basis; namely

$$\Gamma_{\alpha\beta}^{\sigma} = \mathbf{a}_{\alpha,\beta} \cdot \mathbf{a}^{\sigma}. \quad (2.7)$$

The curvature tensor and the Christoffel symbols allow to compute the (covariant or contravariant) derivative with respect to the curvilinear coordinate. In fact, using (2.5), (2.7)

$$\mathbf{a}_{\alpha,\beta} = (\mathbf{a}_{\alpha,\beta} \cdot \mathbf{a}^{\sigma}) \mathbf{a}_{\sigma} + (\mathbf{a}_{\alpha,\beta} \cdot \mathbf{a}_3) \mathbf{a}_3 = \Gamma_{\alpha\beta}^{\sigma} \mathbf{a}_{\sigma} + b_{\alpha\beta} \mathbf{a}_3. \quad (2.8)$$

Also, we have

$$\mathbf{a}_{,\beta}^{\alpha} = (\mathbf{a}_{,\beta}^{\alpha} \cdot \mathbf{a}_{\sigma}) \mathbf{a}^{\sigma} + (\mathbf{a}_{,\beta}^{\alpha} \cdot \mathbf{a}_3) \mathbf{a}_3 = -\Gamma_{\sigma\beta}^{\alpha} \mathbf{a}^{\sigma} + b_{\beta}^{\alpha} \mathbf{a}_3. \quad (2.9)$$

Now, consider a vector field  $\mathbf{v} = v_i \mathbf{a}^i$  defined by the its covariant components; the derivative  $\mathbf{v}_{,\beta}$  of  $\mathbf{v}$  with respect to  $\xi^{\beta}$  can be computed, thanks to the chain rule as

$$\mathbf{v}_{,\beta} = v_{\alpha,\beta} \mathbf{a}^{\alpha} + v_{\sigma} \mathbf{a}_{,\beta}^{\sigma} + v_{3,\beta} \mathbf{a}_3 + v_3 \mathbf{a}_{3,\beta}.$$

Using (2.8) and (2.9), one finally obtains

$$\mathbf{v}_{,\alpha} = (v_{\alpha|\beta} - b_{\alpha\beta} v_3) \mathbf{a}^{\alpha} + (v_{3|\beta} + b_{\beta}^{\sigma} v_{\sigma}) \mathbf{a}_3,$$

where the symbol  $|\beta$  denotes the covariant derivative operation with respect to  $\xi^{\beta}$  defined below

$$\begin{cases} v_{\alpha|\beta} &= v_{\alpha,\beta} - v_{\sigma} \Gamma_{\alpha\beta}^{\sigma} \\ v_{3|\beta} &= v_{3,\beta}. \end{cases} \quad (2.10)$$

### 2.1.2 Differential geometry for curvilinear 3D body

Let  $\Phi$  be an immersion in  $C^2(\omega, \mathcal{E}^3)$  and  $\Omega$  be the surface  $\Omega = \Phi(\omega)$ , we will denote  $\Omega_t$  the following three-dimensional body of thickness  $t$  and middle-surface  $\Omega$ :

$$\Omega_t = \left\{ x \in \mathbb{R}^3, \text{ such that } \mathbf{x} = \Phi(\xi^1, \xi^2) + \xi^3 \mathbf{a}_3 \text{ for all } (\xi^1, \xi^2, \xi^3) \in \omega \times \left[-\frac{t}{2}, \frac{t}{2}\right] \right\} \quad (2.11)$$

where  $\mathbf{a}_3$  is the unit normal vector to the middle-surface and  $\xi^3$  is the normal coordinate along  $\mathbf{a}_3$  at a point  $\Phi(\xi^1, \xi^2)$ .

We may now define the covariant vectors  $\mathbf{g}_\alpha$  at any point  $x \in \Omega_t$  of the three-dimensional body

$$\begin{aligned} \mathbf{g}_\alpha &= \Phi_{t,\alpha} = \mathbf{a}_\alpha + \xi^3 \mathbf{a}_{3,\alpha} = \mathbf{a}_\alpha - \xi^3 b_\alpha^\lambda \mathbf{a}_\lambda = (\delta_\alpha^\lambda - \xi^3 b_\alpha^\lambda) \mathbf{a}_\lambda \\ \mathbf{g}_3 &= \mathbf{a}_3 \end{aligned} \quad (2.12)$$

The element of volume  $dV$  on  $\Omega_t$  is defined as

$$dV = \sqrt{g} d\xi^1 d\xi^2 d\xi^3, \text{ with } \sqrt{g} = (\mathbf{g}_1 \wedge \mathbf{g}_2) \cdot \mathbf{a}_3.$$

As a first step, to compute  $\sqrt{g}$ , we have

$$\mathbf{g}_1 \wedge \mathbf{g}_2 = (\delta_1^\lambda - \xi^3 b_1^\lambda) (\delta_2^\beta - \xi^3 b_2^\beta) \mathbf{a}_\lambda \wedge \mathbf{a}_\beta.$$

Using the formula (2.6), we have

$$\begin{aligned} \mathbf{g}_1 \times \mathbf{g}_2 &= (\delta_1^\lambda - \xi^3 b_1^\lambda) (\delta_2^\beta - \xi^3 b_2^\beta) \sqrt{a} e_{\lambda\beta} \mathbf{a}_3 \\ &= \sqrt{a} [(1 - \xi^3 b_1^1) (1 - \xi^3 b_2^2) - (\xi^3 b_1^2) (\xi^3 b_2^1)] \mathbf{a}_3. \end{aligned}$$

Rearranging as sequence of  $\xi^3$  and taking the scalar product with  $\mathbf{a}_3$ , we obtain

$$\sqrt{g} = (1 - \xi^3 b_\alpha^\alpha + (\xi^3)^2 \det(b_\alpha^\beta)) \sqrt{a}, \text{ with } \det(b_\alpha^\beta) = b_1^1 b_2^2 - b_2^1 b_1^2.$$

It is usual to write  $\sqrt{g}$  as

$$\sqrt{g} = (1 - 2H\xi^3 + K(\xi^3)^2) \sqrt{a}, \quad (2.13)$$

where  $H = \frac{1}{2} b_\alpha^\alpha$  is the mean curvature and  $K = \det(b_\alpha^\beta)$  is the Gaussian curvature of the midsurface.

The thickness is assumed small enough in order to have  $1 - 2H\xi^3 + K(\xi^3)^2 > 0$  for all  $\xi^3 \in [-\frac{t}{2}, \frac{t}{2}]$ . Indeed, if this quantity were negative the definition (2.11) of  $\Omega_t$  does not make sense, i.e negative volume.

Let  $\tilde{e}_{\alpha\beta}$  and  $\tilde{e}^{\alpha\beta}$  be the Levi-Cevita symbols associated to the three-dimensional body

$$\tilde{e}_{\alpha\beta} = \sqrt{g} e_{\alpha\beta} \text{ and } \tilde{e}^{\alpha\beta} = \frac{1}{\sqrt{g}} e^{\alpha\beta}.$$

The contravariant vectors  $\mathbf{g}^j$  associated to  $\mathbf{g}_i$  are such that

$$\mathbf{g}^3 = \mathbf{a}_3 \text{ and } \mathbf{g}_3 \wedge \mathbf{g}_\alpha = \tilde{e}_{\alpha\beta} \mathbf{g}^\beta.$$

We have

$$\mathbf{g}^\beta = \tilde{e}^{\beta\alpha}(e_{\lambda\alpha} - \xi^3 b_\alpha^\sigma e_{\lambda\sigma})\mathbf{a}^\lambda.$$

We conclude this section by defining the covariant derivative corresponding to three-dimensional body, the analogous of formula (2.10) for a surface. Given a three-dimensional vector field  $\mathbf{U} := U_i \mathbf{g}^i$ ,

$$\mathbf{U}_{i||j} := \mathbf{U}_{,j} \cdot \mathbf{g}_i = U_{i,j} - \Gamma_{ij}^k U_k$$

The Christoffel symbols being defined by  $\Gamma_{ij}^k = \mathbf{g}_{i,j} \cdot \mathbf{g}^k$ . Reader interested may refer to the aforementioned reference [27].

## 2.2 Mechanical model

A shell is a structure occupying a region in the three-dimensional space with one dimension small in regards to its two other main characteristic dimensions so that it can be identified with a surface. Hence, given a regular immersion  $\Phi \in C^2(\omega, \mathcal{E}^3)$ , a shell of middle-surface  $\Omega$  and thickness  $t$  will be defined by formula (2.11). The vector  $\mathbf{a}_3$  is the unit vector along the normal fibre to  $\Omega$ .

We focus in this section on the definition of the Naghdi shell model. We start by the kinematical assumptions of this model, compute the corresponding strain tensor and finally, in order to compute the strain energy, we specify the elastic properties feature and state the Naghdi shell equation.

### 2.2.1 Kinematic assumptions

The Naghdi model is based on the following assumptions on the normal fiber:

- the normal fiber is a straight line in the reference configuration which is orthogonal to the middle-surface,
- the normal fiber remains a straight line which does not stretch and is not restricted to stay normal to the middle-surface of the deformed configuration.

Thus, in the Naghdi model, the displacement field of the three-dimensional shell is defined by five functions: three covariant components of displacement and two covariant components of rotation. More precisely, let  $\Psi(\cdot, \cdot)$  be the infinitesimal rotation vector of the normal fiber and  $\mathbf{u}$  be the displacement vector of the middle-surface, we set

$$\mathbf{u} = u_i \mathbf{a}^i, \quad \Psi(\mathbf{u}, \mathbf{s}) = e^{\alpha\lambda} s_\alpha \mathbf{a}_\lambda + \frac{1}{2} e^{\lambda\alpha} u_{\alpha|\lambda} \mathbf{a}_3. \quad (2.14)$$

The displacement  $\mathbf{U}$  of a particle located at  $\Phi(\xi^1, \xi^2) + \xi^3 \mathbf{a}_3$  is defined by

$$\mathbf{U} = \mathbf{u} + \xi^3 \mathbf{a}_3 \wedge \Psi(\mathbf{u}, \mathbf{s}) = \mathbf{u}(\xi^1, \xi^2) + \xi^3 s_\alpha \mathbf{a}^\alpha. \quad (2.15)$$

In the following, for simplicity reasons, we do not note explicitly the dependence of  $u_i$ ,  $s_\alpha$  and  $\mathbf{a}_i$  with respect to the curvilinear coordinates  $\boldsymbol{\xi} = (\xi_\alpha)$ . We note  $\mathbf{u} = (u_i)$  and  $\mathbf{s} = (s_\alpha)$  respectively the vectors composed of covariant components of displacement and rotation. Also, we further noted  $\Psi(\mathbf{u}, \mathbf{s}) = \Psi(\mathbf{u}, \mathbf{s})$ .

### 2.2.2 Constitutive equations

In the case of shell, we assume that the elastic body is curvilinearly anisotropic: the equivalent directions from point to point are not parallel but follow a conventionally chosen coordinate lines. Let then assume that the strain and stress are defined by covariant and contravariant components on the curvilinear basis, i.e  $\sigma := \sigma^{ij}(\mathbf{g}_i \otimes \mathbf{g}_j)$  and  $\epsilon = \epsilon_{ij}(\mathbf{g}^i \otimes \mathbf{g}^j)$  respectively be the Cauchy stress tensor and the three-dimensional linearised strain tensor. The coefficients  $E^{ijkl}$  are then the contravariant components of the elastic tensor written in the local basis of the shell:

$$\mathbb{E} = E^{ijkl}(\mathbf{g}_i \otimes \mathbf{g}_j \otimes \mathbf{g}_k \otimes \mathbf{g}_l).$$

If the material properties are homogeneous throughout the thickness, i.e. independent of  $\xi^3$ , it is commonly assumed that

$$\mathbb{E} = E^{ijkl}(\mathbf{a}_i \otimes \mathbf{a}_j \otimes \mathbf{a}_k \otimes \mathbf{a}_l). \quad (2.16)$$

#### Elastic coefficients in local basis

In general, the elastic properties of the constitutive material of the shell are given in an arbitrary frame, called the material frame and the coefficients  $E^{ijkl}$  in the local basis, (2.16), are not initially known. Thus, for the purpose of setting up the mechanical equations, one has to perform a basis change in order to compute the elastic coefficients  $E^{ijkl}$  from the elastic tensor coefficient given in the material frame.

Let us denote by  $A^{ijkl}$  the coefficients of the tensor  $\mathbb{E}$  in the material frame  $(\mathbf{m}_1, \mathbf{m}_2, \mathbf{m}_3)$ , we have

$$\mathbb{E} = A^{pqrs}(\mathbf{m}_p \otimes \mathbf{m}_q \otimes \mathbf{m}_r \otimes \mathbf{m}_s) = E^{ijkl}(\mathbf{a}_i \otimes \mathbf{a}_j \otimes \mathbf{a}_k \otimes \mathbf{a}_l). \quad (2.17)$$

Let  $G_p^i$  be the contravariant components of the material frame basis vectors  $\mathbf{m}_p$  such that

$$\mathbf{m}_p = G_p^i \mathbf{a}_i. \quad (2.18)$$

Thus injecting the formula (2.18) into (2.17), we have

$$\mathbb{E} = A^{pqrs} G_p^i \mathbf{a}_i \otimes G_q^j \mathbf{a}_j \otimes G_r^k \mathbf{a}_k \otimes G_s^l \mathbf{a}_l.$$

Thus the contravariant components of the elastic tensor are:

$$E^{ijkl} = (G_p^i G_q^j G_r^k G_s^l) A^{pqrs}. \quad (2.19)$$

Formula (2.19) defines the contravariant components in terms of the elastic coefficients given in the material frame. We illustrate below a possible convention for the definition of the material frame.



### Curvilinear material frame

Let us introduce the orthogonal basis vectors  $\mathbf{d}_i$  defined such that

$$\mathbf{d}_3 = \mathbf{a}_3 \text{ and } \mathbf{d}_\beta \in \text{span}\{\mathbf{a}_1, \mathbf{a}_2\}.$$

It is generally assumed that  $\mathbf{m}_3 = \mathbf{d}_3 = \mathbf{a}_3$  so that the vectors  $\mathbf{m}_\alpha$  are defined through a rotation of a given angle  $\theta(\boldsymbol{\xi}) = \theta$  of the vectors  $\mathbf{d}_\alpha$  around the normal vector  $\mathbf{a}_3$ . The angle  $\theta$  fixes the material frame on the geometry and is referred to as the orthotropy angle in chapter 4 and 5.

$$\begin{cases} \mathbf{m}_1 &= \cos \theta \mathbf{d}_1 + \sin \theta \mathbf{d}_2 \\ \mathbf{m}_2 &= -\sin \theta \mathbf{d}_1 + \cos \theta \mathbf{d}_2 \\ \mathbf{m}_3 &= \mathbf{a}_3 \end{cases} \quad (2.20)$$

One can define the reference frame basis vector  $\mathbf{d}_i$  as follows: Given a fixed integer  $\alpha \in \{1, 2\}$

$$\begin{cases} \mathbf{d}_3 &= \mathbf{a}_3 \\ \mathbf{d}_2 &= \frac{\mathbf{a}_\alpha}{\sqrt{a_{\alpha\alpha}}} \\ \mathbf{d}_1 &= \mathbf{d}_2 \wedge \mathbf{d}_3 \end{cases}, \text{ more precisely } \mathbf{d}_1 = \frac{\epsilon_{\beta\alpha} \mathbf{a}^\beta}{\|\epsilon_{\beta\alpha} \mathbf{a}^\beta\|}. \quad (2.21)$$

The orthogonality property in the previous definition results from equation (2.5), page 18. After the definition of the contravariant component of the elastic tensor, we specify subsequently the elastic symmetries of the elastic tensor in any arbitrary material frame.

### Elastic symmetries

For a general anisotropic material, there are 81 elastic coefficients. Thanks to the minor and major symmetry the number of independent elastic coefficients  $A^{ijkl}$  is reduced to 21. But the material can possess some proper symmetries, that give some relations between the elastic coefficients so further reducing the number of independent elastic coefficients. These relations come from the existence of one or more planes of symmetry which leave invariant the elastic properties to reflection operation. More precisely, noting  $\mathcal{R} = (R_p^i)$  the second-rank tensor associated to the reflection transformation, we have

$$A^{ijkl} = R_p^i R_q^j R_r^k R_s^l A^{pqrs}. \quad (2.22)$$

#### Monoclinic symmetry:

A monoclinic material is a material which possesses one plane of symmetry leaving invariant the elastic tensor by reflection. Let us assume that  $\mathbf{m}_3$  is the orthogonal axis to that plane of symmetry. Thus the matrix form of the tensor  $\mathcal{R}$  is

$$\mathcal{R} = \begin{pmatrix} 1 & 0 & 0 \\ 0 & 1 & 0 \\ 0 & 0 & -1 \end{pmatrix}.$$

Using Eq. (2.22), we have the following eight relations (respectively 6 for the first and 2 for the second)

$$A^{ii\alpha 3} = 0 \text{ and } A^{\alpha 333} = 0. \quad (2.23)$$

Thus the total number of independent elastic coefficients is 13.

**Orthotropic material:**

An orthotropic material is a material which posses two mutually perpendicular planes of symmetry. Let us assume the planes of symmetry are  $\text{span}\{\mathbf{m}_1, \mathbf{m}_2\}$  and  $\text{span}\{\mathbf{m}_1, \mathbf{m}_3\}$ . The matrix form of the corresponding tensor is

$$\mathcal{R} = \begin{pmatrix} -1 & 0 & 0 \\ 0 & 1 & 0 \\ 0 & 0 & -1 \end{pmatrix}.$$

This symmetry in fact, turns to add a new plane of symmetry to the one defined above, in (2.23). Symmetry with respect to  $\text{span}\{\mathbf{m}_1, \mathbf{m}_2\}$  induces the following new relations to (2.23)

$$A^{3312} = A^{2212} = A^{1323} = A^{1211} = 0. \quad (2.24)$$

Thus the number of independent elastic coefficients is 9.

REMARK 2.2.1

- Given the vectors  $\mathbf{m}_i$ ; symmetry of principal direction  $\mathbf{m}_i$  yields to the relations consisting of vanishing the elastic coefficients with odd number of index  $i$ .
- One finds in a straightforward fashion that adding a new symmetry of principal direction  $\mathbf{m}_1$  does not add any relations to those defined above. Thus orthotropic material are often referred to as material possessing three mutually orthogonal planes of symmetry.

We subsequently consider orthotropic material

**2.2.3 Strain, stress and energies**

The Hooke's law implies

$$\sigma^{ij} = E^{ijkl} \epsilon_{kl} = E^{ij\lambda\mu} \epsilon_{\lambda\mu} + 2E^{ij\alpha 3} \epsilon_{\alpha 3} + E^{ij33} \epsilon_{33}. \quad (2.25)$$

**Strain and stress tensors definition**

The covariant strain coefficients are defined as [see [27], Theorem 3.2.1 page 117]

$$\epsilon_{ij} = \frac{1}{2}(U_{i||j} + U_{j||i}), \text{ with } U_{i||j} = \mathbf{U}_{,j} \cdot \mathbf{g}_i. \quad (2.26)$$

The plane and anti-plane (transverse shear) components of the strain tensor are

$$\begin{aligned} \epsilon_{\alpha\beta}(\mathbf{u}, \mathbf{s}) &= \gamma_{\alpha\beta}(\mathbf{u}) + \xi^3 \chi_{\alpha\beta}(\mathbf{u}, \mathbf{s}) \\ \epsilon_{\alpha 3}(\mathbf{u}, \mathbf{s}) &= \gamma_{\alpha 3}(\mathbf{u}, \mathbf{s}), \end{aligned}$$

where  $\gamma_{\alpha\beta}$ ,  $\gamma_{\alpha 3}$  and  $\chi_{\alpha\beta}$  are respectively the membrane and bending strain tensors

$$\begin{aligned} \gamma_{\alpha\beta}(\mathbf{u}) &= \frac{1}{2}(u_{\alpha|\beta} + u_{\beta|\alpha}) - b_{\alpha\beta} u_3 \\ \chi_{\alpha\beta}(\mathbf{u}, \mathbf{s}) &= \frac{1}{2} \left( s_{\alpha|\beta} + s_{\beta|\alpha} - b_{\alpha}^{\sigma} d_{\sigma\beta}(\mathbf{u}) - b_{\beta}^{\sigma} d_{\sigma\alpha}(\mathbf{u}) \right) \\ \gamma_{\alpha 3}(\mathbf{u}, \mathbf{s}) &= \frac{1}{2}(s_{\alpha} + b_{\alpha}^{\sigma} u_{\sigma} + u_{3,\alpha}) \end{aligned} \quad (2.27)$$

In the above equation,  $u_{\alpha|\beta}$  designates the covariant derivative of  $u_\alpha$  with respect to the curvilinear coordinate  $\xi^\beta$  and  $d_{\lambda\mu}(\mathbf{u}) := u_{\lambda|\mu} - b_{\lambda\mu}u_3$ .

Shell models are based plane stress state assumption, i.e the transverse normal component of stress is neglected<sup>a</sup>:

$$\sigma^{33} = 0. \quad (2.28)$$

The transverse normal stress component is

$$\sigma^{33} = E^{33kl}\epsilon_{kl} = E^{33\lambda\mu}\epsilon_{\lambda\mu} + 2E^{33\lambda 3}\epsilon_{\lambda 3} + E^{3333}\epsilon_{33},$$

and condition (2.28) yields to

$$\epsilon_{33} = -\frac{E^{33\lambda\mu}\epsilon_{\lambda\mu} + 2E^{33\lambda 3}\epsilon_{\lambda 3}}{E^{3333}}. \quad (2.29)$$

and thanks to the symmetry with respect to the middle-surface ( $A^{33\alpha 3} = 0 \rightarrow E^{33\lambda 3} = 0$ ), we have

$$\epsilon_{33} = -\frac{E^{33\lambda\mu}}{E^{3333}}\epsilon_{\lambda\mu}. \quad (2.30)$$

Injecting (2.30) in (2.25), and using the fact that the middle-surface is a surface of symmetry so that  $E^{\alpha\beta\lambda 3} = 0$ , the Hooke's law is returned as follows:

$$\begin{aligned} \sigma^{\alpha\beta} &= Q^{\alpha\beta\lambda\mu}\epsilon_{\lambda\mu}, \\ \sigma^{\alpha 3} &= 2E^{\alpha 3\beta, 3}\epsilon_{\beta 3} \end{aligned}$$

where  $\mathbb{Q} := (Q^{\alpha\beta\lambda\mu})$  is the plane reduced elastic tensor:

$$Q^{\alpha\beta\lambda\mu} = \left( E^{\alpha\beta\lambda\mu} - \frac{E^{\alpha\beta 33}E^{33\lambda\mu}}{E^{3333}} \right)$$

and  $\mathbf{E} := (E^{\alpha 3\beta 3})$  is the anti-plane part of the elastic tensor.

### Strain energy:

Now we consider the strain energy

$$E_d(\mathbf{u}, \mathbf{s}) = \frac{1}{2} \int_{\hat{\Omega}} \left\{ \sigma^{\alpha\beta}\epsilon_{\alpha\beta} + 4\sigma^{\alpha 3}\epsilon_{\alpha 3} \right\} dV.$$

Making the following approximation  $dV \simeq \sqrt{ad}Sd\xi^3$ , the strain energy is

$$\begin{aligned} E_d(\mathbf{u}, \mathbf{s}) &= \frac{1}{2} \int_{-\frac{t}{2}}^{\frac{t}{2}} \int_{\omega} \left\{ Q^{\alpha\beta\lambda\mu}\gamma_{\lambda\mu}(\mathbf{u})\gamma_{\alpha\beta}(\mathbf{u}) + 2\xi^3 Q^{\alpha\beta\lambda\mu}\chi_{\lambda\mu}(\mathbf{u}, \mathbf{s})\gamma_{\alpha\beta}(\mathbf{u}) \right. \\ &\quad \left. + (\xi^3)^2 Q^{\alpha\beta\lambda\mu}\chi_{\lambda\mu}(\mathbf{u}, \mathbf{s})\chi_{\alpha\beta}(\mathbf{u}, \mathbf{s}) + 4E^{\alpha 3\beta 3}\gamma_{\beta 3}(\mathbf{u}, \mathbf{s})\gamma_{\alpha 3}(\mathbf{u}, \mathbf{s}) \right\} \sqrt{ad}S d\xi^3, \end{aligned} \quad (2.31)$$

---

<sup>a</sup>In addition to (2.28), in the Koiter's model, the transverse strain is assumed to be zero,  $\epsilon_{\alpha 3} = 0$ .

where  $dS$  is the element area on the parametric domain of the shell.

We have, after a through-the-thickness integration

$$E_d(\mathbf{u}, \mathbf{s}) \simeq \frac{1}{2} \int_{\omega} t \{ Q^{\alpha\beta\lambda\mu} \gamma_{\alpha\beta}(\mathbf{u}) \gamma_{\alpha\beta}(\mathbf{v}) + \frac{t^2}{12} \chi_{\lambda\mu}(\mathbf{u}, \mathbf{s}) \chi_{\alpha\beta}(\mathbf{u}, \mathbf{r}) + 4E^{\alpha^3\beta^3} \gamma_{\beta^3}(\mathbf{u}, \mathbf{s}) \gamma_{\alpha^3}(\mathbf{v}, \mathbf{r}) \} \sqrt{ad} dS. \quad (2.32)$$

Let  $N^{\alpha\beta}$ ,  $M^{\alpha\beta}$ ,  $Q^{\alpha}$  respectively the resultant force, moment and shear force per unit of area, defined as

$$N^{\alpha\beta} = \int_{-\frac{t}{2}}^{\frac{t}{2}} \sigma^{\alpha\beta}(\mathbf{u}, \mathbf{s}) d\xi^3, \quad M^{\alpha\beta} = \int_{-\frac{t}{2}}^{\frac{t}{2}} \sigma^{\alpha\beta}(\mathbf{u}, \mathbf{s}) \xi^3 d\xi^3, \quad N^{\alpha^3} = \int_{-\frac{t}{2}}^{\frac{t}{2}} \sigma^{\alpha^3} d\xi^3. \quad (2.33)$$

Then, we finally obtain

$$N^{\alpha\beta} = tQ^{\alpha\beta\lambda\mu} \gamma_{\lambda\mu}(\mathbf{u}), \quad M^{\alpha\beta} = \frac{t^3}{12} Q^{\alpha\beta\lambda\mu} \chi_{\lambda\mu}(\mathbf{u}, \mathbf{s}), \quad N^{\alpha^3} = 2tE^{\alpha^3\beta^3} \gamma_{\beta^3}(\mathbf{u}, \mathbf{s}) \quad (2.34)$$

Now let us define the different parts of the strain energy:

- The bending strain energy, denote with a superscript “b”:

$$E_d^b := \frac{1}{2} \int_{\omega} M^{\alpha\beta} \gamma_{\alpha\beta}(\mathbf{u}, \mathbf{s}) \sqrt{ad} dS.$$

- The shear-membrane (complementary to the bending) strain energy, denoted with a superscript “ $\bar{b}$ ”:

$$E_d^{\bar{b}} = \frac{1}{2} \int_{\omega} \{ N^{\alpha\beta} \gamma_{\alpha\beta}(\mathbf{u}, \mathbf{s}) + 2N^{\alpha^3} \gamma_{\alpha^3}(\mathbf{u}, \mathbf{s}) \} \sqrt{ad} dS.$$

#### 2.2.4 Naghdi's equation

Assume that the middle-surface is subjected to a load  $\mathbf{p} = p^i \mathbf{a}_i$  per element of area, a resultant force  $\mathbf{N} = N^i \mathbf{a}_i$ , a moment  $\mathbf{M} = \hat{e}_{\alpha\beta} M^{\alpha\beta} \mathbf{a}^{\alpha\beta}$  on  $\Gamma_1 := \Phi(\gamma_1)$ ,  $\gamma_1 \in \bar{\omega}$ . The middle-surface is assumed clamped at its boundary.

**PROBLEM 2.2.1** (Principle of virtual work) Let  $V(\omega)$  be an appropriated space of admissible displacement and rotation, with taking into account the boundary condition. The virtual work principle problem associated to the equilibrium problem is: Find  $[\mathbf{u}, \mathbf{s}] \in V(\omega)$  such that

$$a([\mathbf{u}, \mathbf{s}], [\mathbf{v}, \mathbf{r}]) = l([\mathbf{v}, \mathbf{r}]), \quad \text{for all } [\mathbf{v}, \mathbf{r}] \in V(\omega). \quad (2.35)$$

$l$  is the virtual work of the applied loads, defined as

$$l([\mathbf{v}, \mathbf{r}]) = \int_{\omega} p^i v_i \sqrt{ad} dS + \int_{\gamma} (N^i v_i + M^{\alpha} r_{\alpha}) dl \quad (2.36)$$

$dl$  being the element of length on  $\Phi(\gamma_1)$  and  $a(\cdot, \cdot)$  is the strain energy bilinear form

$$a([\mathbf{u}, \mathbf{s}], [\mathbf{v}, \mathbf{r}]) = \int_{\omega} t \{ Q^{\alpha\beta\lambda\mu} \gamma_{\lambda\mu}(\mathbf{u}) \gamma_{\alpha\beta}(\mathbf{v}) + \frac{t^2}{12} Q^{\alpha\beta\lambda\mu} \chi_{\lambda\mu}(\mathbf{u}, \mathbf{s}) \chi_{\alpha\beta}(\mathbf{v}, \mathbf{r}) + E^{\alpha^3\beta^3} \gamma_{\beta^3}(\mathbf{u}, \mathbf{s}) \gamma_{\alpha^3}(\mathbf{v}, \mathbf{r}) \} \sqrt{ad} dS. \quad (2.37)$$

In the previous problem, the bilinear form is associated to the stiffness of the shell. For eigenfrequency analysis one has to defined the bilinear form  $b$  associated to the virtual work associated to the acceleration loads. Let us denote by  $\rho$  the volume density of the shell. We have

$$b([\mathbf{u}, \mathbf{s}], [\mathbf{v}, \mathbf{r}]) = \int \rho \ddot{\mathbf{U}} \mathbf{V} dV$$

where  $\ddot{\mathbf{U}}$  is the acceleration associated to the displacement  $\mathbf{U}$ .

Setting up  $\mathbf{U} = e^{i\lambda t} \underline{\mathbf{U}}$ , with  $t$  the time parameter,  $\lambda$  and  $\mathbf{U}$  respectively the eigenvalue and the corresponding eigenvector, the bilinear form  $b$  is

$$b([\mathbf{u}, \mathbf{s}], [\mathbf{v}, \mathbf{r}]) = -\lambda^2 \int_{\Omega_t} \rho (u_i \mathbf{a}^i + \xi^3 s_\alpha \mathbf{a}^\alpha) (v_j \mathbf{a}^j + \xi^3 r_\beta \mathbf{a}^\beta) \sqrt{ad} S d\xi^3.$$

Taking into account of the fact that  $a^{3\alpha} = a_{\alpha 3} = 0$ ,  $a_{33} = 1$ ; one finally obtains after a throughout-the-thickness integration

$$b([\mathbf{u}, \mathbf{s}], [\mathbf{v}, \mathbf{r}]) \simeq -\lambda^2 \int_{\omega} \rho t \left( u_3 v_3 + a^{\alpha\beta} u_\alpha v_\beta + \frac{t^2}{12} a^{\alpha\beta} s_\alpha r_\beta \right) \sqrt{ad} S. \quad (2.38)$$

Throughout the following, we consider that the shell is unloaded and subjected to a clamping boundary conditions at  $\Gamma_0$

PROBLEM 2.2.2 (Dynamic variational equation) The variational problem is

$$\begin{aligned} \text{Find } [u_i, s_\alpha] \in [V(\omega)]^5, \lambda \in \mathbb{R} \text{ such that} \\ a([\mathbf{u}, \mathbf{s}], [\mathbf{v}, \mathbf{r}]) + b([\mathbf{u}, \mathbf{s}], [\mathbf{v}, \mathbf{r}]) = 0, \text{ for all } [v_i, r_\alpha] \in [V(\omega)]^5 \end{aligned}$$

## 2.3 On the existence results

In order to discuss existence results on the variational problem, we introduce the following Sobolev spaces.

### Sobolev spaces

We define the following Sobolev spaces which will be useful for discussion on the existence results of Naghdi's model.

Let us consider the bounded domain  $\omega \subset \mathbb{R}^2$ , and let  $d \geq 2$  be an integer; we denote by  $\mathbf{L}^2(\omega) := [L^2(\omega)]^d$  and  $\|\cdot\|_{0,\omega}$  the norm in the spaces  $L^2(\omega)$  and  $\mathbf{L}^2(\omega)$  defined as follows: Given  $w \in L^2(\omega)$  and  $\mathbf{w} := (w_i)_{i=1}^d \in \mathbf{L}^d(\omega)$

$$\|w\|_{0,\omega} := \left\{ \int_{\omega} |w|^2 dS \right\}^{1/2}, \text{ and } \|\mathbf{w}\|_{0,\omega} := \left\{ \sum_{i=1}^d \|w_i\|_{0,\omega}^2 \right\}^{1/2}.$$

Given an integer  $m \geq 1$ ,  $H^m(\omega)$  denotes the usual Sobolev space of  $L^2$ -integrable functions with derivatives of order  $\leq m$  also  $L^2$ -integrable. In particular, we consider

$$H^1(\omega) = \{w \in L^2(\omega), \text{ such that } \partial_\alpha w \in L^2(\omega)\}.$$

Let  $\gamma_0 \subset \partial\omega$  be a part of the boundary of positive length, the space  $H_0^1(\omega)$  of functions of  $H^1(\omega)$  vanishing on  $\gamma_0$  is

$$H_0^1(\omega) = \{v \in H^1(\omega), v = 0 \text{ on } \gamma_0\}. \quad (2.39)$$

Analogously to  $\mathbf{L}^2(\omega)$ , we define the space  $\mathbf{H}^1(\omega) := [H^1(\omega)]^d$

$$\mathbf{H}^1(\omega) = \{\mathbf{v} = (v_i)_{i=1}^d \text{ such that } v_i \in H^1(\omega)\}$$

and  $\|\cdot\|_{1,\omega}$  the associated norm defined as

$$\|\mathbf{v}\|_{1,\omega}^2 = \sum_{i=1}^d \|v_i\|_{1,\omega}^2,$$

and

$$\|w\|_{1,\omega}^2 = \|w\|_{0,\omega}^2 + \sum_{\alpha=1}^2 \|w_{,\alpha}\|_{0,\omega}^2. \quad (2.40)$$

After this brief definition of the functional spaces needed.

**THEOREM 2.3.1** *Assume that the plane and anti-plane parts  $Q^{\alpha\beta\lambda\mu}$  and  $E^{\alpha 3\beta 3}$  are such that: for any second order symmetric tensor  $\tau = (\tau_{ij})$  there are two positive constants  $C_q > 0$  and  $C_e > 0$  such that:*

$$Q^{\alpha\beta\lambda\mu} \tau_{\lambda\mu} \tau_{\alpha\beta} \geq C_q \sum_{\alpha\beta} |\tau_{\alpha\beta}|_{1,\omega}^2 \text{ and } E^{\alpha 3\beta 3} \tau_{\beta 3} \tau_{\alpha 3} \geq \sum_{\alpha=1}^2 |\tau_{\alpha 3}|_{1,\omega}^2. \quad (2.41)$$

Then

i) the bilinear form (2.37) is  $V(\omega)$ -elliptic, with  $V(\omega) = [H_0^1(\omega)]^5$

ii) for any applied loads  $\mathbf{p} \in \mathbf{L}^2(\omega)$ ,  $\mathbf{N} \in \mathbf{L}^2(\gamma_1)$  and  $\mathbf{M} \in \mathbf{L}^2(\gamma_1)$ , the problem 2.2.1 have a unique solution in  $[H_0^1(\omega)]^5$

*Sketch of the proof.* As the linear form in (2.36) is continuous on  $\mathbf{H}_0^1(\omega)$ , the claim ii) is a direct consequence of claim i) and of the following Lax-Milgram lemma:

**LEMMA 2.3.1** (Lax-Milgram lemma) *Let  $V$  be a Hilbert space. Assume that the bilinear form  $a : V \times V \rightarrow \mathbb{R}$  is continuous and elliptic, i. e there exists  $M, c > 0$  such that*

$$a(u, v) \leq M \|u\|_V \|v\|_V \text{ and } a(v, v) \geq c \|v\|_V^2. \quad (2.42)$$

*Assume that  $l(\cdot) : V \rightarrow \mathbb{R}$  is linear continuous, i.e there exists  $c_f > 0$  such that*

$$l(v) \leq c_f \|v\|_V, \text{ for all } v \in V.$$

*Then the variational equation*

$$a(u, v) = l(v), \quad \forall v \in V$$

*has a unique solution  $u \in V$ .*

## Chapter 2. Naghdi Shell Model

---

To complete the proof of theorem 2.3.1 it remains to prove *i*). To this end, let us introduce the space  $V_\epsilon(\omega)$

$$V_\epsilon(\omega) := \{[\mathbf{v}, \mathbf{r}] \in [L^2(\omega)]^5 \text{ such that } \gamma_{\alpha\beta}(\mathbf{v}) \in L^2(\omega) \chi_{\alpha\beta}(\mathbf{v}) \in L^2(\omega) \text{ and } \gamma_{\alpha 3}(\mathbf{v}) \in L^2(\omega)\}.$$

Then equipped with

- the semi-norm  $[\mathbf{v}, \mathbf{r}] \mapsto |\cdot|_{\epsilon, \omega}$

$$|\mathbf{r}, \mathbf{s}|_{\epsilon, \omega}^2 = \sum_{\alpha, \beta=1}^2 |\gamma_{\alpha\beta}|_{0, \omega}^2 + |\chi_{\alpha\beta}|_{0, \omega}^2 + \sum_{\alpha=1}^2 |\gamma_{\alpha 3}|_{0, \omega}^2.$$

- and the norm  $[\mathbf{v}, \mathbf{r}] \mapsto \|\cdot\|_{\epsilon, \omega}$

$$\|\mathbf{r}, \mathbf{s}\|_{\epsilon, \omega}^2 = \sum_{i=1}^3 \|v_i\|_{0, \omega}^2 + \sum_{\alpha=1}^2 \|s_\alpha\|_{0, \omega}^2 + |\mathbf{v}, \mathbf{r}|_{0, \omega}^2$$

the space  $V_\epsilon(\omega)$  is an Hilbert space which obviously contains  $\mathbf{H}_0^1(\omega)$ .

Hypothesis (2.41) implies that there exists a constant  $C > 0$  such that

$$a([\mathbf{v}, \mathbf{r}], [\mathbf{v}, \mathbf{r}]) \geq C|\mathbf{v}, \mathbf{r}|_{1, \omega}^2$$

and the remaining of the demonstration consists to prove that:

a) The norms  $\|\cdot\|_{\epsilon, \omega}$  and  $\|\cdot\|_{1, \omega}$  are equivalent over the space  $\mathbf{H}^1(\omega)$ .

b) The semi-norm  $|\cdot|_{\epsilon, \omega}$  is actually equivalent to the norm  $\|\cdot\|_{\epsilon, \omega}$  over the space  $\mathbf{H}_0^1(\omega)$ .

Points a) and b) proves that the bilinear form is  $\mathbf{H}_1^0(\omega)$  elliptic.

Point a) is consequence of the following Korn's inequality given and proved in Ciarlet [25] and [10], [9]

LEMMA 2.3.2 (Korn's inequality) *There exists a constant  $C > 0$  such that*

$$\|(\mathbf{v}, \mathbf{r})\|_{\epsilon, \omega} \geq C\|(\mathbf{v}, \mathbf{r})\|_{1, \omega}, \text{ for all } (\mathbf{v}, \mathbf{r}) \in V_\epsilon(\omega)$$

Hence  $\|\cdot\|_{1, \omega}$  and  $\|\cdot\|_{\epsilon, \omega}$  are equivalent over the space  $V_\epsilon(\omega)$ .

Arguing by contradiction, we can see that if point b) were false, we could find a point  $(\mathbf{v}, \mathbf{r}) \in V_\epsilon(\omega)$  such that  $\|\mathbf{v}, \mathbf{r}\|_1 = 1$  and  $\|\mathbf{v}, \mathbf{r}\|_{\epsilon, \omega} = 0$ . The following lemma 2.3.3 proves that  $\mathbf{v}, \mathbf{r}$  is necessary of the form (2.43) and due to the boundary condition  $(\mathbf{v}, \mathbf{r}) = (0, 0)$ .

LEMMA 2.3.3 *Let  $(\mathbf{u}, \mathbf{s})$  be an element in the space  $\mathbf{H}^1(\omega)$  that satisfies*

$$\gamma_{\alpha\beta}(\mathbf{u}) = \chi_{\alpha\beta}(\mathbf{u}, \mathbf{s}) = \gamma_{\alpha 3}(\mathbf{u}, \mathbf{s}) = 0.$$

Then

- there exist two constant vectors  $\mathbf{c} \in \mathbb{R}^3, \mathbf{d} \in \mathbb{R}^3$  such that

$$u_i \mathbf{a}^i(\boldsymbol{\xi}) = \mathbf{c} + \mathbf{d} \wedge \Phi(\boldsymbol{\xi}), \text{ with } \mathbf{d} = \epsilon^{\alpha\lambda} \beta_\alpha \mathbf{a}_\lambda + \frac{1}{2} \epsilon^{\lambda\alpha} u_{\alpha|\lambda} \mathbf{a}_3. \quad (2.43)$$

- Moreover  $u_i = \beta_\alpha = 0$  if the following boundary conditions are satisfied

$$u_i = \beta_\alpha = 0 \text{ on } \gamma_0 \subset \partial\omega, \text{ length } \gamma_0 > 0.$$

□

## 2.4 Synthesis

We have recalled in this chapter the Naghdi's shell model used for the structural analysis. To do so, we have introduced the essential of differential geometry which allows to define a mechanical problem parameterized by the shape. This bi-dimensional model describes mainly the average mechanical behaviour of the three-dimensional shell, namely the one of its middle-surface. However this model is only valid for shell defined by a single regular mapping. The focus of the next chapter is the definition of problem involving an assembling of shells.





# Naghdi shell junctions with Nonconforming Discretization

---

## Contents

---

<b>3.1</b>	<b>General equations for an assembling of shells . . . . .</b>	<b>32</b>
3.1.1	Geometric decomposition aspects . . . . .	32
3.1.2	Junction conditions . . . . .	35
3.1.3	General mechanical problem . . . . .	36
3.1.3.1	General equilibrium problem . . . . .	36
3.1.3.2	The state equation . . . . .	36
<b>3.2</b>	<b>Finite element space - Mortar method for shell . . . . .</b>	<b>39</b>
3.2.1	Discrete problem . . . . .	39
3.2.1.1	Discrete space . . . . .	40
3.2.1.2	Discrete form of shells assembling problem . . . . .	41
3.2.2	Mortar principle on an abstract problem . . . . .	42
3.2.3	Mortar method implementation for shell junction . . . . .	46
3.2.4	Finite elements implementation . . . . .	48
3.2.4.1	Matrix form of the variational problem . . . . .	48
3.2.4.2	Local discretization . . . . .	50
3.2.4.3	$P_2$ Lagrange interpolation . . . . .	51
<b>3.3</b>	<b>Numerical results . . . . .</b>	<b>52</b>
3.3.1	Vibration frequencies of a plate . . . . .	53
3.3.2	Vibration frequencies of a 3D L-plate . . . . .	57
3.3.3	Frequency analysis of a cylindrical shell . . . . .	60
3.3.4	Rectangular plate under pointwise load . . . . .	61
<b>3.4</b>	<b>Synthesis . . . . .</b>	<b>66</b>

---

## Introduction

Real-life structures met in engineering are commonly heterogeneous structures. This heterogeneity can be structural or geometric. The structural heterogeneity holds when different materials and kind of structures, such as beams, plates, shells, rods, are joined together. The latter comes

from the geometry features, and concerns structures which are defined by a collection of non-overlapping smooth regular sub-structures, joined together through physical interfaces. Then one needs to paid interest to the shell problem in a general geometric decomposition case.

Valuable interest has been devoted to the subject in [48] for plates. The analysis has latter been extended to shells having general shapes [46, 47]. The considered model in these papers is Koiter's. We also mention the work of [43] which has considered the junction between moderately thick shells using a nonconforming finite element. The finite element used is the DKT (Discrete Kirchoff-Triangle) element which allows to enforce the Kirchoff constraints, i.e vanishing of the transverse-shear deformation, at some given points while keep using a  $C^0$  finite element approximation. In [43], the author has used the mortar technique for the construction of the discrete space corresponding to the finite element analysis. We can notice the existence, in the literature, of a formulation of the Naghdi's shell model in Cartesian coordinates [16, 17]. In this formulation, the unknowns are described in Cartesian coordinates instead of local covariant basis. The interest of this formulation is that it is valid for shell with curvature discontinuities. Similar formulation also exists for Koiter model [15]. Reader interested may refer to [18] for the finite element concerns with this formulation in the case of Naghdi's model.

We consider in this chapter the junction between general shells using the Naghdi shell models. In the first part of the chapter, we set the frame of geometric decomposition for shell and the related notations. Further we define the variational problem corresponding to an assembling of shells. This problem is defined from the standard problem described in the previous chapter and taking into account for the continuity of the displacement and rotation. We consider in the remaining of the chapter the finite element aspects and end with some numerical results. The key point in the finite element section is the construction of the discrete space based on a mortar method.

### 3.1 General equations for an assembling of shells

In this section, we focus on the variational problem of generally assembled structures. We start by specifying the geometric decomposition, notations, the junction conditions and the mechanical problem.

#### 3.1.1 Geometric decomposition aspects

Let us suppose that the middle-surface  $\Omega$  is decomposed into  $N$  disjoints non-overlapping regular middle-surfaces ( $\Omega_k$ ) which are defined through a set of bounded parametric domains  $\omega_k \subset \mathbb{R}^2$  and regular mappings  $\Phi_k \in C^2(\omega_k; \mathbb{R}^3)$ :  $\Omega$  is piecewise "regular" and defined by a collection of mappings  $\Phi = (\Phi_k)_{k=1:N}$ , and a product of the parametric domains

$$\omega = \prod_{k=1}^N \omega_k.$$

For the sake of clarity, we use the same curvilinear coordinates notation for the different domains as much as possible; while they should be denoted  $(\xi_{(k)}, \xi_{(k)}^3)$ . Also, for the sake of simplicity, we

### 3.1. General equations for an assembling of shells

suppose that the decomposition is conforming in the following sense: the common part between two middle-surfaces is either empty, a vertex or an entire interface.

$$\bar{\Omega} = \bigcup_{k=1}^N \bar{\Omega}_k, \text{ and } \hat{\Omega}_k \cap \hat{\Omega}_p = \emptyset \ \forall \ k \neq p. \quad (3.1)$$

Let  $\Gamma^l$  denote the interface between the two disjoint middle-surfaces of indexes  $n$  and  $m$ , i.e

$$\Gamma^l = \partial \bar{\Omega}_n \cap \bar{\Omega}_m. \quad (3.2)$$

In order to explicit the middle-surface indexes to which refer the interfaces, we denote  $\Gamma^l = \Gamma^{l(n)} = \Gamma^{l(m)}$ ; and  $\Gamma^{l(k)}$  designates the interface  $\Gamma^l$  view from the middle-surface  $\Omega_k$ . Conversely, the notation  $k(l)$  will refer to the fact that the middle-surface of index  $k$  has  $\Gamma^l$  in common with another middle-surface  $\Omega_{\bar{k}}$ ,  $\bar{k} \neq k$ .

We denote by  $\gamma^{l(k)} \subset \partial \omega_k$ ,  $k \in \{n, m\}$ , the parametric interface associated to  $\Gamma^{l(k)}$ . We also assume that both of the parametric interfaces  $\gamma^{l(k)}$  are defined as the images of a common parametric bounded interval  $\gamma^l$  through their respective bi-dimensional vector value mappings  $\varphi^{l(k)}$ :

$$\varphi_{l(k)} : \eta \in \gamma^l \subset \mathbb{R} \rightarrow \boldsymbol{\xi} = (\varphi_{l(k)}^1(\eta), \varphi_{l(k)}^2(\eta)) \in \gamma^{l(k)} \subset \mathbb{R}^2. \quad (3.3)$$

Thus, the different interfaces are defined as

$$\Gamma^{l(k)} = \left\{ P \in \mathbb{R}^3 \text{ such that } \mathbf{p} = \Phi_k(\varphi_{l(k)}(\eta)), \eta \in \gamma^l \right\}, \ k \in \{n, m\}. \quad (3.4)$$

Figure 3.1 shows an assembling of two shells and the chain of transformations which define the physical interfaces  $\Gamma^{l(k)}$ . Let  $ds_{l(k)}$  be the element of length on  $\Gamma^{l(k)}$  such that  $ds_{l(k)} = s_{l(k)}(\eta)d\eta$ . We have

$$s_{l(k)}^2(\eta) = \frac{\partial \varphi_{l(k)}^\alpha}{\partial \eta} \frac{\partial \varphi_{l(k)}^\beta}{\partial \eta} a_{\alpha\beta(k)}(\varphi_{l(k)}(\eta)), \ \eta \in \gamma^l$$

with  $a_{\alpha\beta(k)}$  the components of the metric tensor associated to  $\Omega_k$ .

**REMARK 3.1.1** For the sake of brevity, throughout the following, we omit the curvilinear coordinate  $\eta$  for the quantities of interface. For instance, we simply write  $a_{\alpha\beta(k)}$  instead of  $a_{\alpha\beta(k)}(\cot)$ . Also, we assume that the index  $l$  is used for interface index and range in  $\{1, \dots, L\}$  while  $k, n$  and  $m$  are used for middle-surface and range in  $\{1, \dots, N\}$ . Hence there is no Einstein summation on the lower and upper repeated indexes  $l, k, n$  and  $m$ .

The  $i$ -th component of the covariant (resp.  $j$ -th contravariant) vector of  $\Omega_k$  is noted  $\mathbf{a}_{i(k)}$  (resp.  $\mathbf{a}^{j(k)}$ ). The corresponding covariant and contravariant components of metric tensor are respectively denoted  $a_{ij(k)}$ ,  $a^{ij(k)}$ . Given two disjoint domains of indexes  $n$  and  $m$ , we denote  $a_{j(n)}^{i(m)} := \mathbf{a}^{i(m)} \cdot \mathbf{a}_{j(n)}$ .

The contravariant and covariant Levi-Civita symbols ( $e^{\alpha\beta(k)}$ ) and  $e_{\alpha\beta(k)}$ , associated to the

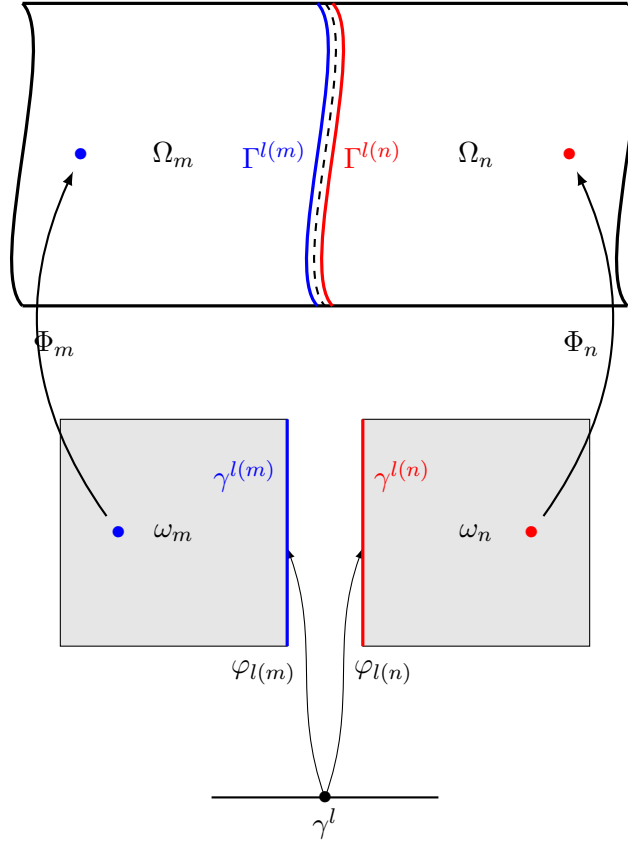


Figure 3.1 Illustration of an assembling of two shells, which are each defined as an image of their respective bi-dimensional domain. The parametric interfaces  $\gamma^{l(k)}$  are the images of a common interval  $\gamma^l$

shell of index  $k$ , are  $e^{\alpha\beta(k)} = \frac{1}{\sqrt{a_k}} \hat{e}^{\alpha\beta}$  and  $e_{\alpha\beta(k)} = \sqrt{a_k} \hat{e}_{\alpha\beta}$ ;  $a_k$  being the element of area,  $a_k = a_{11(k)}a_{22(k)} - a_{12(k)}^2$ . We equip the different interfaces with their unit tangent vector  $\mathbf{t}_{l(k)}$

$$\mathbf{t}_{l(k)} = t_{l(k)}^\alpha \mathbf{a}_{\alpha(k)}.$$

The contravariant components of the unit tangent vector  $t_{l(k)}^\alpha = \frac{\partial \varphi_{l(k)}^\alpha}{\partial \eta} / s_{l(k)}$  are defined conveniently in order to have a consistently oriented global middle-surface  $\Omega$ . The covariant components of the tangent vector are

$$t_\alpha^{l(k)} = a_{\alpha\beta(k)} t_{l(k)}^\beta.$$

Given a boundary  $\Gamma_b \subset \partial\Omega$ , of label “ $b$ ”, we denote  $\mathcal{I}_b$  the following set of indexes

$$\mathcal{I}_b = \{k \in \{1, \dots, N\}, \text{ such } \partial\bar{\Omega}_k \cap \Gamma_b \neq \emptyset\}.$$

For any index  $i \in \mathcal{I}_b$ , we define the parametric curvilinear domain  $\gamma_{b(i)}$

$$\gamma_{b(i)} = \{\boldsymbol{\xi} \in \partial\omega_i \text{ such that } \Phi_i(\boldsymbol{\xi}) \in \bar{\Gamma}_b\}$$

and  $l_{b(i)}$  the corresponding element of length on  $\Gamma_{b(i)} := \Phi(\gamma_{b(i)})$  such that  $\Gamma_b = \bigcup_{i \in \mathcal{I}_b} \Gamma_{b(i)}$ .

### 3.1.2 Junction conditions

Let  $u_{i(k)}$  and  $s_{\alpha(k)}$  be respectively the covariant components of displacement and rotation associated to  $\Omega_k$ . Let  $\mathbf{u}^{(k)} := (u_{i(k)})$ ,  $\mathbf{s}^{(k)} := (s_{\alpha(k)})$  be their corresponding covariant components vectors. The Cartesian displacement vector of  $\Omega_k$  is  $\mathbf{u}^{(k)} = u_{i(k)}\mathbf{a}^{i(k)}$ . Let  $\Psi^{(k)}(\cdot, \cdot)$  denote the Cartesian rotation vector of  $\mathbf{a}_{3(k)}$

$$\Psi^{(k)}(\mathbf{u}, \mathbf{s}) = e^{\alpha\lambda(k)} s_{\alpha(k)} \mathbf{a}_{\lambda(k)} + \frac{1}{2} e^{\alpha\lambda(k)} u_{\lambda(k)|\alpha} \mathbf{a}_{3(k)} \quad (\text{no summation over } k).$$

We suppose that the thickness is constant all over the shell structure. The Cartesian displacement vector  $\mathbf{U}^{(k)}$  associated to a particle located at  $\Phi_k(\boldsymbol{\xi}) + \xi^3 \mathbf{a}_{3(k)}$

$$\mathbf{U}^{(k)} = \mathbf{u}^{(k)} + \xi^3 \mathbf{a}_{3(k)} \times \Psi^{(k)}(\mathbf{u}, \mathbf{s}), \quad \xi^3 \in \left[-\frac{t}{2}, \frac{t}{2}\right].$$

In this present framework of assembling of shells,  $\mathbf{u}$  and  $\mathbf{s}$  designate respectively the covariant components vectors of the displacement and rotation all over the middle-surface  $\Omega$  such that

$$\mathbf{u} := (\mathbf{u}_1, \mathbf{u}_2, \mathbf{u}_3) \in [\mathbf{H}^1(\boldsymbol{\omega})]^3 \quad \text{and} \quad \mathbf{s} := (\mathbf{s}_1, \mathbf{s}_2) \in [\mathbf{H}^1(\boldsymbol{\omega})]^2, \quad (3.5)$$

where

$$\mathbf{H}^1(\boldsymbol{\omega}) := \prod_{k=1}^N H^1(\omega_k) = \{\mathbf{w} := (w_{(k)})_{k=1:N}, \text{ such that } w_{(k)} \in H^1(\omega_k)\}. \quad (3.6)$$

Given a covariant field  $w \in \mathbf{H}^1(\boldsymbol{\omega})$ ,  $w^{l(k)} := w_{(k)|\gamma^{l(k)}}$  denotes the restriction of  $w$  to the parametric interface  $\gamma^{l(k)}$ . We note respectively  $\mathbf{u}^{l(k)}$  and  $\Psi^{l(k)}$  the restrictions of the Cartesian vectors of displacement  $\mathbf{u}^{(k)}$  and rotation  $\Psi^{(k)}$  to the interface  $\Gamma^{l(k)}$

$$\mathbf{u}^{l(k)} = u_i^{l(k)} \mathbf{a}^{i(k)} \quad \text{and} \quad \Psi^{l(k)}(\mathbf{u}, \mathbf{s}) = e^{\alpha\lambda(k)} s_{\alpha}^{l(k)} \mathbf{a}_{\lambda(k)} + \frac{1}{2} e^{\alpha\lambda(k)} u_{\lambda|\alpha}^{l(k)} \mathbf{a}_{3(k)}. \quad (3.7)$$

The junction conditions are basically the following [9]:

$$\mathbf{u}^{l(n)} = \mathbf{u}^{l(m)} \quad \text{and} \quad \Psi^{l(n)} \cdot \mathbf{t}_{l(n)} = \Psi^{l(m)} \cdot \mathbf{t}_{l(n)}, \quad \text{for all } l \in \{1, \dots, L\}. \quad (3.8)$$

The former corresponds to the continuity of the displacement of the middle-surface  $\Omega$  and the latter to the continuity of the tangential rotation along the different interfaces. We emphasize that the relations in Eq. (3.8) are on vectors in Cartesian coordinates. The displacement equality entails componentwise

$$u_i^{l(n)} = a_{i(n)}^{j(m)} u_j^{l(m)}.$$

These continuity conditions on the displacement and rotation are respectively due to the transmission of the internal forces and moments at the interface. The equality of displacements appears natural while the only continuity condition on the tangential component of rotation is due to the plane moment assumption used in shell model.

### 3.1.3 General mechanical problem

In this section, we define the global mechanical problem (virtual work principle). We start by defining the equilibrium problem which corresponds to the minimization of the energy functional under the continuity constraints of the displacement fields.

#### 3.1.3.1 General equilibrium problem

Now, we consider the equilibrium problem of the middle-surface  $\Omega$ . The energy of the assembled shells is defined as

$$J(\mathbf{u}, \mathbf{s}) = \frac{1}{2}a([\mathbf{u}, \mathbf{s}], [\mathbf{u}, \mathbf{s}]) - l([\mathbf{u}, \mathbf{s}]),$$

where  $a$  is the bilinear form defined as  $a : [\mathbf{H}^1(\boldsymbol{\omega})]^5 \times [\mathbf{H}^1(\boldsymbol{\omega})]^5 \rightarrow \mathbb{R}$

$$a([\mathbf{u}, \mathbf{s}], [\mathbf{u}, \mathbf{s}]) = \sum_{k=1}^N a_{(k)}([\mathbf{u}_{(k)}, \mathbf{s}_{(k)}], [\mathbf{u}_{(k)}, \mathbf{s}_{(k)}])$$

and  $l : [\mathbf{H}^1(\boldsymbol{\omega})]^5 \rightarrow \mathbb{R}$  is the linear form of potential energy of the applied loads

$$l([\mathbf{u}, \mathbf{s}]) = \sum_{k=1}^N l_{(k)}([\mathbf{u}_{(k)}, \mathbf{s}_{(k)}]).$$

$a_{(k)}$  and  $l_{(k)}$  are respectively the strain energy bilinear form and the linear form associated to the  $\Omega_k$ . In the case of assembled shells,  $[\mathbf{u}, \mathbf{s}]$  is solution of the minimization problem of  $J(\cdot)$  subjected to the continuity constraints across the interfaces. Let  $\mathbf{V}_b(\boldsymbol{\omega})$  and  $\mathbf{V}_j(\boldsymbol{\omega})$  be two subsets of  $[\mathbf{H}^1(\boldsymbol{\omega})]^5$ .  $\mathbf{V}_b(\boldsymbol{\omega})$  is the space with the essential boundary conditions on a part of  $\partial\Omega$  and  $\mathbf{V}_j(\boldsymbol{\omega})$  is the space with the junction conditions (3.8). The generic form of the variational problem corresponding to the minimization problem is the following

PROBLEM 3.1.1 Find  $[\mathbf{u}, \mathbf{s}] \in \mathbf{V}(\boldsymbol{\omega}) := \mathbf{V}_b(\boldsymbol{\omega}) \cap \mathbf{V}_j(\boldsymbol{\omega})$  such that:

$$a([\mathbf{u}, \mathbf{s}], [\mathbf{v}, \mathbf{r}]) = l([\mathbf{v}, \mathbf{r}]), \quad \forall [\mathbf{v}, \mathbf{r}] \in \mathbf{V}(\boldsymbol{\omega})$$

#### 3.1.3.2 The state equation

We start by specifying the loads acting on  $\Omega$ . Let consider that  $\Omega$  is subjected to applied resultant force and moment at its boundary  $\Gamma_1 \subset \partial\Omega$ . Without loss of generality, consider that the middle-surface undergoes the following system loads

- each  $\Omega_k$  is submitted to a surface load  $\mathbf{p}_k$
- a resultant force and moment  $\mathbf{N}_k$  and  $\mathbf{M}_k$  on  $\Gamma_{1(k)}$ ,  $k \in \mathcal{I}_1$
- clamping boundary condition at  $\Gamma_{0(k)}$ ,  $k \in \mathcal{I}_0$ .

We introduce the space

$$\mathbf{H}_0^1(\omega) = \{ \mathbf{v} \in \mathbf{H}^1(\omega) \text{ such that } v_{0(k)} = 0 \text{ on } \gamma_{0(k)}, k \in \mathcal{I}_0 \}$$

and consider the following product space with boundary conditions

$$\mathbf{V}(\omega) = \{ [\mathbf{v}, \mathbf{r}] \in [\mathbf{H}_0^1(\omega)]^5 \text{ such that (3.8) holds} \}. \quad (3.9)$$

Let  $[\mathbf{v}, \mathbf{r}]$  be the components of an admissible virtual displacement (defined as in 3.5), the corresponding virtual work of applied loads is:

$$l([\mathbf{v}, \mathbf{r}]) = \sum_{k=1}^N \int_{\omega_k} \mathbf{p}_k \cdot \mathbf{v}^{(k)} \sqrt{a_k} d\xi + \sum_{k \in I_1} \int_{\gamma_{1(k)}} \left( \mathbf{N}_k \cdot \mathbf{v}^{(k)} + \mathbf{M}_k \cdot \Psi^{(k)}(\mathbf{v}^{(k)}, \mathbf{r}^{(k)}) \right) dl_{1(k)} \quad (3.10)$$

The variational formulation is:

PROBLEM 3.1.2 Find  $[\mathbf{u}, \mathbf{s}] \in \mathbf{V}(\omega)$  such that:

$$a([\mathbf{u}, \mathbf{s}], [\mathbf{v}, \mathbf{r}]) = l([\mathbf{v}, \mathbf{r}]), \quad \forall [\mathbf{v}, \mathbf{r}] \in \mathbf{V}(\omega)$$

where

$$a([\mathbf{u}, \mathbf{s}], [\mathbf{v}, \mathbf{r}]) = \sum_{k=1}^N a_{(k)}([\mathbf{u}^{(k)}, \mathbf{s}^{(k)}], [\mathbf{v}^{(k)}, \mathbf{r}^{(k)}]).$$

The bilinear form  $a_{(k)}(\cdot, \cdot)$  is defined analogously to (2.37)

$$\begin{aligned} a_{(k)}([\mathbf{u}^{(k)}, \mathbf{s}^{(k)}], [\mathbf{v}^{(k)}, \mathbf{r}^{(k)}]) &= \int_{\omega_k} t \{ Q^{\alpha\beta\lambda\mu(k)} \gamma_{\lambda\mu}(\mathbf{v}^{(k)}) \gamma_{\alpha\beta}(\mathbf{u}^{(k)}) + \\ &\quad \frac{t^2}{12} Q^{\alpha\beta\lambda\mu(k)} \chi_{\lambda\mu}(\mathbf{v}^{(k)}, \mathbf{r}^{(k)}) \chi_{\alpha\beta}(\mathbf{u}^{(k)}, \mathbf{s}^{(k)}) + \\ &\quad E^{\alpha\beta\gamma\delta(k)} \gamma_{\beta\gamma}(\mathbf{v}^{(k)}, \mathbf{r}^{(k)}) \gamma_{\alpha\delta}(\mathbf{u}^{(k)}, \mathbf{s}^{(k)}) \} \sqrt{a_k} dS_k. \end{aligned} \quad (3.11)$$

where  $\mathbb{Q}^{(k)} = (Q^{\alpha\beta\lambda\mu(k)})$ ,  $\mathbf{E}^{(k)} = (E^{\alpha\beta\gamma\delta(k)})$  and  $dS_k$  are respectively the reduced plane, the anti-plane parts of the elastic tensor of the constitutive material associated to  $\Omega_k$  and the element of area aver  $\omega_k$ . We, analogously to  $a_{(k)}(\cdot, \cdot)$ , define the linear form associated to  $\Omega_k$  as

$$l_{(k)}([\mathbf{v}, \mathbf{r}]) = \int_{\omega_k} \mathbf{p}_k \cdot \mathbf{v}^{(k)} \sqrt{a_k} d\xi + \mathbb{1}_{k \in I_1} \int_{\gamma_{1(k)}} \left( \mathbf{N}_k \cdot \mathbf{v}^{(k)} d l_{1(k)} + \mathbf{M}_k \cdot \Psi^{(k)}(\mathbf{v}^{(k)}, \mathbf{r}^{(k)}) \right) d l_{1(k)}$$

with  $\mathbb{1}$  the usual indicator function.

For the subsequent, let us equip the space  $[\mathbf{H}^1(\omega)]^5$  with its corresponding broken norm and semi-norm, respectively denoted  $\|\cdot\|_{1,\omega}$  and  $|\cdot|_{1,\omega}$ : for  $[\mathbf{v}, \mathbf{r}] \in [\mathbf{H}^1(\omega)]^5$

$$\|\mathbf{v}, \mathbf{r}\|_{1,\omega}^2 := \sum_{k=1}^N \|\mathbf{v}^{(k)}, \mathbf{r}^{(k)}\|_{1,\omega_k}^2, \quad \text{and} \quad |\mathbf{v}, \mathbf{r}|_{1,\omega}^2 := \sum_{k=1}^N |\mathbf{v}^{(k)}, \mathbf{r}^{(k)}|_{1,\omega_k}^2.$$



### Chapter 3. Naghdi shell junctions with Nonconforming Discretization

**THEOREM 3.1.1** *Assume for any  $k \in \{1, \dots, N\}$  that  $Q^{\alpha\beta\lambda\mu(k)}$  and  $E^{\alpha\beta\gamma\delta(k)}$  are such that: for any second order symmetric tensor  $\tau = (\tau_{ij})$  there exist two positive constants  $C_q > 0$  and  $C_e > 0$  such that:*

$$Q^{\alpha\beta\lambda\mu(k)}\tau_{\lambda\mu}\tau_{\alpha\beta} \geq C_q \sum_{\alpha,\beta=1}^2 |\tau_{\alpha\beta}|_{1,\omega}^2 \quad \text{and} \quad E^{\alpha\beta\gamma\delta(k)}\tau_{\beta\gamma}\tau_{\alpha\delta} \geq C_e \sum_{\alpha=1}^2 |\tau_{\alpha 3}|_{1,\omega}^2. \quad (3.12)$$

Then

- i) the bilinear form (3.11) is  $\mathbf{V}(\omega)$ -elliptic
- ii) for any applied loads system such that  $\mathbf{p}_k \in \mathbf{L}^2(\omega_k)$ ,  $\mathbf{N}_k \in \mathbf{L}^2(\gamma_{1(k)})$  and  $\mathbf{M}_k \in \mathbf{L}^2(\gamma_{1(k)})$  for any  $k \in \{1, \dots, N\}$ , the Problem 3.1.2 has a unique solution in  $\mathbf{V}(\omega)$ .

The proof stands on the same Lax-Milgram lemma 2.3.1 in page 27 as in the case of mono-shell problem. The clue point for the well-posedness remains the demonstration that the bilinear form  $a(\cdot, \cdot)$  is  $\mathbf{V}(\omega)$ -elliptic and follows the same line as in the case of shell defined through a single injective immersion.

In the present case, one defines, in analogous manner to the mono-shell case, a product space

$\mathbf{V}_\epsilon(\omega) = \prod_{k=1}^N V_\epsilon(\omega_k)$  equipped with its norm and semi-norm respectively denoted by  $\|\cdot\|_{\epsilon,\omega}$  and  $|\cdot|_{\epsilon,\omega}$

$$\|\mathbf{v}, \mathbf{r}\|_{\epsilon,\omega}^2 := \sum_{k=1}^N \|\mathbf{v}^{(k)}, \mathbf{r}^{(k)}\|_{\epsilon,\omega_k}^2, \quad \text{and} \quad |\mathbf{v}, \mathbf{r}|_{\epsilon,\omega}^2 := \sum_{k=1}^N |\mathbf{v}^{(k)}, \mathbf{r}^{(k)}|_{\epsilon,\omega_k}^2;$$

and proves that

- the broken  $H^1$ -norm  $\|\cdot\|_{1,\omega}$  over the space  $\mathbf{H}^1(\omega)$  and the norm  $\|\cdot\|_{\epsilon,\omega}$  are equivalent.
- the semi-norm  $|\cdot|_{\epsilon,\omega}$  is a norm over the space  $[\mathbf{H}_0^1(\omega)]^5$  and is equivalent to the norm  $\|\cdot\|_{1,\omega}$ .

As in the mono-shell case, the infinitesimal displacement lemma and the boundary condition plays a key role in order to have  $a([\mathbf{v}, \mathbf{r}], [\mathbf{v}, \mathbf{r}]) = 0 \implies v_{i(k)} = r_{\alpha(k)} = 0$  for all  $k \in \mathcal{I}_0$  and thanks to the continuity conditions  $v_{i(k)} = r_{\alpha(k)} = 0$  for all  $k \in \{1, \dots, N\}$ .

Now, we focus on the resolution of the global problem using finite element method. We use the mortar method to solve the Problem (3.1.2). The mortar method [11] is based on the fact that the continuity conditions are handled weakly in the equations (3.13),(3.14). Indeed, the conditions are defined in an integral sense, and satisfied against some test functions.

- The first condition in (3.8) is a vector equality which componentwise in an integral sense is

$$\int_{\gamma^l} (u_i^{l(n)} s_{l(n)} - a_{i(n)}^{j(m)} u_j^{l(m)} s_{l(m)}) f \, d\eta = 0, \quad \forall f \in L^2(\gamma^l) \quad i \in \{1, 2, 3\}. \quad (3.13)$$

- In the same manner, the equality of the tangential component of the rotation is

$$\int_{\gamma^l} \left( \Psi_t^{l(n)}(\mathbf{s})s_{l(n)} - \Psi_t^{l(m)}(\mathbf{s})s_{l(m)} \right) f \, d\eta = 0, \quad \forall f \in L^2(\gamma^l), \quad (3.14)$$

where the tangential rotation is noted  $\Psi_t^{l(k)}(\cdot)$  at the interface  $\Gamma^{l(k)}$  and defined as

$$\Psi_t^{l(k)}(\mathbf{s}) = \frac{1}{\sqrt{a_k}} (s_1^{l(k)} t_2^{l(k)} - s_2^{l(k)} t_1^{l(k)}).$$

In the next section we discuss the mortar aspect and the implementation. The key point resides in the appropriate choice of the test functions against which the constraints are stated in (3.13), (3.14).

## 3.2 Finite element space - Mortar method for shell

The mortar method has been originally developed to couple different nonconforming discretizations such as spectral and finite element methods in order to take advantage of both methods. Generally, spectral approximation is well adapted for regular solutions and finite element approximation is used for problems with complex geometries. Different applications have shown that the framework of application of this method is very large and is not only limited to the preconceived idea of spectral and finite element coupling only. The mortar method has further been extended to different finite element elements discretization coupling. The crucial point of the discretization is the construction of the discrete space: the problems on each subdomain are discretized using independent finite dimensional spaces, and the mortar is defined on the interfaces between the subdomains to enforce the transfer or matching conditions. The method is nonconforming because the discrete space is not included in the exact one. The interest of using the mortar method is that the meshes and finite element discretizations can be generated and performed independently, i.e locally to each middle-surface.

The key point of the mortar method is the construction of the discrete space at the interfaces. In the case of Naghdi shell model which is a second-order elliptic partial differential equations, discretized using  $C^0$ -finite element, we use the standard mortar discretization as described in [8]. In fact the mortar principle does not depend on the operator of the partial differential equations of the physics. We emphasize that the mortar technique has been used in the framework of isogeometric analysis in [19]. Reader interested may refer to [74]-chapter 1- for a general overview on the method.

### 3.2.1 Discrete problem

In order to define the discrete problem, we first introduce the triangulation of numerical simulation with aim at defining first the discrete space.

We consider that the domains  $\omega_k$  are polygonal such that they can perfectly be covered with some meshes of triangulation  $\omega_{h(k)}$ ,

$$\omega_{h(k)} = \bigcup_{i=1}^{N_k} T_{i(k)}, \quad T_{i(k)} \text{ being the element of index } i \text{ of the mesh } \omega_{h(k)}.$$

Let  $h_k$  be a mesh diameter associated to  $\omega_{h(k)}$  defined as

$$h_k = \max_i \text{diam} T_{i(k)}, \text{ diam being the diameter}$$

and  $h := \max_{k=1:N} h_k$  be the global mesh parameter.

The meshes are assumed regular in the following sense:

- the intersection of two distinct elements is either empty, a node or an entire common edge.
- considering  $\rho_k^i$  as the biggest inscribed circle's diameter in the element  $T_{i(k)}$ ; there exists  $\sigma > 0$  such that

$$\frac{\rho_k^i}{h_k} \geq \sigma > 0, \forall k \in \{1, \dots, N\}.$$

### 3.2.1.1 Discrete space

For simplicity, we assume that the displacement and rotation components are discretized using the same finite elements. Hence, let  $X_{h(k)}$  be the finite dimensional space corresponding to the discretization of  $u_{i(k)}$  and  $s_{\alpha(k)}$  on the subdomain  $\omega_k$ . Let us then note  $\mathbf{X}_{h(k)} := [X_{h(k)}]^5$  the discrete space associated to both of the displacement and rotation components, and  $\mathbf{X}_h$  the discrete space corresponding to the global problem without taking into account for the matching conditions. The main idea -see [61, 76]- for the discretization of the global problem consists in

extracting from the basis of  $\mathbf{X}_h = \prod_{k=1}^N \mathbf{X}_{h(k)}$  an independent basis for  $\mathbf{V}_h$ , the subspace of  $\mathbf{X}_h$

with the displacement and tangential rotation continuity conditions. To that end, we introduce, for each interface  $\Gamma^l$ ,  $\mathcal{W}(\gamma^l)$  a trace space defined on  $\gamma^l$  which inherits its discretization from one side of the interface  $\gamma^{l(k)}$ . In our case,  $X_{h(k)}$  is the space of continuous piecewise polynomial functions generally interpolated using classical Lagrange polynomials.

$$X_{h(k)} = \{v \in C^0(\omega_{h(k)}) \text{ such that } v|_T \in P_{d_k}(T) \text{ for all } T \in \omega_{h(k)}\}, \quad (3.15)$$

where  $P_{d_k}$  is the space of polynomials of degree  $d_k \geq 0$ . Let  $T^{l(k)}$  be the trace of the mesh associated to the parametric interface  $\gamma^{l(k)}$ . We assume that the space  $\mathcal{W}(\gamma^l)$  is defined using the non-mortar mesh trace as

$$\mathcal{W}(\gamma^l) = \{w \in C^0(\gamma^{l(n)}) \text{ such that } w \in P_{d_n}(e), \bar{e} \in T^{l(n)}\}. \quad (3.16)$$

In the above definition  $e$  is a segment of the trace mesh  $T^{l(n)}$ . On other words,  $\mathcal{W}(\gamma^l)$  is chosen as the trace space of the (Lagrange) test functions of  $X_{h(n)}$  and the junction conditions are then:  $\forall l \in \{1, \dots, L\}$

$$\int_{\gamma^l} (u_i^{l(n)} s_{l(n)} - a_{i(n)}^{j(m)} u_j^{l(m)} s_{l(m)}) f \, d\eta = 0, \forall f \in \mathcal{W}(\gamma^l), \text{ for } i \in \{1, 2, 3\} \quad (3.17)$$

$$\int_{\gamma^l} (\Psi_t^{l(n)}(\mathbf{r})_{s_{l(n)}} - \Psi_t^{l(m)}(\mathbf{r})_{s_{l(m)}}) f = 0, \forall f \in \mathcal{W}(\gamma^l). \quad (3.18)$$

Hence, the global space  $\mathbf{V}_h$  is defined as

$$\mathbf{V}_h = \{[\mathbf{v}, \mathbf{r}] \in \mathbf{X}_h \text{ such that (3.17) and (3.18) hold}\} \quad (3.19)$$

### 3.2.1.2 Discrete form of shells assembling problem

We now consider the definition of the discrete problem defined on the space  $\mathbf{V}_h$ . In the finite element framework, the solution of the discrete problem is distinguished from the one of the continuous problem with a subscript  $h$ , highlighting the approximation of the continuous solution and the dependence with respect to the geometry mesh and the discretization parameter.

PROBLEM 3.2.1 Let us still note  $[\mathbf{u}, \mathbf{s}]$  the discrete solution approximating the continuous solution of Problem 3.1.2. The discrete problem is:

Find  $[\mathbf{u}, \mathbf{s}] \in \mathbf{V}_h$  such that

$$a_h([\mathbf{u}, \mathbf{s}], [\mathbf{v}, \mathbf{r}]) = l_h([\mathbf{v}, \mathbf{r}]), \quad \forall [\mathbf{v}, \mathbf{r}] \in \mathbf{V}_h,$$

$a_h(\cdot, \cdot)$  and  $l_h(\cdot)$  are respectively the bilinear and linear forms written as the sum of integrals over  $\omega_{h(k)}$  and eventually with use of an appropriate integration quadrature.

$$a_h([\mathbf{u}, \mathbf{s}], [\mathbf{v}, \mathbf{r}]) = \sum_{k=1}^N a_{h(k)}([\mathbf{u}_{(k)}, \mathbf{s}_{(k)}], [\mathbf{v}_{(k)}, \mathbf{r}_{(k)}]) \quad \text{and} \quad l_h([\mathbf{v}, \mathbf{r}]) = \sum_{k=1}^N l_{h(k)}([\mathbf{v}_{(k)}, \mathbf{r}_{(k)}])$$

$$a_{h(k)}([\mathbf{u}_{(k)}, \mathbf{s}_{(k)}], [\mathbf{v}_{(k)}, \mathbf{r}_{(k)}]) = \sum_{p=1}^{N_k} \int_{T_p^{(k)}} \sum_{i=1}^{n_q} w_i a_{(k)}([\mathbf{u}_{(k)}(\boldsymbol{\xi}_i), \mathbf{s}_{(k)}(\boldsymbol{\xi}_i)], [\mathbf{v}_{(k)}(\boldsymbol{\xi}_i), \mathbf{r}_{(k)}(\boldsymbol{\xi}_i)]) \quad (3.20)$$

$\boldsymbol{\xi}_i$  and  $w_i$  are respectively the quadrature points and the associated weights; with  $n_q$  the number of quadrature points.

The discrete problem involves the choice of a discretization space for the unknown functions. In the classical finite element framework for  $C^0$  problem such as Naghdi's shell model, a Lagrange interpolation function is a common choice. In the case of mortar method the matching conditions have to be discretized and appropriate space has to be chosen.

The discretization of the general problem is made through the following steps:

- the different local problems (without considering the junctions conditions) are discretized independently as in the "conforming" case using their proper finite elements, which can be of different degrees. This step constitutes on the assembling of the system local to each domain, i.e  $a_{h(k)}([\mathbf{u}_{(k)}, \mathbf{s}_{(k)}], [\mathbf{v}_{(k)}, \mathbf{r}_{(k)}]) = l_{h(k)}(\mathbf{v}_{(k)}, \mathbf{r}_{(k)})$
- at a second step, the junction conditions are considered by using the shape functions of an appropriate space  $\mathcal{W}(\gamma^l)$ , against which the continuity is satisfied. We made the standard choice of  $\mathcal{W}(\gamma^l)$  as the trace space derived from the discrete space  $X_{h(n)}$  over the non-mortar side  $\Omega_{n(l)}$ . This step yields to a matrix form of the conditions (3.17) and (3.18)
- at a third step, one defines some degrees of freedom (at the interface) of the non-mortar side in terms of the (independent) degrees of freedom. The independent degrees of freedom can sometimes involves some non-mortar side degrees of freedom. This step yields to a local junction which defines some non-mortar degrees of freedom in terms of the independent degrees of freedom

- as a last step, one defines a global matrix which allows to take into account for the local junction conditions and defines the global Problem 3.2.1. The link between the initial degrees of freedom and the set of independent degrees of freedom is made through a global junction matrix which involves the local junction matrix.

REMARK 3.2.1 For the second step, we emphasize that the space  $\mathcal{W}(\gamma^l)$  can be set independently of the discretizations used on  $\Omega_{k(l)}$ ,  $k \in \{n, m\}$ . In fact its corresponding shape functions, defined on the interval  $\gamma^l$ , can be totally independent of the discretizations used on  $\Omega_{n(l)}$  and  $\Omega_{m(l)}$ . The only requirement is that the dimension of the space, i.e the number of spanning shape functions, must be of appropriate dimension in order to have a well-posed problem.

### 3.2.2 Mortar principle on an abstract problem

Let us consider the following abstract problem involving the domain decomposition with two domains:

PROBLEM 3.2.2 (Problem for description) Find  $\mathbf{w} = (w^{(1)}, \dots, w^{(N)}) \in H^1(\boldsymbol{\omega})$  such that:  $\forall k \in \{n, m\}$

$$\left| \begin{array}{l} b(w^{(k)}, v^{(k)}) = l(v^{(k)}) \\ w^{l(n)} = w^{l(m)} \end{array} \right., \quad \forall \mathbf{v} \in H^1(\boldsymbol{\omega}) \text{ such that } v^{l(n)} = v^{l(m)}, \quad (3.21)$$

where  $b$  and  $l$  are respectively the bilinear for and linear form of the basic problem.

We recall that the matching condition in integral form is

$$\int_{\gamma^l} (w^{l(n)} s_{l(n)} - w^{l(m)} s_{l(m)}) f = 0, \quad \forall f \in \mathcal{W}(\gamma^l). \quad (3.22)$$

#### Local interpolation

Let  $\boldsymbol{\xi}_i = (\xi_i^1, \xi_i^2)$  be the coordinates of the nodes of the triangulation  $\omega_{h(k)}$  and  $(p_i^{(k)})$  be the corresponding shape functions of  $X_{h(k)}$

$$X_{h(k)} := \text{span} \left\{ \left( p_i^{(k)} \right)_{i=1:N_k} \right\}.$$

Hence the interpolation of the restriction of  $w$  to  $\omega_k$  is

$$w^{(k)}(\boldsymbol{\xi}) = \sum_{i=1}^{d_k} w(\boldsymbol{\xi}_i) p_i^{(k)}(\boldsymbol{\xi})$$

$w_i^{(k)} = w(\boldsymbol{\xi}_i)$  are the degrees of freedom of the function and  $d_k$  is the number of degrees of freedom. The shape functions are assumed independent and satisfy the following unit partition and  $\delta$ -Kronecker properties:

$$\forall \boldsymbol{\xi} \in \omega_k, \quad \sum_{i=1}^{N_k} p_i^{(k)}(\boldsymbol{\xi}) = 1 \quad (3.23)$$

and

$$p_i^{(k)}(\boldsymbol{\xi}_j) = \delta_{ij}, \text{ for } \boldsymbol{\xi}_j \in \omega_{h(k)}. \quad (3.24)$$

We further introduce  $\underline{w}^{(k)} = \left( w_i^{(k)} \right)_{i=1:d_k}$ , the vector of degrees of freedom of the domain  $\omega_k$  and  $\underline{w}$ , the vector of degrees of freedom overall  $\omega$ .

### Construction of the junction

We introduce  $S_{l(k)}$  the set of indexes of degrees of freedom which are on the parametric interface  $\gamma^{l(k)}$

$$S_{l(k)} = \{i \in \{1, \dots, N_k\}, \text{ such that } \boldsymbol{\xi}_i \in \gamma^{l(k)}\}.$$

We define  $S_{0(k)}$  the complement of  $S_{l(k)}$ ,  $\forall l \in \{1, \dots, L\}$ , i.e the set of degrees of freedom which are considered as interior, in the sense that they are not on interface

$$S_{0(k)} = \{i \in \{1, \dots, N_k\}, \text{ such that } i \notin S_{l(k)}, \forall l \in \{1, \dots, L\}\}.$$

Let us note  $d_{l(k)} = \text{Card}(S_{l(k)})$  the number of degrees of freedom of  $w^{(k)}$  on the interface  $\gamma^{l(k)}$ . The dimension of the space  $\mathcal{W}(\gamma^l)$  can be at most equal to  $d_{l(n)}$ . The space  $\mathcal{W}(\gamma^l)$  of trace space associated to the discretization, inherited from the non-mortar side, is

$$\mathcal{W}(\gamma^l) = \{f \in C^0(\gamma^l) \text{ such that } f(\eta) = \sum_{j \in S_{l(n)}} f_j p_j^{(n)}(\boldsymbol{\xi}), \text{ with } \boldsymbol{\xi} = \varphi_{l(n)}(\eta), \eta \in \gamma^l\}. \quad (3.25)$$

Let us denote respectively by  $\underline{w}^{l(k)}$  the ‘‘trace of degrees of freedom’’ on  $T^{l(k)} \subset \gamma^{l(k)}$ ; and  $\underline{w}^{0(k)}$  the interior degrees of freedom of a function  $w^{(k)}$

$$\underline{w}^{l(k)} = \{w_i^{(k)}, \text{ such that } i \in S_{l(k)}\}, \quad (3.26)$$

$$\underline{w}^{0(k)} = \{w_i^{(k)}, \text{ such that } i \in S_{0(k)}\}. \quad (3.27)$$

Let us note  $\mathbf{B}^{(k)}$  and  $\mathbf{f}^{(k)}$  the matrix form of the bilinear and linear forms. The ‘‘discrete’’ form of the considered problem 3.2.2 is

PROBLEM 3.2.3 (Discrete form of the problem) Find  $\underline{w} \in \mathbb{R}^{N_1} \times \mathbb{R}^{N_2}$  such that

$$\left| \begin{array}{l} \underline{v}^{(k)\top} \mathbf{B}^{(k)} \underline{w}^{(k)} \\ w^{l(n)} \end{array} \right. = \underline{v}^{(k)\top} \mathbf{f}^{(k)}, \text{ such that } w^{l(m)}, \quad \forall \underline{v} \in \mathbb{R}^{d_n} \times \mathbb{R}^{d_m} \text{ such that } v^{l(n)} = v^{l(m)}. \quad (3.28)$$

where  $v^{l(k)} = \sum_{j \in S_{l(k)}} w_j^{(k)} p_{j|\gamma^{l(n)}}^{(k)}(\boldsymbol{\xi}), \boldsymbol{\xi} \in \gamma^{l(k)}$ .

The matrix form of the global problem without considering the matching condition is

$$\begin{bmatrix} \underline{v}^{(n)} & \underline{v}^{(m)} \end{bmatrix} \underbrace{\begin{bmatrix} \mathbf{B}^{(n)} \\ \mathbf{B}^{(m)} \end{bmatrix}}_{\mathbf{B}} \begin{bmatrix} \underline{w}^{(n)} \\ \underline{w}^{(m)} \end{bmatrix} = \begin{bmatrix} \underline{v}^{(n)} & \underline{v}^{(m)} \end{bmatrix} \underbrace{\begin{bmatrix} \mathbf{f}^{(n)} \\ \mathbf{f}^{(m)} \end{bmatrix}}_{\mathbf{f}}. \quad (3.29)$$

Our purpose subsequently is to define the global problem which enforces the matching condition in the matrix form associated to the general problem on the assembling of domains.

### Matrix form of the junction

Thanks to the independence of the shape functions  $(p_i^{(n)})_{i \in S_{l(n)}}$ , the continuity in integral sense (3.22), page 42 is satisfied if and only if

$$\int_{\gamma^l} (w^{l(n)}(\boldsymbol{\xi}_{(n)})_{S_{l(n)}}(\eta) - w^{l(m)}(\boldsymbol{\xi}_{(m)})_{S_{l(m)}}(\eta)) p_j^{(n)}(\varphi_{l(n)}(\eta)) = 0, \quad \forall j \in S_{l(n)}$$

where  $\boldsymbol{\xi}_{(k)}$  is the curvilinear coordinates associated to  $\Omega_k$ . In the previous equation we have  $\boldsymbol{\xi}_{(k)} = \varphi_{l(k)}(\eta)$  and the continuity  $\Phi_m(\boldsymbol{\xi}_{(m)}) = \Phi_n(\boldsymbol{\xi}_{(n)})$  for  $\eta \in \gamma^l$ .

The restriction  $w^{l(k)}$  of  $w^{(k)}$  to  $\gamma^{l(k)}$  is defined as

$$w^{l(k)}(\eta) = \sum_{i \in S_{l(k)}} w_i^{(k)} p_i^{(k)}(\varphi_{l(k)}(\eta)).$$

Thus the matrix form of (3.22) is

$$\mathbf{M}^{l(n)} \underline{w}^{l(n)} = \mathbf{M}^{l(m)} \underline{w}^{l(m)},$$

where  $\mathbf{M}^{l(k)}$  is the matrix of dimensions  $(d_{l(n)}, d_{l(k)})$ , of components

$$M_{\hat{i}\hat{j}}^{l(k)} = \int_{\gamma^l} p_i^{(n)}(\boldsymbol{\xi}_{(n)}) p_j^{(k)}(\boldsymbol{\xi}_{(k)})_{S_{l(k)}}(\eta) d\eta, \quad \hat{i} \in \{1, \dots, d_{l(n)}\}, \hat{j} \in \{1, \dots, d_{l(k)}\},$$

where  $i$  (resp  $j$ ) is the global numbering in  $S_{l(n)}$  (resp.  $S_{l(k)}$ ) corresponding to  $\hat{i} \in \{1, \dots, d_{l(n)}\}$  (resp  $\hat{j} \in \{1, \dots, d_{l(k)}\}$ ). We finally define the non-mortar interface degrees of freedom as

$$\underline{w}^{l(n)} = \mathbf{R}^{(l)} \underline{w}^{l(m)}, \quad \text{with } \mathbf{R}^{(l)} = [\mathbf{M}^{l(n)}]^{-1} \mathbf{M}^{l(m)}. \quad (3.30)$$

### Matrix form of the global problem

Using the partition of the degrees of freedom (3.26) and (3.27), we arrange the global vector of degrees of freedom as follows

$$\underline{\mathbf{w}} = (\underline{w}^{0(n)} \quad \underline{w}^{l(n)} \quad \underline{w}^{l(m)} \quad \underline{w}^{0(m)}). \quad (3.31)$$

The definition of the local matching matrix involved in the problem (3.28) is given below.

PROPOSITION 3.2.1 *Let us introduce the following vector of independent degrees of freedom  $\bar{\mathbf{w}}$  associated to global problem*

$$\bar{\mathbf{w}}^\top = (\underline{w}^{0(n)} \quad \underline{w}^{l(m)} \quad \underline{w}^{0(m)}).$$

*The global matching matrix  $\mathbf{M}$  which defines  $\underline{\mathbf{w}}$  in terms of the independent degrees of freedom vector  $\bar{\mathbf{w}}$  is then*

$$\mathbf{M} = \begin{bmatrix} \mathbf{I}_{0(n)} & & \\ & \mathbf{R}^{(l)} & \\ & \mathbf{I}_{0(m)}^l & \\ & & \mathbf{I}_{0(m)}^0 \end{bmatrix} \quad \text{and } \underline{\mathbf{w}} = \mathbf{M}\bar{\mathbf{w}} \quad (3.32)$$

$\mathbf{I}_{0(k)}$  is the identity matrix associated to the free interior degrees of freedom of the domain of index  $k$ . We highlight that  $\mathbf{I}_{0(m)} = \text{diag}(\mathbf{I}_{0(m)}^l, \mathbf{I}_{0(m)}^0)$ , where  $\mathbf{I}_{0(m)}^l$  is the identity matrix associated to the free and independent degrees of freedom on the mortar interface and  $\mathbf{I}_{0(m)}^0$  is the identity matrix associated to the interior degrees of freedom of  $\omega_n$  which are not on the interfaces.

REMARK 3.2.2 Before going further, we recall that likewise as the solution  $\mathbf{w}$ , the admissible function must also satisfy the matching conditions. Thus, given an admissible test function  $\mathbf{v}$ , we have similar relation (3.32) for  $\underline{\mathbf{v}}$  with its corresponding  $\bar{\mathbf{v}}$ .

Now we state the matrix form of the global problem which enforces the matching conditions defined previously.

PROBLEM 3.2.4 The matrix form of the global Problem 3.2.3 is: Find  $\bar{\mathbf{w}} \in \mathbb{R}^{(d_n - d_{l(n)})} \times \mathbb{R}^{d_m}$  such that

$$\bar{\mathbf{v}}^\top \mathbf{B}_m \bar{\mathbf{w}} = \bar{\mathbf{v}}^\top \mathbf{f}_m \quad \text{for all } \bar{\mathbf{v}} \in \mathbb{R}^{d_m} \times \mathbb{R}^{d_n - d_{l(n)}} \iff \mathbf{B}_m \bar{\mathbf{w}} = \mathbf{f}_m \quad \text{with} \quad (3.33)$$

with

$$\mathbf{B}_m = \mathbf{M}^\top \text{diag}(\mathbf{B}^{(n)}, \mathbf{B}^{(m)}) \mathbf{M}, \quad \text{and } \mathbf{f}_m = \mathbf{M}^\top \mathbf{f}, \quad \mathbf{f}^\top = [\mathbf{f}^{(n)} \quad \mathbf{f}^{(m)}].$$

REMARK 3.2.3 We have assumed in the previous problem that the matrices  $\mathbf{B}^{(k)}$  are rearranged conveniently in regards to the new ordering of the degrees of freedom, introduced in Eq. (3.31)

$$\mathbf{B}^{(m)} = \begin{bmatrix} \mathbf{B}_l^{l(m)} & \mathbf{B}_l^{0(m)} \\ \mathbf{B}_0^{l(m)} & \mathbf{B}_0^{0(m)} \end{bmatrix} \quad \text{and } \mathbf{B}^{(n)} = \begin{bmatrix} \mathbf{B}_0^{0(n)} & \mathbf{B}_0^{l(n)} \\ \mathbf{B}_l^{0(n)} & \mathbf{B}_l^{l(n)} \end{bmatrix}.$$

The block-matrix  $\mathbf{B}_r^{c(k)} = ([B_r^{c(k)}]_{\hat{i}\hat{j}})_{\hat{i}\hat{j}}$  is of dimensions  $d_{r(k)} \times d_{c(k)}$  of components

$$[B_r^{c(k)}]_{\hat{i}\hat{j}} = b_{(k)}(p_i^{(k)}, p_j^{(k)}), \quad i \in S_{r(k)} \quad \text{and } j \in S_{c(k)}.$$

Similarly for the right hand side

$$\mathbf{f}^{(n)} = [\mathbf{f}^{0(n)} \quad \mathbf{f}^{l(n)}] \quad \text{and } \mathbf{f}^{(m)} = [\mathbf{f}^{l(m)} \quad \mathbf{f}^{0(m)}],$$

with  $\mathbf{f}^{r(k)} = (f_{\hat{i}}^{r(k)})_{\hat{i}}$  is a column vector of dimension  $d_{r(k)}$  of components

$$f_{\hat{i}}^{r(k)} = l_{(k)}(p_i^{(k)}), \quad i \in S_{r(k)}.$$

Now, we consider in particular the matching conditions of a global shell problem.



### 3.2.3 Mortar method implementation for shell junction

Let  $\underline{\mathbf{u}}_{(k)}$  and  $\underline{\mathbf{s}}_{(k)}$  be respectively the degrees of freedom vectors corresponding to  $\mathbf{u}_{(k)}$  and  $\mathbf{s}_{(k)}$ . In the same vein, as in the above abstract problem, being  $u_i^{l(k)}$  and  $s_\alpha^{l(k)}$  respectively the restriction of  $u_{i(k)}$  and  $s_{\alpha(k)}$  to the parametric interface  $\gamma^{l(k)}$ , we denote by  $\underline{u}_i^{l(k)}$  and  $\underline{s}_\alpha^{l(k)}$  their corresponding vectors of (finite element) degrees of freedom, while  $\underline{u}_i^{0(k)}$  and  $\underline{s}_\alpha^{0(k)}$  are the degrees of freedom vectors in the interior of  $\Omega_k$ . For sake of simplicity, we suppose that both the displacement and rotation components are discretized using the same finite element.

First, we focus on the continuity condition of the displacement fields of the assembling of middle-surfaces. The matrix form of (3.17) reads:

$$\mathbf{M}^{(l)} \underline{u}_i^{l(n)} = [\mathbf{M}^{l(m)}]_i^j \underline{u}_j^{l(m)}, \text{ with summation over } j \in \{1, 2, 3\}.$$

$[\mathbf{M}^{l(m)}]_i^j$  denotes the matrix on the mortar side of dimension  $(d_{l(n)}, d_{l(m)})$ . For a given couple  $(i, j) \in \{1, 2, 3\}^2$ , the components  $[M_{\hat{p}\hat{q}}^{l(m)}]_i^j$  of  $[\mathbf{M}^{l(m)}]_i^j$  are

$$[M_{\hat{p}\hat{q}}^{l(m)}]_i^j = \int_{\gamma^l} a_{i(n)}^{j(m)} p_p^{(n)}(\boldsymbol{\xi}_{(n)}) p_q^{(m)}(\boldsymbol{\xi}_{(m)}) s_{l(m)}(\eta) d\eta.$$

The matrix  $\mathbf{M}^{(l)}$ 's components are defined as

$$M_{\hat{p}\hat{q}}^{(l)} = \int_{\gamma^l} p_p^{(n)}(\boldsymbol{\xi}_{(n)}) p_q^{(n)}(\boldsymbol{\xi}_{(n)}) s_{l(n)}(\eta) d\eta.$$

Thus the matrix form of the continuity of the displacement vector is

$$\mathbf{M}^{l(n)} \underline{\mathbf{u}}^{l(n)} = \mathbf{M}^{l(m)} \underline{\mathbf{u}}^{l(m)}, \text{ with } \mathbf{M}^{l(n)} = \left( [\delta_i^j \times \mathbf{M}^{(l)}]_i^j \right)_{(i,j) \in \{1,2,3\}^2} = \begin{bmatrix} \mathbf{M}^{(l)} & & \\ & \mathbf{M}^{(l)} & \\ & & \mathbf{M}^{(l)} \end{bmatrix}$$

and  $\mathbf{M}^{l(m)}$  is the  $3 \times 3$  block matrix of dimension  $d_{l(n)} \times d_{l(m)}$ :

$$\mathbf{M}^{l(m)} = \left( [\mathbf{M}^{l(m)}]_i^j \right)_{(i,j) \in \{1,2,3\}^2}.$$

Regarding the other junction condition, we introduce the matrices  $\mathbf{M}_\Psi^{l(k)}$  such that

$$\mathbf{M}_\Psi^{l(k)} = ([\mathbf{M}_\Psi^{l(k)}]^\alpha)_{\alpha \in \{1,2\}}.$$

The components  $[\mathbf{M}_\Psi^{l(k)}]_{\hat{p}\hat{q}}^\alpha$  of the (sub-block) matrix  $[\mathbf{M}_\Psi^{l(k)}]^\alpha$  are defined as

$$[\mathbf{M}_\Psi^{l(k)}]_{\hat{p}\hat{q}}^\alpha = (-1)^{\bar{\alpha}} \int_{\gamma^l} t_{\bar{\alpha}}^{l(k)} p_p^{(n)}(\boldsymbol{\xi}_{(n)}) p_q^{(k)}(\boldsymbol{\xi}_{(k)}) s_{l(k)}(\eta) d\eta, \quad \bar{\alpha} = \{1, 2\} \setminus \alpha.$$

Thus the matrix form of Equation (3.18) is

$$\mathbf{M}_\Psi^{l(n)} \underline{\mathbf{s}}^{l(n)} = \mathbf{M}_\Psi^{l(m)} \underline{\mathbf{s}}^{l(m)}. \tag{3.34}$$

The tangential rotation continuity (and the associated corollary, i.e the independence of the normal component of rotation) implies that only one of the rotation covariant components of  $\Omega_{n(l)}$  can be defined through Equation (3.34). Then, one has to extract a sub-matrix of “full rank”, i.e invertible, which corresponding rotation will be defined.

Let us consider a given integer number  $\alpha \in \{1, 2\}$ , and assume that  $t_{\alpha}^{l(n)} \neq 0$  so we can define the rotation  $s_{\alpha}^{l(n)}$ . Thus we have

$$[\mathbf{M}_{\psi}^{l(n)}]_{\alpha} s_{\alpha}^{l(n)} = \mathbf{M}_{\psi}^{(l)} \underline{s}^{(l)} \quad (\text{no summation over } \alpha) \quad (3.35)$$

where

$$\mathbf{M}_{\psi}^{(l)} = \begin{pmatrix} \mathbf{M}_{\psi}^{l(m)} & -[\mathbf{M}_{\psi}^{l(n)}]_{\bar{\alpha}} \end{pmatrix} \quad \text{and} \quad \underline{s}^{(l)} = \begin{pmatrix} \underline{s}^{l(m)} & \underline{s}_{\bar{\alpha}}^{l(n)} \end{pmatrix}^{\top}.$$

Now, for the purpose of defining the global junction, let us note  $\mathbf{R}_u^{(l)}$  and  $\mathbf{R}_{\psi}^{(l)}$  respectively the matrices associated to the junction of the displacement and rotation, such that

$$\underline{\mathbf{u}}^{l(n)} = \mathbf{R}_u^{(l)} \underline{\mathbf{u}}^{l(m)} \quad \text{and} \quad \underline{s}_{\alpha}^{l(n)} = [\mathbf{R}_{\psi}^{(l)}]_{\alpha} \underline{s}^{(l)},$$

where  $\mathbf{R}_u^{(l)} = [\mathbf{M}_u^{l(n)}]^{-1} \mathbf{M}_u^{l(m)}$  and  $[\mathbf{R}_{\psi}^{(l)}]_{\alpha} = ([\mathbf{M}_{\psi}^{l(n)}]_{\alpha})^{-1} \mathbf{M}_{\psi}^{(l)}$ . Let us note  $[\mathbf{R}_{\psi}^{(l)}]_{\alpha} := [\mathbf{R}_{\psi}^{l(m)} \quad \mathbf{R}_{\psi}^{l(n)}]$ .

The matrices  $\mathbf{R}_{\psi}^{l(m)}$  and  $\mathbf{R}_{\psi}^{l(n)}$  are respectively the sub-block matrices associated to the mortar and non-mortar degrees of freedom  $\underline{s}^{l(m)}$  and  $\underline{s}_{\bar{\alpha}}^{l(n)}$ , and are of respective dimensions  $(d_{l(n)}, 2d_{l(m)})$  and  $(d_{l(n)}, d_{l(n)})$

$$\mathbf{R}_{\psi}^{l(m)} = ([\mathbf{M}_{\psi}^{l(n)}]_{\alpha})^{-1} \mathbf{M}_{\psi}^{l(m)}, \quad \mathbf{R}_{\psi}^{l(n)} = ([\mathbf{M}_{\psi}^{l(n)}]_{\alpha})^{-1} [\mathbf{M}_{\psi}^{l(n)}]_{\bar{\alpha}}.$$

From now on, let us note  $\sigma = \bar{\alpha}$ , we introduce the vectors

$$\underline{\mathbf{U}}^{(l)} = \begin{bmatrix} \underline{\mathbf{u}}^{l(n)} & \underline{s}_{\sigma}^{l(n)} & \underline{s}_{\alpha}^{l(n)} & \underline{\mathbf{u}}^{l(m)} & \underline{s}^{l(m)} \end{bmatrix} \quad \text{and} \quad \overline{\mathbf{U}}^{(l)} = \begin{bmatrix} \underline{\mathbf{u}}^{l(m)} & \underline{s}_{\sigma}^{l(n)} & \underline{s}^{l(m)} \end{bmatrix}.$$

Finally, we define the local matching matrix

$$\mathbf{M}^{(l)} = \begin{bmatrix} \mathbf{R}_u^{(l)} & & & & \\ & \mathbf{I}_{\psi}^{l(n)} & & & \\ & \mathbf{R}_{\psi}^{l(n)} & \mathbf{R}_{\psi}^{l(m)} & & \\ \mathbf{I}_u^{l(m)} & & & & \\ & & & \mathbf{I}_{\psi}^{l(m)} & \end{bmatrix} \quad \text{and} \quad \underline{\mathbf{U}}^{(l)} = \mathbf{M}^{(l)} \overline{\mathbf{U}}^{(l)}$$

where  $\mathbf{I}_{\psi}^{l(n)}$ ,  $\mathbf{I}_{\psi}^{l(m)}$  and  $\mathbf{I}_u^{l(m)}$  are respectively the identity matrices of respective sizes  $(d_{l(n)}, d_{l(n)})$ ,  $(2d_{l(m)}, 2d_{l(m)})$  and  $(3d_{l(m)}, 3d_{l(m)})$ .

Let  $\mathbf{U}^{0(k)} := (\underline{\mathbf{u}}^{0(k)}, \underline{\mathbf{s}}^{0(k)})$  be the interior degrees of freedom corresponding to  $\Omega_k$ . We consider the vectors of degrees of freedom

$$\underline{\mathbf{U}}^{\top} = [\mathbf{U}^{0(n)} \quad \underline{\mathbf{U}}^{(l)} \quad \mathbf{U}^{0(m)}] \quad \text{and} \quad \overline{\mathbf{U}}^{\top} = [\mathbf{U}^{0(n)} \quad \overline{\mathbf{U}}^{(l)} \quad \mathbf{U}^{0(m)}].$$

The global matrix is

$$\mathbf{M} = \begin{bmatrix} \mathbf{I}^{0(n)} & & \\ & \mathbf{M}^{(l)} & \\ & & \mathbf{I}^{0(m)} \end{bmatrix}.$$

$\mathbf{I}^{0(k)}$  is the identity matrix of dimensions  $(5 \times d_{0(k)}, 5 \times d_{0(k)})$  associated to interior degrees of freedom  $\mathbf{U}^{0(k)}$

### 3.2.4 Finite elements implementation

There exist several numerical methods for the solving of PDEs problems. Their common purpose is the construction of an approximation of a continuous solution which most of the time cannot be computed analytically. One of them, most widespread used, is the Finite Element Method. In its framework, the approximated solution is the solution of a discrete problem which is commonly a Galerkin approximation of the continuous problem. The key point is then the construction of an appropriate finite dimensional discrete space associated to the problem meshing. Naturally, attached to the meshing, the discrete solution is considered as a piecewise polynomial function (in each element). Its discrete space is characterized by the kind of shape basis functions used and depends of the required regularity by the variational problem solution.

Our purpose subsequently is to define the discrete problem and show the finite element approximation aspects using Lagrange interpolation. For the purpose of ease the discretization the variational problem is first put in matrix form and then the FEM discretization is depicted.

#### 3.2.4.1 Matrix form of the variational problem

Let us define the functional vector  $\mathbf{F}(\cdot, \cdot)$  of the three-dimensional displacement covariant components and their derivatives

$$\mathbf{F}(\mathbf{v}, \mathbf{r}) = [v_i \ v_{i,\alpha} \ r_\beta \ r_{\beta,\alpha}]^\top = [v_1 \ v_{1,1} \ v_{1,2} \ \cdots \ r_2 \ r_{2,1} \ r_{2,2}]$$

Taking into account for the elastic tensor symmetry and using the Voigt notations, we set:

$$\boldsymbol{\gamma} := (\gamma_{11} \ \gamma_{22} \ 2\gamma_{12})^\top, \ \boldsymbol{\chi} := (\chi_{11} \ \chi_{22} \ 2\chi_{12})^\top \text{ and } \boldsymbol{\gamma}_s := (2\gamma_{13} \ 2\gamma_{23})^\top.$$

Let us introduce the matrices  $\mathbf{M}_\gamma$ ,  $\mathbf{M}_\chi$  and  $\mathbf{M}_s$  respectively associated to the membrane, bending and shear tensors.  $\mathbf{M}_\gamma$  and  $\mathbf{M}_\chi$  are both of dimensions  $(3, 15)$  and  $\mathbf{M}_s$  is of dimensions  $(2, 15)$

$$\boldsymbol{\gamma}(\cdot) = \mathbf{M}_\gamma \mathbf{F}(\cdot, \star) \ \boldsymbol{\chi}(\cdot, \star) = \mathbf{M}_\chi \mathbf{F}(\cdot, \star) \text{ and } \boldsymbol{\gamma}_s(\cdot, \star) = \mathbf{M}_s \mathbf{F}(\cdot, \star). \quad (3.36)$$

These different matrices depend explicitly of the geometry through the metric, curvature tensors and Christoffel symbols. Let us define the row vectors of dimension  $15 \times 1$ :

- relatively to the membrane and bending strain components:

$$\boldsymbol{\gamma}^{\alpha\beta} := [-\Gamma_{\alpha\beta}^1 \ \delta_\alpha^1 \delta_\beta^1 \ \frac{1}{2}(\delta_\alpha^1 \delta_\beta^2 + \delta_\alpha^2 \delta_\beta^1) \ -\Gamma_{\alpha\beta}^2 \ \frac{1}{2}(\delta_\alpha^2 \delta_\beta^1 + \delta_\alpha^1 \delta_\beta^2) \ \delta_\alpha^2 \delta_\beta^2 \ -b_{\alpha\beta} \ 0_{1 \times 8}].$$

$$\boldsymbol{\chi}^{\alpha\beta} := [-\chi_{u_1}^{\alpha\beta} \ -\chi_{u_2}^{\alpha\beta} \ \chi_{u_3}^{\alpha\beta} \ \chi_1^{\alpha\beta} \ \chi_2^{\alpha\beta}]$$

◦ finally for the shear strain components

$$2\gamma^{\alpha 3} := [ b_{\alpha}^1 \ 0 \ 0 \ b_{\alpha}^2 \ 0 \ 0 \ 0 \ \delta_{\alpha}^1 \ \delta_{\alpha}^2 \ \delta_{\alpha}^1 \ 0 \ 0 \ \delta_{\alpha}^2 \ 0 \ 0 ].$$

In the previous definitions  $0_{1 \times n}$  represents a zero row vector of dimension  $n$  and

$$\begin{aligned} \chi_{u_{\sigma}}^{\alpha\beta} &:= [(\Gamma_{\alpha\beta}^{\sigma} + b_{\alpha}^{\lambda} b_{\lambda\beta}^{\sigma} + b_{\beta}^{\lambda} \Gamma_{\lambda\alpha}^{\sigma}) \quad b_{\alpha}^{\sigma} \delta_{\beta}^1 + b_{\beta}^{\sigma} \delta_{\alpha}^1 \quad b_{\alpha}^{\sigma} \delta_{\beta}^2 + b_{\beta}^{\sigma} \delta_{\alpha}^2], \quad \sigma \in \{1, 2\} \\ \chi_{u_3}^{\alpha\beta} &:= [b_{\alpha}^{\lambda} b_{\lambda\beta} + b_{\beta}^{\lambda} b_{\lambda\alpha} \quad 0 \quad 0] \\ \chi_1^{\alpha\beta} &:= [0 \quad \delta_{\alpha}^1 \delta_{\beta}^1 \quad \frac{1}{2}(\delta_{\alpha}^1 \delta_{\beta}^2 + \delta_{\alpha}^2 \delta_{\beta}^1)] \\ \chi_2^{\alpha\beta} &:= [0 \quad \frac{1}{2}(\delta_{\alpha}^2 \delta_{\beta}^1 + \delta_{\alpha}^1 \delta_{\beta}^2) \quad \delta_{\alpha}^2 \delta_{\beta}^2]. \end{aligned} \tag{3.37}$$

The matrices  $\mathbf{M}_{\gamma}$ ,  $\mathbf{M}_{\chi}$  and  $\mathbf{M}_s$ 's rows are respectively  $\gamma^{11}$ ,  $\gamma^{22}$ ,  $2\gamma^{12}$ ;  $\chi^{11}$ ,  $\chi^{22}$ ,  $2\chi^{12}$  and  $2\gamma^{13}$ ,  $2\gamma^{23}$ .

PROPOSITION 3.2.2 *Consider an open bounded subset  $\omega \subset \mathbb{R}^2$  and an injective immersion  $\Phi$  which defines the middle-surface  $\Omega$  and let  $t > 0$  be the shell's thickness. Let  $\mathbf{Q}$  and  $\mathbf{E}$  respectively be the reduced plane and anti-plane parts of the elastic tensor. The matrix expression of the bilinear form associated to the strain energy is*

$$a([\mathbf{u}, \mathbf{s}], [\mathbf{v}, \mathbf{r}]) = \int_{\omega} \{ \mathbf{F}^{\top}(\mathbf{v}, \mathbf{r}) \mathbb{A} \mathbf{F}(\mathbf{u}, \mathbf{s}) + \mathbf{F}^{\top}(\mathbf{v}, \mathbf{r})^{\top} \mathbb{D} \mathbf{F}(\mathbf{u}, \mathbf{s}) + \mathbf{F}^{\top}(\mathbf{v}, \mathbf{r}) \mathbf{S} \mathbf{F}(\mathbf{u}, \mathbf{s}) \} \sqrt{ad} d\xi, \tag{3.38}$$

where

- $\mathbb{A} := t \mathbf{M}_{\gamma}^{\top} \mathbf{Q} \mathbf{M}_{\gamma}$  is the matrix associated to the membrane strain
- $\mathbb{D} := \frac{t^3}{12} \mathbf{M}_{\chi}^{\top} \mathbf{Q} \mathbf{M}_{\chi}$  the matrix associated to the bending strain
- $\mathbf{S} := t \mathbf{M}_s^{\top} \mathbf{E} \mathbf{M}_s$  is the matrix associated to the shear strain.

In analogous manner, for the virtual work of the applied loads, we have:

PROPOSITION 3.2.3 *Let us consider that the middle-surface is subjected to a surface load  $\mathbf{p} = p^i \mathbf{a}_i$ , a resultant effort and moment  $\mathbf{N} = N^i \mathbf{a}_i$  and  $\mathbf{M} = \sqrt{a}(M^2 \mathbf{a}^1 - M^1 \mathbf{a}^2)$  on its boundary  $\Phi(\gamma_1)$ . The matrix form of the linear form is*

$$l([\mathbf{v}, \mathbf{r}]) = \int_{\omega} \mathbf{L}_p \cdot \mathbf{F}(\mathbf{v}, \mathbf{r}) \sqrt{ad} d\xi + \int_{\gamma_1} (\mathbf{L}_n \cdot \mathbf{F}(\mathbf{v}, \mathbf{r}) + \mathbf{L}_m \cdot \mathbf{F}(\mathbf{v}, \mathbf{r})) d l_1,$$

where

$$\begin{aligned} \mathbf{L}_p^{\top} &:= [p^1 \quad 0_{1 \times 2} \quad p^2 \quad 0_{1 \times 2} \quad p^3 \quad 0_{1 \times 2} \quad 0_{1 \times 6}] \\ \mathbf{L}_n^{\top} &:= [N^1 \quad 0_{1 \times 2} \quad N^2 \quad 0_{1 \times 2} \quad N^3 \quad 0_{1 \times 2} \quad 0_{1 \times 6}] \\ \mathbf{L}_m^{\top} &:= [0_{1 \times 3} \quad 0_{1 \times 3} \quad 0_{1 \times 3} \quad M^1 \quad 0_{1 \times 2} \quad M^2 \quad 0_{1 \times 2}]. \end{aligned}$$

### 3.2.4.2 Local discretization

Let  $u_i^j$  (resp.  $s_\alpha^j$ ) be the  $j$ -th degree of freedom of the  $i$ -th displacement vector component  $u_i^h$  (resp.  $\alpha$ -th rotation vector component  $s_\alpha^h$ ). We have

$$u_i^h(\boldsymbol{\xi}) = \sum_{j=1}^{n_K} u_i^j p_j(\boldsymbol{\xi}) \text{ and } s_\alpha^h = \sum_{j=1}^{n_K} s_\alpha^j p_j(\boldsymbol{\xi}).$$

where  $p_j$ ,  $j = 1 : n_K$  are the Lagrange polynomial basis functions.

Given a polynomial  $w^h(\boldsymbol{\xi}) = \sum_{j=1}^{n_K} w^j p_j(\boldsymbol{\xi})$ , the derivative  $w_{,\sigma}^h(\boldsymbol{\xi})$  of  $w^h$  with respect to  $\xi^\sigma$  is

$$w_{,\sigma}^h(\boldsymbol{\xi}) = \sum_{j=1}^{n_K} w^j p_{j,\sigma}(\boldsymbol{\xi}).$$

Adopting the convention  $\partial_0 f = f$ , we define the matrix  $\mathbf{D} := (D_{ij} = \partial_{i-1} p_j(\boldsymbol{\xi}))_{i=1:3, j=1:n_K}$  of size  $3 \times n_K$  such that:

$$[w(\boldsymbol{\xi}) \quad w_{,1}(\boldsymbol{\xi}) \quad w_{,2}(\boldsymbol{\xi})]^\top = \mathbf{D}(\boldsymbol{\xi}) [w^1 \quad w^2 \quad \dots \quad w^{n_K}]^\top.$$

Let us consider the matrix  $\mathbf{DP}_n$  of dimension  $15 \times (5n_K)$

$$\mathbf{DP}_n = \begin{pmatrix} \mathbf{D} & & & & \\ & \mathbf{D} & & & \\ & & \mathbf{D} & & \\ & & & \mathbf{D} & \\ & & & & \mathbf{D} \end{pmatrix}.$$

Let now  $\underline{\mathbf{U}}^h$  be the vector of dimension  $5 n_K$  composed of the degrees of freedom of displacement and rotation arranged consecutively

$$\underline{\mathbf{U}}^h = \left[ (u_i^j)_{j=1:n_K} \quad (s_\alpha^j)_{j=1:n_K} \right]^\top,$$

hence  $\mathbf{F}(\mathbf{u}^h, \mathbf{s}^h) = \mathbf{DP}_n \underline{\mathbf{U}}^h$ .

Let  $a_K(\cdot, \cdot)$  denote the restriction to the element  $K$  of the bilinear form  $a(\cdot, \cdot)$

$$\begin{aligned} a_K([\mathbf{u}^h, \mathbf{s}^h], [\mathbf{v}^h, \mathbf{r}^h]) &= \int_K \{ \underline{\mathbf{V}}_h^\top \mathbf{DP}_n^\top \mathbf{A} \mathbf{DP}_n \underline{\mathbf{U}}_h + \underline{\mathbf{V}}_h^\top \mathbf{DP}_n^\top \mathbb{D} \mathbf{DP}_n \underline{\mathbf{U}}_h \\ &\quad + \underline{\mathbf{V}}_h^\top \mathbf{DP}_n^\top \mathbf{S} \mathbf{DP}_n \underline{\mathbf{U}}_h \} \sqrt{a} dS \end{aligned} \quad (3.39)$$

$\mathbf{A}_K$  is the elementary stiffness matrix (restricted to the element  $K$ ), of dimensions  $5n_K \times 5n_K$ , associated to the discretization of the bilinear form

$$\mathbf{A}_K = \int_K A_K(\boldsymbol{\xi}) dS$$

where

$$A_K(\boldsymbol{\xi}) = \{ \mathbf{DP}_n^\top(\boldsymbol{\xi}) \mathbf{A}(\boldsymbol{\xi}) \mathbf{DP}_n(\boldsymbol{\xi}) + \mathbf{DP}_n^\top(\boldsymbol{\xi}) \mathbb{D}(\boldsymbol{\xi}) \mathbf{DP}_n(\boldsymbol{\xi}) + \mathbf{DP}_n^\top(\boldsymbol{\xi}) \mathbf{S}(\boldsymbol{\xi}) \mathbf{DP}_n(\boldsymbol{\xi}) \} \sqrt{a}(\boldsymbol{\xi}).$$

The elementary stiffness matrix  $\mathbf{A}_K$  is computed after an appropriate integration scheme in order to compute the integral in equation (3.39) -as recall in (3.20). There exist various quadrature rules for numerical integrations [30]. One usually uses a Gauss-quadrature integration, which for  $n_p$  points of quadrature is exact for the integration of a polynomial of degree  $2n_p - 1$ . After the local evaluation, one finally assembles the global matrix by adding the elementary contributions from the different finite elements. Reader may refer to [26, 24] for a deep insight on the finite element aspects.

### 3.2.4.3 $P_2$ Lagrange interpolation

We have used a  $P_2$ -Lagrange interpolation for the displacement and rotation components. Consider a non-degenerated element of vertexes  $A_i$  of coordinates  $(\eta_1^i, \eta_2^i)$ ,  $i = 1 : 3$ . The dimension of the polynomial space is  $\dim(P_n) = \frac{(n+1)(n+2)}{2} = n_K$ . Let us consider a point  $X$  of coordinates  $\boldsymbol{\xi} = (\xi^1, \xi^2)$  and let  $\lambda_i$  denote its barycentric coordinates

$$\lambda_i(\boldsymbol{\xi}) = \lambda_i := \frac{\|XA_{i+1} \wedge XA_{i+2}\|}{\|A_1A_2 \wedge A_1A_3\|},$$

where  $i + 1$  and  $i + 2$  are defined from a cyclic permutation of the indexes (1, 2, 3); for instance “3 + 1 = 1, 3 + 2 = 2”. For a  $P_2$ -Lagrange approximation the degrees of freedom are defined at the three vertexes and the middle nodes of the three edges, as shown in Figure 3.2. Their local (barycentric) coordinates are reported on Table 3.1.

Point	$(\lambda_1, \lambda_2, \lambda_3)$
$A_1$	$(1, 0, 0)$
$A_2$	$(0, 1, 0)$
$A_3$	$(0, 0, 1)$
$b_1$	$(0, \frac{1}{2}, \frac{1}{2})$
$b_2$	$(\frac{1}{2}, 0, \frac{1}{2})$
$b_3$	$(\frac{1}{2}, \frac{1}{2}, 0)$

Table 3.1 Barycentric coordinates of a  $P_2$  interpolation.

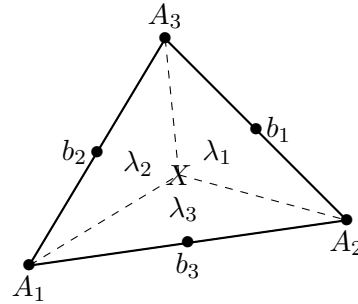


Figure 3.2  $P_2$ -finite element

The six polynomial basis functions are defined by

$$\begin{aligned}
 p_1(\boldsymbol{\xi}) &= \lambda_1^2(\boldsymbol{\xi}) \\
 p_2(\boldsymbol{\xi}) &= \lambda_2^2(\boldsymbol{\xi}) \\
 p_3(\boldsymbol{\xi}) &= \lambda_3^2(\boldsymbol{\xi}) \\
 p_4(\boldsymbol{\xi}) &= 4\lambda_2(\boldsymbol{\xi})\lambda_3(\boldsymbol{\xi}) \\
 p_5(\boldsymbol{\xi}) &= 4\lambda_1(\boldsymbol{\xi})\lambda_3(\boldsymbol{\xi}) \\
 p_6(\boldsymbol{\xi}) &= 4\lambda_1(\boldsymbol{\xi})\lambda_2(\boldsymbol{\xi}).
 \end{aligned} \tag{3.40}$$

The polynomials effectively satisfy the properties (3.23) and (3.24). Figure 3.3 shows the shapes of the trace functions used for the mortar-method. The representation at the left corresponds to the middle-nodes  $b_i$  and the one at the right side corresponds to the vertexes  $A_i$ .

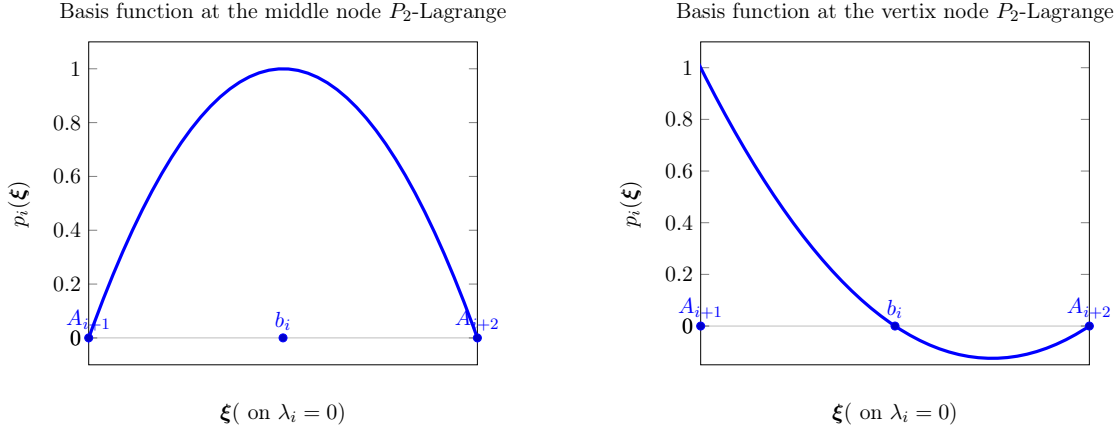


Figure 3.3 Trace functions of the Lagrange  $P_2$  basis functions.

We give some numerical results in the next section.

### 3.3 Numerical results

We first start by specifying the parameterization of the mid-surfaces.

#### Shape parameterization:

The shape functions  $\Phi_k$  are Bezier polynomial functions (of class  $C^\infty$ ) of order 4 and the parametric domain is the unit square  $\omega_k := \omega = [0, 1]^2$ . The middle-surface  $\Omega_k$  is thus defined by mean of 16 control points noted  $p_{ij(k)}$ ,  $(i, j) \in \{0, \dots, n = 3\}^2$ . Their corresponding bivariate Bernstein polynomials  $B_{ij} : \omega \rightarrow [0, 1]$  are defined as usual through tensor product of the univariate Bernstein polynomial  $b_i^n : [0, 1] \rightarrow [0, 1]$  of order  $n + 1$ , with  $n = 3$ :

$$b_i^n(\eta) = C_n^i(1 - \eta)^{(n-i)}\eta^i, \text{ and } B_{ij}(\xi^1, \xi^2) = b_i^n(\xi^1)b_j^n(\xi^2), \text{ with } C_n^i = \frac{n!}{i!(n-i)!}.$$

The shape function  $\Phi_k$  is defined as

$$\Phi_k(\xi^1, \xi^2) = \sum_{i,j=0}^3 p_{ij(k)} B_{ij}(\xi^1, \xi^2).$$

The global geometric continuity conditions, in the case of shell assembling, are simply reduced to the equivalence between the control points of different domains which have a common interface, i.e the equalities of their coordinates. In such a kind of configuration, the domain  $\gamma^l = \gamma = [0, 1]$ , for all  $1 \leq l \leq L$ , and the interface parametric functions  $\varphi^{l(k)}$  are simply one of the following vector value functions  $\varphi_i$ ,  $i \in \{1, \dots, 4\}$ , parameterizing the boundary  $\partial\bar{\omega}$ , as shown on Figure 3.4.

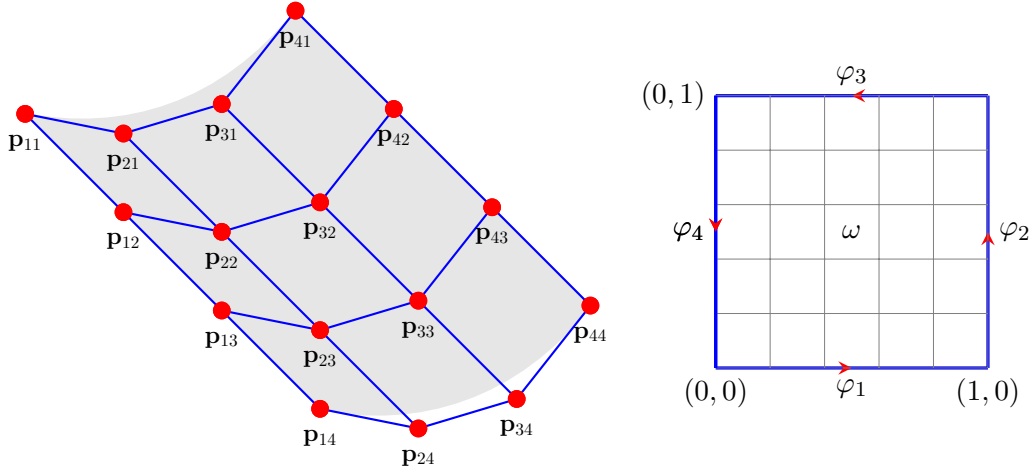


Figure 3.4 From left to right an example of middle-surface with the associated control points and the parametric interfaces with their associated mappings defined as follows:

$$\varphi_1(\eta) = (\eta, 0), \quad \varphi_2 = (1, \eta), \quad \varphi_3 = (1 - \eta, 1) \quad \text{and} \quad \varphi_4(\eta) = (0, 1 - \eta).$$

REMARK 3.3.1 As can be seen from the parametric functions  $\varphi_i$  of the interfaces, the tangent vectors are just one of the in-plane covariant basis vectors. More precisely, the tangent vector corresponding to  $\varphi_i$ ,  $i \in \{1, 3\}$  is co-linear to  $\mathbf{a}_1$  and for  $i \in \{2, 4\}$  it is co-linear to  $\mathbf{a}_2$ . Thus in regards to the covariant component of the rotation which is defined with the tangential continuity constraint -see Equation (3.35)-:

- in the case where  $\varphi^{l(n)} = \varphi_i$  with  $i \in \{1, 3\}$ , one can define  $\underline{s}_2^{l(n)}$  in terms of  $\underline{s}^{(m)}$  and  $\underline{s}_1^{l(n)}$ .
- while, for  $i \in \{2, 4\}$  one will define  $\underline{s}_1^{l(n)}$  in terms of  $\underline{s}^{(m)}$  and  $\underline{s}_2^{l(n)}$ .

### 3.3.1 Vibration frequencies of a plate

The first example concerns the vibration analysis of a plate shell. The unit square plate is free without boundary condition, and is made of isotropic material of following characteristics

$$E = 210 \text{ GPa and } \nu = 0.3, \quad \rho = 7300 \text{ Kg/m}^3.$$

The first six eigenvalues correspond to rigid body motion. For the frequencies of rank greater than six, comparison is made with theoretical values  $f_i^{ex}$  given in formula 3.41

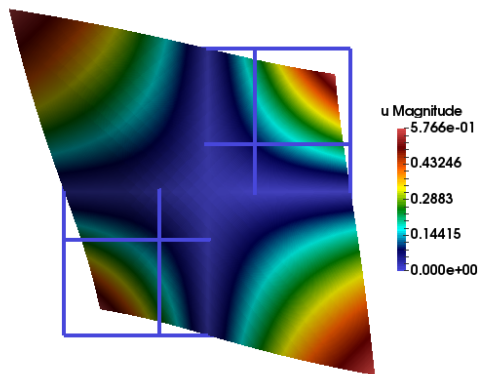
$$(f_i^{ex})^2 = \frac{1}{2\pi l^2} \lambda_i^2 \frac{tE}{12\rho(1-\nu^2)}, \quad (3.41)$$

i	$\lambda_i^2$
7	13.49
8	19.79
9	24.43
10	35.02
11	35.02

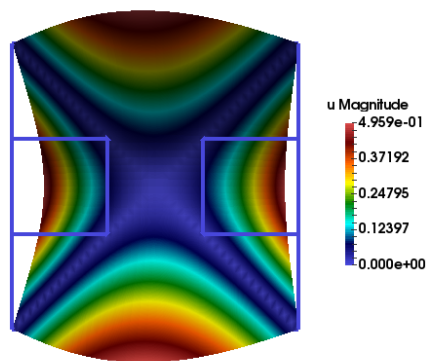


Mono-shell case

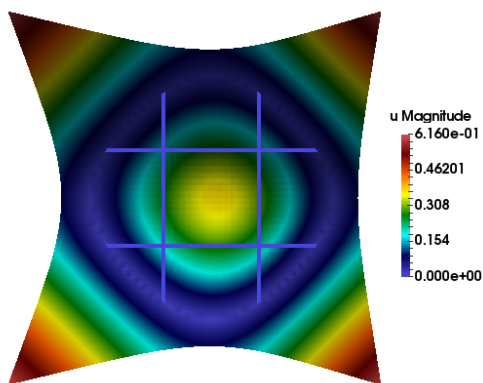
Figure 3.5 shows the non rigid vibration modes of rank seven to eleventh.



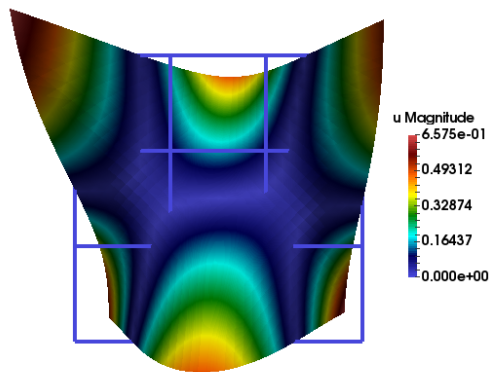
3.5.a – 7th eigenvector deformation



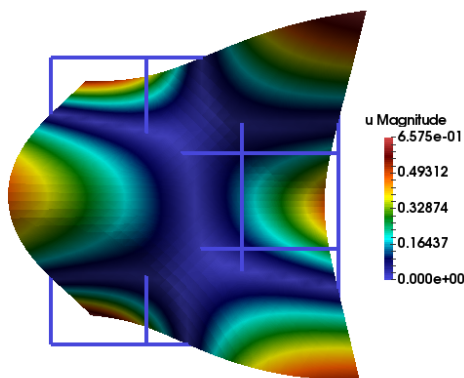
3.5.b – 8th eigenvector deformation



3.5.c – 9th eigenvector deformation



3.5.d – 10th eigenvector deformation



3.5.e – 11th eigenvector deformation

Figure 3.5 Representation of the vibration modes 7 to 12 for the free plate

Table 3.2 shows the comparison of the computed eigenvalues with the theoretical. We remark that the maximum relative error is less than 1%, which proves the validity of the implementation. We further adopt the following notations: given an index  $i$ ,  $f_i^{ex}$ ,  $f_i^n$  and  $r_i^n$  stand respectively for the exact eigenvalue, the computed eigenvalue for the geometric decomposition with  $n$  patches and the percentage of relative error,  $r_i^n = \frac{f_i^{ex} - f_i^n}{f_i^{ex}} \times 100$ .

$N^o$	$f_i^{ex}$ (Hz)	$f_i^1$ (Hz)	$r_i^1$ (%)
7	10.454	10.454	0.000
8	15.336	15.20	0.887
9	18.932	18.84	0.487
10	27.139	27.129	0.037
11	27.139	27.130	0.033

Table 3.2 Comparison of the computed eigenvalues corresponding to free-plate with the theoretical ones. The analysis was performed with a mesh of 1681 nodes and 3200 elements: the total number of degrees of freedom is 8405.

Even if the results are satisfactory, a general remark on the convergence of the eigenvalues is that the convergence is by superior values, i.e. the eigenvalues tend to the theoretical values by superior values, see Figure 3.6.

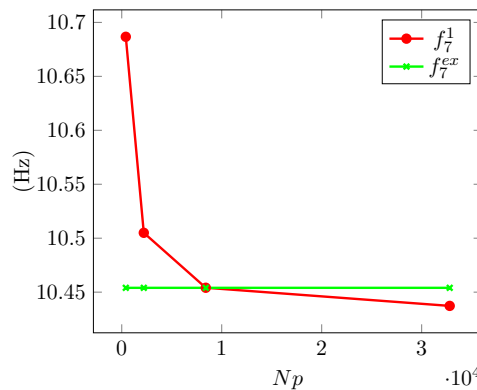


Figure 3.6 Illustration of the convergence of the 7th eigenvalue as the meshing step diminishes.  $Np$  represents the number of degrees of freedom.

This is explained by the fact that the stiffness matrix becomes over-stiffened as the discretization parameter tends to zero. This observation may correspond to the numerical locking phenomenon which induces spurious modes [3]. The reference frequencies  $f_i^{ex}$ , said exact, against which the computed frequencies are compared correspond to a Kirchoff-Love plate and are solution of a

bi-Laplacian problem. This may explain the fact that the convergence curve of  $f_7^1$  passes under the line of the reference value  $f_7^{ex}$ . Indeed, we use a Naghdi's shell model which corresponds to a Reissner-Mindlin's plate.

### Assembling of plate-shells

In order to validate the implementation of the junction, we also made the same analysis with a  $2 \times 2$  checkboard decomposition of the initial plate. The total number of degrees of freedom corresponding to the overall assembling is 8820 (8491 after considering the junction). Thus the total numbers of degrees of freedom for the both cases are almost similar so the results are comparable.

Table 3.3 shows the comparison of the computed eigenvalues with the theoretical ones, the relative differences with respect to the exact eigenvalues and also the relative differences  $\Delta f_i$  between the frequencies  $f_i^1$  and  $f_i^4$ .

$N^o$	$f_i^4$ (Hz)	$r_i^4$ (%)	$\Delta f_i$ (%)
7	10.449	0.048	-0.048
8	15.205	0.854	-0.007
9	18.843	0.471	-0.005
10	27.125	0.052	-0.015
11	27.125	0.052	-0.018

Table 3.3 Comparison of the computed eigenvalues corresponding to free-plate decomposed into  $2 \times 2$  patches. Comparison is made with respect to the theoretical values and we also compute the relative error between the eigenvalues of the two cases.  $\Delta f_i = \frac{f_i^4 - f_i^1}{f_i^4} \times 100$ .

The maximum relative error  $\Delta f_i$  between the eigenvalues of the different cases is less than  $5 \times 10^{-2}\%$  proving that the junction technique gives good results.

### Non-conforming meshes case

We conclude this example by illustrating the flexibility of our implementation of junction. We consider a non-conforming meshing discretization of the plate. The plate is still decomposed into a  $2 \times 2$  patches and the sub-plates located at the bottom-left and upper-right have 8405 degrees of freedom while the other two sub-plates have 2205 degrees of freedom. The total number of degrees of freedom is 21220 and finally 20894 after taking into account the junction conditions. Table 3.4 shows the values of the eigenvalues and the relative errors  $r_i^4$  in respect to the exact eigenvalues. One remarks that while gaining a flexibility in one hand, the drawback on the other hand is the lost of accuracy on the double eigenvalues 10th and 11th, which are not equal.

$N^o$	$f_i^A$ (Hz)	$r_i^A$ (%)
7	10.440	0.134
8	15.21	0.822
9	18.823	0.577
10	27.062	0.284
11	27.065	0.273

Table 3.4 Eigenvalues and errors corresponding to the nonconforming meshing of the  $2 \times 2$  decomposition of the plate.

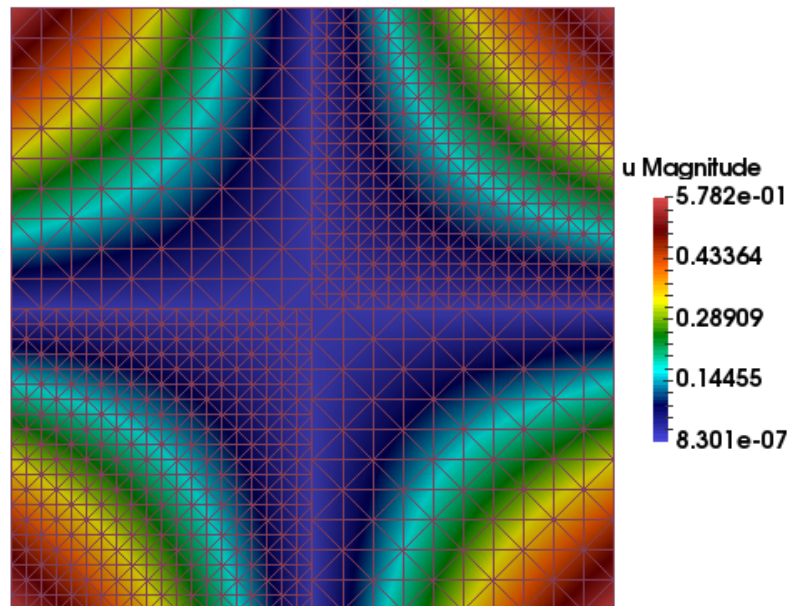


Figure 3.7 7th frequency corresponding to the nonconforming discretization of the  $2 \times 2$ -plate.

We remark that we have gained some accuracy in the computed eighth frequency to the detriment of the other frequencies. However the maximum value of the relative error is less than 0.82% (better than 0.85% in the previous case of conforming meshings). Figure 3.7 shows the magnitude of the displacement field corresponding to the seventh eigenfrequency and the representation of the physical mesh on the plate.

### 3.3.2 Vibration frequencies of a 3D L-plate

We now consider a L-plate composed of two unit square plate-shells joined orthogonally and *non-coplanar*. The structure is free and made of the same isotropic material as in the previous example. The validation is made by comparing the computed eigenfrequencies with some references ones

given in [39] and obtained with the Code-Aster (an open FEA software developed by Électricité de France - EDF).

The analysis was performed using a mesh with 1089 nodes and 2048 elements. The total number of degrees of freedom is 41990. The first six deformation corresponding to the rigid body motion are plotted on Figure 3.8.

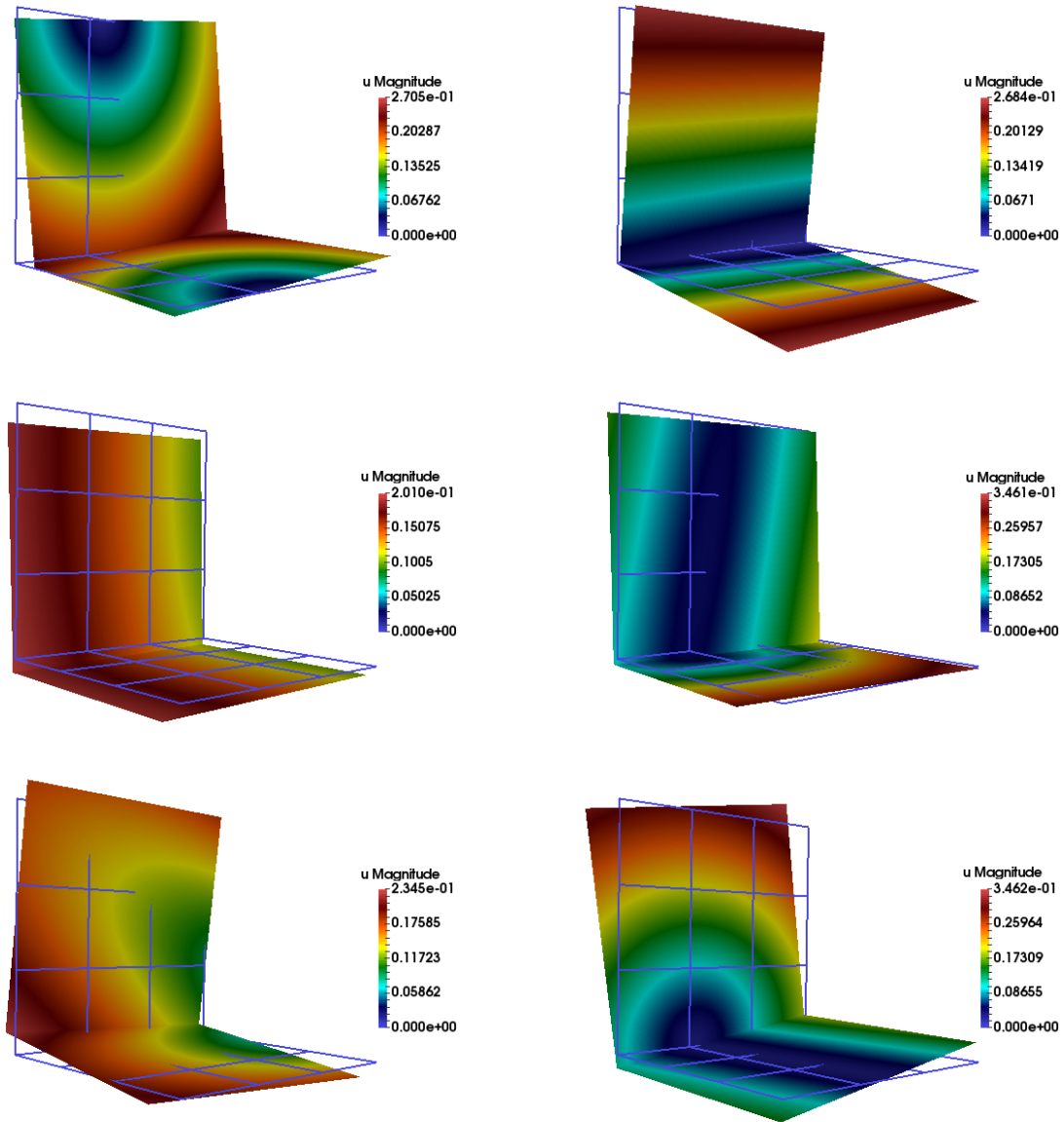
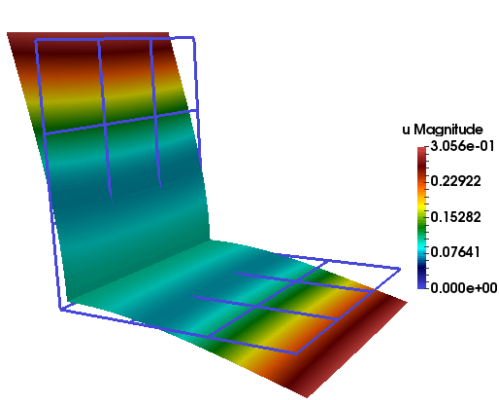
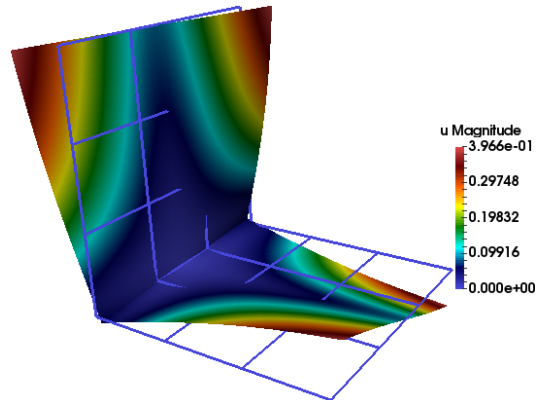


Figure 3.8 Representation of the first six eigenmodes of deformation of the L-plate.

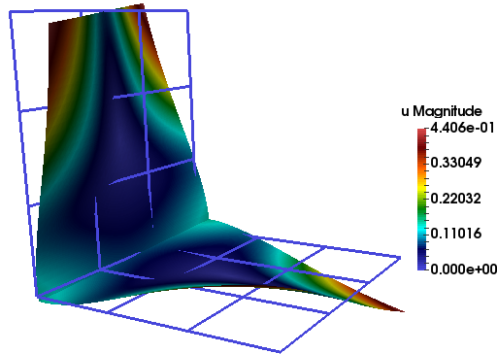
And the following first six non rigid modes are plotted in Figure 3.9.



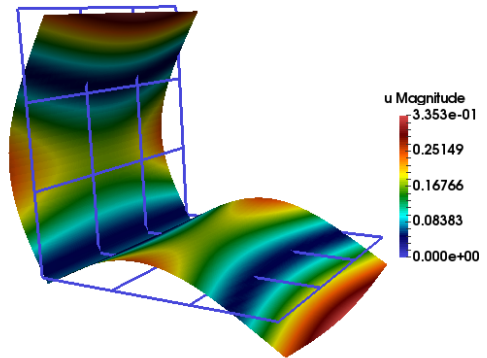
3.9.a – 7th eigenvector deformation



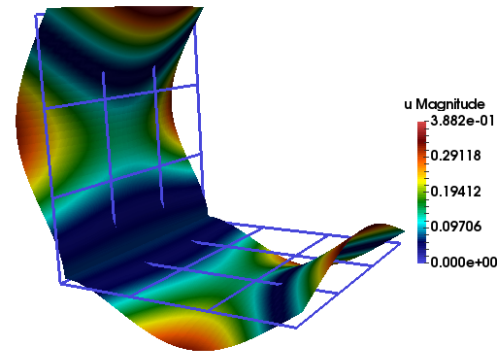
3.9.b – 8th eigenvector deformation



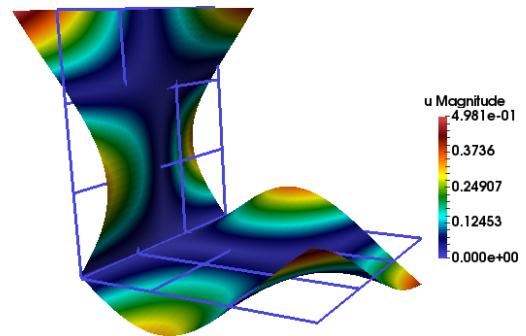
3.9.c – 9th eigenvector deformation



3.9.d – 10th eigenvector deformation



3.9.e – 11th eigenvector deformation



3.9.f – 12th eigenvector deformation

Figure 3.9 Representation of the first six eigenvectors of deformation corresponding to the free L-plate.

The values of the first six eigenvalues of deformation are given in Table 3.5. The reference values used are computed with 79056 degrees of freedom. The notations  $f_i^2$ ,  $f_i^{ast}$  and  $r_i^2$  stand respectively for the computed eigenvalues with the two orthogonal plates, the Code Aster reference

values and the percentage of relative error  $r_i^2 = \frac{f_i^{ast} - f_i^2}{f_i^{ast}} \times 100$ .

$N^o$	$f_i^2$ (Hz)	$f_i^{ast}$ (Hz)	$r_i^2$ (%)
7	3.227	3.224	-0.093
8	5.527	5.526	-0.018
9	7.525	7.503	-0.293
10	12.224	12.216	-0.065
11	17.649	17.614	-0.199
12	19.924	19.85	-0.373

Table 3.5 Comparison of the computed eigenvalues corresponding to free-L-plate with the reference eigenvalues computed with the Code-Aster software.

The computed frequencies are acceptable. Indeed, the maximum of relative error is  $\simeq 0.3\%$ .

### 3.3.3 Frequency analysis of a cylindrical shell

We consider a cylindrical shell with the following geometric and material characteristics

$$R = 0.3\text{m}, H = 0.6\text{m}, \nu = 0.3, E = 3 \times 10^6 \text{ MPa and } \rho = 7.3 \text{ kg/m}^3.$$

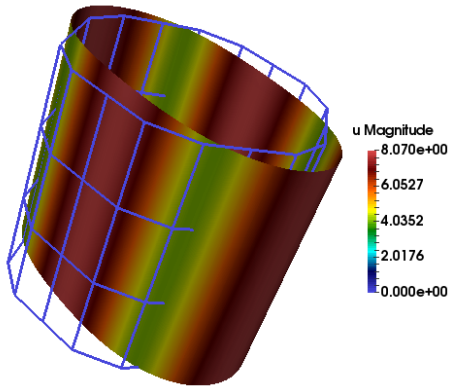
Here also, we compare the computed eigenvalues with those found with Code Aster. The values of the eigenfrequencies are reported in Table 3.6. We remark that the errors are relatively small (less than 2.5%).

$N^o$	$f_i$ (Hz)	$f_i^{ast}$ (Hz)	$r_i$ (%)
1	$1.66 \times 10^{-5}$	-	-
2	$1.11 \times 10^{-2}$	-	-
3	$1.11 \times 10^{-2}$	-	-
4	$3.43 \times 10^{-2}$	-	-
5	$1.72 \times 10^{-1}$	-	-
6	$1.72 \times 10^{-1}$	-	-
7	2.7679	2.7523	-0.569
8	2.7679	2.7523	-0.568
9	3.7712	3.6815	-2.437
10	3.7712	3.6816	-2.435
11	7.8116	7.7846	-0.347
12	7.8560	7.7846	-0.917

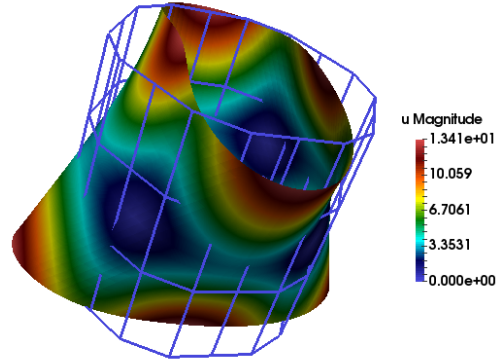
Table 3.6 Eigenvalues corresponding to a free cylindrical shell and the relative errors with respect to the reference values.

We emphasize that the rigid body motion eigenvalues are not exactly zero. This is one of the drawbacks of the  $C^0$  finite element, which needs a very fine mesh for convergence. Figure 3.10 shows the first four non rigid body modes.

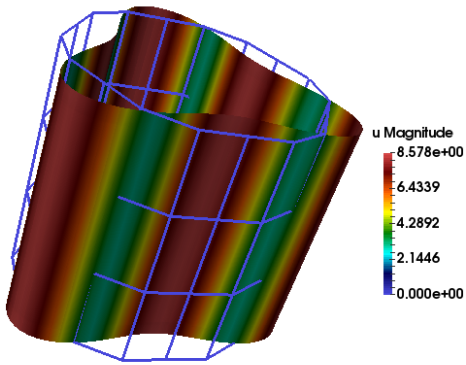




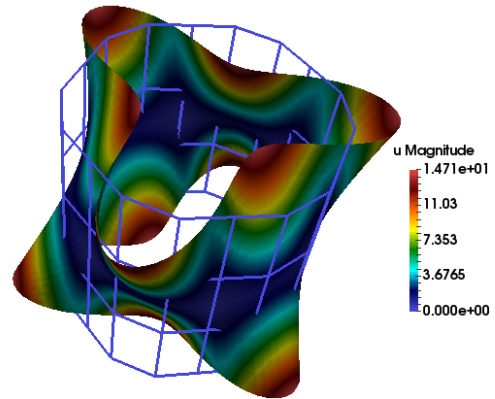
3.10.a – 7-8th eigenvector deformation



3.10.b – 9-10th eigenvector deformation



3.10.c – 11-12th eigenvector deformation

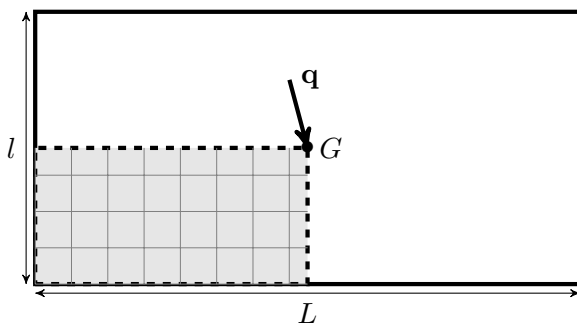


3.10.d – 13-14th eigenvector deformation

Figure 3.10 Representation of the first four non rigid body modes.

### 3.3.4 Rectangular plate under pointwise load

Now we consider a rectangular plate benchmark, as described in [49]. The geometric and material characteristics of the plate are described on Figure 3.11.



$$\begin{aligned}
 L &= l = 2 \\
 E &= 1.7472 \times 10^7, \nu = 0.3 \\
 \rho &= 1, t = 10^{-2} \\
 \mathbf{q} &= 4 \times 10^{-4} \mathbf{a}_3.
 \end{aligned}$$

Figure 3.11 Geometric and material characteristics of the plate



The validation is based on the reference value of displacement amplitude at the center of the plate which is  $u_G = 5.60 \times 10^{-6}$ . For symmetry reasons, we consider in our simulation only the quarter of the plate, and the load is  $\frac{q}{4}$ . The displacement field magnitude of the plate is plotted on Figure 3.12. The number of elements and nodes are respectively 512 and 289, and the total number of degrees of freedom 21125.

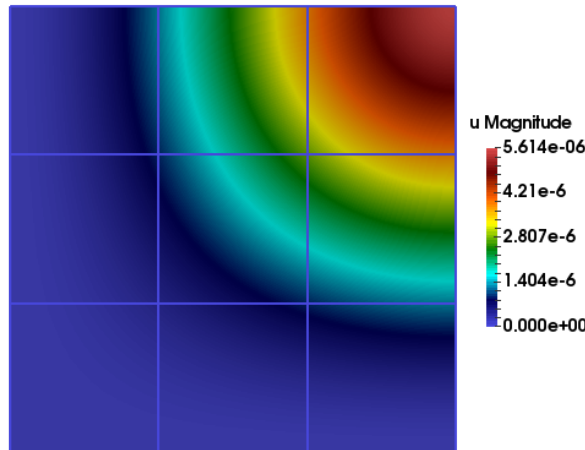


Figure 3.12 Displacement field corresponding to the plate under concentrated load and the control polygon associated to the shape mapping

Table 3.7 shows the relative error on the third component of the displacement, at  $G$ , in the case of one patch and four patches.

1 patch			$2 \times 2$ patches		
$ddl_s$	$u_G^1 (\times 10^{-6})$	$r^1 (\%)$	$ddl_s$	$u_G^4 (\times 10^{-6})$	$r^4 (\%)$
245	1.00	82.074	-	-	-
405	2.32	58.530	980	4.29	23.476
1445	5.02	10.287	1620	5.03	10.205
5445	5.54	1.101	5780	5.55	0.975
21125 <sup>a</sup>	5.61	-0.159	21780	5.62	-0.370

Table 3.7 Relative errors on the vertical component of displacements.  $u_G^n$  represents the third component of the displacement computed with  $n$  patches and  $r^n = \frac{u_G - u_G^n}{u_G} \times 100$  is the relative error

Figure 3.13 shows the variation of  $u_G^1$  with respect to the number of degrees of freedom.

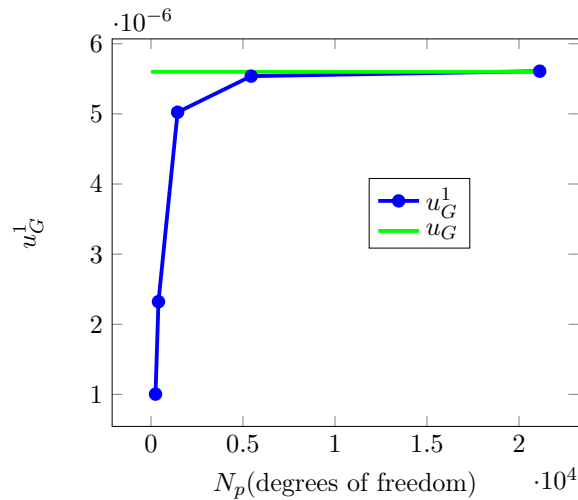


Figure 3.13 Convergence of the displacement vertical component. The reference value  $u_G$  is plotted in green and the values  $u_G^1$  in blue

### Non-conforming case

We also perform the same analysis with taking into account for a geometric decomposition and non-conforming meshings. We assume that the plate is decomposed into a  $2 \times 2$  square plates. The plate which contains the point supporting the concentrated load has a finest mesh. We consider the following case of local refinement: the finest mesh over the plate supporting the concentrated load is left fixed and the meshings associated the other three plates are refined. Table 3.8 shows the relative errors with respect to the total number of DOFs. One remarks that with only 9780 DOFs, one attains an acceptable relative error of 0.032%, which is surprisingly better than the relative error for a uniformly refined mesh with only one patch and 21125 DOFs.

$2 \times 2$ patches		
$ddl_s$	$u_G^1 (\times 10^{-6})$	$r^4 (\%)$
5820	4.04	27.914
6180	5.08	9.361
6660	5.40	3.625
9780	5.60	0.032

Table 3.8 Relative errors on the vertical component of displacement. The number of degrees of freedom of the plate with the fixed finest mesh is 5445

One draws that the local refinement allows to set the meshing optimally and obtain a good approximation in regards to the reference solution, through using a minimal number of DOFs.

The displacement field magnitude corresponding to this analysis is plotted on Figure 3.14. The physical mesh is plotted on the same figure.

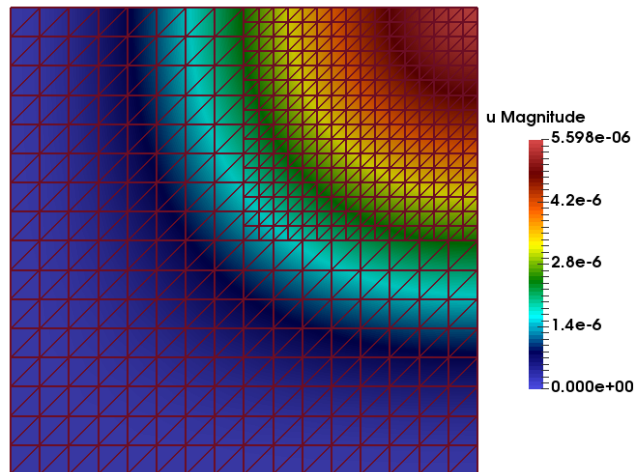


Figure 3.14 Displacement field with local refinement with a fixed finest mesh for the sub-plate supporting the concentrated load. The total number of DOFs is 9780

#### Local discretization error

We close this section by considering the study of the local discretization error in case of junction. We consider as reference solution the one corresponding to the finest discretization, obtained using one mapping and discretized with 21125 degrees of freedom, see Table 3.7. We perform the analysis for a  $2 \times 2$  geometric decomposition. Let  $u_h^l$  denoted the approximated displacement for the  $l$ -th level of refinement and  $u_h^r$  be the reference solution obtained with the finest mesh.

$i$	$ u_h^i - u_h^r _1$	$\ u_h^i - u_h^r\ _0$
1	$3.73 \times 10^{-7}$	$1.55 \times 10^{-8}$
2	$2.97 \times 10^{-7}$	$1.05 \times 10^{-8}$
3	$2.95 \times 10^{-7}$	$2.24 \times 10^{-8}$
4	$1.02 \times 10^{-7}$	$2.55 \times 10^{-9}$
5	$0.84 \times 10^{-7}$	$1.18 \times 10^{-10}$

a – Error corresponding to the first patch

$i$	$ u_h^i - u_h^r _1$	$\ u_h^i - u_h^r\ _0$
1	$5.73 \times 10^{-7}$	$9.28 \times 10^{-8}$
2	$4.39 \times 10^{-7}$	$6.43 \times 10^{-8}$
3	$3.91 \times 10^{-7}$	$4.73 \times 10^{-8}$
4	$1.47 \times 10^{-7}$	$4.60 \times 10^{-9}$
5	$0.85 \times 10^{-7}$	$7.66 \times 10^{-10}$

c – Error corresponding to the third patch

$i$	$ u_h^i - u_h^r _1$	$\ u_h^i - u_h^r\ _0$
1	$12.95 \times 10^{-7}$	$35.56 \times 10^{-8}$
2	$10.88 \times 10^{-7}$	$24.44 \times 10^{-8}$
3	$8.92 \times 10^{-7}$	$15.98 \times 10^{-8}$
4	$3.10 \times 10^{-7}$	$13.70 \times 10^{-9}$
5	$1.16 \times 10^{-7}$	$37.88 \times 10^{-10}$

d – Error corresponding to the fourth patch

Table 3.9 Discretization errors local to each patch.  $| \cdot |_1$  stands for the strain energy semi norm and  $\| \cdot \|_0$  for the standard  $L_2$ -norm

One remarks on the Table 3.9 that the local discretization errors of the patches of indexes 1 and 3 are similar. In fact the mechanical problems in these patches are the same: they both have the clamping and symmetry boundary conditions and are unloaded. The global discretization errors (sum of the local errors) are reported on Table 3.10.

$N^o$	$ u - u _1$	$L_2$
1	$1.57 \times 10^{-6}$	$37.94 \times 10^{-8}$
2	$1.28 \times 10^{-6}$	$26.04 \times 10^{-8}$
3	$1.09 \times 10^{-6}$	$17.47 \times 10^{-8}$
4	$0.39 \times 10^{-6}$	$1.54 \times 10^{-8}$
5	$0.19 \times 10^{-6}$	$0.39 \times 10^{-8}$

Table 3.10 Global discretization error

Figure 3.15 illustrates the variation of the error as the mesh refinement is performed. One remarks that the global discretization error diminishes.

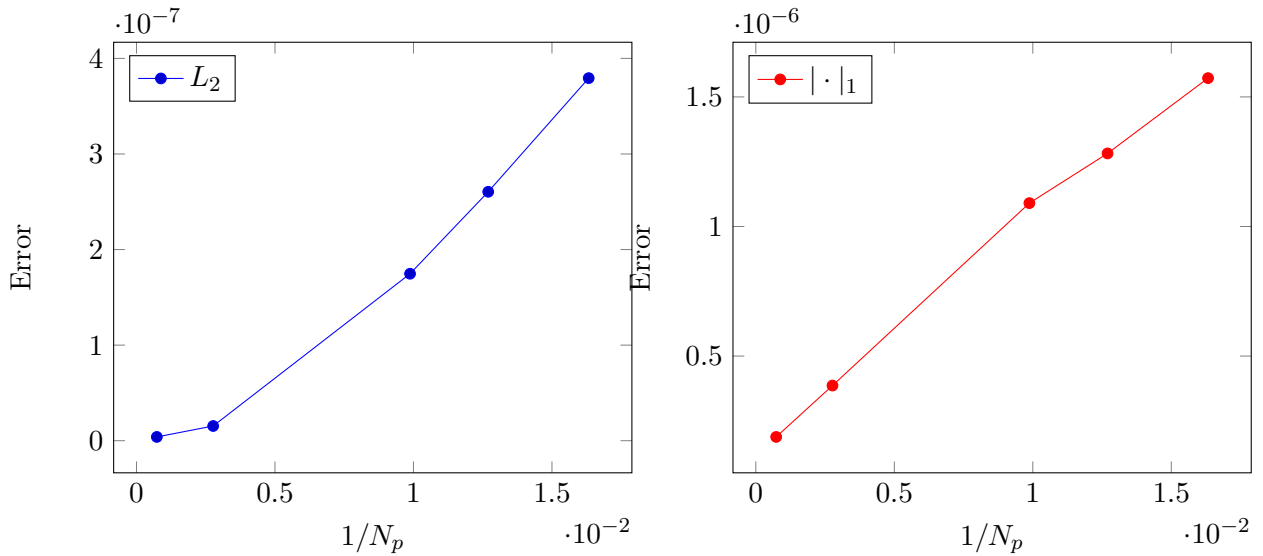


Figure 3.15 Global discretization error

### 3.4 Synthesis

In this chapter, we have discussed the junction for Naghdi shell structures. The junction involves the continuity of displacement and tangential rotation fields. The finite element used for the discretisation of the classical mono shell problem is a Lagrange one. In this case of junction, the continuity or matching conditions have been weakly enforced in the variational space as well as in the discrete space using the mortar technique. The approach involves the choice of an appropriate space of functions against which the continuities are stated. We have made the standard choice of defining the mortar space as the trace space associated to the discretization of the non-mortar side. The proved interest of the method, through the numerical results, is its suitability which allows to mesh each domain independently and thus using nonconforming meshes.

The numerical results have been shown in the case of conforming geometric assembling and finite element discretization. A perspective from the finite element approximation point of view can be the coupling of different orders of Lagrange finite elements. Regarding the geometry, the extension to the assembling of shells defined through mappings of different degrees can be investigated, but is complex since it involves many tricky points. For instance the definition of the interface, the careful computation of the intersections of elements along the interface, the ensuring of the coherence of the integration quadrature points from side to side for the definition of the mortar conditions.

## Part II

# Anisotropy and shape optimal design



# Anisotropy properties and material optimization

---

## Contents

---

<b>4.1</b>	<b>Introduction</b>	<b>69</b>
<b>4.2</b>	<b>The polar formalism</b>	<b>71</b>
4.2.1	Polar formalism representation	71
4.2.2	Constraints on the parameters	73
<b>4.3</b>	<b>Parametrization tailored to the polar formalism</b>	<b>74</b>
4.3.1	Conformal parameterization	77
4.3.2	Direct parameterization	78
<b>4.4</b>	<b>Formulation of the optimization problem</b>	<b>81</b>
4.4.1	Design parameters	82
4.4.2	Derivatives with respect to the polar parameters	82
4.4.2.1	Derivatives of the compliance	83
4.4.2.2	Derivatives of the stiffness	83
<b>4.5</b>	<b>Numerical Results</b>	<b>84</b>
4.5.1	Plate under two in-plane concentrated loads	86
4.5.2	Anisotropy design of a cantilever	90
4.5.3	Cylinder shell under torsional load	94
4.5.4	Anisotropy design of a plate submitted to torsion	97
<b>4.6</b>	<b>Synthesis</b>	<b>99</b>

---

## 4.1 Introduction

The optimization of distributed, i.e. locally varying, material properties is an interesting challenge for modern structure design. Such type of structures can today be manufactured using numerically controlled machines for the deposition of reinforcing fibers in an isotropic matrix. Anisotropic laminates having elastic properties varying point-wise can so be realized. The possibility of tailoring locally the elastic properties gives new interesting possibilities or flexibilities to designers, who, in turn, need effective mathematical methods for the design of the optimal elastic fields. In practice, one or more elastic tensor fields  $\mathbb{E}(x)$  are to be designed over a structure  $\Omega$ .



To this purpose, we propose here a new method to formulate problems concerning the optimal distribution of material properties for anisotropic plates and shells with given geometry.

Assume that  $\Omega$  is submitted to a system of loads  $\mathbf{f}$ , the optimization problem dealt with in this chapter can be stated as follows:

PROBLEM 4.1.1 Find an optimal elastic tensor field  $\mathbb{E}^* : x \in \Omega \mapsto \mathbb{E}^*(x)$  such that

$$\mathbb{E}^* = \arg \min J(\mathbb{E}), \quad J \text{ is the compliance } J(\mathbb{E}) := \int_{\Omega} \mathbf{f} \cdot \mathbf{u} \, d\Omega$$

where  $\mathbf{u}$  is solution of a state equation.

For static problems, this last is the equation of equilibrium that can be given in a variational form as

$$\int_{\Omega} \epsilon(\mathbf{v}) : \mathbb{E} : \epsilon(\mathbf{u}) \, dx = \int_{\Omega} \mathbf{f} \cdot \mathbf{v} \, d\Omega, \quad \text{for all } \mathbf{v} \in \mathcal{V},$$

where:

- $\mathcal{V}$  is an appropriate functional vector space tuned to take into account for the boundary conditions
- $\epsilon$  is the symmetric linearized strain tensor.

In structural analysis, the variational problem is commonly solved by the Finite Element Method. The problem is discretized through a mesh  $\Omega_h$  of the structure,  $h$  being a mesh parameter. Within this framework, the discretization of the material properties is generally based on the Finite Element mesh and the material properties defined as constant per element, see [20], [38], [50].

This technique does not yield to a convenient discretization for the structural optimization problem 4.1.1 and has serious shortcomings: the number of design variables (DV) is mesh-dependent and can be of thousands; and the elastic properties (mainly the fiber orientations) are not continuous.

Also, the value of the elastic variables cannot be free: for a single-layer structure, the elastic moduli must respect some bounds on the elastic constraints, see [44], imposed by the positiveness of the work done by the applied forces. For a laminate, the elastic variables must satisfy similar but more restrictive bounds [68], called “geometrical bounds”. These bounds correspond to the impossibility of realizing, by a laminate, all the admissible combinations of the values of the elastic moduli.

It is apparent that if such a kind of discretization is adopted for the structural design, the optimization problem will have a large, sometimes huge, number of DV and constraints. Hence it should be interesting to formulate the optimization problem using a different discretization of the anisotropic elastic fields, so as to reduce the number of DV and constraints, though still using a Finite Element Discretization (as fine as needed) for the structural analysis.

To such a purpose, in this chapter, we propose an approach based on one side on the polar formalism for the representation of the elastic tensor and, on the other side, on the parameterization of the polar parameters fields by means of B-spline functions. This allows a drastic reduction of the number of DV that are reduced to just the parameters of the B-spline and, most important, to use a unique set of elastic or geometric constraints for the polar parameters instead of a set for each finite element.

Some recent papers [51], [75], concerning variable angle tow, and elastic properties design, discuss parameterization of elastic properties with B-spline functions. The first is based on the polar formalism and concerns the case of multi-scale level optimization of laminates. The considered criteria for both papers is the first buckling load. In this chapter, we discuss the parameterization problem of the elastic tensor and highlight the relevant B-spline properties which allow to have an efficient parameterization and sufficient finite set of constraint for optimization problem. We propose two parameterizations: one that we call *conformal* in regards to the constraints to be respected. In that case all the power functions, which appear in the constraint, are approximated with B-spline functions of the same orders and basis functions. The second case is called *direct parameterization* and is conformal with respect to the parameterized fields, namely the polar moduli. In this case the parameterization concerns directly the polar parameters fields and not their power functions intervening in the constraints. These polar moduli are still parameterized using B-spline functions of the same orders and basis functions.

The chapter is organized as follows:

- in Section 4.2, we recall the essentials of the polar formalism
- in Section 4.3, we detail the representation of the polar parameters fields by B-spline functions and the sufficient conditions on the control parameters. We distinguish two kinds of parameterization, and discuss a B-spline flexibility helping to ensure a good exploration of the admissible space
- section 4.4 is dedicated to the formalization of optimal problems for anisotropic structures with locally varying properties. The considered criterion is the compliance
- finally, Section 4.5 contains some examples showing the effectiveness of the method.

## 4.2 The polar formalism

An anisotropic material has elastic properties changing with the direction. Such properties are expressed by the elastic tensor. The main goal when designing such material is to set up the optimal distribution of the elastic properties. In optimal design of anisotropy, it is suitable to make use of the polar formalism, introduced by Verchery [72] in 1979, to represent the elastic tensor using just invariants and angles. This formalism allows to easily represent rotations and the constraints on the design variables (polar parameters) due to the mutual dependence of the elastic coefficients.

Moreover, the polar formalism allows to split the elastic tensor into its isotropic and anisotropic parts; hence it offers the possibility to target and explicitly tune the anisotropy. More details on the polar formalism can be found in [66], [68], and [71]. This formalism has successfully been applied to different plane anisotropy problems, see e.g. [20], [52].

### 4.2.1 Polar formalism representation

For a second order symmetric tensor

$$\mathbf{L} = \begin{pmatrix} L^{11} & L^{12} \\ L^{12} & L^{22} \end{pmatrix},$$

the polar parameters  $T, R, \Phi$  are defined by:

$$\begin{aligned}
 T &= \frac{1}{2} \text{tr}(\mathbf{L}) = \frac{1}{2}(L^{11} + L^{22}) \\
 R &= \sqrt{\left(\frac{L^{11} - L^{22}}{2}\right)^2 + (L^{12})^2} \implies \begin{aligned} L^{11} &= T + R \cos 2\Phi \\ L^{12} &= R \sin 2\Phi \\ L^{22} &= T - R \cos 2\Phi \end{aligned} \\
 \tan 2\Phi &= \frac{2L^{12}}{L^{11} - L^{22}}
 \end{aligned} \tag{4.1}$$

$T$  and  $R$  are invariants;  $T$  represents the spherical part and  $R$  the deviatoric one. The parameter  $\Phi$  is an angle whose choice fixes the frame.

Now, assume that  $\mathbb{E}$  is the plane elastic tensor in the material frame  $(\mathbf{m}_1, \mathbf{m}_2)$  and let  $\mathbb{E}^p$  be its representing matrix

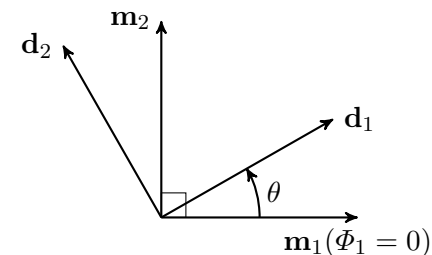
$$\mathbb{E}^p = \begin{pmatrix} E^{1111} & E^{1122} & E^{1112} \\ E^{1122} & E^{2222} & E^{2212} \\ E^{1112} & E^{2212} & E^{1212} \end{pmatrix}.$$

The independent elastic coefficients  $E^{\alpha\beta\lambda\mu}$  are expressed in the polar formalism as:

$$\begin{cases} E^{1111} = T_0 + 2T_1 + R_0 \cos 4\Phi_0 + 4R_1 \cos 2\Phi_1. \\ E^{1112} = R_0 \sin 4\Phi_0 + 2R_1 \sin 2\Phi_1. \\ E^{1122} = -T_0 + 2T_1 - R_0 \cos 4\Phi_0. \\ E^{1212} = T_0 - R_0 \cos 4\Phi_0. \\ E^{1222} = -R_0 \sin 4\Phi_0 + 2R_1 \sin 2\Phi_1. \\ E^{2222} = T_0 + 2T_1 + R_0 \cos 4\Phi_0 - 4R_1 \cos 2\Phi_1. \end{cases} \tag{4.2}$$

where  $T_0, T_1$  are the isotropy invariants and  $R_0, R_1, \Phi_0 - \Phi_1$  are the invariants of the anisotropic part. The choice of one of the two polar angles fixes the frame. As  $\Phi_0 - \Phi_1$  is an invariant, choosing  $\Phi_0$  or  $\Phi_1$  corresponds to choose a frame and to fix the value of the other angle. Usually, the axis  $\mathbf{m}_1$  is set in the direction of the highest elastic modulus  $E^{1111}$ , so that  $\Phi_1 = 0$ .

This formalism is also convenient to compute the elastic tensor in a rotated frame. Let us consider  $(\mathbf{d}_1, \mathbf{d}_2)$  a basis obtained by a counter clockwise rotation through an angle  $\theta$ .

$$\begin{aligned}
 \mathbf{d}_1 &= \cos \theta \mathbf{m}_1 + \sin \theta \mathbf{m}_2 \\
 \mathbf{d}_2 &= -\sin \theta \mathbf{m}_1 + \cos \theta \mathbf{m}_2
 \end{aligned} \tag{4.3}$$


The components  $E^{\alpha\beta\lambda\mu}(\theta)$ , of  $\mathbb{E}$  in the frame  $(\mathbf{d}_1, \mathbf{d}_2)$ , are obtained by changing  $\Phi_\alpha$  into  $\Phi_\alpha - \theta, \alpha \in \{0, 1\}$  in Equation (4.2).

It can be shown, see [66], that the polar invariants are linked to the elastic symmetries. In particular, ordinary orthotropy corresponds to the condition

$$\Phi_0 - \Phi_1 = K \frac{\pi}{4}; \quad K = 0, 1. \tag{4.4}$$

The value of  $K$  is very important in optimization problems; in fact, it has been seen in several cases [67] that changing  $K$  from 0 to 1 or vice-versa transforms an optimal solution into an anti-optimal one (i.e the best to the worst). If we fix the frame choosing  $\Phi_1 = 0$ , then  $\Phi_0 = K\frac{\pi}{4}$ , so, for an orthotropic layer, we have:

$$\begin{cases} E^{1111}(\theta) &= T_0 + 2T_1 + R_0^K \cos 4\theta + 4R_1 \cos 2\theta \\ E^{1112}(\theta) &= -R_0^K \sin 4\theta - 2R_1 \sin 2\theta \\ E^{1122}(\theta) &= -T_0 + 2T_1 - R_0^K \cos 4\theta \\ E^{1212}(\theta) &= T_0 - R_0^K \cos 4\theta \\ E^{1222}(\theta) &= R_0^K \sin 4\theta - 2R_1 \sin 2\theta \\ E^{2222}(\theta) &= T_0 + 2T_1 + R_0^K \cos 4\theta - 4R_1 \cos 2\theta \end{cases} \quad (4.5)$$

with  $R_0^K = (-1)^K R_0$ .

Two other special orthotropies exist: square symmetry (i.e of elastic properties periodic of  $\frac{\pi}{2}$ ), corresponding to the condition  $R_1 = 0$  and  $R_0$ -orthotropy, corresponding to  $R_0 = 0$ . For more details on this subject, the reader is referred to [65], [66].

REMARK 4.2.1 To summarize, in the polar formalism, the following six parameters define the elastic tensor in any frame:

- two isotropic invariants  $T_0, T_1$ ;
- three anisotropic invariants  $R_0, R_1, \Phi_0 - \Phi_1$ . For ordinarily orthotropic layers, these can be replaced by the two quantities  $R_0^K$  and  $R_1$ , still representing the three invariants
- the angle  $\Phi_1$  fixing the frame.

For the case considered in the following, that of orthotropic tensors, a further reduction is possible using the variable  $R_0^K$ : in the end, the only DV are  $R_0^K, R_1$  and  $\Phi_1$ ; the sign of  $R_0^K$  gives the value of  $K$ , i.e the type of orthotropy. We finally remark that isotropy corresponds to  $R_0 = R_1 = 0$ .

REMARK 4.2.2 (Reduction of the number of DV)

Let us consider the particular case of a laminate composed by identical layers of polar parameters  $T_0^L, T_1^L, R_0^L, R_1^L, \Phi_0^L, \Phi_1^L$ , and let  $T_0, T_1, R_0, R_1, \Phi_0, \Phi_1$  be the polar parameters of the laminate. It has been shown in the [70] that for laminates with identical layers it is:

$$\begin{aligned} T_0 &= T_0^L, \\ T_1 &= T_1^L. \end{aligned} \quad (4.6)$$

Hence, in design problems where the basic material is chosen (i.e the constituents are chosen for each layer and remain constant everywhere in  $\Omega$ )  $T_0$  and  $T_1$  cannot be modified, they are no more DV. This is a real advantage given by the use of the polar formalism: the number of unknown is reduced from six to four:  $R_0, R_1, \Phi_0 - \Phi_1$  and  $\Phi_1$ ; this last fixing the orientation. In the particular case of ordinary orthotropic material they are just three  $R_0^K, R_1, \Phi_1$ , as said above.

### 4.2.2 Constraints on the parameters

The elastic moduli are submitted to two types of constraints:

- Elastic constraints, see [69], resulting from the positive definiteness of the matrix  $\mathbb{E}^P$ :

$$\begin{aligned} T_1[T_0 + R_0^K] &> 2R_1^2 \\ T_0 &> |R_0^K| \\ R_1 &\geq 0 \end{aligned} \tag{4.7}$$

- Geometric constraints: it can be shown, see [68], that laminates composed by identical layers cannot realize all the possible combinations of the values of the elastic moduli. We could say, in some words, that laminates form a “more restricted” elastic class. Mathematically speaking, this corresponds to the fact that the bounds of the laminate elastic tensors are not (4.7) but some other more restrictive ones. For laminates composed by identical layers, the elastic tensors for extension and bending are respectively

$$\begin{aligned} \mathbb{A} &= \frac{1}{h} \int_{-\frac{t}{2}}^{\frac{t}{2}} \mathbb{E} dz \\ \mathbb{D} &= \frac{12}{h^3} \int_{-\frac{t}{2}}^{\frac{t}{2}} z^2 \mathbb{E} dz \end{aligned} \tag{4.8}$$

where  $t$  is the laminate thickness and  $z$  the vertical coordinate, with  $z = 0$  corresponding to the location of the mid-surface of the laminate.

Then it can be shown, see [68], that for  $\mathbb{A}$  and  $\mathbb{D}$ , bounds (4.7) must be replaced by other constraints called the geometric bounds that for ordinary orthotropy are:

$$\begin{aligned} 2 \left( \frac{R_1}{R_1^L} \right)^2 - 1 &\leq \frac{R_0^K}{R_0^{KL}}, \\ R_0^K &\leq R_0^L, \\ R_1 &\leq R_1^L. \end{aligned} \tag{4.9}$$

Since equation (4.9) is more restrictive than (4.7), when the problem concerns the design of a laminated structure, eq. (4.7) must be replaced by eq. (4.9), otherwise, one could obtain some values for the components of  $\mathbb{A}$  or  $\mathbb{D}$  that cannot be realized in practice through a laminate composed by identical plies.

### 4.3 Parametrization tailored to the polar formalism

We assume the elastic tensor field to be designed under the form of B-spline functions; the question is then to define a set of constraints on the control points of the B-spline which ensure that the inequalities (4.7) or (4.9) are satisfied pointwise. Two parameterizations for  $R_1$  are relevant:

- a conformal parameterization:  $R_1$  is parametrized as the square root of a positive B-spline; the interest of this change of variable is to simplify the constraints (4.7), (4.9) which become linear. The drawback is that the elastic coefficients and the constraints are no more differentiable at  $R_1 = 0$ ;

### 4.3. Parametrization tailored to the polar formalism

---

- a direct parametrization:  $R_1$  is parameterized by a B-spline but –see Propostion 4.3.4– the constraints on the control points depend on the number of control points. However it offers the advantage to make the elasticity tensor differentiable with respect to the control points of the polar parameters.

The main results of this Section, given in the Propositions 4.3.2 , 4.3.3 and 4.3.4, are direct consequences of the following definition of a B-spline.

DEFINITION 4.3.1 (B-spline curve) Let  $\mathcal{K} = (\xi_j)_{j=0}^{n+d}$  be a non decreasing sequence of real numbers such that  $\xi_0 = 0$  and  $\xi_{n+d} = 1$ ,

1. the  $j$ -th B-spline basis function of degree  $d$  (or order  $d + 1$ ) is the numerical mapping  $N_d^j$  defined recursively as follows: for  $1 \leq k \leq d$  and  $0 \leq j \leq n + d - (k + 1)$

$$N_k^j(\xi) = \omega_{j,d}(\xi)N_{k-1}^j(\xi) + (1 - \omega_{j+1,d}(\xi))N_{k-1}^{j+1}(\xi), \quad (4.10)$$

where

- $N_0^j(\xi) = \begin{cases} 1 & \text{if } \xi_j < \xi < \xi_{j+1} \\ 0 & \text{elsewhere} \end{cases}$  , for  $0 \leq j \leq n + d - 1$  starts the recurrence
- $\omega_{j,k}$  is defined by

$$\xi \mapsto \omega_{j,k}(\xi) = \begin{cases} \frac{\xi - \xi_j}{\xi_j - \xi_{j+k}} & \text{if } \xi_j \leq \xi \leq \xi_{j+k}, \\ 0 & \text{otherwise .} \end{cases}$$

In the above definition of  $\omega_{j,k}$ , it is adopted the convention  $\frac{0}{0} = 1$ .

2. A B-spline of degree  $d$  is a numerical mapping  $C$  which is in the  $n$ -dimensional space  $Sp(\mathcal{K}, d)$  spanned by the set of functions  $N_d(\mathcal{K}) := \left(N_d^j\right)_{j=0}^{n-1}$ .
3. The coordinates  $p_j$  of  $C \in Sp(\mathcal{K}, d)$ , in this basis, are called control points of the B-spline  $C$ ; in other words, a B-spline is written as

$$C(\xi) = \sum_{j=0}^{n-1} N_d^j(\xi)p_j \quad \text{for } \xi \in \mathbb{R}. \quad (4.11)$$

We define in the following Remarks some commonly used terminology.

REMARKS 4.3.1 1) The set  $\mathcal{K}$  will be called knot vector of the B-spline and the number  $n_c$  of control points of a given B-spline is linked to its degree  $d$  by

$$\text{card}(\mathcal{K}) = n_c + d + 1 \implies n_c = n.$$

- 2) The distinct knots are called break-points. A break-point  $\xi$  is said of multiplicity  $m$  if there exists an index  $j$  and there are  $m$  knots  $\xi_{j+k} \in \mathcal{K}$  ( $0 \leq k \leq m - 1$ ) such that  $\xi_j = \xi_{j+1} = \dots = \xi_{j+m-1} = \xi$ . A break-point is said of full multiplicity if its multiplicity order is equal to the B-spline order  $d + 1$ .

## Chapter 4. Anisotropy properties and material optimization

EXAMPLE 4.3.1 If the knot vector  $\mathcal{K}$  is  $\{0, 0, 0, 0, 1, 1, 1, 1\}$  and  $d = 3$ , the restriction to  $[0, 1]$  of the basis functions of  $Sp(\mathcal{K}, d)$  are the polynomials

$$N_3^0(\xi) = (1 - \xi)^3 \quad N_3^1(\xi) = 3(1 - \xi)^2\xi \quad N_3^2(\xi) = 3(1 - \xi)\xi^2 \quad N_3^3(\xi) = \xi^3$$

In this case 0 and 1 are break-points of full multiplicities, the generic B-spline

$$C(\xi) = \sum_{i=0}^3 p_i N_3^i(\xi)$$

satisfies  $C(0) = p_0$  and  $C(1) = p_3$  and is called clamped B-spline.

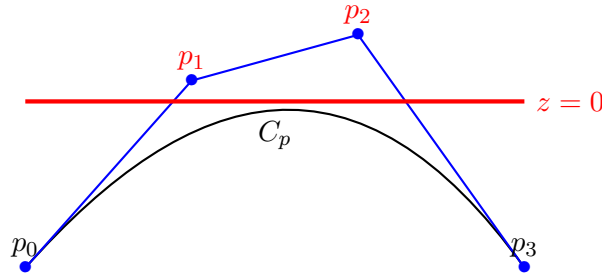


Figure 4.1 *Example of clamped B-spline.* In this particular case, the control points:  $p_0 = -2.0$ ,  $p_1 = 0.25$ ,  $p_2 = 0.8$  and  $p_3 = -2.0$  are not all negative while  $C(\xi) < 0$  for all  $\xi \in [0, 1]$ .

DEFINITION 4.3.2 (Bivariate B-spline) Let  $\mathbf{d} = (d_1, d_2)$  and  $\mathcal{K} = (\mathcal{K}_1, \mathcal{K}_2)$  be two pairs of integer numbers and knot-vectors. A bivariate B-spline is a mapping in the vector space spanned by the tensor products

$$B_{\mathbf{d}}^{ij} : \boldsymbol{\xi} := (\xi^1, \xi^2) \in \mathbb{R}^2 \mapsto B_{\mathbf{d}}^{i,j}(\boldsymbol{\xi}) := N_{d_1}^i(\xi^1)M_{d_2}^j(\xi^2),$$

where  $N_{d_1}^i \in N_{d_1}(\mathcal{K}_1)$  and  $M_{d_2}^j \in N_{d_2}(\mathcal{K}_2)$ . This space will be still denoted by  $Sp(\mathcal{K}, \mathbf{d})$ , being understood that  $\mathcal{K}$  is a Cartesian product of the knot vectors in the two coordinate directions and  $\mathbf{d} := (d_1, d_2)$  is a couple of degrees when the B-spline is bivariate.

From now on, for notation simplicity reasons, we use a unique index instead of the multi-index such that: for each given  $(p, q) \in \{0, \dots, n_1 - 1\} \times \{0, \dots, n_2 - 1\}$  we associate a conveniently defined unique index  $i := i(p, q) = q \times n_1 + p$ , with  $i \in \{0, \dots, n_{12} - 1\}$  and  $n_{12} = n_1 \times n_2$ . Hence the B-spline  $B_{\mathbf{d}}^{pq}$  is denoted  $B_{\mathbf{d}}^i$ .

We summarize in the following Proposition the properties of the bivariate B-splines which are used in the paper.

PROPOSITION 4.3.1 *Let  $\mathcal{K} = (\mathcal{K}_1, \mathcal{K}_2)$  and  $\mathbf{d} = (d_1, d_2)$  be two couples of knot vectors and integer numbers.*

*i)* The B-spline basis functions of  $Sp(\mathcal{K}, \mathbf{d})$  are such that

$$\forall \boldsymbol{\xi} \in \omega := [\xi_0^1, \xi^{n_1+d_1}] \times [\xi_0^2, \xi^{n_2+d_2}] \text{ and } i \in \{0, \dots, n_{12} - 1\} \quad 0 \leq B_d^i(\boldsymbol{\xi}) \leq 1. \quad (4.12)$$

*ii)* Moreover if the end knot-points are of full multiplicity the B-spline functions satisfy the unit partition property

$$\forall \boldsymbol{\xi} \in \omega, \quad \sum_{i=0}^{n_{12}-1} B_d^i(\boldsymbol{\xi}) = 1. \quad (4.13)$$

*iii)* If  $C$  is a B-spline in  $Sp(\mathcal{K}, \mathbf{d})$  of control points  $c^i$  then the relationships  $c^i \leq 0$  for all  $i$  entail that  $C(\boldsymbol{\xi}) \leq 0$  for any  $\boldsymbol{\xi} \in \omega$ . The example 4.3.1 shows that the converse is false.

*iv)* If  $P$  and  $Q$  are two B-splines in  $Sp(\mathcal{K}, \mathbf{d})$  then for any  $(a, b, c) \in \mathbb{R}^3$  the linear combination  $C = aP + bQ + c$  is a B-spline which belongs to  $Sp(\mathcal{K}, \mathbf{d})$ . Moreover, if  $p^i$  and  $q^i$  denote respectively the control points of  $P$  and  $Q$ , the control points  $c^i$  of  $C$  are given by

$$c^i = ap^i + bq^i + c$$

*Proof.* The proofs of properties *i)* and *ii)* are given in [31]. Property *iii)* is a consequence of the positiveness property of the B-spline basis functions. For the property *iv)*, we see from the equation (4.13) that the constant function  $\boldsymbol{\xi} \mapsto c$  can be written as

$$c = \sum_{i=0}^{n_{12}-1} cB_d^i(\boldsymbol{\xi}) \text{ for all } \boldsymbol{\xi} \in \omega$$

and thus  $c$  is a ‘‘B-spline function’’ in  $Sp(\mathcal{K}, \mathbf{d})$ ; and the result falls from the fact that  $Sp(\mathcal{K}, \mathbf{d})$  is a vector space. □

**REMARK 4.3.2** B-splines do not generally interpolate the endpoints of the control polygon. Their associated knot vectors define the influence of the control points or parameters. The control polygon will coincide with the B-spline’s surface at a knot of full multiplicity. We will consider knot vectors with first and last knot breakpoints of full multiplicity with respect to the orders of the B-spline function. This point is necessary for the property 4.12 in the Proposition 4.3.1.

#### 4.3.1 Conformal parameterization

In this case, the polar parameters  $R_0^K$  and  $R_1^2$  are parametrized by B-splines and we show in the Proposition 4.3.2 that this allows to reduce the non-linear constraints (4.7) to the linear constraints (4.15) set on the control points.

**PROPOSITION 4.3.2** Let  $\mathbf{d} = (d_1, d_2)$  and  $\mathcal{K} = (\mathcal{K}_1, \mathcal{K}_2)$  be two pairs of integers and knot-vectors. Assume that  $\mathcal{R}$  and  $\mathcal{R}_0$  are two B-spline parametrizations of  $R_1^2$  and  $R_0^K$  in  $Sp(\mathcal{K}, \mathbf{d})$ , written as

$$\mathcal{R}(\boldsymbol{\xi}) = \sum_{i=0}^{n_{12}-1} r^i B_d^i(\boldsymbol{\xi}), \quad \mathcal{R}_0(\boldsymbol{\xi}) = \sum_{i=0}^{n_{12}-1} r_0^i B_d^i(\boldsymbol{\xi}) \quad (4.14)$$



where  $n_i = \text{card}(\mathcal{K}_\alpha) - d_\alpha - 1$  ( $\alpha = 1, 2$ ). If the following inequalities

$$\begin{aligned} -T_0 &< r_0^i < T_0 \\ r^i &\geq 0 \\ T_1[T_0 + r_0^i] &> 2r^i \end{aligned} \tag{4.15}$$

are satisfied  $\forall (i, j) \in \{0, \dots, n_1\} \times \{0, \dots, n_2\}$  then the inequalities (4.7) are satisfied for all  $\boldsymbol{\xi} \in \omega$ .

*Proof.* As  $T_0$  can be written as

$$T_0 = \sum_{i=0}^{n_{12}-1} T_0 B_d^i(\boldsymbol{\xi}) \quad \forall \boldsymbol{\xi} \in \omega,$$

the property *iii*) of Proposition 4.3.1 shows that if  $r_0^i < T_0$  for all  $i$  then we have  $\mathcal{R}_0(\boldsymbol{\xi}) - T_0 < 0$  for all  $\boldsymbol{\xi} \in \omega$ , which is precisely the first of the inequalities (4.7). The other inequalities can be proved in the same manner.  $\square$

REMARK 4.3.3 As the angle  $\Phi_1$  does not appear nor in the geometric nor in the elastic constraints, different parametrizations can be considered for the orthotropy angle. Of course, the box constraints  $-\pi \leq \Phi_1 \leq \pi$  exist for  $\Phi_1$ . Then, we give in the following Proposition a result for  $\Phi_1$  analogous to that of Proposition 4.3.2.

PROPOSITION 4.3.3 Let  $\mathcal{K}^\phi = (\mathcal{K}_1^\phi, \mathcal{K}_2^\phi)$  and  $\mathbf{d}^\phi = (d_1^\phi, d_2^\phi)$  be two couples of knot-vectors and integers. Assume that the polar variable  $\Phi_1 \in \text{Sp}(\mathcal{K}^\phi, \mathbf{d}^\phi)$  is written as follows:

$$\Phi_1(\boldsymbol{\xi}) = \sum_{i=0}^{n_{12}^\phi-1} \Phi_1^i B_{\mathbf{d}^\phi}^i(\boldsymbol{\xi}).$$

Then the inequalities

$$-\pi \leq \Phi_1^i \leq \pi, \quad \forall i \in \{0, \dots, n_{12} - 1\} \tag{4.16}$$

imply  $-\pi \leq \Phi_1(\boldsymbol{\xi}) \leq \pi$  for all  $\boldsymbol{\xi} \in \omega$ .

REMARK 4.3.4 The bounds specified in the previous proposition take into account for the periodicity of the trigonometric functions which appear in the polar expressions of the elasticity tensor components.

### 4.3.2 Direct parameterization

In this subsection, we assume that the polar parameter  $R_1$  is parametrized by a B-spline and we have the following result:

PROPOSITION 4.3.4 Let  $\mathcal{R}_1$  and  $\mathcal{R}_0$  be two B-spline parametrizations of the polar moduli  $R_1$  and  $R_0^K$ , written as:

$$\mathcal{R}_1(\boldsymbol{\xi}) = \sum_{i=0}^{n_{12}-1} r_1^i B_d^i(\boldsymbol{\xi}) \quad \text{and} \quad \mathcal{R}_0(\boldsymbol{\xi}) = \sum_{i=0}^{n_{12}-1} r_0^i B_d^i(\boldsymbol{\xi}).$$

Then the inequalities

$$2(r_1^i)^2 - \frac{T_1(T_0 + r_0^i)}{n_{12}} < 0, \quad \forall i \in \{0, \dots, n_{12} - 1\} \quad (4.17)$$

imply the inequality (4.7)<sub>1</sub> to be satisfied for every  $\xi \in \omega$ .

*Proof.* We start the proof with the following technical Lemma which shows that the square  $\mathcal{R}^2$  of a B-spline  $\mathcal{R} \in Sp(\mathcal{K}, \mathbf{d})$  can be bounded above by a B-spline  $\mathcal{R}_a \in Sp(\mathcal{K}, \mathbf{d})$ .

LEMMA 4.3.1 *Let then  $\mathcal{F}$  be the vector space spanned by a  $(n + 1)$ -uple  $(f_i)_{i=0}^n$  of real valued mappings defined on  $\omega$ , satisfying the following conditions:*

$$0 \leq f^i(\xi) \leq 1 \text{ and } \sum_{i=0}^n f^i(\xi) = 1 \text{ for all } \xi \in \omega.$$

Then for any  $f \in \mathcal{F}$  there is  $f_a \in \mathcal{F}$  such that

$$f(\xi)^2 \leq f_a(\xi) \text{ for all } \xi \in \omega.$$

Moreover if  $f = \sum_{k=0}^n v_k f^k$  then  $f_a$  can be chosen as the following linear combination of the basis-functions  $(f^i)_{i=0}^n$

$$f_a = (n + 1) \sum_{k=0}^n (v_k)^2 f^k \quad (4.18)$$

*Proof.* we have

$$f(\xi)^2 = \sum_{k=0}^n (v_k)^2 (f^k)^2 + 2 \sum_{k=0}^{n-1} \sum_{l>k}^n (v_k f^k(\xi))(v_l f^l(\xi)). \quad (4.19)$$

The second term of the right hand side of (4.19) is bounded above as follows:

$$\begin{aligned} 2 \sum_{k=0}^{n-1} \sum_{l>k}^n (v_k f^k(\xi))(v_l f^l(\xi)) &\leq \\ &\leq \sum_{k=0}^{n-1} \sum_{l>k}^n \{(v_k f^k(\xi))^2 + (v_l f^l(\xi))^2\} \text{ (by Young's inequality)} \\ &\leq \sum_{k=0}^{n-1} \sum_{l>k}^n \{(v_k)^2 f^k(\xi) + (v_l)^2 f^l(\xi)\} \text{ (as } 0 \leq f^k(\xi) \leq 1); \end{aligned} \quad (4.20)$$

then, rearranging the indexes in an appropriate manner, we have

$$\sum_{k=0}^{n-1} \sum_{l>k}^n \{(v_k)^2 f^k(\xi) + (v_l)^2 f^l(\xi)\} = n \sum_{k=0}^n (v_k)^2 f^k(\xi). \quad (4.21)$$

Using the inequalities (4.20), (4.21) in (4.19), one gets:

$$f(\boldsymbol{\xi})^2 \leq (n + 1) \sum_{k=0}^n (v_k)^2 f^k(\boldsymbol{\xi})$$

which proves the formula (4.18). □

To complete the proof of Proposition 4.3.4 we use the Lemma 4.3.1 with  $\mathcal{F} = Sp(\mathcal{K}, \mathbf{d})$  and  $f = \mathcal{R}_1$ ; then there is a B-spline  $\mathcal{R}_a$  in  $Sp(\mathcal{K}, \mathbf{d})$  such that

$$(\mathcal{R}_1(\boldsymbol{\xi}))^2 \leq \mathcal{R}_a(\boldsymbol{\xi}) \quad \forall \boldsymbol{\xi} \in \omega;$$

now the property *iii*) of the Proposition 4.3.1 shows that the inequalities of Proposition 4.3.4 entail

$$T_1(T_0 + \mathcal{R}_0(\boldsymbol{\xi})) - 2\mathcal{R}_a(\boldsymbol{\xi}) \geq 0 \quad \forall \boldsymbol{\xi} \in \omega.$$

By definition of  $\mathcal{R}_a$ , this last inequality implies

$$T_1(T_0 + \mathcal{R}_0(\boldsymbol{\xi})) - 2(\mathcal{R}_1(\boldsymbol{\xi}))^2 \geq 0 \quad \forall \boldsymbol{\xi} \in \omega,$$

which is precisely (4.7)<sub>1</sub>. □

The parameterizations stated above for the polar parameters allow, when considering the optimization problem (4.1.1), to reduce the number of design variables which are now the control points of their parameterizing B-spline functions. But the Example 4.3.1 and Figure 4.1 shows that defining the constraints directly on the control points (see Propositions 4.3.4, 4.3.3, 4.3.2) can lead to a reduction of the design space exploration. However it is possible to use B-spline flexibility to define that constraint on new control parameters in order to enlarge the admissible space exploration. More specifically, once the parametrizations of the polar parameters are set, considering the resulting B-spline constraint function, one can use subdivision or knot insertion flexibility of B-spline to define some new more interpolating control points. By doing so, we can define new control parameters which are linear combinations of the original control points and more suitable for the definition of more accurate constraints. This yields to “relax” the bounds of variation on the design variables (control points) and allow to enlarge the admissible space exploration. The constraints will then be checked on the new control points.

**EXAMPLE 4.3.2** (B-spline flexibility for the constraints). Subdivision operation is a well known flexibility given by B-spline function. The idea was first defined for Bezier curves and surfaces with the *Casteljau algorithm*, see [58]. This algorithm allows to evaluate a Bezier function at some given parametric coordinates and also, at the same time, to split or subdivide the Bezier curve at that specific parametric coordinate. The subdivision technique has been generalized for B-spline functions by Cox-De-Boor [31], [62].

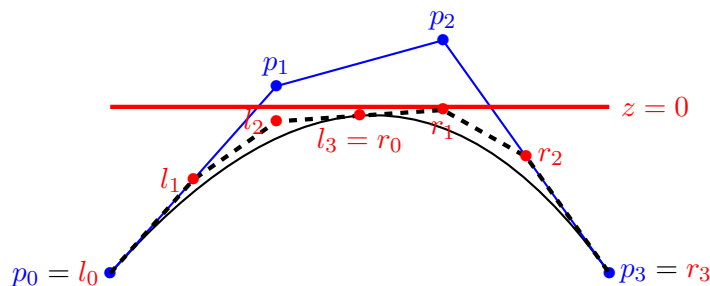


Figure 4.2 *Illustration of subdivision on the B-spline curve  $C_p$ , with the control points  $\{l_i, r_i\}$ ,  $i \in \{0, \dots, 3\}$  of its two subdividing B-spline curve  $C_l$  and  $C_r$ . The *new* calculated control points satisfy the sufficient conditions*

Looking at Figure 4.2, the control parameters  $p_i$  are the design variables while the parameters  $\{l_i, r_i\}$  are just used to check the admissibility of the control parameters  $p_i$ . One can choose *a priori* a certain level of subdivision at which the “sufficient constraints” will be checked on the new computed control points.

These flexibilities help to increase the number of interpolated control parameters and also make the control polygon be much closer to the function, see [62]. By doing so, we tend to sufficient and necessary conditions but we also increase the number of constraints. However, we propose to keep optimizing on the initial control points. In fact, the *new added control points* by subdivision are linked to the initial ones thanks to the linear recursive relations, see [62], and are just useful for more refined or accurate constraints.

REMARK 4.3.5 It appears clearly, on one hand, that the choice of the proposed B-spline based parameterizations yields to an acceptable number of design parameters but to some sufficient constraints on the control points which can induce a restriction on the design space exploration. On the other hand, the search of good exploration, by means of B-spline flexibility, of the design space by defining some more precise or accurate constraints on new control points obtained by subdivision, can be expensive. One has to tradeoff the number of constraints versus accuracy or design parameters space exploration.

## 4.4 Formulation of the optimization problem

Let us consider the optimization problem (4.1.1) which consists in the minimization of an objective function  $J(\mathbb{E})$ .

We focus on an optimization problem which consists in minimizing the compliance of  $\Omega$ . The structural response depends on the reduced plane elastic tensor, thus we note the compliance  $J(\mathbb{E}^P)$

$$J(\mathbb{E}^P) = \int_{\omega} \mathbf{f} \mathbf{u} \, ds.$$

Without loss of generality the following developments are made in the case of geometric bound constraints on the elastic properties.

#### 4.4.1 Design parameters

We recall that for the sake of simplicity, we subsequently use the notation  $R_0$  and  $R_1$  respectively for  $R_0^K$  and  $R_1^2$ . Given a basic layer of polar parameters  $T_0^L, T_1^L, R_0^L, R_1^L$ , we introduce the dimensionless parameters

$$\rho_\alpha = \frac{R_\alpha}{R_\alpha^L}, \alpha \in \{0, 1\}, \rho_\alpha \in [l_\alpha, u_\alpha]$$

where  $l_\alpha$  and  $u_\alpha$  are the lower and upper bounds of the dimensionless parameters:  $[l_0, u_0] = [-1, 1]$ , and  $[l_1, u_1] = [0, 1]$ . So the geometric constraints (4.9) can be rewritten as:

$$\begin{aligned} 2\rho_1 - 1 &\leq \rho_0 \\ \rho_0 &\in [-1, 1] \\ \rho_1 &\in [0, 1] \end{aligned} \quad (4.22)$$

Then, we consider equivalently the optimization of the dimensionless parameters

$$\rho_\alpha : \omega \rightarrow [l_\alpha, u_\alpha] \text{ and the polar angle } \Phi_1 : \omega \rightarrow [-\pi, \pi].$$

Let  $(\mathcal{K}_\rho, \mathbf{d}_\rho)$  and  $(\mathcal{K}_\Phi, \mathbf{d}_\Phi)$  be the knot vectors and orders of the B-spline parameterizations of  $\rho_\alpha$ , and of  $\Phi_1$ . We note by  $B_\rho^i$  and  $B_\Phi^i$  the B-spline basis functions of  $\rho_\alpha$  and  $\Phi_1$

$$\rho_\alpha(\boldsymbol{\xi}) = \sum_{i=0}^{n_{12}^\rho-1} \rho_\alpha^i B_\rho^i(\boldsymbol{\xi}), \alpha \in \{0, 1\}, \Phi_1(\boldsymbol{\xi}) = \sum_{i=0}^{n_{12}^\Phi-1} \Phi_1^i B_\Phi^i(\boldsymbol{\xi}).$$

The admissible spaces of the discretized problem  $\mathcal{P}_\rho$  and  $\mathcal{P}_\Phi$  are

$$\mathcal{P}_\rho = \{ \rho_\alpha \in Sp(\mathcal{K}_\rho, \mathbf{d}_\rho) \text{ such that } \rho_\alpha \in [l_\alpha, u_\alpha] \text{ and } 2\rho_1^i - \rho_0^i - 1 \leq 0, \text{ for all } i = 0 : n_{12}^\rho - 1 \},$$

$$\mathcal{P}_\Phi = \{ \Phi_1 \in Sp(\mathcal{K}_\Phi, \mathbf{d}_\Phi) \text{ such that } \Phi_1^i \in [-\pi, \pi], \text{ for all } i = 1 : n_{12}^\Phi - 1 \}$$

Then the global discrete parameters admissible space is

$$\mathcal{P} = \mathcal{P}_\rho \otimes \mathcal{P}_\Phi.$$

For the optimal design problem is: Find the polar parameters  $(\rho_\alpha^*, \Phi_1)$  such that

$$(\rho_\alpha^*, \Phi_1^*) = \arg \min_{(\rho_0, \rho_1, \Phi_1) \in \mathcal{P}} J(\rho_0, \rho_1, \Phi_1).$$

In order to use a gradient-based method for the optimization the objective function and the constraints have to be derivated with respect to the polar parameters.

#### 4.4.2 Derivatives with respect to the polar parameters

Let us denote by  $\mathbf{K}$  the stiffness matrix, associated to the FEM discretization of the bilinear form  $a$  in state equation -Problem 2.2.1,  $\mathbf{F}$  the vector of applied loads and  $\mathbf{u}$  the FEM vector of degrees of freedom, i.e the components of the displacement  $[\mathbf{u}, \mathbf{s}]$ .

#### 4.4.2.1 Derivatives of the compliance

The matrix form of the Eq. (2.35), page 25 is then:

$$\mathbf{K}\mathbf{u} = \mathbf{F} \quad (4.23)$$

and the compliance is then

$$J(\rho_0, \sqrt{\rho_1}, \Phi_1) = \mathbf{F} \cdot \mathbf{u}.$$

The applied loads being independent of the elastic tensor, the derivative of the compliance with respect to a given parameter  $p$  is

$$\partial_p J(\rho_0, \sqrt{\rho_1}, \Phi_1) = \mathbf{F} \cdot \partial_p \mathbf{u}, \quad p \in \{\rho_\nu, \Phi_1\} \text{ and } \nu \in \{0, 1\}.$$

Also, the derivative of the state equation (4.23) with respect to  $p$  is

$$\partial_p \mathbf{K} \mathbf{u} + \mathbf{K} \partial_p \mathbf{u} = \partial_p \mathbf{F} = 0 \implies \partial_p \mathbf{u} = -\mathbf{K}^{-1} [\partial_p \mathbf{K} \mathbf{u}]. \quad (4.24)$$

So the derivatives of the compliance with respect to the anisotropic polar parameters  $p \in \{\rho_\alpha, \Phi_1\}$  are:

$$\partial_p J(\rho_0, \sqrt{\rho_1}, \Phi_1) = \partial_p (\mathbf{F} \cdot \mathbf{u}) = \mathbf{F} \cdot \partial_p \mathbf{u} = -\mathbf{F} \cdot \mathbf{K}^{-1} [\partial_p \mathbf{K} \mathbf{u}] = -\mathbf{u} \cdot \partial_p \mathbf{K} \mathbf{u}.$$

The last equality falls from the symmetry of  $\mathbf{K}$ . To compute the derivative of the compliance with respect to the polar parameters, one needs the derivative of the stiffness matrix with respect to these parameters.

#### 4.4.2.2 Derivatives of the stiffness

The bilinear form  $a$  being linear in terms of the stiffness elastic tensor, the derivative  $\partial_p \mathbf{K}$  of the stiffness matrix with respect to the polar parameters is equal to the matrix associated to the following symmetric bilinear form:

$$\begin{aligned} \partial_p a(\mathbf{u}, \mathbf{v}) = & \int_{\omega} t \{ \boldsymbol{\gamma}(\mathbf{v}) : [\partial_p \mathbb{E}^p(\rho_0, \sqrt{\rho_1}, \Phi_1)] : \boldsymbol{\gamma}(\mathbf{u}) + \\ & \frac{t^2}{12} \boldsymbol{\chi}(\mathbf{v}) : [\partial_p \mathbb{E}^p(\rho_0, \sqrt{\rho_1}, \Phi_1)] : \boldsymbol{\chi}(\mathbf{u}) + \boldsymbol{\gamma}_3(\mathbf{v}) : [\partial_p \mathbf{E}^a(\Phi_1)] : \boldsymbol{\gamma}_3(\mathbf{u}) \} d\Omega \end{aligned} \quad (4.25)$$

where  $\mathbb{E}^p = \mathbb{Q} = (Q^{\alpha\beta\lambda\mu})$  and  $\mathbf{E}^a$  are respectively the reduced plane and anti-plane parts of the elasticity tensor, see Equation (2.37) page 25.

Let  $p^i$  be the control points associated to the B-spline parameterization  $p$ . The derivative of the elastic tensor with respect to the  $p^i$  is:

$$\partial_{p^i} \mathbb{E}^p(\rho_0, \sqrt{\rho_1}, \Phi_1) = \partial_p \mathbb{E}^p(\rho_0, \sqrt{\rho_1}, \Phi_1) \partial_{p^i} p, \quad \text{with } p \in \{\rho_0, \rho_1, \Phi_1\}. \quad (4.26)$$

Before computing the derivative of the elastic tensor with respect to those design control parameters, we specify the derivatives with respect to the different polar parameter fields  $p$ .

- Derivative with respect to  $\rho_0$

$$\partial_{\rho_0} \mathbb{E}^p(\rho_0, \sqrt{\rho_1}, \Phi_1) = R_0^L \begin{pmatrix} \cos 4\Phi_1 & -\cos 4\Phi_1 & -\sin 4\Phi_1 \\ -\cos 4\Phi_1 & \cos 4\Phi_1 & \sin 4\Phi_1 \\ -\sin 4\Phi_1 & \sin 4\Phi_1 & -\cos 4\Phi_1 \end{pmatrix}.$$

- Derivative with respect to  $\rho_1$

$$\partial_{\rho_1} \mathbb{E}^p(\rho_0, \sqrt{\rho_1}, \Phi_1) = \frac{R_1^L}{2\sqrt{\rho_1}} \begin{pmatrix} 4\cos 2\Phi_1 & 0 & -2\sin 2\Phi_1 \\ 0 & -4\cos 2\Phi_1 & -2\sin 2\Phi_1 \\ -2\sin 2\Phi_1 & -2\sin 2\Phi_1 & 0 \end{pmatrix}.$$

- Derivative with respect to  $\Phi_1$

$$\begin{aligned} \partial_{\Phi_1} \mathbb{E}^p(\rho_0, \sqrt{\rho_1}, \Phi_1) = \\ \begin{pmatrix} -4R_0 \sin 4\Phi_1 - 8R_1 \sin 2\Phi_1 & 4R_0 \sin 4\Phi_1 & -4R_0 \cos 4\Phi_1 - 4R_1 \cos 2\Phi_1 \\ 4R_0 \sin 4\Phi_1 & 8R_1 \sin 2\Phi_1 - R_0 \sin 4\Phi_1 & 4R_0 \cos 4\Phi_1 - 4R_1 \cos 2\Phi_1 \\ -R_0 \cos 4\Phi_1 - 4R_1 \cos 2\Phi_1 & 4R_0 \cos 4\Phi_1 - 4R_1 \cos 2\Phi_1 & 4R_0 \sin 4\Phi_1 \end{pmatrix}. \end{aligned}$$

Now, to compute the derivative of the antiplane part of  $\mathbf{E}^a = (E^{3\alpha 3\beta})_{\alpha, \beta=1:2}$  with respect to the orthotropy angle we use its polar representation, as for any (*plane*) second order tensor, which allows to have the derivative in a straightforward manner. Let  $T$ ,  $R$  and  $\varphi$  be the polar parameters associated to  $\mathbf{E}^a$ , defined through Equation (4.1). The derivative with respect to the orthotropy angle  $\Phi_1$  is:

$$\partial_{\Phi_1} \mathbf{E}^a(\Phi_1) = 2R_a \begin{pmatrix} \sin 2(\varphi - \Phi_1) & -\cos 2(\varphi - \Phi_1) \\ -\cos 2(\varphi - \Phi_1) & -\sin 2(\varphi - \Phi_1) \end{pmatrix}, \quad \partial_{\rho^\alpha} \mathbf{E}^a = )_{2 \times 2}.$$

Finally, the derivatives with respect to the design variables  $p^i$  are obtained by applying a chain rule:

$$\begin{aligned} \partial_{p^i} \mathbb{E}^p(\rho_0, \sqrt{\rho_1}, \Phi_1)(\boldsymbol{\xi}) &= B_p^i(\boldsymbol{\xi}) \times \partial_p \mathbb{E}^p(\rho_0, \sqrt{\rho_1}, \Phi_1) \text{ and} \\ \partial_{p^i} \mathbf{E}^a(\Phi_1)(\boldsymbol{\xi}) &= B_p^i(\boldsymbol{\xi}) \times \partial_p \mathbf{E}^a(\Phi_1) \end{aligned} \quad (4.27)$$

## 4.5 Numerical Results

In the following, we show some examples of material design of anisotropic shell structures.

### Parameterization:

The B-spline functions representing the different polar parameters are defined through open knot vectors of the form

$$\mathcal{K}_p^\alpha = \{\underbrace{0, \dots, 0}_{d_p+1}, \underbrace{1, \dots, 1}_{d_p+1}\}, \quad \alpha \in \{1, 2\}$$

with  $d_p$  the function degree. Thus the number of control parameters, for a given polar parameter field  $p \in \{\rho_\alpha, \Phi\}$ , is  $(d^p + 1) \times (d^p + 1)$ .

In practice, shell geometries are usually defined using several patches joined together in a conforming manner; i.e. the common part between two geometries is either empty, a vertex or an

entire edge. In that case, the polar parameters associated to each shell are interpolated using the same B-spline basis functions so that the continuity constraint on the elastic properties is set in a straightforward manner by equating the values of the control points corresponding to their common interfaces for each polar parameter field.

**Algorithm:**

For the numerical results, we have used NLOpt, a free/open-source library for NonLinear OP-Timization. It includes the implementation of numerous optimization algorithms adapted for global and local optimizations. The library involves different types of algorithm such as Moving Asymptote Method (MMA), COBYLA (Constrained Optimization by Linear Approximation) which can be gradient-based or derivative-free, for local and global optimization searches. We have used the Cobyla algorithm which appears to yield to the best optimization results among the different algorithms.

**Material properties of the basic layer:**

We consider a material with the following properties for all the numerical examples:

$$\begin{aligned} E_1 &= 9000 \text{ MPa}, \\ E_2 &= E_3 = 161 \text{ MPa}, \\ \nu_{21} &= \nu_{31} = 0.26, \text{ and } \nu_{23} = 0.26, \\ G_{13} &= G_{12} = 61 \text{ MPa}, \quad G_{23} = \frac{E_2}{2(1+\nu_{23})} = 61.54 \text{ MPa} \end{aligned}$$

which corresponds to a transversally isotropic material of principal direction along the axis 1. The polar parameters of the reduced and anti-plane parts of the elastic tensor are:

<i>In plane elastic behaviour</i>	$\mathbb{E}_p$
<i>Polars parameters</i>	
$T_0$ [MPa]	1166.53
$T_1$ [MPa]	1156.99
$R_0^K$ [MPa]	1105.53
$R_1$ [MPa]	1106.21
$\Phi_1$ (deg)	0
<i>Out plane elastic behaviour</i>	$\mathbb{E}_a$
<i>Polar parameters</i>	
$T$ [MPa]	62.44
$R$ [MPa]	1.44
$\Phi$ (deg)	0

Table 4.1 Table of polar parameters corresponding to the different part of the elastic tensor.

The volume density and the thickness of the shells are:

$$\begin{aligned} \rho &= 1.58 \times 10^3 \text{ kg/m}^3 \\ t &= 3 \times 10^{-3} \text{ m}. \end{aligned} \tag{4.28}$$



We further consider different cases of optimization:

- one with orthotropy angle as design variable, within which one is seeking for the optimal orientation of a given fixed material
- the second with  $R_0^K$  and  $R_1$  as design variables corresponds to seek to the optimal material with a given fixed orthotropy orientation
- the last concerning the joint optimization of the polar moduli and angle corresponds to seek for the optimal material and the appropriate orientation on the geometry.

For the last two cases, we consider that the resulting optimal properties  $R_0^K$  and  $R_1$  achieved a laminate composed of identical basic layer. Hence the isotropic polar parameters are disregarded for the optimization. As consequence, we use the geometric bound constraints on the polar moduli  $R_0^K, R_1$ .

#### 4.5.1 Plate under two in-plane concentrated loads

We consider a plate clamped at its side  $[DC]$  and subjected to two concentrated loads  $\mathbf{F}_A$  and  $\mathbf{F}_B$  at the two vertexes  $A, B$ :

$$\mathbf{F}_A = (N_x, N_y, 0) \text{ and } \mathbf{F}_B = (-N_x, N_y, 0), \text{ with } N_x = N_y = 1000\text{N}.$$

Figure 4.3 shows the boundary and the loading conditions on the plate

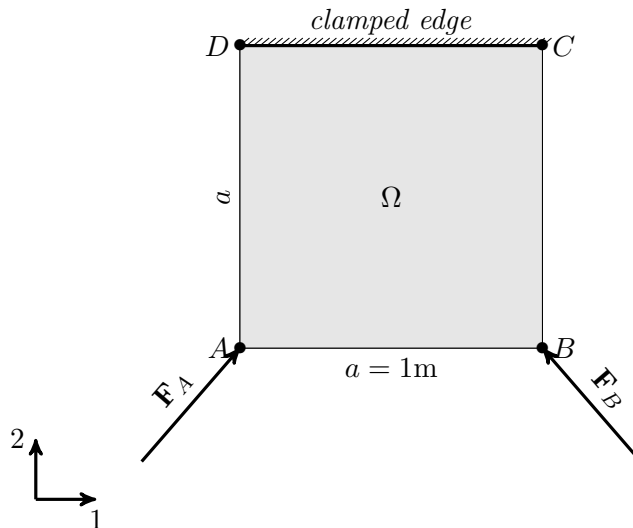


Figure 4.3 Boundary and loading conditions of the plate.

**Orthotropy direction optimization:**

We first consider the exclusive optimization of the material frame orientation,  $\Phi_1$ . Initially, the axis with the highest stiffness is put along the axis 2,  $\Phi_1 = \frac{\pi}{2}$ .

The Figure 4.4 shows the optimal orthotropy direction.

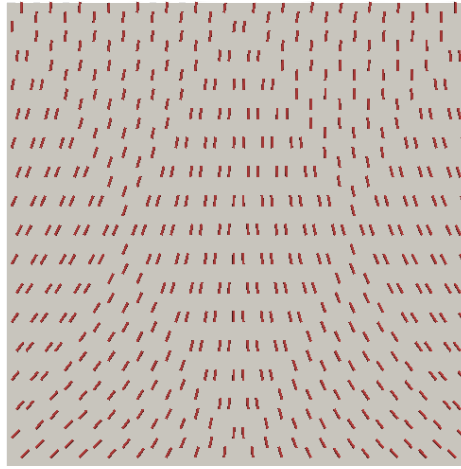


Figure 4.4 Optimal orthotropy direction distribution and the corresponding displacement field

The structure is stressed in compression then the optimal fibers are in the loading direction, near the points  $A$  and  $B$ .

**Optimization of the moduli  $R_0^K$  and  $R_1$ :**

In the present case of optimization, the initial orthotropy angle  $\Phi_1 = \frac{\pi}{2}$  is kept fixed and we consider the design of the moduli  $R_0^K$  and  $R_1$ . The initial distributions of  $R_0^K$  and  $R_1$  are constant fields, equal to those of the basic layer. Figure 4.5 shows the optimal distributions of  $R_0^K$  and  $R_1$ .

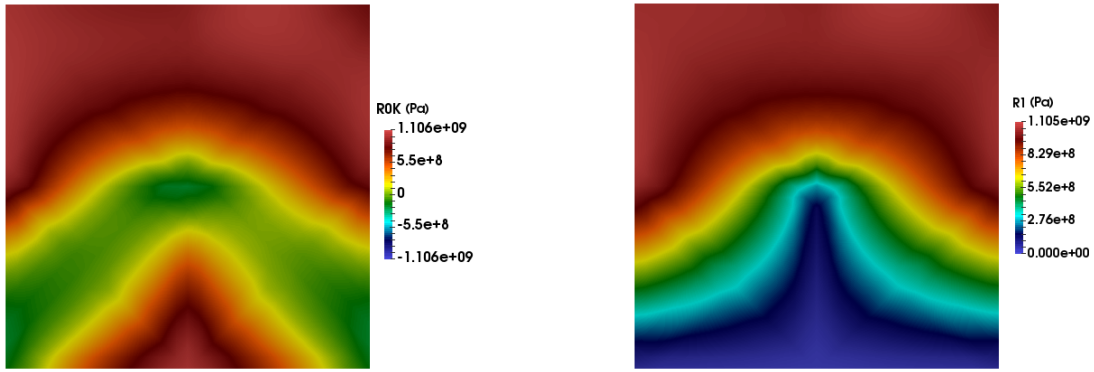


Figure 4.5 From left to the right the optimal distribution of  $R_0^K$  and  $R_1$

We remark that the values of  $R_0^K$  are negatives near the two loading regions, which means that in the plate there are present at the same time the two types of orthotropy, those with  $K = 0$  and with  $K = 1$ . The former is present near the loading points while the latter is anywhere else.

**Optimization of  $\Phi_1$ ,  $R_0^K$  and  $R_1$ :**

As last case, we consider the joint optimization of the elastic moduli and of the orientation of the material frame, i.e the orthotropy direction.

Figure 4.6 shows the distribution of the different moduli. In this case, we remark that  $R_0^K$  is nonnegative which means that all the plate has the same type of ordinary orthotropy everywhere.

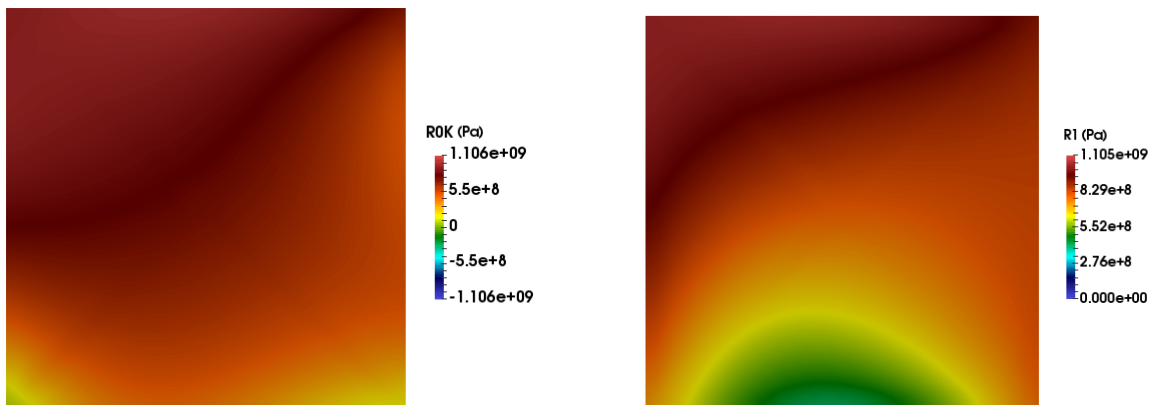


Figure 4.6 Optimal distribution of the polar parameters  $R_0^K$  and  $R_1$  corresponding to the plate under two concentrated loads.

Figure 4.7 shows the optimal orthotropy direction. The fiber are oriented on the loading direction near the points  $A$  and  $B$ .

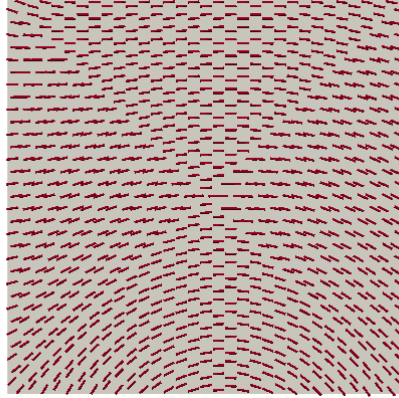


Figure 4.7 Optimal orthotropy direction orientation: the fibers are locally in the loading directions and anywhere else in the 1 axis direction.

We remark that close to the loaded region, the orthotropy orientation constitutes a kind of arch which imposts are at the loading points and the keystone located at the middle line perpendicular to the edge  $[AB]$  and  $[CD]$ .

Table 4.2 shows the optimal design compliances corresponding to the different cases of optimization.

	compliance	$\Delta_{opt}J(\%)$	NoP
<b>initial</b>	23.13	0	-
$(\Phi_1, 4)$	3.41	85.256	16
$(R_0^K, 4), (R_1, 4)$	1.72	92.570	32
$(\Phi_1, 4), (R_0^K, 4), (R_1, 4)$	1.10	95.231	48

Table 4.2 Information related to the different cases of optimization (*plate under point-wise loads*)

In the above table the notation  $(p, d + 1)$  designate that the parameter  $p$  has been parameterized with the B-spline of open knot vector of degree  $d$  and  $d + 1$  control points in each parametric coordinate direction. The notation **NoP** designates the number of parameters,  $\Delta_{opt}J = \frac{J_{opt} - J_{init}}{J_{init}} \times 100$  the percentage of the relative gain on the compliance with respect to the initial compliance;  $J_{init}$  and  $J_{opt}$  being respectively the compliance with the initial and optimal elastic tensor fields.

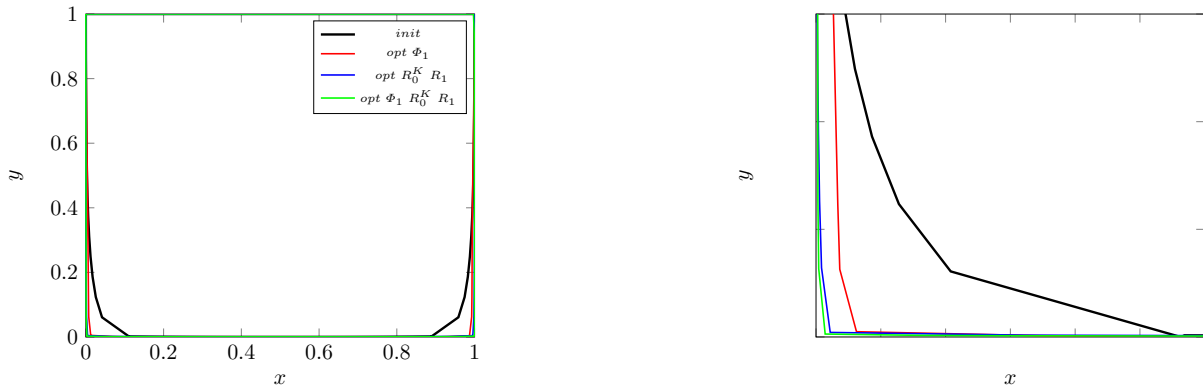


Figure 4.8 Comparison of the deformations corresponding to the different cases of optimization: at the left the entire plate deformations and at the right the zooms near the loading region

One remarks on Figure 4.8 that the deformation of each different cases of optimization is better than the deformation corresponding to the initial material. The diminishing of the compliance and the ranks of performance after the different optimizations are also noticeable on Figure 4.8 and are consistent with the Table 4.2.

### 4.5.2 Anisotropy design of a cantilever

Now, we consider the optimal anisotropy design of a cantilever, see Fig 4.9. More precisely, the plate is clamped along its left boundary and subjected along the opposite side to a uniform tangential force. The considered design criterion is the compliance. The polar parameters are subjected to geometric bound constraints. Thus the design problem corresponds to the optimization of the elastic properties distribution of the homogenized properties of a laminate.

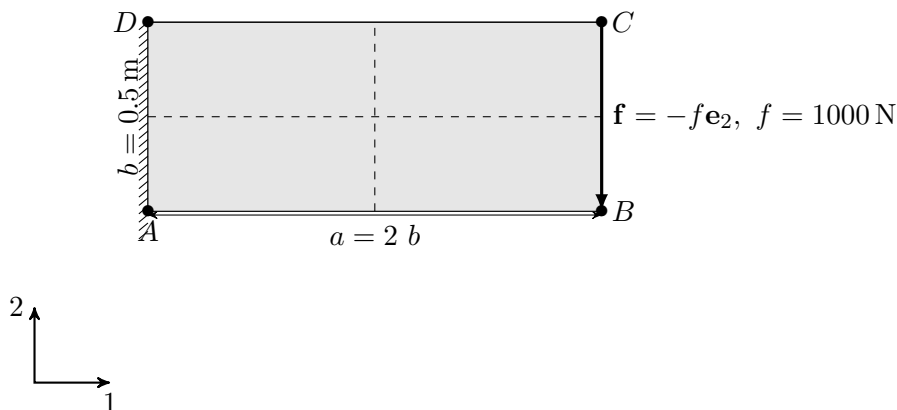


Figure 4.9 Boundary and loading conditions of the plate with tangential load.

The geometry is defined through a  $2 \times 2$  assembled plates. The polar parameters are parameterized with a B-spline of order 3 of open uniform knot vector  $\Sigma = \{0, 0, 0, 1, 1, 1\}$ . The number of control points per polar parameter field is 9 is over each sub-plate. Taking into account for the continuity condition across the different interfaces, the total number of variables per type of polar field is further reduced to 21.

### Orthotropy orientation design

We first optimize the orthotropy direction of the material. The fiber was initially along the direction  $\mathbf{e}_1$ . Figure 4.10 shows the optimal orthotropy direction.

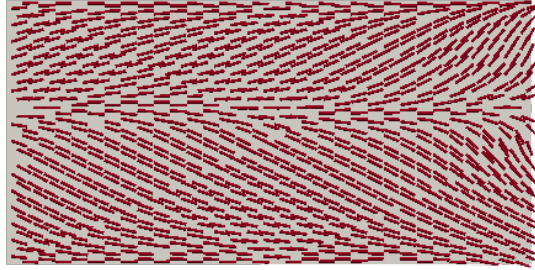


Figure 4.10 Optimal distribution of the orthotropy direction.

### Polar moduli $R_0^K$ and $R_1$ design

Now, we consider the optimization of the two anisotropic polar moduli. Their distributions were initially uniform, i.e of constant value over all the plate. We emphasize that the considered constraint is the geometric bound and not the elastic one. The distribution of the optimal field  $R_0^K$  is plotted on figure 4.11. We remark that there exist two kinds of orthotropy. The orthotropy  $K = 0$  is in both the lower and upper sides of the plate.

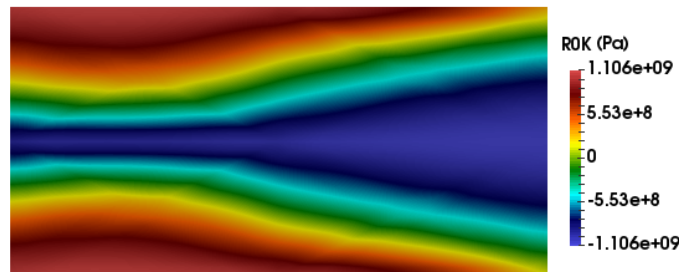


Figure 4.11 Optimal distribution of the polar modulus  $R_0^K$ .

Figure 4.12 shows the optimal distribution of the polar parameter  $R_1$ . The field is also symmetric with respect to the median line of  $[BC]$ , the loading edge.

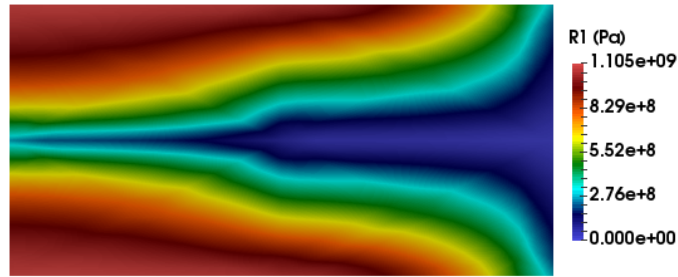


Figure 4.12 Optimal distribution of the polar modulus  $R_1^K$ .

The parameters are tailored so as that the lower and upper edges have the highest elastic coefficient  $E^{1111}$  which allows to resist to flexure; in fact  $E_{1111} = T_0 + 2T_1 + R_0^K + 4R_1$ . Secondly, the stress inside the structure being mostly shear, the elastic properties are tailored in order to have highest value for  $E^{1122}$ , by setting  $R_0^K < 0$ . Indeed, to increase the stiffness to a shear with an orthotropy angle  $\Phi = \frac{\pi}{2}$  deg one needs a  $K = 1$  orthotropy.

### Polar moduli and orientation design

At last, we consider the joint optimization of the orthotropy direction and the polar moduli. The optimal orthotropy direction field is represented in Figure 4.13.

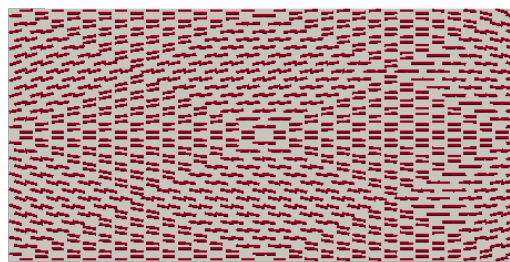


Figure 4.13 Optimal distribution of the orthotropy

Figures 4.14 and 4.15 respectively show the optimal distribution of the polar moduli  $R_0^K$  and  $R_1$ .

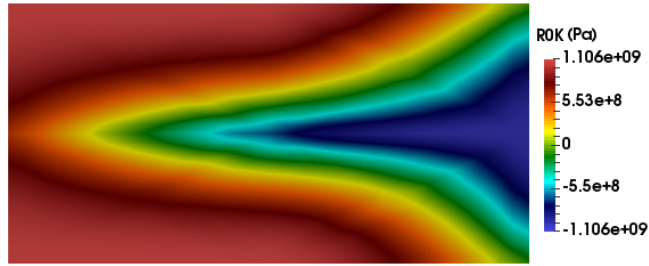


Figure 4.14 Optimal distribution of the parameter  $R_0^K$

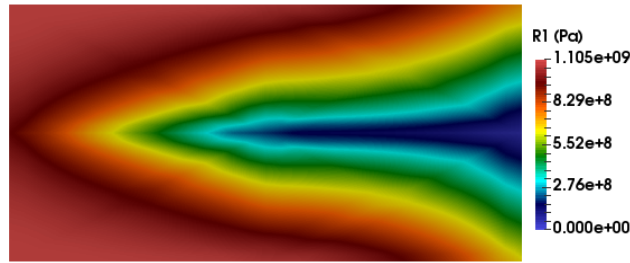


Figure 4.15 Optimal distribution of the parameter  $R_1$

The orthotropy direction is orthogonal to the edge  $[AD]$ , with clamping boundary condition. The upper and lower sides of the plate have a  $K = 0$  orthotropy with  $\Phi_1 \simeq \frac{\pi}{2}$ . These settings of orthotropy and angle orientation allow to resist to flexural stresses. We still notice, as in the previous optimization, the presence of a  $K = 1$  orthotropy inside the plate where there is a shear stress.

Table 4.3 summarize the informations relative to the different cases of design.

	$J$	$\Delta_{opt}J(\%)$	NoP
<b>initial</b>	0.21	0	-
$(\Phi_1, 3)$	0.05	74.286	9
$(R_0^K, 3), (R_1, 3)$	0.03	84.810	42
$(\Phi_1, 3), (R_0^K, 3), (R_1, 3)$	0.03	86.286	63

Table 4.3 Informations relative to the different cases of design (*plate with tangential edge load*)

Figure 4.16 shows the deformations corresponding to the initial material and those associated to the different cases of optimization.



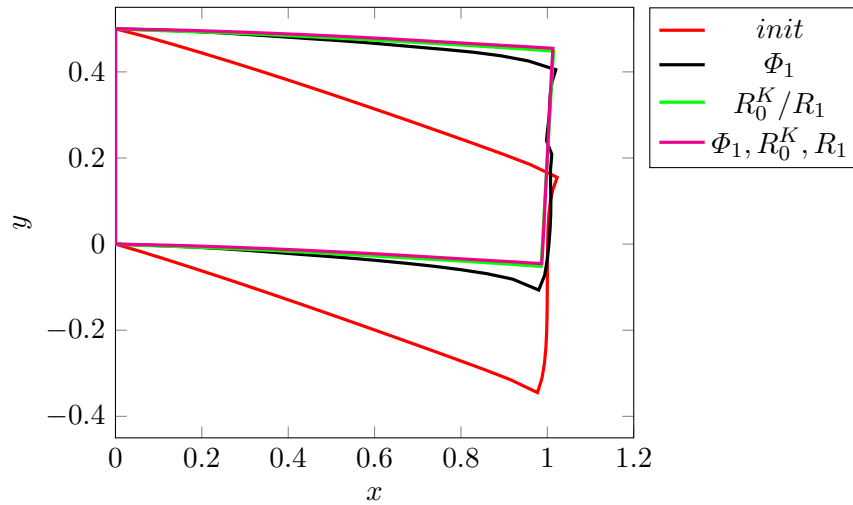


Figure 4.16 Deformation corresponding to the different case of design of the plate subjected to vertical edge force, with an amplification factor  $\times 200$ .

One remarks that the deformed configuration associated to the optimal designs of  $R_0^K$ ,  $R_1$  and  $\Phi_1$ ,  $R_0^K$  and  $R_1$  are almost confounded to the reference state of the initial design: the most influent parameters are the moduli  $R_0^K$  and  $R_1$ .

### 4.5.3 Cylinder shell under torsional load

This case deals with a cylindrical shell which is subjected to a torsional load. The cylinder is of radius  $r = 0.18\text{m}$ , of height  $h = 0.5\text{m}$ , and is clamped at its basis. The applied loads correspond to a twisting moment at the upper circular boundary. Letting  $\mathbf{a}_1$  be the tangent vector to the circular boundary, the applied load is  $\mathbf{f} = f \mathbf{a}_1$ , with  $f = 2 \times 10^4 \text{N}$ .

The orthotropy direction is initially oriented along the generatrix, i.e  $\Phi_1 = \frac{\pi}{2}$ . The cylinder is defined through five patches, on the circumference. Thus, the parameterization of the different polar parameters is made through five piecewise continuous bivariate B-spline polynomials.

The deformation being axial, we only post-process the field of displacement. Figure 4.17 shows the initial displacement field.

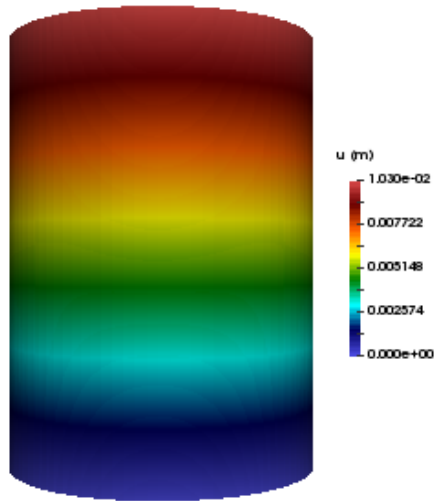


Figure 4.17 Initial displacement field induced by the torsional load on the cylindrical shell.

#### Orthotropy direction design:

We first start with an optimization of the orthotropy direction only. The optimal angle is obtained through a third order B-spline polynomials: the total number of control parameters is equal to 30. The optimal angle field is globally constant,  $\Phi_1 = \frac{\pi}{4}$ . Figure 4.18 shows the optimal orthotropy direction.

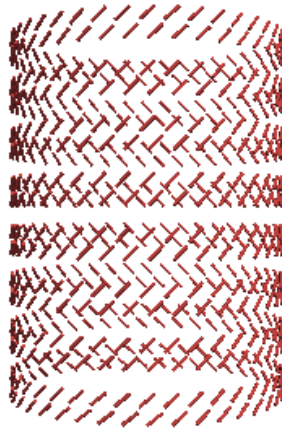


Figure 4.18 The optimal orthotropy direction.

Although the angle was parameterized with a biquadratic B-spline function, the optimizer was able to find the constant solution.

#### Polar moduli $R_0^K$ and $R_1$ design:

We again consider an optimization case in which the design variables are the two moduli  $R_0^K$  and  $R_1$ . The different parameters were also parameterized with a third order B-spline functions: the number of variables is equal to 60. Figure 4.19 shows the different distributions of the moduli  $R_0^K$  (at the left) and  $R_1$  (at the right).

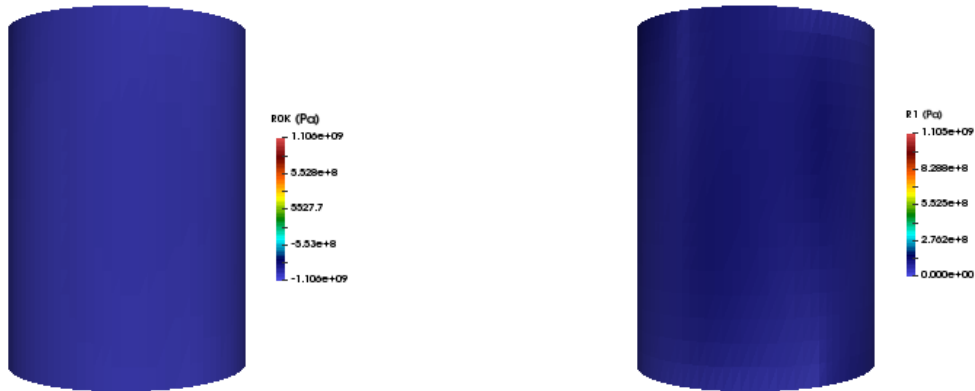


Figure 4.19  $R_0^K$  and  $R_1$  optimal distributions

We remark that  $R_0^K$  is uniformly negative, i.e there exists only one kind of orthotropy with  $K = 1$ .

**Angle and polar moduli design:**

For this example, we optimize conjointly all the polar parameters. Figure 4.20 shows the optimal distributions of  $R_0^K$ ,  $R_1$ . We remark on Figure 4.21 that the angle is almost  $\Phi_1 = \frac{\pi}{4}$  everywhere and the modulus  $R_0^K$  is now positive. Indeed, the orthotropy phase here was explicitly designed, through the angle  $\Phi_1$ .

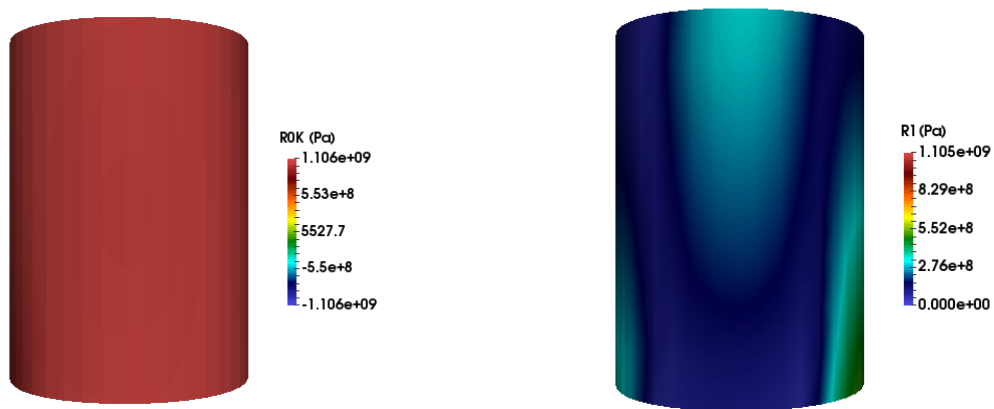


Figure 4.20 The distributions of the polar parameters

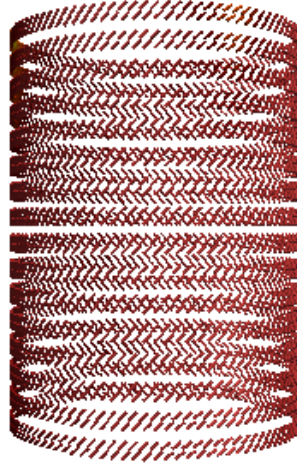


Figure 4.21 Optimal orthotropy direction corresponding to the optimal material on the cylinder under torsion.

Table 4.4 summarizes the informations relative to the different cases of optimization.

	compliance	ratio (%)	NoP
<b>initial</b>	62.62	0	-
$(\Phi_1, 3)$	23.67	62.201	30
$(R_0^K, 3), (R_1, 3)$	1.75	97.205	60
$(\Phi_1, 3), (R_0^K, 3), (R_1, 3)$	1.68	97.317	90

Table 4.4 Informations related to the different cases of optimization (*cylindrical shell under torsional load*)

#### 4.5.4 Anisotropy design of a plate submitted to torsion

We conclude the numerical results with a case of joint optimization of the polar parameters. In what follows, we are given a plate clamped at a boundary and subjected to torsional load at the opposite side. The torsion is produced by two concentrated loads of opposite directions  $\mathbf{f}_\pm = \pm f \mathbf{e}_3$ ,  $f = 1 \times 10^3$  N. The description of the problem is similar to the one described in Figure 4.3, replacing the loads at the points A and B respectively by  $\mathbf{F}_A = \mathbf{f}_-$  and  $\mathbf{F}_B = \mathbf{f}_+$ .

All the polar parameters are parameterized using 4 control points in each parametric direction, i.e 16 control points for each. The optimal orthotropy orientation is plotted in Figure 4.22.

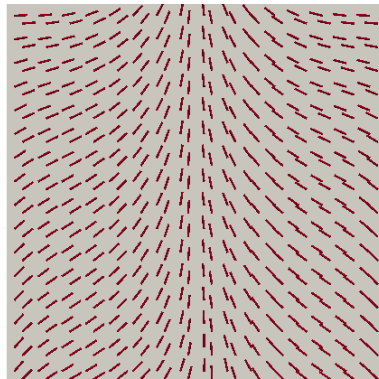


Figure 4.22 Optimal orthotropy direction corresponding to the optimal design.

Figure 4.23 shows from left to right the optimal polar moduli  $R_0^K$  and  $R_1$ .

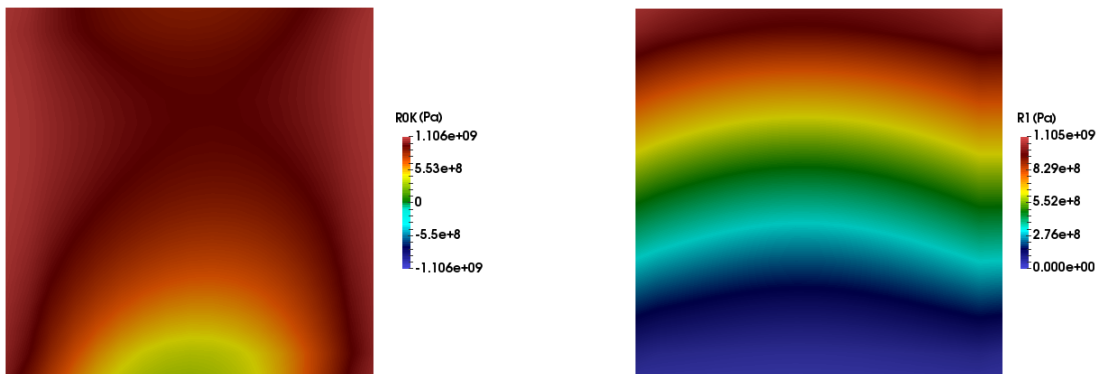


Figure 4.23 From left to right, the optimal polar parameters  $R_0^K$  and  $R_1$  for a plate submitted to torsional load.

The fibers are orientated so that they are perpendicular to the edge with boundary condition at the middle-line region and are distributed almost symmetrically from the edge with boundary condition towards the points with concentrated loads.

Figure 4.24 shows the deformation of the frame of the plate corresponding to the initial material and the optimal one.

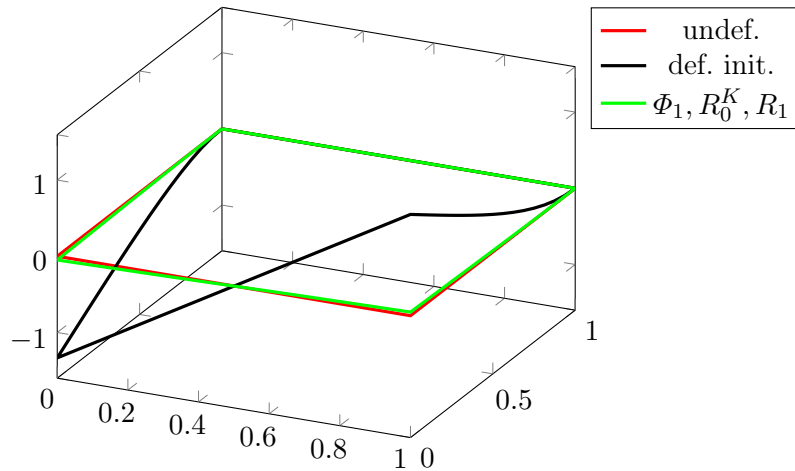


Figure 4.24 Comparison of the deformations of the plate corresponding to the initial and optimal material. In red color the plate in its reference configuration, in black the deformation corresponding to the initial material, finally in green the deformation obtained with the optimal elastic properties.

One remarks in Figure 4.24 that the deformed configuration corresponding to the optimal material is almost coincident with the undeformed plate. The compliance was initially equal to  $1.331 \times 10^6$  and for the optimal design found  $4.791 \times 10^4$ , which represents a drastic reduction of 96.400 %.

## 4.6 Synthesis

The optimal design of anisotropy is of crucial importance in industry. Such kind of problem has generally large number of variables. We have proposed here two relevant parameterizations based on the use of B-spline properties. At first stage, the interest is that they allow to reduce the number of DV. In the other hand, the semi-infinite pointwise elastic or geometric constraints on the elastic tensor field are replaced with a finite set of constraints defined on the control points of the elastic parameters. The price to paid is that the derived constraints are sufficient and not necessary. This sufficiency condition can be weakened and tends to necessary one by using B-spline flexibilities such as subdivision or knot insertion. We have shown some applications by considering several optimization problems with compliance criterion. For almost each example we have considered different combinations of polar parameters design. The numerical results show that the parameterizations allow to obtain optimal solution and to tailor continuous elastic properties with possible significant local variations.



# Simultaneous optimization of shape and anisotropy

## Contents

---

<b>5.1</b>	<b>Introduction</b>	<b>102</b>
<b>5.2</b>	<b>Isogeometric shape parameterization</b>	<b>103</b>
5.2.1	Multiple patches	105
5.2.1.1	Curve junction conditions	106
5.2.1.2	Surface junction conditions	107
5.2.1.3	Matrix associated to the geometric regularity	108
<b>5.3</b>	<b>Anisotropy and shape optimization</b>	<b>110</b>
5.3.1	Derivatives with respect to the shape	112
5.3.2	Derivatives of the strain bilinear form	113
5.3.3	Derivatives of the linear form	115
5.3.3.1	Geometry dependent loads	115
5.3.3.2	Geometry independent loads	115
<b>5.4</b>	<b>Sensitivity for an assembling of shells</b>	<b>116</b>
5.4.1	Problem setting	116
5.4.2	Gradient for an assembling of shells	117
5.4.3	Constraints on the design's geometry	117
5.4.4	General overview on the derivative of the junction	119
5.4.5	Sensitivity of the shells junction	121
5.4.5.1	Matrix form of the junction conditions	121
5.4.5.2	Derivatives of the junction matrix	123
<b>5.5</b>	<b>Numerical results</b>	<b>127</b>
5.5.1	Optimal design of a circular plate	127
5.5.1.1	Optimal shape design	128
5.5.1.2	Anisotropy and shape design	132
5.5.2	Optimization of a holed circular plate	136
5.5.2.1	Optimal shape with isotropic material	137
5.5.2.2	Optimal shape for the anisotropic circular plate	139
5.5.2.3	Shape and anisotropy optimal design	142
5.5.3	Plate submitted to torsional load	146



5.5.4 Optimal design of a square plate under weight-load . . . . . 149  
5.6 Synthesis . . . . . 152

---

## 5.1 Introduction

A shell model allows to parameterize the mechanical equation by the shape thanks to geometric quantities such as Christoffel symbols, metric and curvature tensors. The dependence of the mechanical problem to the material properties is naturally integrated, through the constitutive laws by means of the elastic tensor coefficients. This enables to optimize elegantly the shape using exact parameterization. As for the second aspect of the structure, the constituting material, we have discussed and derived in the previous chapter a material property discretization which allows to describe continuously the elastic properties. This formulation was based on B-spline function parameterization and allows to reduce the size of the design problem. We focus in this chapter on the development of both shape and material optimal design in the isogeometric framework. Geometry and material properties of the structure are both defined by B-spline functions and the design parameters are the control points coordinates. Different kinds of regularity constraints can be taken into account for the shape.

We focus in this chapter on the optimal design of shape and anisotropy of shell structures. The optimization process implemented to do so can rapidly become complex and heterogeneous. Indeed shape optimization is quite interdisciplinary, it combines many counterparts such as modelling, design, simulation, mathematical programming and computer science techniques. On the one hand, the design is defined on a CAD software. On the other hand, the analysis of the mechanical response, needed for computing the objective function, is commonly made using the finite element method based on a mesh approximating the exact geometry in a CAE environment. And finally, the optimization problem is set on this mesh [14]. Hence the so-defined optimization problem does not fit the original one which should involve the exact geometry. Nevertheless, once performed, the resulting optimal design has to be integrated in the CAD design environment. This involves a very costly step of mesh-CAD conversion process.

During the last few, a new method called isogeometric was developed to intend to reduce the gap between the design environment and those of structural response analysis and optimization. In fact isogeometric refers to numerical techniques in which the solution or a quantity of interest of a given problem is discretized with the basis functions describing the exact geometry in an isoparametric sense. Introduced by T.R. Hugues [37], these methods were first implemented in the frame of structural and computational fluid dynamic coupling.

Extensive works and researches have recently been devoted to the Isogeometric method which principle is based on a direct link and integration of the numerical analysis, optimization and the design process in the same environment. For optimization, the design variables are the control points associated to the NURBS functions [23] and sometimes their weights [60].

Our optimization problem is set in an isogeometric framework which, in fact, appears quite naturally when using shell models. These models offer a natural setting towards the integration of the isogeometric method since the mechanical problem is parameterized by the exact geometry mapping.

This chapter is organized as follows: we start by describing the parameterization using B-splines functions. We further focus on optimization problem. At a first instance, we consider the case of

simple geometry defined through one shell, and after consider a multi-shell geometry. In order to perform the sensitivity analysis which would be useful in the case of gradient-based optimization algorithms, we compute the derivatives of the stiffness matrix and the work of the applied loads with respect to the design parameters. The sensitivity is directly carried out with respect to the discrete parameters (control points co-ordinates) and mechanical problem is considered under its discrete (matrix) form.

## 5.2 Isogeometric shape parameterization

The isogeometric approach is based on the parameterization of fields of interest by mean of the blending functions associated to the geometry. In CAD environment, these functions are typically some Bézier, B-spline and NURBS functions. Splines are a more general form of Bezier functions introduced in [13], which are further generalized by NURBS functions. The idea of Bezier was to define curves and surfaces as polynomial functions with vectorial coefficients, e.g. the control points coordinates. The basis functions are the Bernstein polynomials. The advantage of doing so is that it enables to define smooth curves and surfaces. The aim of this section is to briefly recall the parameterization with B-spline functions [62].

Let  $\omega := [0, 1]^2$  denote the bi-dimensional parametric set, often referred to as a patch. Let us note  $\boldsymbol{\xi} := (\xi^1, \xi^2)$  the parametric coordinates in  $\omega$ . Assume that each parametric direction is partitioned using a knot vector  $\Sigma^\alpha$  comprising a non-decreasing sequence of real numbers called knots

$$\Sigma^\alpha = \{\xi_1^\alpha, \xi_2^\alpha, \dots, \xi_{n_\alpha + d_\alpha + 1}^\alpha\}, \text{ with } \xi_k^\alpha \leq \xi_{k+1}^\alpha,$$

where  $\xi_k^\alpha$ ,  $n_\alpha$ , and  $d_\alpha$  represent a knot, the number of univariate spline basis functions defined with the  $\alpha$ -th knot vector, and the polynomial degree. Also  $d_\alpha + 1$  is called order of the spline function. The knots do not require to be distinct, they can have a given multiplicity. The multiplicities define the influence of the control points. Let us assume that the number of distinct knot elements is  $k_\alpha \leq n_\alpha + d_\alpha + 1$ . The distinct knot points are called breakpoint knots and are denoted  $\hat{\xi}_i^\alpha$ ,  $i \in \{1, \dots, k_\alpha\}$  and their corresponding multiplicity, integer numbers noted  $m_i^\alpha$ , satisfy

$$\sum_{i=1}^{k_\alpha} m_i^\alpha = n_\alpha + d_\alpha + 1.$$

The multivariate spline basis polynomials are defined in a straightforward manner as tensor product of the univariate spline basis polynomial functions  $b_p^\alpha$ , which are defined recursively as follows.

**DEFINITION 5.2.1** Let  $\hat{\omega} := [0, 1]$  be the parametric domain partitioned with the knot vector  $\Sigma := (\xi_i)$ ,  $i \in \{1, \dots, n + d + 1\}$ , where  $n$  and  $d$  are respectively the number of spline basis polynomial functions and their degree. The univariate spline functions  $b_i^d$  are defined recursively from (the Cox-de-Boor formula) [32]

$$b_i^0(\xi) = \begin{cases} 1 & \text{if } \xi_i \leq \xi \leq \xi_{i+1} \\ 0 & \text{otherwise} \end{cases}, \quad i \in \{1, \dots, n + d\} \quad (5.1)$$

and for all  $p > 0$

$$b_i^p(\xi) = \frac{\xi - \xi_i}{\xi_{i+p} - \xi_i} b_i^{p-1}(\xi) + \frac{\xi_{i+p+1} - \xi}{\xi_{i+p+1} - \xi_{i+1}} b_{i+1}^{p-1}(\xi), \quad i \in \{1, \dots, n + d + 1 - p\} \quad (5.2)$$

where the convention  $\frac{0}{0} = 0$  is adopted in (5.2).

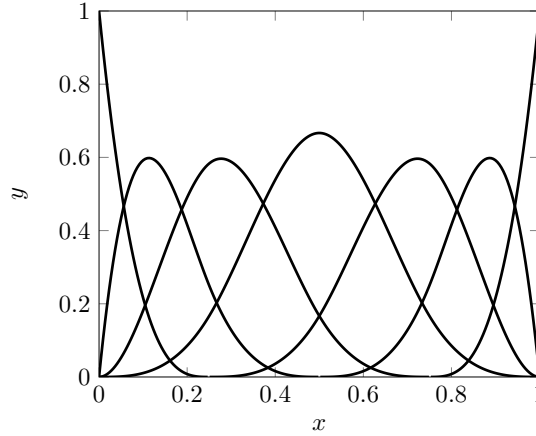


Figure 5.1 B-splines basis functions corresponding to the knot vector  $\Sigma = \{0, 0, 0, 0, 0.25, 0.5, 0.75, 1, 1, 1, 1\}$ , with  $d = 3$ .

Let us note  $\mathcal{B}_1(\Sigma, d)$  the space of univariate B-spline polynomial functions

$$\mathcal{B}_1(\Sigma, d) = \text{span}\{b_i^d, i \in \{1, \dots, n\}\}.$$

Figure 5.1 shows the B-spline basis function  $(b_i^3)_{i=1:7}$  corresponding to the knot vector  $\Sigma = \{0, 0, 0, 0, 0.25, 0.5, 0.75, 1, 1, 1, 1\}$ .

A univariate B-spline function is defined as a linear combination of the basis functions  $b_i^d$ . Letting  $c_i$  be the coefficients associated to the definition of a function  $C \in \mathcal{B}_1(\Sigma, d)$ , we have

$$C(\xi) := \sum_{i=1}^n c_i b_i^d(\xi). \quad (5.3)$$

A curve is defined by means of some control points weighted by their associated B-spline basis polynomial. Let us denote by  $\mathcal{C}$  the curve defined through the parametric function  $\phi \in \mathcal{B}_1(\Sigma, d) : \hat{\omega} \mapsto \mathcal{C} \in \mathbb{R}^3$

$$\phi(\xi) := \sum_{i=1}^n p_i b_i^d(\xi).$$

The shell's middle-surface is defined through a mapping from a bi-dimensional parametric domain  $\omega$  into  $\mathbb{R}^3$ . We thus focus on bivariate spline definition.

DEFINITION 5.2.2 Given two knot vectors  $\Sigma^\alpha = (\xi_i^\alpha)_{i=1:n_\alpha+d_\alpha+1}$  partitioning each direction of  $\omega$ , the corresponding bivariate spline functions of degree  $d$  are defined in a straightforward fashion as

$$b_{ij}^{\mathbf{d}}(\boldsymbol{\xi}) = b_i^{d_1}(\xi^1)b_j^{d_2}(\xi^2), \quad (5.4)$$

where  $\mathbf{d} = (d_\alpha)$  and  $b_i^{d_\alpha}$  are the univariate spline basis functions of degree  $d_\alpha$  defined through the knot vector  $\Sigma^\alpha$ .

Let's now recall some general properties of the B-spline functions:

- they are non-negative:  $b_i^{d_\alpha}(\xi) \geq 0$  for all  $\xi$
- they have local supports:  $\text{supp}(b_i^{d_\alpha}) = [\xi_i^\alpha, \xi_{i+d_\alpha+1}^\alpha]$ .
- the functions  $b_i^{d_\alpha}$  are at least of regularity  $C^{d_\alpha-m_\alpha}$ ,  $m_\alpha$  being the maximum multiplicity of the knot breakpoint in the  $\alpha$ -th direction.

We will assume subsequently that  $\hat{\xi}_1^\alpha = \hat{\xi}_{k_\alpha}^\alpha - 1 = 0$  and also that the knot vector is opened or clamped, i.e the multiplicity numbers  $m_1^\alpha = m_{k_\alpha}^\alpha = d_\alpha + 1$ . This in fact yields to a geometry (surface) which interpolates the end-points.

Let  $\mathcal{B}_2(\boldsymbol{\Sigma}, \mathbf{d})$  denote the spline space defined as

$$\mathcal{B}_2(\boldsymbol{\Sigma}, \mathbf{d}) = \text{span}\left\{\left(b_{ij}^{\mathbf{d}}\right)_{i=1:n_1}^{j=1:n_2}\right\}.$$

The properties recalled above are naturally inherited by multivariate spline basis.

Assume that the middle-surface is defined through a bivariate function  $\Phi : \omega \rightarrow \mathbb{R}^3$  of the space  $\mathcal{B}_2(\boldsymbol{\Sigma}, \mathbf{d})$ , by a finite set of weighting coefficients  $p_{ij} := (x_{ij}, y_{ij}, z_{ij}) \in \mathbb{R}^3$  called control points. More precisely

$$\Phi(\boldsymbol{\xi}) := \sum_{i,j=1}^{n_1, n_2} p_{ij} b_{ij}^{\mathbf{d}}(\boldsymbol{\xi}).$$

For simplicity reasons, we introduce and use as much as possible a unique-index for the numbering of the control points:  $i = i(p, q) \rightarrow i = (q-1)n_1 + p$ , and  $i \in \{1, \dots, n_{12} = n_1 n_2\}$ . So the function  $\Phi$  can be rewritten as

$$\Phi(\boldsymbol{\xi}) = \sum_{i=1}^{n_{12}} p_i b_i^{\mathbf{d}}(\boldsymbol{\xi}) \quad (5.5)$$

### 5.2.1 Multiple patches

A general curve (resp. surface) can be defined through many parametric curves (resp. surfaces) joined together. One of the most important advantages of a B-spline based parameterization is that the continuity and regularity constraints of the general curve (resp. surface) are defined through a finite set of algebraic relations on the control points. We, further, assume that the

joining is conforming in the sense that the common part between two surfaces is either empty or an entire boundary curve. We state below the regularity constraint on curve and surface. Subsequently, we denote by  $p_{i(k)}$  (resp.  $p_{i,j(k)}$ ) the control point of index  $i$  (resp.  $(i, j)$ ) associated to the patch of index  $k$ ; and  $q$  is used to denote the control points of any given interface. Hence  $q_{i(l)}$  is the  $i$ -th control point of the interface  $\Gamma^l$ .

### 5.2.1.1 Curve junction conditions

Let us consider two sets of control points  $(p_{i(k)})_{i=1:n}$ ,  $k \in \{n, m\}$  which define the curves  $\mathcal{C}_k$ , images of the parametric domains  $\omega_k := [0, 1]$  by the polynomial functions  $\phi_k \in \mathcal{B}_1(\Sigma^{(k)}, d_k)$ ;  $\Sigma^{(k)}$  being their respective open knot vector of length  $n_k + d_k + 1$  and  $d_k$  the degree of the associated B-spline basis functions.

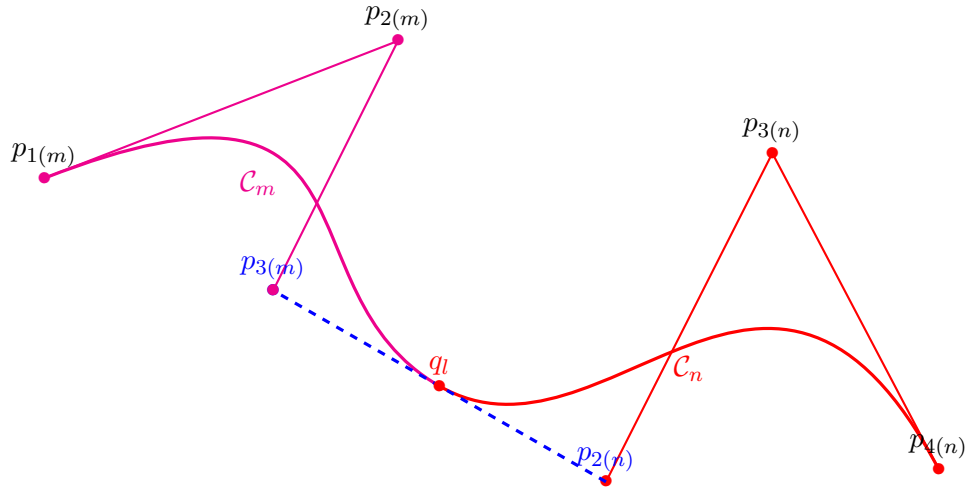


Figure 5.2 Illustration of a  $C^1$ -regularity on the junction of two B-splines curves of order 4 and of knot vector  $\Sigma^{(k)} = \{0, 0, 0, 0, 1, 1, 1, 1\}$ ,  $k \in \{n, m\}$ .

Let us assume that the curve  $C_m$  and  $C_n$  are respectively joined at the endpoint and the starting point, i.e respectively at the parametric coordinates  $\xi = 1$  and  $\xi = 0$ . One writes the continuity constraint

$$\phi_m(1) = \phi_n(0) \Rightarrow p_{n(m)} = p_{1(n)} := q_l. \tag{5.6}$$

For a  $C^1$ -continuity, we have the condition

$$\phi'_m(1) = \phi'_n(0).$$

The derivative of the B-spline basis function - see [59] page 59 - is

$$b_i^{p'}(\xi) = \frac{P}{\xi_{i+p} - \xi_i} b_i^{p-1}(\xi) - \frac{P}{\xi_{i+p+1} - \xi_{i+1}} b_{i+1}^{p-1}(\xi).$$

Since the knot vector is clamped such that  $\xi_1 = \dots = \xi_{d+1} = 0$ ,  $\xi_{n+1} = \dots = \xi_{n+d+1} = 1$ :

- for  $\xi = 0$  the only non-zero basis functions are:

$$b_1^{d'}(0) = -\frac{d}{\xi_{p+2} - \xi_2} b_2^{d-1}(\xi) \text{ and } b_2^{d'}(0) = \frac{d}{\xi_{d+2} - \xi_2} b_2^{d-1}(0)$$

- for  $\xi = 1$  the only non-zero basis functions are:

$$b_n^{d'}(1) = \frac{d}{\xi_{n+d} - \xi_n} b_n^{d-1}(1) \text{ and } b_{n-1}^{d'}(1) = -\frac{d}{\xi_{n+d} - \xi_n} b_n^{d-1}(1).$$

Moreover because  $b_{n-1}^{d-1}(1) = b_2^{d-1}(0) = 1$ , then we have

$$b_2^{d'}(0) = -b_1^{d'}(0) = \frac{d}{\xi_{d+2}} \text{ and } b_n^{d'}(1) = -b_{n-1}^{d'}(1) = \frac{d}{1 - \xi_n}.$$

Hence for a  $C^1$ -regularity, in addition to the condition (5.6), we have

$$\frac{1}{1 - \xi_n} (q_l - p_{n-1(m)}) = \frac{1}{\xi_{d+2}} (p_{2(n)} - q_l) \implies p_{2(n)} = (1 + \frac{\xi_{d+2}}{1 - \xi_n}) q_l - \frac{\xi_{d+2}}{1 - \xi_n} p_{n-1(m)}. \quad (5.7)$$

For a  $C^\alpha$ -regularity the number of independent control points is  $2 \times n - (\alpha + 1)$ :  $(p_{i(m)})_{i=1:n}$  and  $(p_{i(n)})_{i=\alpha+2:n}$ . Indeed, the control points  $(p_{i(n)})_{i=1:\alpha+1}$  are defined from some control points of the (mortar) patch of index  $m$ .

### 5.2.1.2 Surface junction conditions

Now, let us consider two B-spline surfaces  $\Omega_k$ ,  $k \in \{n, m\}$  defined as the images of the parametric domains  $\omega_k := [0, 1]^2$  by the bivariate polynomial functions  $\Phi_k \in \mathcal{B}_2(\Sigma^k, \mathbf{d}_k)$

$$\text{with } \Sigma^{(k)} = \left( \Sigma^{\alpha(k)} := \left( \xi_i^{\alpha(k)} \right)_{i=1:n_{\alpha(k)}+d_{\alpha(k)}+1} \right) \text{ and } \mathbf{d}_k = (d_{\alpha(k)}).$$

Let  $(p_{i,j(k)})$ ,  $i \in \{1, \dots, n_1(k)\}$ ,  $j \in \{1, \dots, n_2(k)\}$  be the control points associated to the mapping  $\Phi_k$ . Let us assume for the illustrative case that the two adjacent surfaces are joined along an interface (a curve)  $\Gamma^l$  corresponding to the image of the parametric lines  $\xi \in [0, 1] \rightarrow \varphi_{l(m)}(1, \xi^2 = \xi)$  by  $\Phi_m$  for  $\Omega_m$  and  $\xi \rightarrow \varphi_{l(n)}(\xi) = (0, \xi^2 = \xi)$  by  $\Phi_n$  for  $\Omega_n$ . The joining being assumed conforming  $n_{2(k)} = n_2$ ,  $d_{2(k)} = d_2$  and  $\Sigma^{2(k)} = \Sigma^2$ ,  $\forall k \in \{n, m\}$ . Hence

- the continuity condition is

$$\begin{aligned} \forall \xi \in [0, 1], \Phi_m(1, \xi) &= \Phi_n(0, \xi) \\ p_{n_1, j(m)} &= p_{1, j(n)} := q_{j(l)} \quad \forall j \in \{1, \dots, n_2\} \end{aligned} \quad (5.8)$$

- moreover the  $C^1$ -continuity entails  $\forall j \in \{1, \dots, n_2\}$

$$\begin{aligned} \forall \xi \in [0, 1], \Phi_m'(1, \xi) &= \Phi_n'(0, \xi) \\ \Leftrightarrow \frac{d_{1(m)}}{1 - \xi_{n_1(m)}} (q_{j(l)} - p_{n_1(m)-1, j(m)}) &= \frac{d_{1(n)}}{\xi_{d_1(n)+2}} (p_{2, j(n)} - q_{j(l)}) \\ \text{i.e. } p_{2, j(n)} &= \frac{d_{1(m)}}{d_{1(n)}} \frac{\xi_{d_1(n)+2}}{1 - \xi_{n_1(m)}} (q_{j(l)} - p_{n_1(m)-1, j(m)}) + q_{j(l)} \end{aligned} \quad (5.9)$$

In the case where  $\Sigma^{1(m)} = \Sigma^{1(n)} = \Sigma^1$  and  $d_{1(n)} = d_{1(m)} = d_1$ , we have

$$p_{2,j(n)} = \left(1 + \frac{\xi_{d_1+2}^1}{1 - \xi_{n_1}^1}\right) q_{j(l)} - \frac{\xi_{d_1+2}^1}{1 - \xi_{n_1}^1} p_{n-1,j(m)}.$$

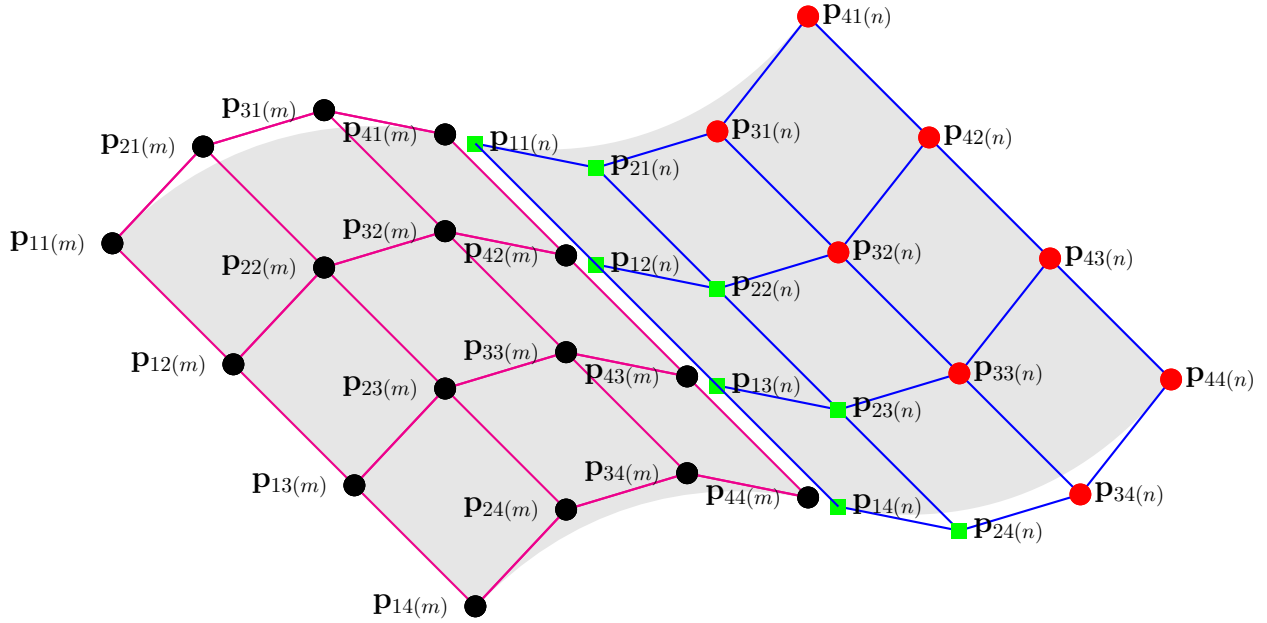


Figure 5.3 Illustration of the junction between the patches  $\Omega_n$  and  $\Omega_m$ . The control points colored in green are defined from the mortar control points. In case of  $C^0$  continuity, only the green control points on the interface are defined from the mortar control points. For  $C^1$ -continuity all the green control points are defined from the mortar control points

Figure 5.3 illustrates the junction between two patches and the linking between the control points. The control points colored in black and red are certainly independent.

In the next sections, we will assume that the geometry parameterization is conforming in the sense that the elementary curves or surfaces composing a general curve or surface are defined using the same knot vectors and same orders.

### 5.2.1.3 Matrix associated to the geometric regularity

In the case of a  $C^\alpha$ -regularity,  $\alpha \in \{0, 1\}$ , the number of independent control points is  $n_{12}^\alpha = 2 \times n_{12} - (\alpha + 1)n_2$ . Let us denote by  $\hat{\mathbf{p}} = (\hat{p}_i)_{i=1:n_{12}^\alpha}$  the set of independent control points, arranged as follows:

- the  $n_{12}$  independent control points of the patch  $\Omega_m$

$$\hat{p}_{I(i,j)} = p_{i,j(m)} \quad I(i,j) = (j-1) \times n_2 + i \quad \text{with } i \in \{1, \dots, n_1\} \text{ and } j \in \{1, \dots, n_2\}$$

- the  $n_{12} - (\alpha + 1) \times n_2$  independent control points of the patch  $\Omega_n$

$$\hat{p}_{I(i,j)} = p_{i,j(m)} \quad I(i,j) = (j-1) \times n_2 + i \text{ with } i \in \{\alpha+2, \dots, n_1\} \text{ and } j \in \{1, \dots, n_2\}.$$

The set of control points of the surface  $\Omega = \Omega_m \cup \Omega_n$  is denoted  $\mathbf{p} = (p_i)_{i=1:2 \times n_{12}}$  such that: for  $i \in \{1, \dots, n_1\}$ ,  $j \in \{1, \dots, n_2\}$  and  $I(i,j) = (j-1) \times n_2 + i$

$$\begin{aligned} p_{I(i,j)} &= p_{i,j(m)}, \text{ with } I_n(i,j) = n_{12} + I(i,j). \\ p_{I_n(i,j)} &= p_{i,j(n)} \end{aligned}$$

Let  $\mathcal{G}^\alpha$  be the matrix of geometric definition for the  $C^\alpha$ -regularity, such that

$$\mathbf{p} = \mathcal{G}^\alpha \hat{\mathbf{p}}.$$

The previous equality is to be understood coordinate-wise. The matrix  $\mathcal{G}^\alpha = \left( g_{i,j}^\alpha \right)_{i=1:2 \times n_{12}}^{j=1:n_{12}^\alpha}$  is defined as follows:

1. for the independent control points of  $\Omega_m$

$$g_{i,i}^\alpha = 1, \quad i \in \{1, \dots, n_{12}\}$$

2. the independent control points of  $\Omega_n$ ; for all  $i \in \{\alpha+2, n_1\}$  and  $j \in \{1, \dots, n_2\}$

$$g_{I(i,j), J(i,j)}^\alpha = 1,$$

where  $I(i,j) = n_{12} + (j-1) \times n_2 + i$  and  $J(i,j) = n_{12} + (j-1) \times (n_1 - (\alpha+1)) + (i - (\alpha+1))$ ;

3. for the interface control points  $(p_{1,j(n)})_{j=1:n_2}$  of  $\Omega_n$  -continuity-; for  $j \in \{1, \dots, n_2\}$

$$g_{I(j), J(j)}^\alpha = 1 \text{ and } I(j) = n_{12} + (j-1) \times n_2 + 1, \quad J(j) = j \times n_2$$

4. Specifically for a  $C^1$ -regularity, we have for the control points  $p_{2,j(n)}$ ,  $j \in \{1, \dots, n_2\}$

$$g_{I(j), J(n_1-\beta, j)}^\alpha = c_\beta, \text{ and } \beta \in \{0, 1\},$$

where the real number  $c_\beta$  is defined as

$$c_\beta = \begin{cases} 1 + \frac{\xi_{d_1+2}^1}{1-\xi_{n_1}^1} & \text{if } \beta = 0 \\ -\frac{\xi_{d_1+2}^1}{1-\xi_{n_1}^1} & \text{if } \beta = 1 \end{cases}$$

and the indices  $I(j)$  and  $J(i,j)$  are defined as

$$I(j) = n_{12} + (j-1) \times n_1 + 1, \quad J(i,j) = (j-1) \times n_2 + i.$$

REMARK 5.2.1 In an analogous manner to the geometry, we introduce the following notations in regards to the discretization of the polar parameters:



- $(\Phi_1^{i(k)})_{i=1:n_{12}^\Phi}$  denote the *control points* associated to the discretization of the orthotropy angle field  $\Phi_1$  on the patch  $\Omega_k$
- $(\rho_0^{i(k)})_{i=1:n_{12}^\rho}$  (resp.  $(\rho_1^{i(k)})_{i=1:n_{12}^\rho}$ ) are the *control points* associated to the discretization of the dimensionless moduli  $\rho_0 = \frac{R_0^K}{R_0^{KL}}$  (resp.  $\rho_1 = \frac{R_1}{R_1^L}$ ), for a conforming parameterization of  $R_1$ .

We introduce  $\Phi$  (resp.  $\rho_\alpha$ ) and  $\hat{\Phi}_1$  (resp.  $\hat{\rho}_\alpha$ ), analogue of  $\mathbf{p}$  (resp.  $\hat{\mathbf{p}}$ ) for the polar parameters. They are related through their respective matrices denoted  $\mathcal{G}_\Phi^0$  and  $\mathcal{G}_\rho^0$ ;  $\mathcal{G}_e^0$  is of dimensions  $2 n_{12}^e \times (2 n_{12}^e - n_2^e)$ , for  $e \in \{\Phi, \rho\}$ . We only consider a continuity conditions on the polar parameters. Hence we introduce  $\hat{\mathbf{d}} = (\hat{\mathbf{p}}, \hat{\Phi}_1, \hat{\rho}_0, \hat{\rho}_1)$  the set of independent shape and material design variables and  $\mathbf{d} = (\mathbf{p}, \Phi_1, \rho_0, \rho_1)$  the set of control points associated to the assembling of patches. Obviously, in the case of geometry composed of one patch  $\hat{\mathbf{d}} = \mathbf{d}$ .

After the previous geometric considerations, we focus in the next section on the optimization problem in the case of a middle-surface defined by one patch and we present the related sensitivity study aspects.

### 5.3 Anisotropy and shape optimization

Subsequently, for the sake of simplicity,  $\mathbf{u} := [\mathbf{u}, \mathbf{s}]$  and  $\mathbf{v} := [\mathbf{v}, \mathbf{r}]$  stand respectively for the three-dimensional displacement vector of the middle-surface and a given admissible virtual displacement.

Let us consider the optimization problem which consists in the minimization of the compliance with respect to the shape and material:

$$\begin{aligned} \mathbf{d}^* &= \arg \min_{\mathbf{d} \in \mathcal{E}_{ad}} J(\mathbf{u}), \text{ with } J(\mathbf{u}) = l(\mathbf{u}) \\ \text{s. t. } &a(\mathbf{u}, \mathbf{v}) = l(\mathbf{v}), \text{ for all } \mathbf{v} \in V(\omega) \end{aligned} \quad (5.10)$$

where  $\mathbf{d}$  is the set of both elastic and shape design variables.  $\mathcal{E}_{ad}$  is a properly specified admissible design space which takes into account the constraints on the polar parameters as described in chapter 4 and those on the geometry which will be laid out further in subsection 5.4.3.

Using the polar formalism, one can express the plane elastic tensor components  $Q^{\alpha\beta\lambda\mu}$  as

$$Q^{\alpha\beta\lambda\mu}(\Phi_1) = G_{\alpha'}^\alpha G_{\beta'}^\beta G_{\lambda'}^\lambda G_{\mu'}^\mu \hat{Q}^{\alpha'\beta'\lambda'\mu'}(\Phi_1),$$

where  $\mathbf{G} = (G_j^i)$  is the transformation matrix from the orthonormal frame  $(\mathbf{d}_1, \mathbf{d}_2, \mathbf{d}_3)$  onto the covariant frame

$$G_j^i = \mathbf{a}^i \cdot \mathbf{d}_j, \quad \mathbf{d}_j = G_j^i \mathbf{a}_i.$$

and  $\hat{\mathbb{Q}} := (\hat{Q}^{\alpha\beta\lambda\mu})$  is the plane reduced elastic tensor in the material frame defined as

$$\hat{Q}^{\alpha\beta\lambda\mu} = A^{\alpha\beta\lambda\mu} - \frac{A^{\alpha\beta 33} A^{33\lambda\mu}}{A^{3333}}.$$

Analogously, for the anti-plane writes

$$E^{\alpha 3 \beta 3}(\Phi_1) = G_\lambda^\alpha G_\lambda^\beta A^{\lambda 3 \lambda 3}(\Phi_1).$$

In the previous expression  $A^{ijkl}$  are the components of the elastic tensor given in the material framework as introduced in chapter 2.

In order to use a gradient based optimization method one has to study the sensitivity of the objective function and constraints, namely the mechanical state equation, with respect to the design variables. There exists two main ways to compute the sensitivity: the direct and the adjoint approach. The latter is a classical approach in optimal control theory [45] and also in structural optimization [21] and [42]. The adjoint method relies on the definition of a Lagrangian function to compute the objective function derivative, and thus on the introduction of some Lagrange multipliers associated to the constraints. Both sensitivity can be performed on the continuum problem or on its discretized form [2, 63]. The present minimization problem of compliance criterion subjected to the mechanical equation constraint is self-adjoint because the Lagrange multiplier associated to the mechanical equation is solution of the same mechanical. Hence the derivative can be computed by the direct approach. We consider the compliance objective function in its discrete form, i.e

$$J(\mathbf{d}, \mathbf{u}(\mathbf{d})) = \mathbf{f} \cdot \mathbf{u}$$

where  $\mathbf{f}$  is a vector depending on the applied load and  $\mathbf{u}$  the vector of degrees of freedom associated to the discretization of the displacement field.

PROPOSITION 5.3.1 *Let us consider the discrete form of the state equation*

$$\mathbf{K}\mathbf{u} = \mathbf{f} \text{ with } \mathbf{K} \text{ the stiffness matrix.}$$

*The derivative of the objective function with respect to the design variable  $d$  is*

$$\partial_d J(\mathbf{d}, \mathbf{u}(\mathbf{d})) = 2\partial_d \mathbf{f} \cdot \mathbf{u} - \mathbf{u} \partial_d \mathbf{K} \mathbf{u}. \quad (5.11)$$

*Proof.* Indeed, the derivative of the discrete form of the state equation yields to

$$\partial_d \mathbf{K} \mathbf{u} + \mathbf{K} \partial_d \mathbf{u} = \partial_d \mathbf{f} \implies \partial_d \mathbf{u} = \mathbf{K}^{-1}(\partial_d \mathbf{f} - \partial_d \mathbf{K} \mathbf{u}). \quad (5.12)$$

Thus the derivative of the objective function with respect to  $p$  is

$$\partial_d J(\mathbf{d}, \mathbf{u}) = \partial_d \mathbf{f} \cdot \mathbf{u} + \mathbf{f} \cdot \partial_d \mathbf{u}. \quad (5.13)$$

By substituting the (5.12) in (5.13), we obtain

$$\partial_d J(\mathbf{d}, \mathbf{u}) = \partial_d \mathbf{f} \cdot \mathbf{u} + \mathbf{f} \cdot \mathbf{K}^{-1}(\partial_d \mathbf{f} - \partial_d \mathbf{K} \mathbf{u}),$$

and finally we have

$$\partial_d J(\mathbf{d}, \mathbf{u}) = 2\partial_d \mathbf{f} \cdot \mathbf{u} - \mathbf{u} \partial_d \mathbf{K} \mathbf{u}. \quad (5.14)$$

□

In order to compute the gradient of the objective function with respect to the design parameters, we focus on the derivatives of the elementary quantities with respect to the parameters.

### 5.3.1 Derivatives with respect to the shape

The derivative of the strain energy bilinear form with respect to the control point coordinates involves the derivatives of the metric, curvature tensors and the Christoffel symbols. These quantities are expressed through some derivatives of the shape mapping with respect to the curvilinear coordinates. The derivative of these elementary quantities are obtained by the usual chain rule.

PROPOSITION 5.3.2 *Let us consider a shape function  $\Phi \in \mathcal{B}_2(\boldsymbol{\Sigma}, \mathbf{d}) \cap C^2(\omega, \mathbb{R}^3)$ , i.e*

$$\Phi(\boldsymbol{\xi}) = \Phi_k(\boldsymbol{\xi}) \mathbf{e}^k, \text{ with } \Phi_k(\boldsymbol{\xi}) = \sum_{i=1}^{n_{12}} [p_i]_k b_i^{\mathbf{d}}(\boldsymbol{\xi}),$$

*with  $[p_i]_k = p_i \cdot \mathbf{e}_k$  the  $k$ -th coordinate of the  $i$  control point  $p_i \in \mathbb{R}^3$ . The first two derivatives of  $\Phi$ ,  $\mathbf{a}_\alpha$  and  $\mathbf{a}_{\alpha,\beta}$ , are defined by*

$$\mathbf{a}_\alpha(\boldsymbol{\xi}) = \sum_{i=1}^{n_{12}} p_i \partial_\alpha b_i^{\mathbf{d}}(\boldsymbol{\xi}), \quad \mathbf{a}_{\alpha,\beta} = \sum_{i=1}^{n_{12}} p_i \partial_{\alpha\beta} b_i^{\mathbf{d}}(\boldsymbol{\xi}).$$

We emphasize that, according to the previous proposition, the metric tensor components are defined in a straightforward way. Using the contravariant metric, one can define the contravariant vectors, the Christoffel symbols and the different curvature tensor components. Let's now get interested in the derivatives with respect to the control points and their coordinates.

PROPOSITION 5.3.3 *Let us consider the function  $\Phi \in \mathcal{B}_2(\boldsymbol{\Sigma}, \mathbf{d}) \cap C^2(\omega, \mathbb{R}^3)$ , we define*

$$\partial_i \Phi(\boldsymbol{\xi}) := b_i^{\mathbf{d}}(\boldsymbol{\xi}) \text{ and } \partial_i^k \Phi(\boldsymbol{\xi}) := b_i^{\mathbf{d}}(\boldsymbol{\xi}) \mathbf{e}_k, \quad k \in \{1, 2, 3\}.$$

*$\partial_i$  is the derivative with respect to the control point  $\mathbf{p}_i$  and  $\partial_i^k$  is the derivative with respect to the  $k$ -th coordinate of the control point of index  $i$ .*

*Analogously, the derivatives of the vectors  $\mathbf{a}_\alpha$  and  $\mathbf{a}_{\alpha,\beta}$  with respect to the  $i$ -th control point are:*

$$\partial_i \mathbf{a}_\alpha(\boldsymbol{\xi}) = \partial_\alpha b_i^{\mathbf{d}}(\boldsymbol{\xi}) \text{ and } \partial_i \mathbf{a}_{\alpha,\beta} = \partial_{\alpha\beta} b_i^{\mathbf{d}}(\boldsymbol{\xi}).$$

*Finally the derivatives with respect to  $k$ -th coordinate of the  $i$ -th control point is*

$$\partial_i^k \mathbf{a}_\alpha(\boldsymbol{\xi}) = \mathbf{e}_k \partial_\alpha b_i^{\mathbf{d}}(\boldsymbol{\xi}) \text{ and } \partial_i^k \mathbf{a}_{\alpha,\beta} = \mathbf{e}_k \partial_{\alpha\beta} b_i^{\mathbf{d}}(\boldsymbol{\xi})$$

The derivatives of the mapping function  $\Phi$  with respect to a control point is simply equal to the corresponding blending function of that control point. Also, the derivative with respect to a given coordinate is equal to the Euclidean space canonical basis vector (of that coordinate) weighted by the corresponding blending function of its control point.

We state in the next lemma the derivative of the different quantities of the strain energy bilinear form -see (2.35) page 25- with respect to the control point coordinates.

LEMMA 5.3.1 *Let  $\Phi \in \mathcal{B}_2(\Sigma, \mathbf{d}) \cap C^2(\omega, \mathbb{R}^3)$  such that  $\mathbf{a}_\alpha$ ,  $\alpha \in \{1, 2\}$  are linearly independent. Then:*

$$\begin{aligned}
 \partial_i^k \mathbf{a}_\alpha &= \partial_\alpha b_i^d(\boldsymbol{\xi}) \mathbf{e}_k \\
 \partial_i^k a_{\alpha\beta} &= [\mathbf{a}_\beta]_k \partial_\alpha b_i^d(\boldsymbol{\xi}) + [\mathbf{a}_\alpha]_k \partial_\beta b_i^d(\boldsymbol{\xi}) \\
 \partial_i^k a &= 2a [\mathbf{a}^\mu]_k \partial_\mu b_i^d(\boldsymbol{\xi}) \\
 \partial_i^k \mathbf{a}_3 &= -[\mathbf{a}_3]_k (\partial_\mu b_i^d(\boldsymbol{\xi}) \mathbf{a}^\mu) \\
 \partial_i^k \mathbf{a}^\alpha &= -[\mathbf{a}^\alpha]_k (\partial_\mu b_i^d \mathbf{a}^\mu) + [\mathbf{a}_3]_k (a^{\alpha\mu} \partial_\mu b_i^d) \mathbf{a}_3 \\
 \partial_i^k a^{\alpha\beta} &= -\{a^{\beta\mu} [\mathbf{a}^\alpha]_k + a^{\alpha\mu} [\mathbf{a}^\beta]_k\} \partial_\mu b_i^d \\
 \partial_i^k \mathbf{a}_{\alpha,\beta} &= \partial_{\alpha\beta} b_i^d(\boldsymbol{\xi}) \mathbf{e}_k \\
 \partial_i^k \Gamma_{\beta\sigma}^\alpha &= [\mathbf{a}_3]_k \partial_{\beta\sigma} b_i^d + \{a^{\alpha\mu} b_{\beta\sigma} [\mathbf{a}_3]_k - \Gamma_{\beta\sigma}^\mu [\mathbf{a}^\alpha]_k\} \partial_\mu b_i^d(\boldsymbol{\xi}) \\
 \partial_i^k b_{\alpha\beta} &= [\mathbf{a}_3]_k \partial_{\alpha\beta} b_i^d(\boldsymbol{\xi}) - \Gamma_{\alpha\beta}^\mu [\mathbf{a}_3]_k \partial_\mu b_i^d(\boldsymbol{\xi}) \\
 \partial_i^k b_\beta^\alpha &= [\mathbf{a}_3]_k (a^{\alpha\mu} \partial_{\beta\mu} b_i^d) - \{b_\beta^\mu [\mathbf{a}^\alpha]_k + a^{\alpha\mu} b_{\beta\lambda} [\mathbf{a}^\lambda]_k + \\
 &\quad \Gamma_{\beta\lambda}^\mu a^{\alpha\lambda} [\mathbf{a}_3]_k\} \partial_\mu b_i^d(\boldsymbol{\xi})
 \end{aligned} \tag{5.15}$$

The proof uses the following lemma which is proven in [9]- Lemma 3.2.1, page 299-.

LEMMA 5.3.2 *Let  $\Phi \in \mathcal{B}_2(\Sigma, \mathbf{d}) \cap C^2(\omega, \mathbb{R}^3)$  be an injective mapping such that  $\mathbf{a}_\alpha$ ,  $\alpha \in \{1, 2\}$  are linearly independent. For all  $\Psi \in C^2(\omega, \mathbb{R}^3)$ , we have*

$$\begin{aligned}
 \partial_\Phi \mathbf{a}_\alpha \Psi &= \Psi_{,\alpha} \\
 \partial_\Phi a_{\alpha\beta}(\Phi) \Psi &= \mathbf{a}_\beta \cdot \Psi_{,\alpha} + \mathbf{a}_\alpha \cdot \Psi_{,\beta} \\
 \partial_\Phi a(\Phi) \Psi &= 2a(\Phi) (\mathbf{a}^\mu \cdot \Psi_{,\mu}) \\
 \partial_\Phi \mathbf{a}_3(\Phi) \Psi &= -(\mathbf{a}_3 \cdot \Psi_{,\mu}) \mathbf{a}^\mu(\Phi) \\
 \partial_\Phi \mathbf{a}^\alpha \Psi &= -(\mathbf{a}^\alpha \cdot \Psi_{,\mu}) \mathbf{a}^\mu(\Phi) + a^{\alpha\mu}(\Phi) (\mathbf{a}_3(\Phi) \cdot \Psi_{,\mu}) \mathbf{a}_3(\Phi) \\
 \partial_\Phi a^{\alpha\beta}(\Phi) \Psi &= -[a^{\beta\mu}(\Phi) \mathbf{a}^\alpha(\Phi) + a^{\alpha\mu}(\Phi) \mathbf{a}^\beta(\Phi)] \cdot \Psi_{,\mu} \\
 \partial_\Phi \mathbf{a}_{\alpha,\beta}(\Phi) \Psi &= \Psi_{,\alpha\beta} \\
 \partial_\Phi \Gamma_{\beta\sigma}^\alpha \Psi &= \mathbf{a}^\alpha(\Phi) \cdot \Psi_{,\beta\sigma} + [a^{\alpha\mu}(\Phi) b_{\beta\sigma}(\Phi) \mathbf{a}_3(\Phi) - \Gamma_{\beta\sigma}^\mu(\Phi) \mathbf{a}^\alpha(\Phi)] \cdot \Psi_{,\mu} \\
 \partial_\Phi b_{\alpha\beta}(\Phi) \Psi &= \mathbf{a}_3(\Phi) \cdot \Psi_{,\alpha\beta} - \Gamma_{\alpha\beta}^\mu(\Phi) (\mathbf{a}_3(\Phi) \cdot \Psi_{,\mu}) \\
 \partial_\Phi b_\beta^\alpha(\Phi) \Psi &= a^{\alpha\mu}(\Phi) (\mathbf{a}_3(\Phi) \cdot \Psi_{,\beta\mu}) - [b_\beta^\mu(\Phi) \mathbf{a}^\alpha(\Phi) + a^{\alpha\mu}(\Phi) b_{\beta\lambda}(\Phi) \mathbf{a}^\lambda(\Phi) + \\
 &\quad \Gamma_{\beta\lambda}^\mu(\Phi) a^{\alpha\lambda}(\Phi) \mathbf{a}_3(\Phi)] \cdot \Psi_{,\mu}
 \end{aligned} \tag{5.16}$$

Readers may refer to [9] for the proof which is most technical with the use of the classical chain rule.

The derivative in the Lemma 5.3.1 are straightforwardly obtained from the Lemma 5.3.2 by substituting  $\Psi$  with the corresponding derivative of the mapping with respect to the control point coordinates. More precisely, for the computation of a given derivative with respect to the  $k$ -th coordinate of the control point of index  $i$ , one sets  $\Psi = \partial_i^k \Phi(\boldsymbol{\xi}) = b_i^d \mathbf{e}_k$ .

### 5.3.2 Derivatives of the strain bilinear form

In the next proposition, we specify the derivative of the bilinear form with respect to any given shape parameter  $d$ .

PROPOSITION 5.3.4 *Let  $\partial_d$  denotes the derivative with respect to a given parameter  $d \in \mathbf{d}$ . We*

have

$$\begin{aligned} \partial_d a([\mathbf{u}, \mathbf{s}], [\mathbf{v}, \mathbf{r}]) &= \int_{\omega} t \{ \partial_d Q^{\alpha\beta\lambda\mu} \gamma_{\lambda\mu\cdot\alpha\beta}(\mathbf{u}; \mathbf{v}) + Q^{\alpha\beta\lambda\mu} \partial_d \gamma_{\lambda\mu\cdot\alpha\beta}(\mathbf{u}; \mathbf{v}) \\ &\quad + t^2 \{ \partial_d Q^{\alpha\beta\lambda\mu} \chi_{\lambda\mu\cdot\alpha\beta}([\mathbf{u}, \mathbf{s}]; [\mathbf{v}, \mathbf{r}]) + Q^{\alpha\beta\lambda\mu} \partial_d \chi_{\lambda\mu\cdot\alpha\beta}([\mathbf{u}, \mathbf{s}], [\mathbf{v}, \mathbf{r}]) \} \\ &\quad + \partial_d E^{3\alpha 3\beta} \gamma_{3,\alpha\cdot\beta}([\mathbf{u}, \mathbf{s}]; [\mathbf{v}, \mathbf{r}]) + E^{\alpha 3\beta 3} \partial_d \gamma_{3,\alpha\cdot\beta}([\mathbf{u}, \mathbf{s}]; [\mathbf{v}, \mathbf{r}]) \} \sqrt{ad} d\xi \\ &\quad + \int_{\omega} t \{ Q^{\alpha\beta\lambda\mu} \gamma_{\lambda\mu\cdot\alpha\beta}(\mathbf{u}; \mathbf{v}) + t^2 Q^{\alpha\beta\lambda\mu} \chi_{\lambda\mu\cdot\alpha\beta}(\mathbf{u}; \mathbf{v}) \\ &\quad + E^{3\alpha 3\beta} \gamma_{3,\alpha\cdot\beta}([\mathbf{u}, \mathbf{s}]; [\mathbf{v}, \mathbf{r}]) \} 2^{-1} a^{-1/2} \partial_d a \, d\xi \end{aligned}$$

where for expansion reduction, we set for  $z \in \{\gamma, \chi\}$

$$\begin{aligned} z_{\lambda\mu\cdot\alpha\beta}(\cdot, *) &:= z_{\lambda\mu}(\cdot) z_{\alpha\beta}(*) \text{ and } \partial_p z_{\lambda\mu\cdot\alpha\beta}(\cdot, *) := \partial_d z_{\lambda\mu}(\cdot) z_{\alpha\beta}(*) + z_{\lambda\mu}(\cdot) \partial_d z_{\alpha\beta}(*) \\ z_{3,\alpha\cdot\beta}(\cdot, *) &:= z_{3\alpha}(\cdot) z_{3\beta}(*) \text{ and } \partial_p z_{3,\alpha\cdot\beta}(\cdot, *) := \partial_d z_{3\alpha}(\cdot) z_{3\beta}(*) + z_{3\alpha}(\cdot) \partial_d z_{3\beta}(*) \end{aligned}$$

- o The derivatives of the elastic tensor components with respect to the shape parameter  $d$  are expressed as follows:

$$\begin{aligned} \partial_d Q^{\alpha\beta\lambda\mu} &:= \partial_d (G_{\alpha'}^{\alpha} G_{\beta'}^{\beta} G_{\lambda'}^{\lambda} G_{\mu'}^{\mu}) \hat{Q}^{\alpha'\beta'\lambda'\mu'}(\Phi_1) \\ \partial_d E^{3\alpha 3\beta} &:= \partial_d (G_{\lambda}^{\alpha} G_{\lambda}^{\beta}) A^{3\lambda 3\lambda}(\Phi_1) \end{aligned}$$

- o The derivatives with respect to a material properties design variable are expressed by

$$\begin{aligned} \partial_d Q^{\alpha\beta\lambda\mu} &:= (G_{\alpha'}^{\alpha} G_{\beta'}^{\beta} G_{\lambda'}^{\lambda} G_{\mu'}^{\mu}) \partial_d \hat{Q}^{\alpha'\beta'\lambda'\mu'}(\Phi_1) \\ \partial_d E^{3\alpha 3\beta} &:= (G_{\lambda}^{\alpha} G_{\lambda}^{\beta}) \partial_d A^{3\lambda 3\lambda}(\Phi_1). \end{aligned}$$

The following proposition gives the derivative of the strain components with respect to the control point coordinates.

PROPOSITION 5.3.5 *Let consider a mapping function  $\Phi \in C^2(\omega, \mathbb{R}^3)$  and  $\Psi \in C^2(\omega, \mathbb{R}^3)$ .*

- o The derivative of the membrane, bending and shear strains covariant components with respect to  $\Phi$  are:

$$\begin{aligned} \partial_{\Phi} \gamma_{\alpha\beta} \Psi &= -\partial_{\Phi} \Gamma_{\alpha\beta}^{\sigma} \Psi u_{\sigma} - \partial_{\Phi} b_{\alpha\beta} \Psi u_3 \\ \partial_{\Phi} \chi_{\alpha\beta} \Psi &= -\partial_{\Phi} \Gamma_{\alpha\beta}^{\sigma} \Psi s_{\sigma} - \partial_{\Phi} b_{\alpha}^{\lambda} \Psi d_{\lambda\beta}(\mathbf{u}) - \partial_{\Phi} b_{\beta}^{\lambda} \Psi d_{\lambda\alpha}(\mathbf{u}) \\ &\quad + b_{\alpha}^{\lambda} (\Gamma_{\lambda\beta}^{\sigma} \Psi u_{\sigma} + \partial_{\Phi} b_{\lambda\beta} \Psi u_3) + b_{\beta}^{\lambda} (\partial_{\Phi} \Gamma_{\lambda\alpha}^{\sigma} \Psi u_{\sigma} + \partial_{\Phi} b_{\lambda\alpha} \Psi u_3) \\ \partial_{\Phi} \gamma_{\alpha 3} \Psi &= \partial_{\Phi} b_{\alpha}^{\sigma} \Psi u_{\sigma}. \end{aligned}$$

- o Assume that  $\Phi \in C^2(\omega, \mathbb{R}^3) \cap \mathcal{B}_2(\Sigma, \mathbf{d})$ , the derivative with respect to the control point coordinates are then:

$$\begin{aligned} \partial_i^k \gamma_{\alpha\beta} &= -\partial_i^k \Gamma_{\alpha\beta}^{\sigma} u_{\sigma} - \partial_i^k b_{\alpha\beta} u_3 \\ \partial_i^k \chi_{\alpha\beta} &= -\partial_i^k \Gamma_{\alpha\beta}^{\sigma} \Psi s_{\sigma} - \partial_i^k b_{\alpha}^{\lambda} \Psi d_{\lambda\beta}(\mathbf{u}) - \partial_i^k b_{\beta}^{\lambda} \Psi d_{\lambda\alpha}(\mathbf{u}) \\ &\quad + b_{\alpha}^{\lambda} (\partial_i^k \Gamma_{\lambda\beta}^{\sigma} \Psi u_{\sigma} + \partial_i^k b_{\lambda\beta} u_3) + b_{\beta}^{\lambda} (\partial_i^k \Gamma_{\lambda\alpha}^{\sigma} \Psi u_{\sigma} + \partial_i^k b_{\lambda\alpha} u_3) \\ \partial_i^k \gamma_{\alpha 3} &= \partial_i^k b_{\alpha}^{\sigma} u_{\sigma}. \end{aligned}$$

Now we focus on the linear form, i.e the work of the applied loads.

### 5.3.3 Derivatives of the linear form

In order to define the derivatives of the linear associated to the applied loads, we have to distinguish two cases: when the applied loads are geometry dependent and when the applied loads are independent from the geometry.

#### 5.3.3.1 Geometry dependent loads

Assume that the middle-surface is subjected to applied resultant force  $\mathbf{N} = N^i \mathbf{a}_j$ , a moment vector  $\mathbf{M} := \mathbf{M} \times \mathbf{a}_3 = e_{\alpha\beta} M^{\alpha\beta} \mathbf{a}^{\beta}$  on its edge  $\Gamma_1 = \Phi(\gamma_1)$  and a surface force  $\mathbf{p} = p^i \mathbf{a}_i$ . Let us denote by  $l_g$  the linear form associated to that geometric dependent loads

$$l_g(\mathbf{u}, \mathbf{s}) = \int_{\omega} p^i v_i \sqrt{a} d\xi + \int_{I_1} (N^i v_i + M^{\alpha} s_{\alpha}) L(\eta) d\eta$$

where  $dL(\eta) = L(\eta) d\eta$  is the element of length along  $\Gamma_1 = \Phi(\gamma_1)$  and

$$L(\eta) := \left\{ \frac{\partial \varphi^{\alpha}}{\partial \eta} a_{\alpha\beta} \frac{\partial \varphi^{\beta}}{\partial \eta} \right\}^{1/2}.$$

It is assumed that  $\gamma_1$  is defined as the image on a bounded interval  $I$  through a bidimensional vector mapping  $\varphi$ , i.e.  $(\varphi^{\alpha}) : \eta \rightarrow (\xi^{\alpha} = \varphi^{\alpha}(\eta)) \in \gamma_1$ .

The derivative with respect to the  $k$ -th coordinate of the control point of index  $i$  is

$$\partial_i^k l_g(\mathbf{u}, \mathbf{s}) = \int_{\omega} p^i u_i (2^{-1} a^{-1/2} \partial_i^k a) d\xi + \int_{I_1} (N^i u_i + M^{\alpha} s_{\alpha}) \partial_i^k L(\eta) d\eta,$$

with

$$\partial_i^k L(\eta) = 2^{-1} L(\eta)^{-1/2} \left\{ \frac{\partial \varphi^{\alpha}}{\partial \eta} \partial_i^k a_{\alpha\beta} \frac{\partial \varphi^{\beta}}{\partial \eta} \right\}.$$

We notice that a particular geometry dependent load is the normal pressure, which for a geometry with sufficiently small thickness is of the form  $\mathbf{p} = p \mathbf{a}_3$ ;  $p$  being the amplitude of the applied pressure per area.

#### 5.3.3.2 Geometry independent loads

Now we suppose that the applied loads are defined by means of their Cartesian components, denoted by a hat symbol:

$$\mathbf{g} = \hat{g}^i \mathbf{e}_i = g^j \mathbf{a}_j, \text{ with } g \in \{p, N\}.$$

with  $g^j := \mathbf{g} \cdot \mathbf{a}^j = \hat{g}^i [\mathbf{a}^j]^i$  the contravariant components. Thus the derivative of the corresponding contravariant components with respect to  $(i, k)$  is

$$\partial_i^k g^q = (\mathbf{g} \cdot \partial_i^k \mathbf{a}^q) = \hat{g}^r [\partial_i^k \mathbf{a}^q]^r.$$

We stress the point that we do not assume applied moment to be independent of the geometry. This could not be consistent with the fact that it must hold the plane moment constraint for

each admissible design:  $\mathbf{M} \cdot \mathbf{a}_3 = 0$ .

Then the derivative of the linear form is

$$\begin{aligned} \partial_i^k l_i(\mathbf{u}, \mathbf{s}) &= \int_{\omega} p^i u_i (2^{-1} a^{-1/2} \partial_i^k a) d\xi + \int_{\omega} N^i u_i \partial_i^k L(\eta) d\eta \\ &+ \int_{\omega} \partial_i^k p^i u_i \sqrt{a} d\xi + \int_{\omega} \partial_i^k N_i u_i L(\eta) d\eta \end{aligned}$$

**For pointwise loads:**

Let  $l_p$  be the work of some pointwise concentrated loads  $\mathbf{f}_p = \hat{f}_p^i \mathbf{e}_i$ , at some points  $P_p = \Phi(\xi_p) \in \bar{\Omega}$ .  $r$  being the number of points. The corresponding linear form and its derivative are respectively

$$l_p(\mathbf{u}, \mathbf{s}) = \sum_{p=1}^r \hat{f}_p^i u_i(\xi_p)$$

and

$$\partial_i^k l_p(\mathbf{u}, \mathbf{s}) = \sum_{p=1}^r \partial_i^k \hat{f}_p^j u_j(\xi_p)$$

At this step, the design problem takes account of a shell defined through one chart. We have defined the derivative with respect to the control points coordinate of the strain energy bilinear form and the linear form. We recall that the applied loads and the corresponding linear form is considered independent of the material properties with respect to which the bilinear form's derivatives have already been computed in Chapter 4.

We consider in the next section the design problem corresponding to a structure defined from a set of connected piecewise regular shells. We will mostly focus on the derivative of the junction conditions (matching of the displacement and rotation) which are involved in the definition of the global mechanical problem.

## 5.4 Sensitivity for an assembling of shells

General shell structures cannot be defined from a single regular surface or mapping, as presented so far. This section is devoted to the sensitivity of the junction operator defined in chapter 3 which is involved in the definition of shell assembling problem. In fact, one has to study the sensitivity of the junction conditions with respect to the shape design parameters and also take into account the geometry continuity when defining the derivatives of the mechanical problem.

### 5.4.1 Problem setting

Now, we assume that the optimization problem involves an assembling of shells. The mechanical problem is of the form: Find  $\bar{\mathbf{u}}$  such that

$$\bar{\mathbf{K}}\bar{\mathbf{u}} = \bar{\mathbf{f}}.$$

$\bar{\mathbf{u}}$  is the vector of independent degrees of freedom,  $\bar{\mathbf{f}} = \mathbf{M}^T \mathbf{f}$  is the corresponding load vector and  $\bar{\mathbf{K}}$  is the stiffness matrix

$$\bar{\mathbf{K}} = \mathbf{M}^T \mathbf{K} \mathbf{M},$$

where  $\mathbf{M}$  is the mechanical junction matrix.

Now we consider that the minimization problem is: Find  $p^*$  such that

$$\begin{aligned} \hat{\mathbf{d}}^* = \arg \min_{\mathbf{d} \in \mathcal{E}_{ad}} J(\bar{\mathbf{u}}), \quad \text{with } J(\bar{\mathbf{u}}) = \bar{\mathbf{f}}^T \bar{\mathbf{u}} \\ \text{s. t. } \bar{\mathbf{K}} \bar{\mathbf{u}} = \bar{\mathbf{f}} \end{aligned} \quad (5.17)$$

### 5.4.2 Gradient for an assembling of shells

We consider the matrix  $\mathcal{G}^\alpha$  which takes into account the algebraic relations between the control points of the multi-patches and the independent control points, for a  $C^\alpha$ -continuity.

Let  $\partial_j^{i(k)}$  denote the derivative with respect to the  $i$ -th coordinate of the control point  $p_{j(k)}$  of index  $j$  associated to patch  $\Omega_k$ , for  $i \in \{1, 2, 3\}$  and  $j \in \{1, \dots, n_{12}\}$ . We introduce the derivatives vector  $\nabla^i$  defined as

$$\nabla^i = \left( \partial_1^{i(m)} \quad \partial_2^{i(m)} \quad \dots \quad \partial_{n_{12}}^{i(m)} \quad \partial_1^{i(n)} \quad \partial_2^{i(n)} \quad \dots \quad \partial_{n_{12}}^{i(n)} \right) := (\partial_j^i)_{j=1:2 \times n_{12}}.$$

$\hat{\partial}_j^i$  denote the derivative with respect to the  $i$ -th coordinate of the  $j$ -th independent control point  $\hat{p}_j$  and set  $\hat{\nabla}^i = \left( \hat{\partial}_j^i \right)_{j=1:n_{12}^\alpha}$  the vector of derivatives with respect to the  $i$ -th coordinate of the independent control points  $\hat{\mathbf{p}}$ . Hence, we have

$$\hat{\nabla}^i = [\mathcal{G}^\alpha]^T \nabla^i$$

which componentwise, for given a function  $f$ , is

$$\hat{\partial}_j^i f = \sum_{r=1}^{2 \times n_{12}} g_{r,j}^\alpha \times \partial_r^i f.$$

The gradient of derivatives with respect to coordinates of the set of control points  $\hat{\mathbf{p}}$  is

$$\hat{\nabla} = [\hat{\nabla}^1 \quad \hat{\nabla}^2 \quad \hat{\nabla}^3] \quad \text{and} \quad \hat{\nabla} f = [\hat{\nabla}^1 f \quad \hat{\nabla}^2 f \quad \hat{\nabla}^3 f].$$

### 5.4.3 Constraints on the design's geometry

#### Bounded area constraint

Let us consider two nonnegative real numbers  $\mathcal{A}_l$  and  $\mathcal{A}_u$ . One can assume that the problem is subjected to a bounded area constraint on  $\mathcal{A}$  the area of the assembling of shells:

$$\mathcal{A}_l \leq \mathcal{A} \leq \mathcal{A}_u$$



with  $\mathcal{A}$  defined as

$$\mathcal{A} = \sum_{k \in \{n, m\}} \int_{\omega_k} \sqrt{a_k} d\xi.$$

The derivative with respect to  $[\hat{p}_j]_i$  -the  $i$ -th coordinate of the  $j$ -th independent control point is

$$\begin{aligned} \hat{\partial}_j^i \mathcal{A} &= \sum_{r=1}^{2 \times n_{12}} \partial_r^i \mathcal{A} \\ &= \sum_{r=1}^{n_{12}} g_{r,j}^\alpha \partial_r^{i(m)} \mathcal{A} + \sum_{r=1}^{n_{12}} g_{n_{12}+r,j}^\alpha \partial_r^{i(n)} \mathcal{A} \end{aligned}$$

where  $\partial_r^{i(k)} \mathcal{A} = \partial_r^{i(k)} \sqrt{a_k}$ .

REMARK 5.4.1 The structure could also be subjected to a bounded constraint on the perimeter (length)  $\mathcal{L} := \sum_{k \in \{n, m\}} l_k$  of a given boundary of the assembling denoted  $\mathcal{C} = \mathcal{C}_m \cup \mathcal{C}_n$ . The derivative  $\hat{\partial}_i^k \mathcal{L}$  with respect to the design variable  $[\hat{p}_i]_k$  is computed in an analogous manner as depicted previously for the area  $\mathcal{A}$ ;  $l_k$  being the length of  $\mathcal{C}_k$ . Also, we emphasize that since the patches are assumed to be defined with clamped knot vectors, the only meaningful derivatives of  $\mathcal{L}$ ,  $\partial_r^{i(k)} \mathcal{L}$ , to be computed are those such that  $p_r$  is related to definition of the boundaries  $\mathcal{C}_k$ ,  $k \in \{n, m\}$ .

### Location or place constraint

In practice, a structure is subjected to location or place constraint often called box constraint. This constraint is expressed as bounded constraints on a given set of control points. Let  $\mathcal{B}_c$  denote the set of indices of control points  $p_i$  with bound constraints. Typically  $\mathcal{B} \subset \{1, \dots, 2 \times n_{12}\}$ . Let  $\mathbf{l}_i$  and  $\mathbf{u}_i$  respectively denote the lower and upper bound on the control point  $p_i$  such that  $\mathbf{l}_i \leq \mathbf{u}_i$ :

$$\mathbf{l}_i \leq p_i \leq \mathbf{u}_i$$

which componentwise is

$$[\mathbf{l}_i]_j \leq [p_i]_k \leq [\mathbf{u}_i]_j, \text{ for all } j \in \{1, 2, 3\}.$$

We recall that: given  $\mathbf{v} \in \mathbb{R}^3$ , the notation  $[\mathbf{v}]_j$  designates the  $j$ -th coordinate of  $\mathbf{v}$ . The control point  $p_i$  being defined as

$$p_i = \sum_{r=1}^{n_{12}^\alpha} g_{i,r}^\alpha \hat{p}_r \text{ and componentwise } [p_i]_j = \sum_{r=1}^{n_{12}^\alpha} g_{i,r}^\alpha [\hat{p}_r]_j,$$

we have

$$\hat{\partial}_r^j [p_i]_k = \delta_k^j g_{i,r}^\alpha.$$

REMARK 5.4.2 A short comment on the set  $\mathcal{B}_c$ .  $\mathcal{B}_c$  is typically composed of the set of indices of the control points that allow to have independent constraints, which are independent:

$$\mathcal{B}_c = \mathcal{B}_{c(m)} \cup \mathcal{B}_{c(n)}$$

with

- for a  $C^0$ -continuity

$$\begin{aligned} \mathcal{B}_{c(m)} &= \{1, \dots, n_{12(m)}\} \\ \mathcal{B}_{c(n)} &= \{n_{12(m)} + (j-1) \times n_{1(n)} + j, \text{ for } i \in \{2, \dots, n_{1(n)}\} \text{ and } j \in \{1, \dots, n_2\}\} \end{aligned}$$

- for a  $C^1$ -continuity

$$\begin{aligned} \mathcal{B}_{c(m)} &= \{(j-1) \times n_{1(m)} + j, i \in \{1, \dots, n_{1(m)} - 1\}, j \in \{1, \dots, n_2\}\} \\ \mathcal{B}_{c(n)} &= \{n_{12(m)} + (j-1) \times n_{1(n)} + j, \text{ for } i \in \{2, \dots, n_{1(n)}\} \text{ and } j \in \{1, \dots, n_2\}\}. \end{aligned}$$

Concretely, considering the case depicted on Figure 5.2

- for a  $C^0$ -continuity the bounded variations will bear on the control points  $p_{1(m)}, p_{2(m)}, p_{3(m)}, p_{4(m)} = q_l; p_{2(n)}, p_{3(n)}$  and  $p_{4(n)}$
- for a  $C^1$ -continuity, the bounded variations will bear on the control points  $p_{1(m)}, p_{2(m)}, p_{3(m)}, p_{2(n)}, p_{3(n)}$  and  $p_{4(n)}$  since the point  $q_l$  belong to the segment  $[p_{3(m)}, p_{2(n)}]$ .

The derivatives with respect to the design variables involve the computation of the elementary derivatives with respect to the control points coordinates, which are linked or defined by means of the design variables. The derivative of the objective function is still computed as in (5.11). This implies that one needs to compute some derivatives of the junction matrix with respect to the design parameters. Indeed, the derivative with respect to any design variable is

$$\hat{\partial}_j^i J(\hat{\mathbf{d}}, \underline{\mathbf{u}}(\hat{\mathbf{d}})) = 2\hat{\partial}_j^i \bar{\mathbf{f}} \cdot \bar{\mathbf{u}} - \bar{\mathbf{u}} \hat{\partial}_j^i \bar{\mathbf{K}} \bar{\mathbf{u}} \quad (5.18)$$

where

$$\hat{\partial}_j^i \bar{\mathbf{K}} = \hat{\partial}_j^i \mathbf{M}^\top \mathbf{K} \mathbf{M} + \mathbf{M}^\top \hat{\partial}_j^i \mathbf{K} \mathbf{M} + \mathbf{M}^\top \mathbf{K} \hat{\partial}_j^i \mathbf{M} \text{ and } \hat{\partial}_j^i \bar{\mathbf{f}} = \hat{\partial}_j^i \mathbf{M}^\top \mathbf{f}.$$

Subsequently, we define the junction matrix sensitivity principle on a general problem and then focus on the specific case of shell problem. For the sake of simplicity, we do not consider the boundary condition aspects.

#### 5.4.4 General overview on the derivative of the junction

Let's here again consider the general form of the domain decomposition problem 3.2.3, described at page 43 with  $\mathbf{B}^{(k)}$  and  $\mathbf{f}^{(k)}$  respectively the matrix form of the bilinear and linear forms of a given variational problem. Consider the problem under its matrix form

$$\mathbf{B}_m \bar{\mathbf{w}} = \mathbf{f}_m, \text{ with}$$

$$\mathbf{B}_m = \mathbf{M}^\top \text{diag}(\mathbf{B}^{(n)}, \mathbf{B}^{(m)}) \mathbf{M}, \text{ and } \mathbf{f}_m = \mathbf{M}^\top \mathbf{f}, \mathbf{f}^\top = [\mathbf{f}^{(n)} \quad \mathbf{f}^{(m)}].$$

The derivative of  $\mathbf{B}_m$  would obviously be computed using a chain rule through the derivatives of  $\mathbf{M}$  and those of  $\mathbf{B}^{(k)}$ .

Considering the derivative of the global matching matrix defined in 3.2.1, one notices that the derivative of the block matrices which define the “interior”, i.e independent, degrees of freedom with respect to any arbitrary shape parameter equals zero. In fact these degrees of freedom are identically conserved, and this, independently to the geometry; concretely

$$\partial_d \mathbf{M} = \begin{bmatrix} \mathbf{0}_{0(n)} & & & \\ & \partial_d \mathbf{R}^{(l)} & & \\ & \mathbf{0}_{0(m)}^l & & \\ & & & \mathbf{0}_{0(m)}^0 \end{bmatrix}$$

where  $\mathbf{0}_{0(n)}$ ,  $\mathbf{0}_{0(m)}^l$ , and  $\mathbf{0}_{0(m)}^0$  are zero matrices of consistent dimensions with respect to the definition of  $\mathbf{M}$ . Using the chain rule and the following well-known result on the derivative of the inverse of a matrix:

$$\text{for a given invertible matrix } \mathbf{N}, \quad \partial_d \mathbf{N}^{-1} = -\mathbf{N}^{-1} \partial_d \mathbf{N} \mathbf{N}^{-1},$$

we can define the derivative of  $\mathbf{R}^{(l)}$  by

$$\partial_d \mathbf{R}^{(l)} = -[\mathbf{M}^{l(n)}]^{-1} \partial_d \mathbf{M}^{l(n)} \mathbf{R}^l + [\mathbf{M}^{l(n)}]^{-1} \partial_d \mathbf{M}^{l(m)}.$$

The derivative of the objective function involves the computation of quantities of the form  $\bar{\mathbf{v}}^\top \partial_d \mathbf{B}_m \bar{\mathbf{w}}$ . Using the chain rule, one obtains

$$\partial_d \mathbf{B}_m = \mathbf{M}^\top \partial_d \mathbf{B} \mathbf{M} + \mathbf{M}^\top \mathbf{B} \partial_d \mathbf{M} + [\partial_d \mathbf{M}]^\top \mathbf{B} \mathbf{M}.$$

PROPOSITION 5.4.1 *Based on the partitioning introduced in (3.26), (3.27), let us consider the corresponding arrangement of the matrix  $\mathbf{B}^{(n)}$*

$$\mathbf{B}^{(n)} = \begin{bmatrix} \mathbf{B}_{0(n)}^{0(n)} & \mathbf{B}_{l(n)}^{0(n)} \\ \mathbf{B}_{0(n)}^{l(n)} & \mathbf{B}_{l(n)}^{l(n)} \end{bmatrix},$$

where  $\mathbf{B}_{i(k)}^{j(k)}$  is the matrix part of  $\mathbf{B}^{(k)}$  whose rows and columns are respectively restricted to the degrees of freedom of type  $i$  and  $j$ .

And we have the following relations:

◦

$$\begin{aligned} \bar{\mathbf{v}}^\top \partial_d \mathbf{M}^\top \mathbf{B} \mathbf{M} \bar{\mathbf{w}} &= \bar{\mathbf{v}}^\top \partial_d \mathbf{M}^\top \mathbf{B}^{(n)} \underline{\mathbf{w}} \\ &= \underline{\mathbf{v}}_{l(m)}^\top \left[ [\partial_d \mathbf{R}^{(l)}]^\top \mathbf{B}_{l(n)}^{0(n)} \underline{\mathbf{w}}_{0(n)} + [\partial_d \mathbf{R}^{(l)}]^\top \mathbf{B}_{l(n)}^{l(n)} \underline{\mathbf{w}}_{l(n)} \right]. \end{aligned}$$

◦

$$\begin{aligned} \bar{\mathbf{v}}^\top \mathbf{M}^\top \mathbf{B} \partial_d \mathbf{M} \bar{\mathbf{w}} &= \underline{\mathbf{v}}^\top \mathbf{B}^{(n)} \partial_d \mathbf{M} \underline{\mathbf{w}} \\ &= \left[ \underline{v}_{0(n)}^\top \mathbf{B}_{0(n)}^{l(n)} \partial_d \mathbf{R}^{(l)} + \underline{v}_{l(n)}^\top \mathbf{B}_{l(n)}^{l(n)} \partial_d \mathbf{R}^{(l)} \right] \underline{\mathbf{w}}_{l(m)}. \end{aligned}$$

REMARK 5.4.3 The decomposition in the previous computation can be further refined for  $B_{l(n)}^{0(n)}$  and  $B_{0(n)}^{l(n)}$  to strictly consider only the rows and columns corresponding to the set of interior degrees of freedom which are connected to the interface degrees of freedom.

After having presented the principle for a general problem, we now focus on the derivative of the shell's junction conditions with respect to the shape parameters.

### 5.4.5 Sensitivity of the shells junction

In the following, we respectively denote by  $u_i^{l(k)}$  and  $s_\alpha^{l(k)}$  the restrictions of  $u_i^{(k)}$  and  $s_\alpha^{(k)}$  to  $\gamma^{l(k)}$ ;  $\underline{u}_i^{l(k)}$  and  $\underline{s}_\alpha^{l(k)}$  their corresponding finite element degrees of freedom; while  $u_i^{0(k)}$  and  $s_\alpha^{0(k)}$  denote the interior degrees of freedom vectors. We set  $\underline{\mathbf{u}} = \left( \underline{u}_i^{l(k)} \right)_{i=1:3}$  and  $\underline{\mathbf{s}} = \left( \underline{s}_\alpha^{l(k)} \right)_{\alpha=1:2}$ .

#### 5.4.5.1 Matrix form of the junction conditions

For the sake of simplicity, we suppose that the displacement and rotation are discretized using the same finite elements.

#### Displacement continuity

We recall that the matrix form corresponding to the displacement continuity condition (3.13) is

$$\mathbf{M}^{(l)} \underline{u}_i^{l(n)} = [\mathbf{M}^{l(m)}]_i^j \underline{u}_j^{l(m)}, \text{ with summation over } j \in \{1, 2, 3\}.$$

$[\mathbf{M}^{l(m)}]_i^j$  denotes the matrix on the mortar side of dimension  $(d_{l(n)}, d_{l(m)})$ .

For a given  $(i, j) \in \{1, 2, 3\}^2$ , the  $(\hat{p}, \hat{q})$ -th component  $[(M_{pq}^{l(m)})]_i^j$  of  $[\mathbf{M}^{l(m)}]_i^j$  is set as

$$[M_{\hat{p}\hat{q}}^{l(m)}]_i^j = \int_{\gamma^l} a_{i(n)}^{j(m)} p_{\hat{p}}^{(n)}(\boldsymbol{\xi}_{(n)}) p_{\hat{q}}^{(m)}(\boldsymbol{\xi}_{(m)}) s_{l(m)}(\eta) d\eta, \quad q \in S_{l(m)}.$$

The matrix  $\mathbf{M}^{(l)}$ 's components are defined as

$$M_{\hat{p}\hat{q}}^{(l)} = \int_{\gamma^l} p_{\hat{p}}^{(n)}(\boldsymbol{\xi}_{(n)}) p_{\hat{q}}^{(n)}(\boldsymbol{\xi}_{(n)}) s_{l(n)}(\eta) d\eta, \quad q \in S_{l(n)}$$

Thus the matrix form of the continuity of the displacement vector is

$$\mathbf{M}^{l(n)} \underline{\mathbf{u}}^{l(n)} = \mathbf{M}^{l(m)} \underline{\mathbf{u}}^{l(m)}, \text{ with } \mathbf{M}^{l(n)} = \left( [\delta_j^i \times \mathbf{M}^{(l)}]_i^j \right)_{i,j}$$

$\mathbf{M}^{l(m)}$  is the  $3 \times 3$  block matrix of dimension  $d_{l(n)} \times d_{l(m)}$ :

$$\mathbf{M}^{l(m)} = \left( [\mathbf{M}^{l(m)}]_i^j \right)_{(i,j) \in \{1,2,3\}^2}.$$

$\mathbf{M}^{l(n)} = \left( \delta_j^i \times \mathbf{M}^{(l)} \right)_{(i,j) \in \{1,2,3\}^2}$  is a  $3 \times 3$  diagonal block-matrix of diagonal matrix equal to  $\mathbf{M}^{(l)}$ .

### Tangential rotation continuity

Regarding the other junction condition (3.14), we introduce the matrices  $\mathbf{M}_{\Psi}^{l(k)}$ ,  $k \in \{n, m\}$  such that

$$\mathbf{M}_{\Psi}^{l(k)} = ([\mathbf{M}_{\Psi}^{l(k)}]_{\alpha})_{\alpha \in \{1,2\}}.$$

The components  $[\mathbf{M}_{\Psi}^{l(k)}]_{\hat{p}\hat{q}}^{\alpha}$  of the block matrix  $[\mathbf{M}_{\Psi}^{l(k)}]^{\alpha}$  are defined as

$$[\mathbf{M}_{\Psi}^{l(k)}]_{\hat{p}\hat{q}}^{\alpha} = (-1)^{\bar{\alpha}} \int_{\gamma^l} a_k^{-\frac{1}{2}} t_{\bar{\alpha}}^{l(k)} p_p^{(n)}(\boldsymbol{\xi}_{(n)}) p_q^{(k)}(\boldsymbol{\xi}_{(k)}) c_{l(k)} s_{l(k)}(\eta) d\eta, \quad \bar{\alpha} = \{1, 2\} \setminus \alpha,$$

with  $c_{l(k)}$  defined as follows

$$c_{l(n)} = 1, \text{ and } c_{l(m)} = \mathbf{t}_{l(n)} \cdot \mathbf{t}_{l(m)}.$$

The matrix form of the rotation continuity condition is

$$\mathbf{M}_{\Psi}^{l(n)} \underline{\mathbf{s}}^{l(n)} = \mathbf{M}_{\Psi}^{l(m)} \underline{\mathbf{s}}^{l(m)}. \quad (5.19)$$

We emphasize that special attention must be paid to this condition: in fact one agrees that we have one equation for two covariant components of rotation. Thus only one of the (non-mortar) rotation covariant components can be defined from (5.19). So we have to extract a sub-matrix of “full rank”, i.e invertible, whose corresponding rotation will be defined.

Given  $\alpha \in \{1, 2\}$ , we set  $\sigma = \bar{\alpha} \in \{1, 2\} \setminus \{\alpha\}$ , we suppose that the matrix  $[\mathbf{M}_{\Psi}^{l(k)}]^{\sigma}$  is of full-rank so we can define the rotation  $\underline{\mathbf{s}}_{\alpha}^{l(n)}$ . Thus we have

$$[\mathbf{M}_{\Psi}^{l(k)}]^{\sigma} \underline{\mathbf{s}}_{\alpha}^{l(n)} = \mathbf{M}_{\Psi}^{(l)} \underline{\mathbf{s}}^{(l)} \quad (\text{no summation over } \alpha),$$

where

$$\mathbf{M}_{\Psi}^{(l)} = \begin{pmatrix} \mathbf{M}_{\Psi}^{l(m)} & [\mathbf{M}_{\Psi}^{l(n)}]^{\alpha} \end{pmatrix}, \text{ and } \underline{\mathbf{s}}^{(l)} = \begin{pmatrix} \underline{\mathbf{s}}^{l(m)} & \underline{\mathbf{s}}_{\sigma}^{l(n)} \end{pmatrix}^{\top}. \quad (5.20)$$

In this case, we insist on the fact that the independent degrees of freedom are not exclusively from the mortar side like for the displacement;  $\underline{\mathbf{s}}^{(l)}$  are the independent degrees of freedom of rotations associated to the interface  $\Gamma^l$  which allows to define the non-mortar rotation degrees of freedom  $\underline{\mathbf{s}}_{\alpha}^{l(n)}$ .

### Local displacement and rotation matrix junction

Let us note  $\mathbf{R}_u^{(l)}$  and  $\mathbf{R}_{\Psi}^{(l)}$  respectively the matrices associated to the junction of the displacement and rotation, such that

$$\underline{\mathbf{u}}^{l(n)} = \mathbf{R}_u^{(l)} \underline{\mathbf{u}}^{l(m)} \text{ and } \underline{\mathbf{s}}_{\alpha}^{l(n)} = [\mathbf{R}_{\Psi}^{(l)}]^{\alpha} \underline{\mathbf{s}}^{(l)}, \quad (5.21)$$

where  $\mathbf{R}_u^{(l)} = [\mathbf{M}_u^{l(n)}]^{-1} \mathbf{M}_u^{l(m)}$  and  $[\mathbf{R}_{\Psi}^{(l)}] = \left([\mathbf{M}_{\Psi}^{l(n)}]^{\bar{\alpha}}\right)^{-1} \mathbf{M}_{\Psi}^{(l)}$ .

Let us note  $[\mathbf{R}_{\Psi}^{(l)}] := \begin{bmatrix} \mathbf{R}_{\Psi}^{l(m)} & \mathbf{R}_{\Psi}^{l(n)} \end{bmatrix}$ . The matrices  $\mathbf{R}_{\Psi}^{l(m)}$  and  $\mathbf{R}_{\Psi}^{l(n)}$  are respectively the block



the control point  $p_{j^{(k)}}$  -see 5.4.2 page 117-, we denote  $\partial_d^{(k)}$  the derivative with respect to the geometric parameter  $d$  of the patch of index  $k$ . When the belonging patch of these parameters is unimportant we simply use the notation  $\partial_d$ .

PROPOSITION 5.4.2 *The derivative  $\partial_d \mathbf{M}$  of the global junction matrix (5.23) is*

$$\partial_d \mathbf{M} = \begin{bmatrix} \mathbf{0}^{0(n)} & & \\ & \partial_d \mathbf{M}^{(l)} & \\ & & \mathbf{0}^{0(m)} \end{bmatrix}.$$

The derivative  $\partial_d \mathbf{M}^{(l)}$  of the local junction matrix associated to the  $l$ -th interface, (5.22) is defined as follows

$$\partial_d \mathbf{M}^{(l)} = \begin{bmatrix} \partial_d \mathbf{R}_u^{(l)} & & & \\ & \mathbf{0}_\psi^{l(n)} & & \\ & \partial_d \mathbf{R}_\psi^{l(n)} & \partial_d \mathbf{R}_\psi^{l(m)} & \\ \mathbf{0}_u^{l(m)} & & & \\ & & & \mathbf{0}_\psi^{l(m)} \end{bmatrix} \quad (5.24)$$

where  $\mathbf{0}^{l(k)}$  and  $\mathbf{0}^{0(k)}$  are null matrices of dimensions consistent with the definition of  $\mathbf{M}$ .

Before going further, we stress the point that, in order to compute the derivative  $\hat{\partial}_d \mathbf{M}^{(l)}$ , the matrices on the *non-mortar side*, namely  $[\mathbf{M}_\psi^{l(n)}]^\alpha$  and  $\mathbf{M}^{l(n)}$ , formally depend only of the non-mortar geometry, while the matrices  $\mathbf{M}^{l(m)}$  and  $\mathbf{M}_\psi^{l(l)}$  depend on both the non-mortar and mortar geometric quantities, respectively through the basis change matrix  $\mathbf{A}_m^n = (a_{i^{(n)}}^{j^{(m)}})$  for  $\mathbf{u}$  and the tangent vector transformation  $c_{l(m)}$  and the passage of the matrix  $[\mathbf{M}_\psi^{l(n)}]^\sigma$  from the left hand side of (5.19) to the right hand side of (5.20).

Now, we focus on the derivative of the local junction matrices with respect to a shape design parameters.

### Displacement junction matrix

The following propositions lead to the computation of the derivative of the junction matrix  $\mathbf{R}_u^{(l)}$  associated to the displacement continuity.

PROPOSITION 5.4.3 *The derivatives of the matrices associated to the displacement continuity are*

$$\partial_d \mathbf{M}^{l(k)} = \left( [\partial_d \mathbf{M}^{l(k)}]_i^j \right)_{i,j},$$

with

$$[\partial_d \mathbf{M}^{l(k)}]_i^j = \left( [\partial_d M_{\hat{p}\hat{q}}^{l(k)}]_i^j \right)_{\hat{p},\hat{q}}, \quad \hat{p} \in \{1, \dots, d_{l(n)}\} \text{ and } \hat{q} \in \{1, \dots, d_{l(l)}\}.$$

In respect of the *non-mortar side*,  $\mathbf{M}^{l(n)}$  being exclusively dependent on non-mortar geometric parameters, we have

$$\partial_d \mathbf{M}^{l(n)} = \left( \delta_{ij} \partial_d \mathbf{M}^{(l)} \right)_{i,j} \text{ with } \partial_d^{(k)} \mathbf{M}^{(l)} = \delta^{nk} \left( \partial_d^{(k)} M_{\hat{p}\hat{q}}^{(l)} \right)_{\hat{p},\hat{q}}.$$

The components of  $\partial_d \mathbf{M}^{(l)}$  are defined as follows

$$\partial_d \mathbf{M}_{\hat{p}\hat{q}}^{(l)} = \int_{\gamma^l} p_p^{(n)}(\boldsymbol{\xi}_{(n)}) p_q^{(n)}(\boldsymbol{\xi}_{(n)}) \partial_d s_{l(n)}(\eta) d\eta.$$

As for the derivative associated to the mortar side, we first define the derivative of the basis change matrix  $\mathbf{A}_{(m)}^{(n)} = (a_{i(n)}^{j(m)})$ :

$$\partial_d^{(m)} a_{i(n)}^{j(m)} = \mathbf{a}_{i(n)} \cdot \partial_d^{(m)} \mathbf{a}^{j(m)}, \quad \text{and} \quad \partial_d^{(n)} a_{i(n)}^{j(m)} = \mathbf{a}_{j(m)} \cdot \partial_d^{(n)} \mathbf{a}^{i(n)}.$$

So we have

$$\begin{aligned} \partial_d^{(n)} [M_{\hat{p}\hat{q}}^{l(m)}]_i^j &= \int_{\gamma^l} \partial_d^{(n)} a_{i(n)}^{j(m)} p_p^{(n)}(\boldsymbol{\xi}_{(n)}) p_q^{(m)}(\boldsymbol{\xi}_{(n)}) s_{l(m)}(\eta) d\eta, \\ \partial_d^{(m)} [M_{\hat{p}\hat{q}}^{l(m)}]_i^j &= \int_{\gamma^l} \left( \partial_d^{(m)} a_{i(n)}^{j(m)} s_{l(m)} + a_{i(n)}^{j(m)} \partial_d^{(m)} s_{l(m)}(\eta) \right) p_p^{(n)}(\boldsymbol{\xi}_{(n)}) p_q^{(m)}(\boldsymbol{\xi}_{(n)}) d\eta. \end{aligned}$$

Thus the derivative of the local matching matrix, associated to the displacement constraint, with respect to

- a non-mortar shape design variable is:

$$\partial_d^{(n)} \mathbf{R}_u^{(l)} = -[\mathbf{M}^{l(n)}]^{-1} \partial_d^{(n)} \mathbf{M}^{l(n)} \mathbf{R}_u^{(l)} + [\mathbf{M}^{l(n)}]^{-1} \partial_d^{(n)} \mathbf{M}^{l(m)}$$

- the mortar shape design variable is:

$$\partial_d^{(m)} \mathbf{R}_u^{(l)} = [\mathbf{M}^{l(n)}]^{-1} \partial_d^{(m)} \mathbf{M}^{l(m)}.$$

### Tangential rotation matrix junction

Now, we focus on the derivative of the junction matrix defining one of the rotation covariant components.

PROPOSITION 5.4.4 *Considering the junction matrix (5.21) associated to the tangential continuity of the rotation, and assuming that the defined rotation is  $\underline{s}_\alpha^{l(n)}$ , i.e.*

$$[\mathbf{R}_\psi^{(l)}]^\alpha = \left( [\mathbf{M}_\psi^{l(n)}]^\alpha \right)^{-1} \mathbf{M}_\psi^{(l)};$$

the derivative with respect to a geometric parameter  $d$  from either  $n(l)$  or  $m(l)$  side is

$$\partial_d [\mathbf{R}_\psi^{(l)}]^\alpha = \partial_d \left( [\mathbf{M}_\psi^{l(n)}]^\alpha \right)^{-1} \mathbf{M}_\psi^{(l)} + \left( [\mathbf{M}_\psi^{l(n)}]^\alpha \right)^{-1} \partial_d \mathbf{M}_\psi^{(l)}.$$

The first term of the r.h.s is obviously equal to

$$- \left( [\mathbf{M}_\psi^{l(n)}]^\alpha \right)^{-1} \partial_d [\mathbf{M}_\psi^{l(n)}]^\alpha \mathbf{R}_\psi^{(l)}.$$

Now, focussing on  $\partial_d \mathbf{M}_\psi^{(l)}$ , we have

$$\partial_d \mathbf{M}_\psi^{(l)} = \left( \partial_d \mathbf{M}_\psi^{l(m)} \quad \partial_d [\mathbf{M}_\psi^{l(n)}]^\alpha \right),$$

where the derivative with respect to



- a non-mortar design variable is thus

$$\partial_d^{(n)} \mathbf{M}_\Psi^{(l)} = \left( \partial_d^{(n)} \mathbf{M}_\Psi^{l(m)} \quad \partial_d^{(n)} [\mathbf{M}_\Psi^{l(n)}]^\alpha \right)$$

- a mortar design variable, on the other hand, is

$$\partial_d^{(m)} \mathbf{M}_\Psi^{(l)} = \left( \partial_d^{(m)} \mathbf{M}_\Psi^{l(m)} \quad \mathbf{0}_\Psi^{l(n)} \right).$$

Where  $\mathbf{0}_\Psi^{l(n)}$  is a zero matrix of size  $(d_{l(n)}, d_{l(n)})$ .

Hence, the derivative of the junction  $[\mathbf{R}_\Psi^{(l)}]^\alpha$  with respect to

- a non-mortar design variable is

$$\partial_d^{(n)} [\mathbf{R}_\Psi^{(l)}]^\alpha = - \left( [\mathbf{M}_\Psi^{l(n)}]^\alpha \right)^{-1} \partial_d^{(n)} [\mathbf{M}_\Psi^{l(n)}]^\alpha \mathbf{R}_\Psi^{(l)} + \left( [\mathbf{M}_\Psi^{l(n)}]^\alpha \right)^{-1} \partial_d^{(n)} \mathbf{M}_\Psi^{(l)}.$$

- a mortar design variable

$$\partial_d^{(m)} [\mathbf{R}_\Psi^{(l)}]^\alpha = \left( [\mathbf{M}_\Psi^{l(n)}]^\alpha \right)^{-1} \partial_d^{(m)} \mathbf{M}_\Psi^{(l)} = \left[ \left( [\mathbf{M}_\Psi^{l(n)}]^\alpha \right)^{-1} \partial_d^{(m)} \mathbf{M}_\Psi^{l(m)} \quad \mathbf{0}_\Psi^{l(n)} \right].$$

We specify below the derivatives  $\partial_d \mathbf{M}_\Psi^{l(n)}$  and  $\partial_d \mathbf{M}_\Psi^{l(m)}$  which serve to the computation of the derivatives of the junction matrix described above.

PROPOSITION 5.4.5 *The derivative of the scalar  $c_{l(k)}$  associated to the tangent vector transformation is*

$$\partial_d^{(k)} c_{l(m)} = \partial_d^{(k)} \mathbf{t}_{l(k)} \cdot \mathbf{t}_{l(\bar{k})}, \quad \partial_d^{(k)} c_{l(n)} = 0, \quad k \in \{n, m\} \text{ and } \bar{k} \in \{m, n\} \setminus \{k\}.$$

The derivative of  $\mathbf{M}_\Psi^{l(k)}$  with respect to a shape variable  $d$  from either non-mortar or mortar side is

$$\partial_d \mathbf{M}_\Psi^{l(k)} = \left( [\partial_d \mathbf{M}_\Psi^{l(k)}]^\alpha \right)_{\alpha \in \{1,2\}}.$$

The components of the matrix  $[\partial_d \mathbf{M}_\Psi^{l(k)}]^\alpha$  are

$$[\partial_d \mathbf{M}_\Psi^{l(k)}]_{\hat{p}, \hat{q}}^\alpha = (-1)^{\bar{\alpha}} \int_{\gamma^l} \partial_d (a_k^{-\frac{1}{2}} t_\alpha^{l(k)} c_{l(k)} s_{l(k)}) p_p^{(n)}(\boldsymbol{\xi}_{(n)}) p_q^{(k)}(\boldsymbol{\xi}_{(n)}) d\eta.$$

The derivative  $\partial_d (a_k^{-\frac{1}{2}} t_\alpha^{l(k)} c_{l(k)} s_{l(k)})$  is defined using the chain rule

$$\begin{aligned} \partial_d (a_k^{-1/2} t_\alpha^{l(k)} c_{l(k)} s_{l(k)}) &= \left( -\frac{1}{2} \partial_d a_k a_k^{-\frac{3}{2}} t_\alpha^{l(k)} + a_k^{-\frac{1}{2}} \partial_d t_\alpha^{l(k)} \right) c_{l(k)} s_{l(k)} \\ &\quad + a_k^{-\frac{1}{2}} t_\alpha^{l(k)} (\partial_d c_{l(k)} s_{l(k)} + c_{l(k)} \partial_d s_{l(k)}). \end{aligned}$$

We have described above the computation of all the necessary quantities needed for the sensitivity analysis in the case of structure composed of assembled patches. The next section is devoted to some optimization numerical results.

## 5.5 Numerical results

### 5.5.1 Optimal design of a circular plate

Now, we consider the joint optimal design with respect to the shape and the material properties. Each polar parameter is parameterized through a five order B-spline function of open knot vector and five control points in each parametric direction. Because of symmetry reasons, the optimization is performed on the quarter of the structure.

In this subsection, we consider the optimal design problem of a circular plate which is subjected to its own weight. The shell is simply supported at its circular boundary. The geometry and the problem data are represented on Figure 5.4.

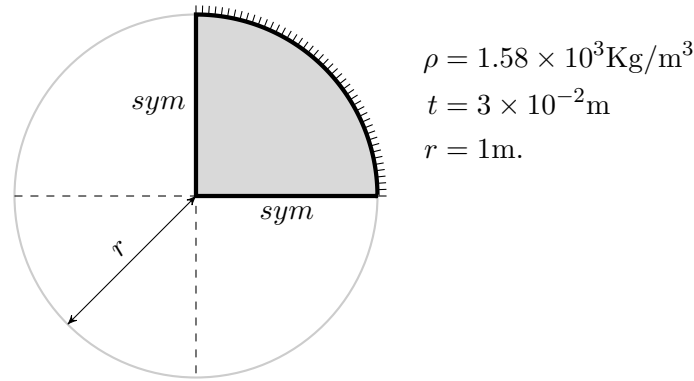


Figure 5.4 Circular plate geometry and boundary condition.

The elastic properties are:

$$E_2 = E = 9000 \times 10^6 \text{Pa}$$

$$E_1 = E_3 = 161 \times 10^6 \text{Pa}$$

$$\nu_{12} = \nu_{23} = \nu = 0.26$$

$$\nu_{13} = 0.26 \text{ and } G_{13} = \frac{E}{1 + \nu}$$

$$G_{12} = G_{23} = 61 \times 10^6 \text{Pa.}$$

The polar parameters corresponding to the plane reduced elastic tensor are:

$$T_0 = 1.17 \times 10^9 \text{Pa}, T_1 = 1.16 \times 10^9 \text{Pa}$$

$$R_0^K = 1.11 \times 10^9 \text{Pa}, R_1 = 1.11 \times 10^9 \text{Pa}, \text{ and } \Phi_1 = 0.$$

The polar parameters of the anti-plane part of the elastic tensor are:

$$T = 62.44 \times 10^6, R = 1.44 \times 10^6, \vartheta = 0.$$

We first consider the optimal design for an optimization of the shape, and then consider the joint optimization of both shape and elastic properties.

5.5.1.1 Optimal shape design

The problem is subjected to bound constraints on the control points which are allowed to take only positive  $z$ -coordinate. The edge with simply-supported boundary condition is subjected to fix place constraint, i.e the control points defining this boundary are kept fixed. The design is also subjected to bounded area and symmetry constraint. Let  $\epsilon_{tol}$  be the tolerance on the variation of the design area denoted by  $\mathcal{A}$ . The constraint is:

$$\mathcal{A}_l \leq \mathcal{A} \leq \mathcal{A}_u, \text{ with } \mathcal{A}_u = (1 + \epsilon_{tol})\mathcal{A}_0, \text{ and } \mathcal{A}_l = (1 - \epsilon_{tol})\mathcal{A}_0.$$

where  $\mathcal{A}_0$ ,  $\mathcal{A}_l$  and  $\mathcal{A}_u$  are respectively the initial design area, the lower and upper bound on the design area. For the following optimization  $\epsilon_{tol} = 0.3$ .

Let  $d$  be a non-negative integer. The polar parameters are defined through open knot vector of the form

$$\Sigma^\alpha = \{\underbrace{0, \dots, 0}_{d+1}, \underbrace{1, \dots, 1}_{d+1}\}, \alpha \in \{1, 2\}.$$

**Isotropic material:**

We first suppose that the structure is made of isotropic material and set  $R_0^K = R_1 = 0$ . The optimal shape computed is represented on Figure 5.5. In this case the three coordinates of the control points are optimized. Hence the number of design parameters is 12. The number of constraints is 26 (2 for the bounded area constraint and  $2 \times 12$  for the bound constraints on the control points coordinates).



Figure 5.5 Optimal shape corresponding to the circular plate with isotropic material under weight-load.

This structure is a cupola, and is the most optimal shape to carry the strain energy in a membrane and minimize the bending. Indeed, the membrane energy part was initially equal to  $E_{\bar{v}} = 1.35\%$  and for the optimal solution it is  $E_{\bar{v}} = 98.35\%$ . Figure 5.6 shows the history of the compliance during optimization.

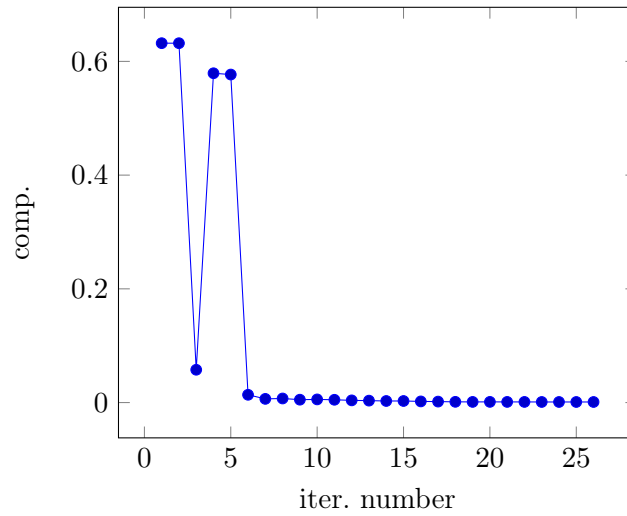


Figure 5.6 History of the compliance for the shape optimal design of the circular plate with isotropic material.

The history of the contributions of the membrane-shear and bending parts of the strain energy (compliance) is plotted on Figure 5.7.

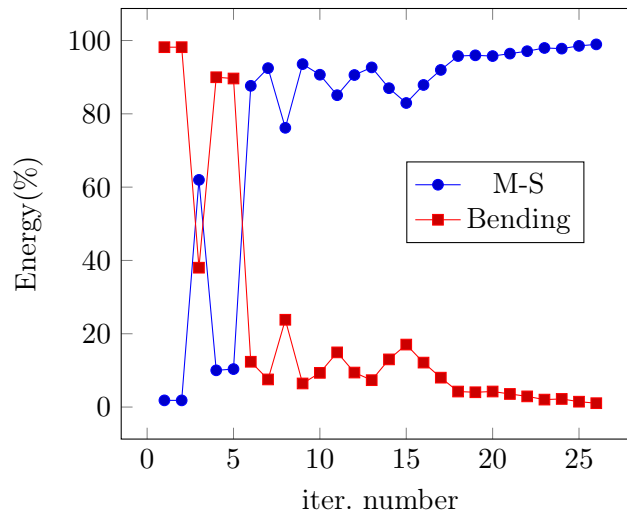


Figure 5.7 History of the variations of the different internal energies to the total strain energy (compliance) for the optimal design of the isotropic circular plate.

The initial structure of which energy is carried by the bending term while the optimal structure's energy is carried on the Membrane-Shear (M-S) term. The figure illustrates the transition from the bending dominant state to the membrane one.

Figure 5.8 shows the area variation throughout the iterations.

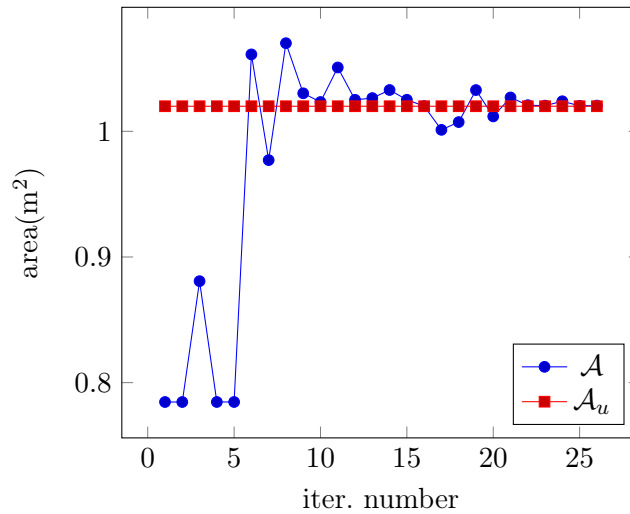


Figure 5.8 Shape design: Variation of the area of the shell during optimization.  $\mathcal{A}_u$  is the upper bound of the area variation and  $\mathcal{A}$  is the area of the design.

We remark that the optimizer tends to increase rapidly the area and that there are few iterations during which the upper bound constraint is violated. During the last iteration, the optimizer ensures the constraint.

**Orthotropy orientation and shape design:**

We consider the optimal design of the shape and orthotropy orientation. In that case, for a given material, one is looking for the optimal shape and the optimal orthotropy orientation. The orthotropy angle, initially  $\Phi_1 = \frac{\pi}{4}$  rad, is parameterized with the open knot vector of degree 3 and four control points in each parametric direction.

The optimal shape is represented on Figure 5.9



Figure 5.9 Orthotropy and shape design: Illustration of the optimal shape corresponding to the circular plate under weight-load.

Figure 5.10 represents the orthotropy direction on the geometry.

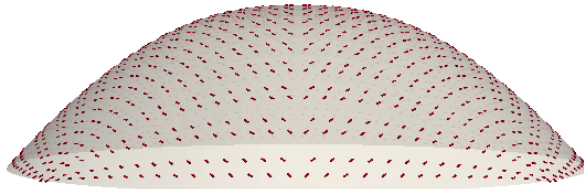


Figure 5.10 Orthotropy direction for the joint design of orthotropy and angle.

Comparing Figure 5.10 to the initial orthotropy, we remark that the orientation did not change, the optimal geometry is still a membrane shell. One can thus conclude, from the results, that the stiffness and optimality come mostly from the geometry.

The history of the objective function associated to this optimization is plotted on Figure 5.11.

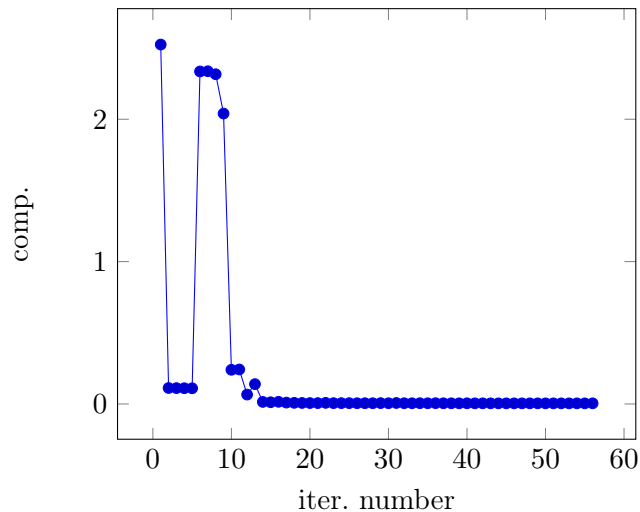


Figure 5.11 Orthotropy and shape optimization: History of the objective function throughout optimization.

The variation of the contributions of  $E_b$  and  $E_{\bar{b}}$  are plotted in Figure 5.12. In this case, similarly to the previous example, the transition from bending to membrane state is visible.

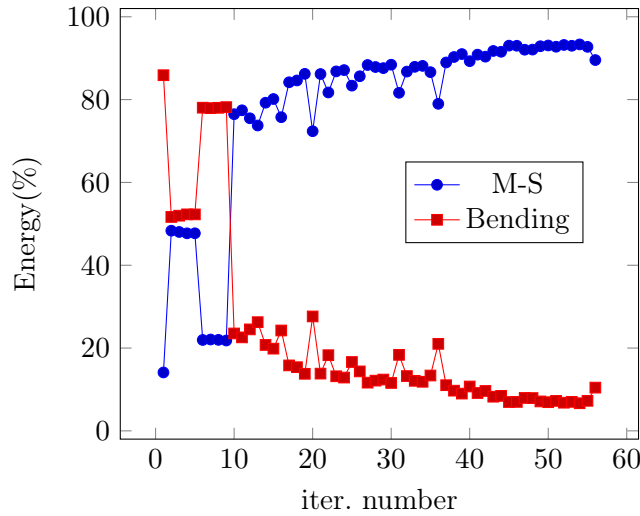


Figure 5.12 History of the contribution the different internal energies to the total strain energy (compliance) throughout optimization.

Initially, we have  $E_b = 86\%$  and for the optimal design  $E_b = 10\%$ , and  $E_{\bar{b}} = 90\%$ . We emphasize that, in comparison to the initial bending part of the isotropic case, the initial bending part in this present anisotropic case is lower. This highlights the role of the anisotropic part of the material properties.

Regarding the history of the objective function 5.11 there is a sudden rise of the objective cost after the first six iterations. These first steps, indeed, correspond to the initial phase of the optimization routine which at the beginning perform some evaluation of some disturbances of the initial design in order to construct an approximation of the objective function. The rising corresponds to the starting of disturbance with respect to the orthotropy angle control parameters. These first iterations illustrate the impact or influence of the shape design parameters on the objective function. The variation of the area, see Figure 5.13, corroborates the fact that the sudden variation of the cost function after six iterations corresponds to disturbances of only the orthotropy control parameters. In fact the area of the following iterations are equal to the initial area.

The energy state of the design become stable after the 45th iteration, i.e convergence has been reached after approximatively 45 iterations.

### 5.5.1.2 Anisotropy and shape design

We finally consider the joint optimization of the polar parameters and shape. The polar parameters are subjected to geometric bound on their control parameters and the orthotropy angle to bound constraints on its corresponding control parameters.

The polar parameters are still defined through using an open knot vector of order 3 and 4 control points for each coordinate direction. The number of design variables is thus equal to 60 and the number of constraints is 173. Among the constraints there is 49 constraints on the angle control parameters which corresponds to one level of refinement (using subdivision flexibility) in each coordinate direction, 16 for the geometric bound constraints for the two polar parameters moduli

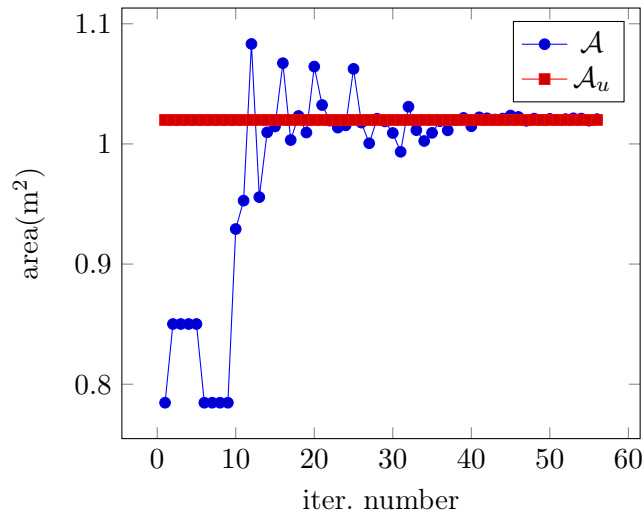


Figure 5.13 Orthotropy and shape design: Variation of the area of the shell during optimization.  $\mathcal{A}_u$  is the upper bound of the area variation and  $\mathcal{A}$  is the area of the design.

and the remaining for the geometric constraints (bounded variations of the control points and two inequality constraints for the upper and lower bounds on the area).

The optimal shape is plotted on Figure 5.14.



Figure 5.14 anisotropy and shape design: Optimal shape corresponding to the circular plate under weight-load.

As in the previous case the optimal design's shape is a cupola, which is the most optimal membrane structure. The direction of orthotropy field is plotted on Figure 5.15.





Figure 5.15 Anisotropy and shape design: Optimal orthotropy direction field of the optimal design corresponding to the circular plate under weight-load.

The optimal orthotropy direction tends to be along the meridional lines. The polar parameters moduli are plotted on Figure 5.16.

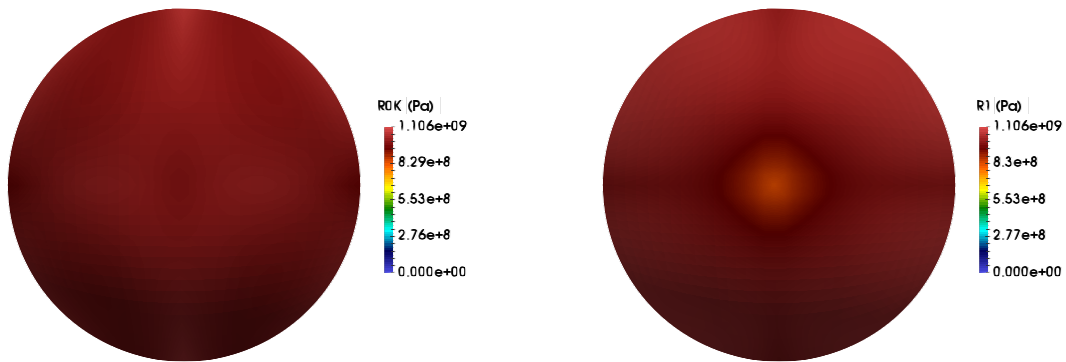


Figure 5.16 Anisotropy and shape design: Optimal polar moduli fields of the optimal design corresponding to the circular plate under weight-load.

One remarks that these parameters are uniform on the structure and the only present orthotropy is for  $K = 1$ .

Figure 5.17 shows the variation of the compliance throughout the optimization.

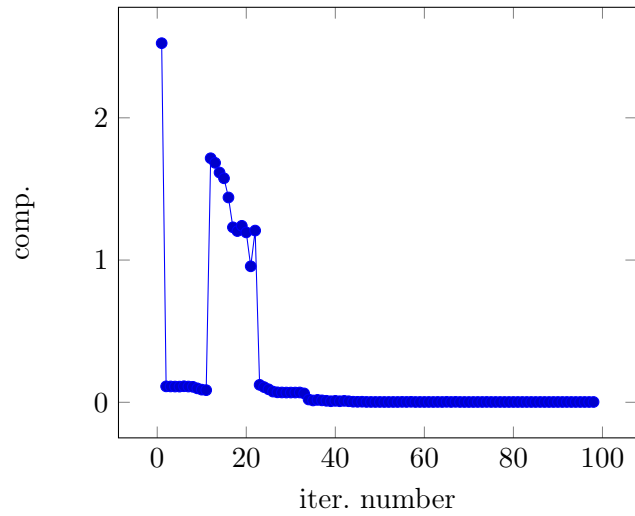


Figure 5.17 Anisotropy and shape optimization: History of the objective function throughout optimization.

The membrane energy part to the total strain energy of the optimal design is 93.34%. The Figure 5.18 shows the transition of the energy from bending to membrane.

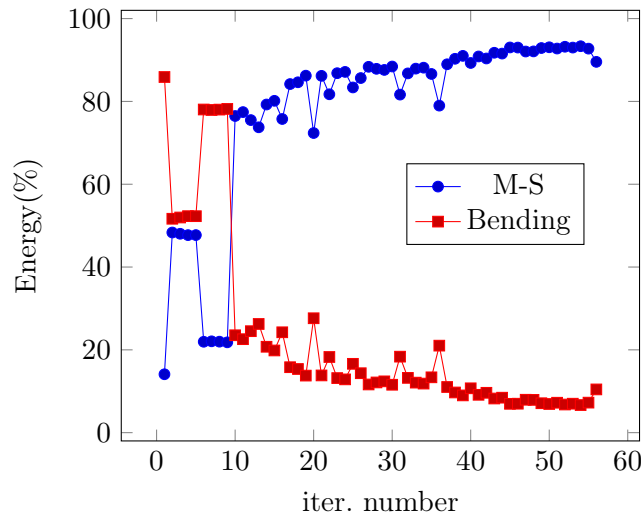


Figure 5.18 Anisotropy and shape design: History of the contribution the different internal energies to the total strain energy (compliance) throughout optimization.

Figure 5.19 shows the variation of the area during the optimization.

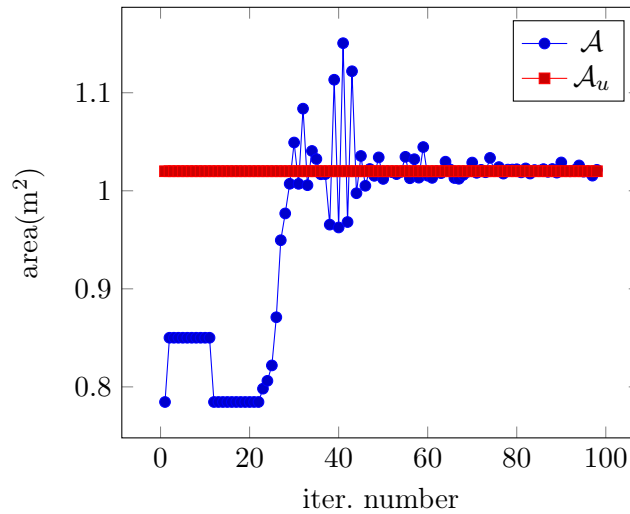


Figure 5.19 Anisotropy and shape design: Variation of the area of the shell during optimization.

As in the case of orthotropy and shape design, we remark that at the beginning of the optimization procedure, the iterations with  $\mathcal{A} = \mathcal{A}_0$  corresponding to design having the initial shape and disturbed angle and/or polar parameters, the objective function rises. This confirms that the geometry has an important incidence on the objective function. After the initial phase iterations of the optimizer which helps to define the approximation of the objective function, the objective function decreases “continuously”. The optimizer decreases rapidly the compliance by increasing the area of the shell to the extent that the bound constraints on the area are violated at some iterations. However, the final optimal design computed satisfies the constraints.

One can conclude from the previous results that the stiffness mostly comes from the geometry. In fact the polar moduli are distributed uniformly and are almost constant over the shell. The joint optimization of the anisotropy and shape yields to a more optimal design. Indeed for the orthotropy and shape design, we have  $E_{ms} = 90\%$ , while for the joint anisotropy and shape optimization we have  $E_{ms} = 93.34\%$ .

### 5.5.2 Optimization of a holed circular plate

In the present case, we consider the optimization of a holed circular plate which is simply supported at its external boundary and subjected to a uniformly distributed vertical load at its inner smallest crown. The geometric feature and conditions are represented on Figure 5.20.

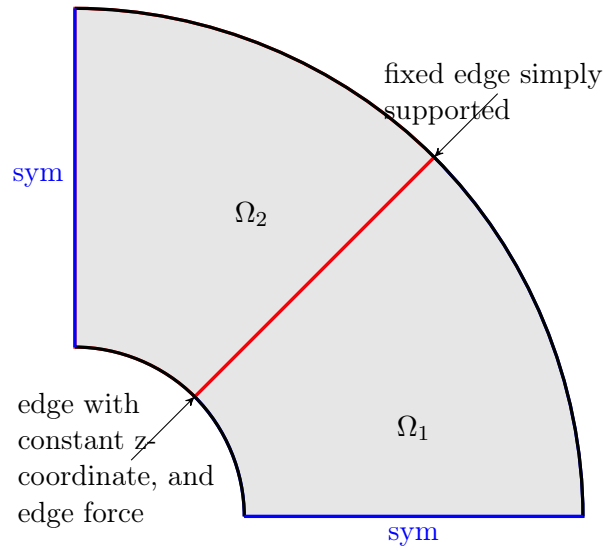


Figure 5.20 Geometric and boundary conditions of the circular holed plate

The elastic properties, thickness and volume density are the same as in the first example. For symmetry reason, the optimization is performed on the quarter of the structure. The geometry is defined by two sub-structures joined together as described in Figure 5.20. The design is subject to  $C^1$  regularity constraints between the two parts and to a  $G$ -continuity through the two planes containing the edges with symmetry conditions.

Different configurations of optimal design are also considered in this case.

### 5.5.2.1 Optimal shape with isotropic material

We start by the optimal design of the structure made of isotropic material, by getting rid of the anisotropic part, i.e setting  $R_0^K = R_1 = 0$ .

The tolerance on the upper bound of the area is  $\epsilon_{tol} = \frac{3}{2}$ . The control points associated to the circular boundary with simply-supported condition are kept fixed while those defining the internal circular crown, which carries the applied load, are constrained to have the same  $z$ -coordinate. The number of design variables is 25.

The optimal shape found is plotted on Figure 5.21.



Figure 5.21 Shape design: Optimal shape corresponding to the holed circular plate under edge load.

The history of the compliance and the variation of membrane-shear and bending energy describing the state of the design during the optimization are respectively plotted on Figure 5.22 and 5.23.

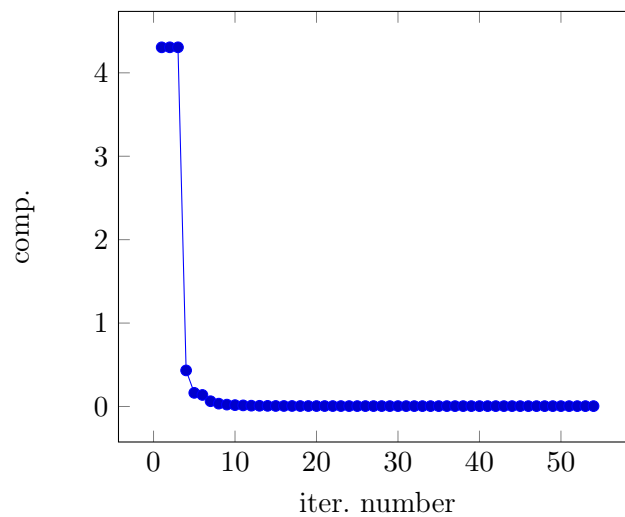


Figure 5.22 Circular holed plate: History of the objective function throughout shape optimization for the isotropic case.

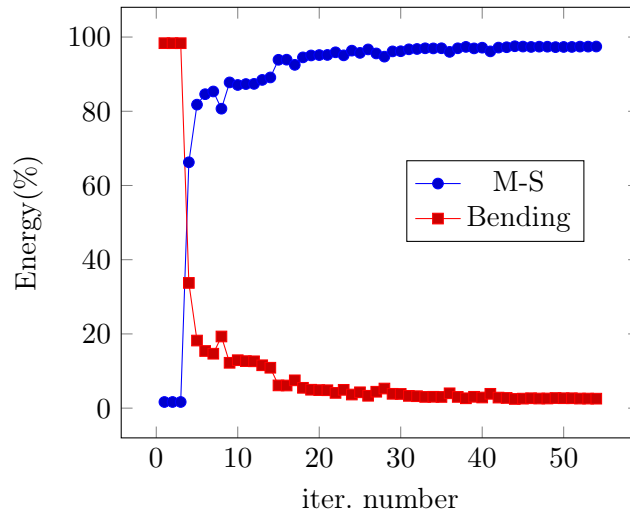


Figure 5.23 Contribution of the different internal energies to the total strain energy (compliance) throughout the optimization of the holed circular plate with isotropic material.

The scalar  $E_b$  was initially equal to 98.35% and the one corresponding to the optimal design is equal to 1.12%. The Figure 5.23 illustrates the changeover from the bending dominant state to the membrane one.

The Figure 5.24 shows the variation of the area throughout optimization.

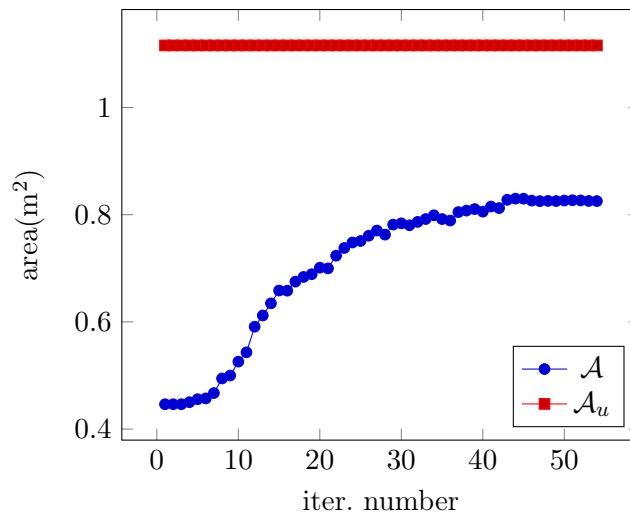


Figure 5.24 Variation of the area of the shell during shape optimization of the holed circular plate with isotropic material.

### 5.5.2.2 Optimal shape for the anisotropic circular plate

We consider the optimization of the shape of the circular plate with anisotropic material and impose the same constraints as in the previous case. Here, the control points are allowed to change

but only along the  $z$ -direction. The number of design variables after considering the constraints is 9. The total number of constraints associated is 24. The angle of orthotropy is  $\Phi_1 = \frac{\pi}{4}$ . The optimal shape is plotted on Figure 5.25.



Figure 5.25 Shape design with anisotropy material with an orthotropy angle  $\Phi_1 = \frac{\pi}{4}$ : Optimal shape corresponding to the holed circular plate under edge load.

and the orthotropy direction associated on Figure 5.26.

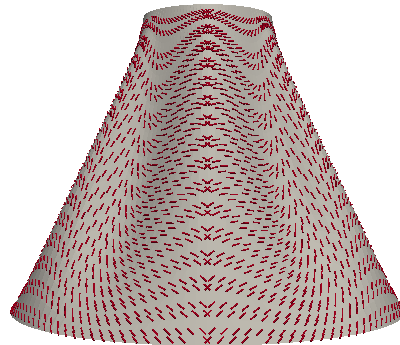


Figure 5.26 Orthotropy direction on the optimal shape design

The optimizer finds a structure with important outline and curvature which creates some pronounced load patches allowing the transmission of the load to the basis of the structure. Figure 5.27 shows the history of the objective function throughout optimization.

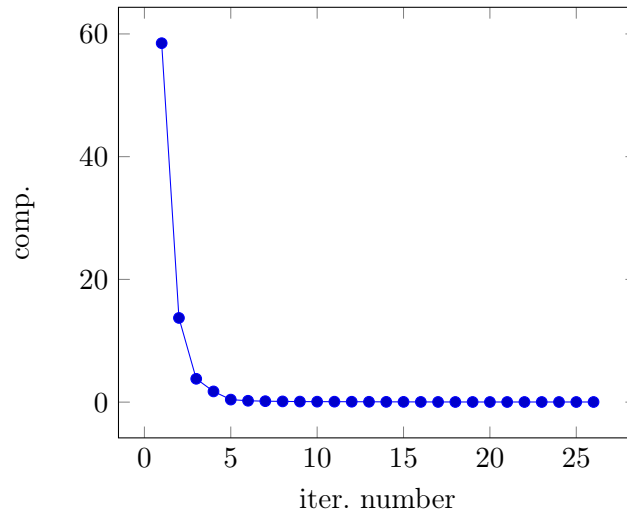


Figure 5.27 Circular holed plate: History of the objective function throughout shape optimization for the anisotropic material case.

The compliance was initially equal to 58.5 and for the optimal computed shape it is  $2.14 \times 10^{-2}$ . We have a significant stiffening of 99.963%.

Figure 5.28 shows the variation of the energy states of the design. However the bending part of energy remains substantially high.

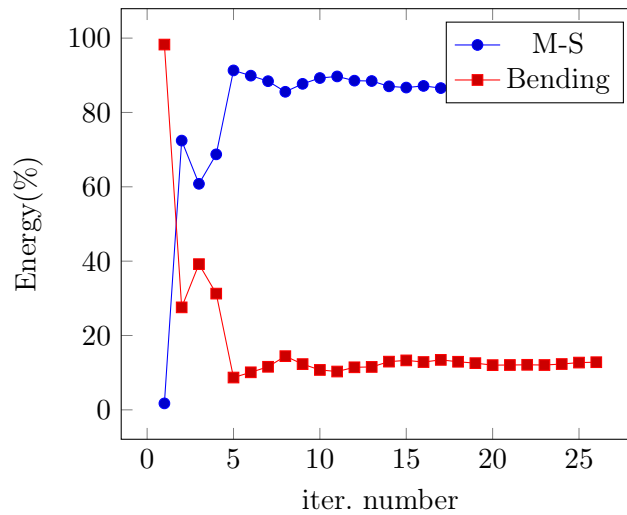


Figure 5.28 Shape design of anisotropic holed circular plate: History of the contribution of the different internal energies to the total strain energy (compliance) throughout optimization.

As in the previous case, we remark that the initial part of the bending energy to the total strain energy drops from 98.26% to 12.7% for the optimal design.

Figure 5.29 shows the variation of the area during the optimization.



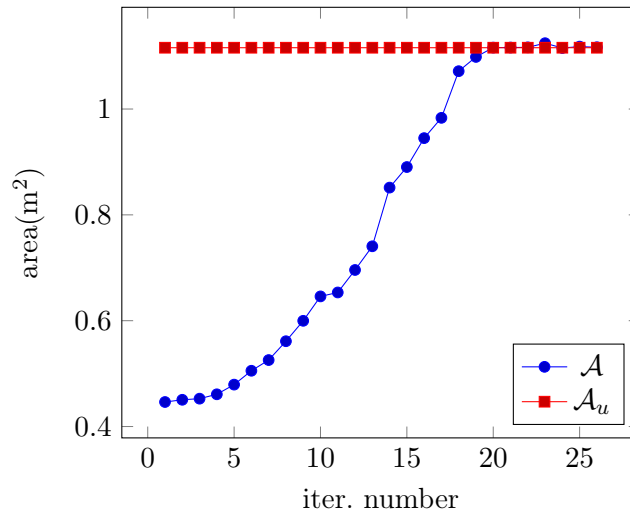


Figure 5.29 Shape design of holed circular plate: Variation of the area of the shell during optimization.

One remarks that the optimizer continuously increases the area of the design and that the upper bound constraint is perfectly satisfied.

### 5.5.2.3 Shape and anisotropy optimal design

We presently consider the joint optimization of the shape and material properties of the circular holed plate. The initial orthotropy angle is still  $\Phi_1 = \frac{\pi}{4}$ . The polar parameters are defined through open knot vector of order 3 and 3 control points in each coordinate direction. Thus in addition to the 9 shape design variables, one have 15 design variables for each polar parameters; in fact  $18 = 9 \times 2$  control parameters, reduced to 15 thanks to the continuity constraint. The total number of constraints is 159.

Figure 5.30 shows the optimal shape obtained and the orthotropy direction.



Figure 5.30 Optimal shape for the joint anisotropy and shape design of the holed circular plate.

The optimal structure is almost a cone frustum. This can either be explained by the fact that the load is applied in the  $\mathbf{e}_3$  direction, and there is a slight curvature on the trunk in order to carry in membrane as much as possible the applied load or because the tolerance on the area variation which could be too restrictive, see Figure 5.35. Figure 5.31 shows the orthotropy direction on the geometry. We remark that the fiber are clearly oriented towards the loading direction. In this case the geometry is regular without any particular outline and the role of the fiber in the stiffening and optimal design is highlighted.

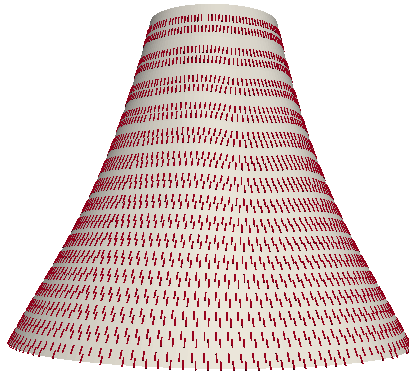


Figure 5.31 Optimal orthotropy direction corresponding to the joint anisotropy and shape design of the holed circular plate.

Figure 5.32 shows the optimal polar moduli  $R_0^K$  and  $R_1$ .



Figure 5.32 Distribution of the optimal polar moduli  $R_0^K$  and  $R_1$ .

The field of the parameter  $R_0^K$  is uniform and seemingly constant over all the structure and we note the presence of only one kind of orthotropy  $K = 0$ . Considering, the definition of the elastic tensors in term of the polar parameters, one can see that the joint positive values of the polar moduli with an orthotropy angle equal to zero corresponds to increasing the elastic coefficient  $E^{1111}$  which is an effective design in the present example. Indeed, the 1-axis in our case is initially the radial direction of the holed circular plate. The values of the polar modulus  $R_1$  indicates that the stiffness is set increasing from the top to the circular ground of the design, to which the load and effort are transmitted.

The applied load is normal to the initial flat middle-surface, and thus the structure is in a bending dominant state. The optimal design is the one which maximizes the membrane-shear energy part of the total energy. Figure 5.33 shows the transition of the energy from a bending state to the membrane-shear one.

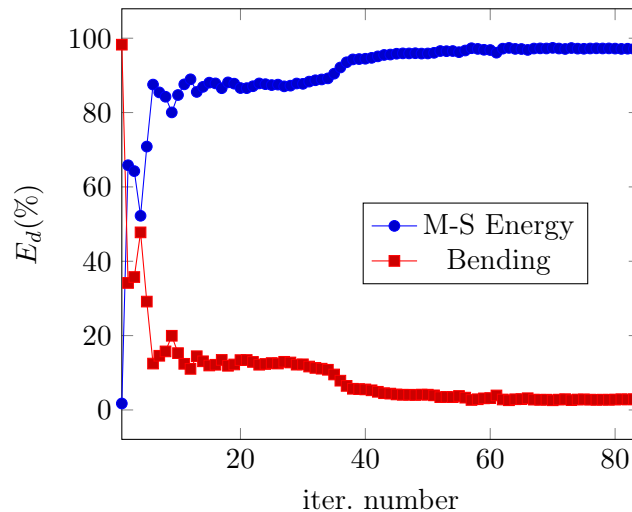


Figure 5.33 Contribution of the different internal energies to the total strain energy (compliance) throughout optimization.

The energy of the initial structure is carried by the bending term while the optimal structure's energy is carried by the Membrane-Shear (M-S) term. The figure illustrates the transition from the bending dominant state to the membrane one.

As can be seen in Figure 5.33, the convergence in the standpoint of energy state has already been attained after 60 iterations. The strain energy which initially was bending predominant  $E_b = 98.3\%$  is membrane dominant for the optimal shell  $\simeq 97.2\%$ .

Figure 5.34 shows the history of the objective function.

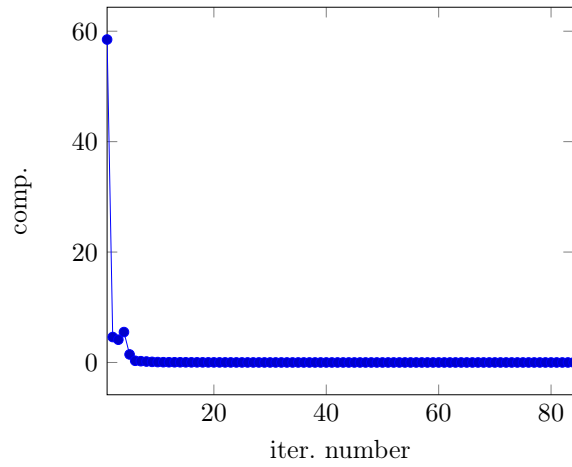


Figure 5.34 History of the objective function

Figure 5.35 represents the variation of the area during the optimization.

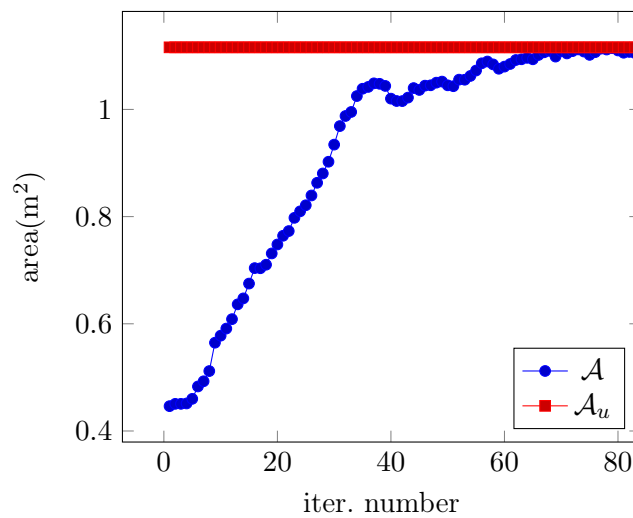


Figure 5.35 Variation of the area of the shell during optimization corresponding to the joint shape and anisotropy design of the holed circular plate

On notices that the area continuously increases and the upper bound constraint on the area is always satisfied. The results of the different optimizations performed are gathered in Table 5.1.

Design	Material					
	Anisotropic				Isotropic	
	0	1	2	4	0	1
Compliance	58.5	$2.14 \times 10^{-2}$	N/O	$2.78 \times 10^{-3}$	4.3	$4.52 \times 10^{-3}$
$E_m(\%)$	1.74	87.19		97.54	1.65	97.45

Table 5.1 Summary of the different optimizations concerning the holed circular plate.

In the previous table the integer numbers have the following meanings: initial design (0), shape optimization (1), orthotropy angle and shape design (2), the three polar parameters and shape design (4) and finally N/O stands for Not Optimized.

### 5.5.3 Plate submitted to torsional load

In what follows, we consider a square plate of unit length clamped at one boundary and subjected to torsional load at the opposite side. The torsion is produced by two concentrated loads at the two vertices of this edge, see Figure 5.36 with  $\mathbf{f} = f \mathbf{e}_3$ , and  $f = 1000\text{N}$ .

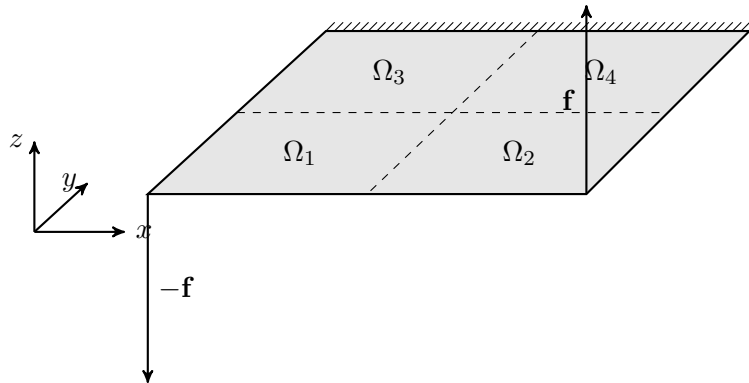


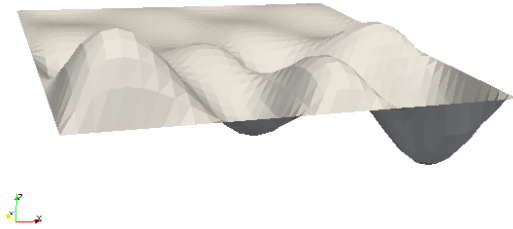
Figure 5.36 Geometric description of the plate under torsion

In order to satisfy iso-loading, the design is subjected to fix place constraint on the four edges, i.e the corresponding control points are kept fixed. The orthotropy is initially oriented with an angle  $\Phi_1 = 0$  and along the  $x$ -axis direction. The design is subjected to bounded area constraints of tolerance  $\epsilon_{tol} = 0.2$ . The plate is defined by an assembling of  $2 \times 2$  square plates of length 0.25m, each parameterized through a cubic B-splines with open knot vectors and four control points.

We consider different cases of optimization. The first one concerns the optimal shape when the design is composed of isotropic material; after we consider the shape design when the material is anisotropic, the joint design of shape and the orthotropy orientation, and at last the joint design of the anisotropy and the shape. Figure 5.37 shows, respectively from left to right, the optimal shape obtained in the case of isotropic and anisotropic materials.



5.37.a – Isotropic material case



5.37.b – Anisotropic material case

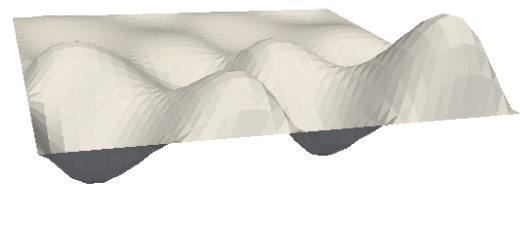
Figure 5.37 Optimal design corresponding to the shape optimizations with isotropic and anisotropic material for the plate under torsion

We remark that in the case of isotropic material, the outline is global whereas in the case of anisotropic material it is localized nearby the loading region.

Figure 5.38 shows the optimal design corresponding to the cases (2) and (4).



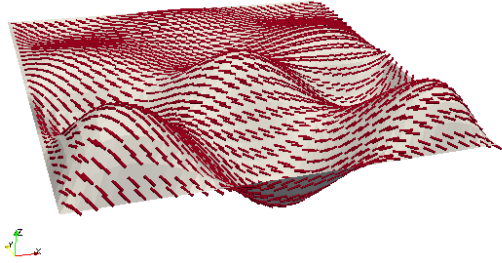
5.38.a – Shape and orthotropy



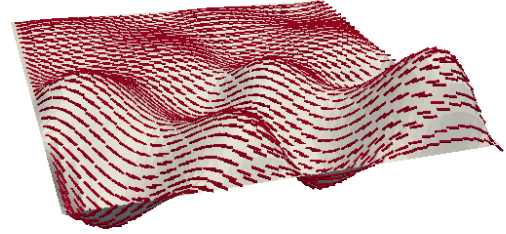
5.38.b – Anisotropy and shape

Figure 5.38 Optimal shape corresponding to the joint orthotropy/shape design and global anisotropy/shape design

The associated orthotropy direction fields are represented on figure 5.39.



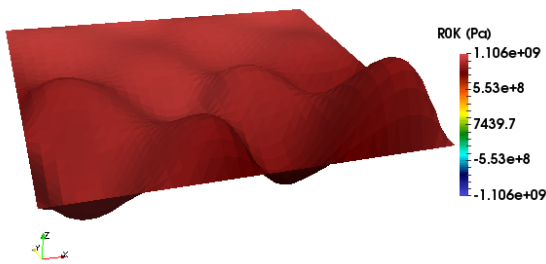
5.39.a – Shape and orthotropy



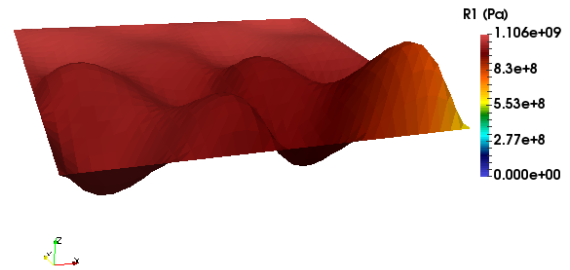
5.39.b – Anisotropy and shape

Figure 5.39 Optimal orthotropy direction corresponding to the joint orthotropy/shape design and global anisotropy/shape design

The polar moduli  $R_0^K$  and  $R_1$  corresponding to the optimization (4) are represented on Figure 5.40.



5.40.a – Optimal distribution of the parameter  $R_0^K$



5.40.b – Optimal distribution of the parameter  $R_1$

Figure 5.40 Optimal polar moduli corresponding to the joint design of the global anisotropy and the shape.

Table 5.2 summarizes the different optimization results.

Design	Material					
	Anisotropic				Isotropic	
	0	1	2	4	0	1
Compliance	1471.83	14.73	5.59	3.77	96.69	4.98
$E_m(\%)$	3.28	91.71	94.78	94.98	16.48	93.05

Table 5.2 Summary of the different optimizations concerning the plate under torsional load.

The common characteristic in the different optimization cases is that the optimal shape presents interesting curvatures. For isotropic material the curvature is smooth, and global while in the design optimization involving the anisotropic material the curvature is mostly localized nearby the loaded region. We remark also that the optimal shape corresponds to those which are in membrane dominated state, see 5.2. We can mention that the joint optimization of anisotropy and shape yields to a substantially better structure according to the values of the compliance and  $E_m$ .

#### 5.5.4 Optimal design of a square plate under weight-load

We consider in this example a plate subjected to its own weight. The constitutive material composing the plate is the same as in the previous examples. The plate's thickness is  $t = 3 \times 10^{-2}m$ . The orthotropy angle is initially  $\Phi_1 = \frac{\pi}{4}$ . The plate is assumed to be clamped at two opposite sides; which are also considered to be fixed for the optimization problem. The tolerance on the area bounds is  $\epsilon_{tol} = 0.3$ . Each polar parameter is parameterized with a quadratic spline, i.e the total number of control points are 9.

#### Shape and material design

We finally consider the joint optimization of the shape and the polar parameters. The total number of design variables is 35; 8 for the shape and 27 for the polar parameters. Figure 5.41 shows the optimal shape and the orthotropy direction.



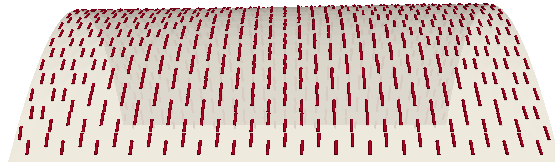
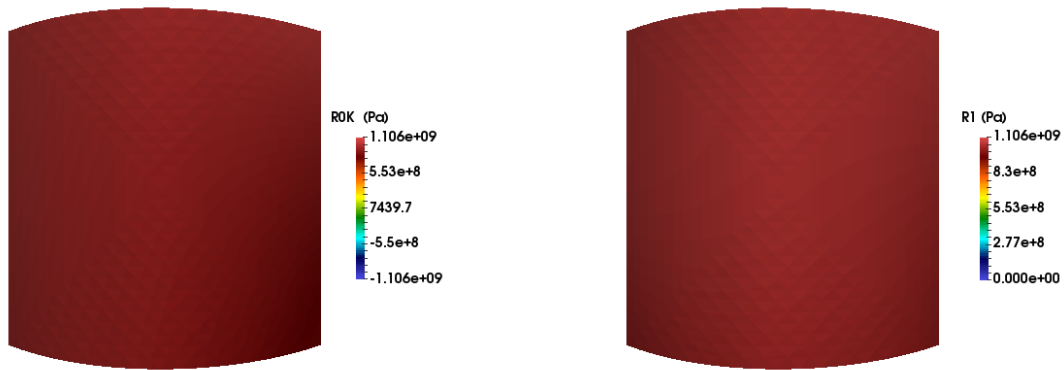


Figure 5.41 Optimal shape for the joint anisotropy and shape design of the plate under weight-load

The optimal fibres are oriented uniformly perpendicular to the edges with clamping conditions and the shape is like a reverse catenary, which in fact is the shape which minimizes the bending. The parameters  $R_0^K$  and  $R_1$  are represented on Figure 5.42.

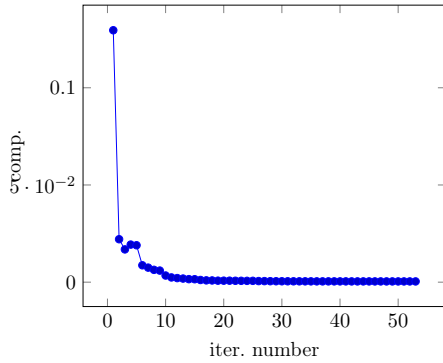


5.42.a – Distribution of  $R_0^K$

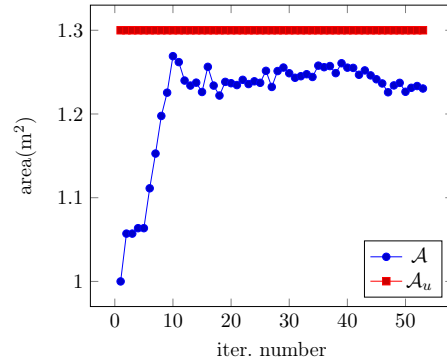
5.42.b – Distribution of  $R_1$

Figure 5.42 Distribution of the optimal polar moduli  $R_0^K$  and  $R_1$  of the joint shape and material design of the plate under weight-load

One remarks that the moduli are constant over the optimal shape. The set of polar parameters found, namely  $\Phi_1 = 0$  rad,  $R_0^K = R_0^L$  and  $R_1 = R_1^L$ , are in fact those which maximize at the same time the elastic moduli  $E^{1111}$  and  $E^{2222}$ . The evolution of the compliance and the area throughout optimization are plotted on Figure 5.43.



5.43.a – Objective function



5.43.b – Design area

Figure 5.43 History of the objective function and area respectively from left to right.

	Material					
	Anisotropic				Isotropic	
Design	0	1	2	4	0	1
Compliance	$12.96 \times 10^{-2}$	$1.04 \times 10^{-2}$	$1.55 \times 10^{-3}$	$3.80 \times 10^{-4}$	$4.88 \times 10^{-2}$	$9.29 \times 10^{-4}$
$E_m(\%)$	18.51	94.69	96.68	95.56	20.33	95.31

Table 5.3 Summary of the different optimizations concerning the plate under weight-load.

In these different cases the optimal shapes are similar. Analyzing the results in Table 5.3, one concludes that, for the optimizations which involve the anisotropic material, the best design is obtained when a joint design of the shape and all the polar parameters is performed. A common characteristic of the optimal design is that the membrane-shear contribution to the total strain energy is  $\simeq 95\%$ .

Figure 5.44 shows the history of the internal energy through the optimization. We emphasize that in both cases of anisotropic and material design, the substantially high part of membrane energy  $\simeq 20\%$ , corresponding to the initial designs is due to the shear forces contribution.

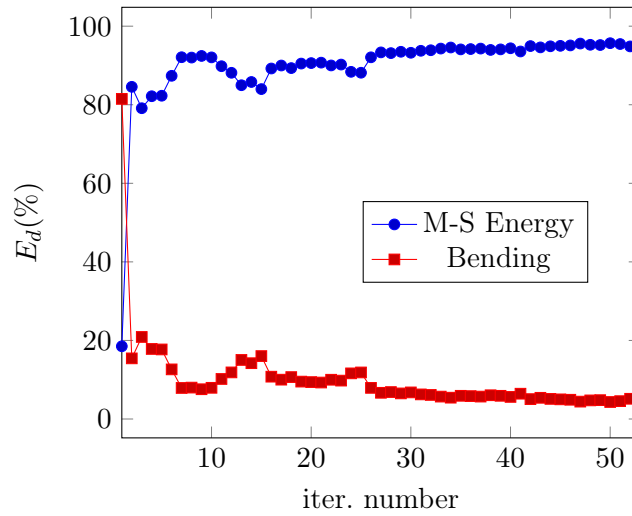


Figure 5.44 History corresponding to the internal energies.

## 5.6 Synthesis

We focused in this chapter on the optimal design involving the shape design. Some joint optimization of both shape and material have been considered. The first part of this chapter was devoted to the shape parameterization using B-spline functions. We have further specified the derivatives with respect to the shape design variables which can allow to use gradient-based optimization algorithms. The derivative when the design involves assembling of shells is computed in the standard way but involves the derivative of the local junction matrix (of displacement and rotation continuities). Several examples presented show the interest of the joint isogeometric-polar formalism coupling.

# Conclusion and Perspectives

---

## Conclusion

The first part of this thesis was mostly devoted to shell analysis aspects. We proposed in chapter 3 a new approach for the analysis of shells assembling. The method described involves the well-known mortar technique which is commonly used in domain decomposition. The advantage of this technique is that the meshing of each shell can be performed independently thanks to the enhancement of nonconforming discretizations.

The second part of this manuscript dealt with the optimization of shell structures. In the first half, we focused on a suitable parameterization of the elastic tensor using on one side a polar formalism, which allows to represent the elastic tensor by means of invariants and angles (the so-called polar parameters), and on the other an isogeometric approach through a B-spline based parameterization for the above polar parameters. The proposed approach possesses several advantages. First, it allows to exhibit the different aspects of the elastic material and to properly reveal the anisotropy features, i.e the dependence of the elastic behavior with respect to the fiber reinforcement direction. Second, the different parameters of the elastic tensor are explicit, i.e the isotropic and the anisotropic parts to be designed are clearly identified. And third, the parameterization introduced allows to reduce the number of design variables and constraints satisfied by the elastic tensor coefficients. Several material design problems have been solved to show the effectiveness of the method and its capability to tailor locally the material properties distribution.

The last topic treated in this work was the shape and anisotropy design of shells. For that purpose we have considered the case of a structure defined through a unique regular mapping and also the case of an assembling of shells. A polar formalism for the elastic tensor representation and an isogeometric (B-spline) parameterization for the polar parameters and the shape are applied. Several optimization examples are performed involving structures in bending dominated state.

## Perspectives

From a mechanical analysis standpoint, further works can be done by implementing a nonconforming discretization, i.e an analysis with finite elements of different orders from one shell to another. The approach developed in this work can be extended to nonconforming junctions for which the interface between shells is not necessarily an entire parametric curve. Another perspective could be to work on techniques allowing to avoid the numerical locking which is inherent to most of shell finite elements.

## Conclusion and Perspectives

---

As for the shell structure optimization, the computation of the derivatives performed can further be useful for an optimizer using a gradient-based algorithm. Future works and applications may consider more complex geometries such as those found in an industrial context. This task is not trivial since the geometry from CAD software is often made of trimmed surfaces. Finally the optimal design of composite shells might further be investigated. In fact the optimization problem involving the optimal design of anisotropy tackled in this thesis can be viewed as a first step towards the design of composite structures through a bilevel optimization: one level concerning the design of the homogenized elastic properties of the laminate and the second level relative to the definition of the optimal stacking sequences corresponding to the global homogenized elastic properties retrieved at that first level. The second level optimal design could be performed through a genetic algorithm such as BIANCA [73], [53].

# Appendix



# Résumé de thèse

---

## Contents

---

<b>A.1 Motivations</b>	<b>157</b>
<b>A.2 Modèle de coques de Naghdi</b>	<b>160</b>
<b>A.3 Jonction de coques de Naghdi et discrétisation non-conformes</b>	<b>163</b>
A.3.1 Considérations géométriques	163
A.3.2 Raccordement entre coques	164
A.3.3 Méthode mortier	166
<b>A.4 Optimisation d'anisotropie et propriétés matériaux</b>	<b>169</b>
A.4.1 Formalisme polaire	169
A.4.2 Discrétisation des paramètres polaires	172
A.4.3 Prise en compte de contraintes	173
<b>A.5 Optimisation conjointe de formes et propriétés matériaux</b>	<b>173</b>
A.5.1 Géométrie et paramétrage de la forme	173
A.5.2 Optimisation	176

---

## A.1 Motivations

Le conception (design) optimale est une question naturelle qui se pose dans de nombreuses tâches quotidiennes. Cette question est rencontrée dans plusieurs domaines tels que le génie civil, l'aéronautique et l'automobile où le défi de construction de structures légères, respectueuses de l'environnement et consommant moins de carburant, est d'une importance primordiale. Une telle tâche présente beaucoup de challenges car la conception optimale est soumise à beaucoup de contraintes. En effet, la conception optimale, par exemple la plus légère, doit permettre d'assurer de bonnes fonctionnalités ou performances. Différents types de structures sont concernés, à savoir les structures de surfaciques telles que les plaques et les coques qui représentent une part prépondérante des constructions; par exemple, les structures surfaciques représentent plus de 70% d'une automobile (voir Figure 1.1 page 6).

Depuis de nombreuses décennies, les structures composites sont intensivement utilisées grâce à leur comportement mécanique et à leur intéressant rapport rigidité-poids élevé etc... Les progrès perpétuels dans la technologie des matériaux composites favorisent leur fabrication par différentes techniques telles que l'enroulement filamentaire, la RTM (Resin Transfert Molding) -injection de résine- et la fabrication additive (impression 3D) et réduisent les obstacles à leur intégration dans



les constructions. Ces structures offrent de nombreux avantages d'un point de vue géométrique et, concernant l'aspect matériau, une réelle flexibilité d'ajustement ou de dimensionnement des propriétés élastiques comparativement aux matériaux standards comme l'acier. L'exploitation de cette flexibilité nécessite l'utilisation des techniques d'optimisation et de programmation mathématique pour l'optimisation structurelle.

L'optimisation structurelle peut être envisagée à différentes échelles d'une structure, à savoir la forme et le matériau constituant. La conception admissible dépend du type d'optimisation considéré. On distingue habituellement trois classes d'optimisation : l'optimisation de forme, de dimensionnement et l'optimisation topologique. Le premier implique la forme comme variable de conception et la topologie n'est pas modifiée, c'est-à-dire aucune apparition ou disparition de trous par rapport à la conception initiale. Dans le deuxième type d'optimisation, les variables sont les paramètres géométriques tels que la longueur, section de poutre, la largeur ou l'épaisseur, ainsi que les coefficients de propriétés élastiques du matériau tels que le module Young et le coefficient de Poisson. Le dernier type d'optimisation citée est le plus complexe mais il permet de gérer des géométries complexes. Dans ce type d'optimisation, la topologie peut changer et le paramètre de conception est généralement une fonction de densité qui définit la distribution du matériau. Cette classe d'optimisation concerne principalement les problèmes de réduction de masse. Il convient de souligner, au vue de cette classification, que le dimensionnement semble à une première vue le plus "simple" en raison du fait que la topologie est connue et fixe. Mais cette classe d'optimisation englobe diverses optimisations et cache une réelle complexité. Par exemple, l'optimisation topologique peut aussi être considérée comme un dimensionnement des propriétés de matériaux composés de deux phases (une forte et l'autre faible, définissant le vide). Ainsi, l'optimisation de matériaux peut également être considérée comme un type d'optimisation structurelle à part entière, au même titre que l'optimisation topologique.

Dans cette thèse, nous considérons l'optimisation à la fois de la forme et des propriétés matériaux de structures surfaciques, qui représentent une part prépondérante d'une automobile. Le processus d'optimisation standard dans l'industrie est complexe et hétérogène. En effet, l'optimisation est interdisciplinaire et associe plusieurs composantes telles que les techniques de conception, de simulation et de calcul scientifique. Toutes ces composantes ne cohabitent pas naturellement de manière homogène. En effet, la structure initialement conçue, à l'aide d'un logiciel de conception assistée par ordinateur (CAO), doit être fournie à un logiciel de simulation pour une analyse structurale, dans un environnement d'Ingénierie Assistée par Ordinateur (IAO), afin de calculer la réponse structurelle à l'aide de méthodes numériques telles que l'analyse par une méthode d'éléments finis (MEF) qui permet en outre de calculer la performance (fonction objectif) à optimiser. L'analyse MEF étant faite sur un maillage de la structure, le passage de la CAO à l'IAO se fait au prix d'une coûteuse étape de maillage. D'une part, l'optimisation de forme, de manière classique, est effectuée sur le même maillage ayant servi à l'analyse structurelle et les variables de conception de forme sont, dans ce contexte, les coordonnées des points de maillage. D'autre part, lorsqu'une conception de matériau est abordée, les variables de conception des propriétés du matériau sont habituellement définies discrètes par éléments finis.

Cette approche présente plusieurs inconvénients. Premièrement, la conversion CAO-maillage qui prend un temps considérable détériore la conception initiale et donc la réponse structurelle; et par conséquent, l'optimisation effectuée ne correspond pas exactement à celle de la conception originale. Il a été démontré dans [4] que pour les structures complexes, la conversion entre la géométrie d'origine (CAO) et le maillage représente près de 80% du temps total de l'analyse. Cette procédure est également intrusive. En raison du manque de générateur de maillage efficace,

l'étape de maillage doit être contrôlée et ajustée par un spécialiste. Deuxièmement, la complexité du problème d'optimisation est très importante et demande d'énormes ressources numériques. En outre, la conception optimale est soumise à de nombreuses contraintes relatives à la régularité de la forme qui ne peuvent être prises en compte facilement. Les propriétés matériaux doivent aussi satisfaire des contraintes de continuité (des fibres) et de fabricabilité par des outils qui sont contrôlés numériquement.

En résumé, la conversion de la géométrie de CAO, considérée comme exacte, en maillage (une approximation) affecte la qualité de l'analyse structurelle qui, de ce fait, détériore sévèrement la solution optimale. La conception résultant du processus d'optimisation n'étant plus une CAO mais un maillage, une étape de conversion de maillage-CAO est donc indispensable mais coûteuse. Ces dernières années ont vu l'émergence d'une nouvelle technique appelée isogéométrie qui permet de réduire le fossé entre les environnements de CAO et de IAO. L'analyse isogéométrique, développée par R.T Hughes [28], offre la possibilité d'intégrer les outils d'IAO aux outils de conception CAO. Dans ce cadre, les fonctions de base d'interpolation classiques de MEF sont remplacées par les fonctions de base CAO, c'est-à-dire des fonctions de Bézier, Splines et NURBS. La désignation isogéométrie a ensuite été élargie à l'ensemble des techniques qui utilisent les fonctions de base décrivant la géométrie pour définir une quantité d'intérêt donnée.

L'optimisation standard de la forme et des propriétés matériaux basée sur les méthodes éléments finis implique différentes représentations géométriques, à savoir la conception de la CAO et son approximation (maillage). La méthode isogéométrique vise donc à réduire cette hétérogénéité. En effet, cette méthode englobe le concept isoparamétrique qui consiste à approcher la solution d'un problème donné ou une quantité d'intérêt donné en utilisant le même paramétrage que celui de "l'objet" auquel elle est associée. Ceci se traduit dans le cadre de résolution d'équations aux dérivées partielles par la substitution des fonctions classiques d'éléments finis par celles associées à la représentation géométrique de la structure. Les fonctions test utilisées sont donc les fonctions NURBS, B-Spline ou de Bézier. Un tel choix est possible car ces fonctions satisfont les propriétés des fonctions test classiques de MEF; notamment l'indépendance linéaire et la propriété de partition de l'unité. Le concept a été élargi aux problèmes d'optimisation. Dans ce cadre, les variables de conception sont des paramètres de CAO, notamment les coordonnées des points de contrôle. Parmi les références, nous pouvons citer non-exhaustivement [40, 23], et spécialement mentionné [56] qui concerne la conception optimale de la forme et du matériau.

Cette thèse découle de la volonté de Renault de disposer d'outils capables d'aider à la conception optimale des structures surfaciques et est dans la continuité des recherches effectuées ces dernières années avec la thèse de P. de Nazelle [35] et S. Julisson [39]. Nous nous concentrons spécifiquement dans cette thèse sur la conception optimale de formes et de propriétés matériaux pour les structures surfaciques (coques) anisotropes.

Le manuscrit est principalement composée de cinq chapitres. Un premier chapitre introductif de rappel rapide de l'état de l'art (voir chapitre 1, page 1). Les deux chapitres suivants concernent le modèle mécanique d'analyse structurelle sachant que les deux derniers traitent de la conception optimale de structure. Dans le chapitre 4 nous abordons la discrétisation et l'optimisation des propriétés matériaux. Et pour finir, dans le chapitre 5, nous nous intéressons à l'optimisation de forme.

## A.2 Modèle de coques de Naghdi

Nous rappelons dans ce chapitre le modèle mécanique qui définit le comportement mécanique de structure utilisé dans la suite de la thèse. Nous introduisons les notations classiques de géométrie différentielle. Les indices grecs prennent leurs valeurs dans l'ensemble  $\{1, 2\}$  et les indices latins dans l'ensemble  $\{1, 2, 3\}$ , quand ils ne se rapportent pas à une suite et sauf mention contraire. Il est régulièrement, sauf mention contraire, fait usage de la convention de sommation d'Einstein sur les indices répétés permettant une brièveté dans la définition d'une somme; par exemple

$$u_i v^i = u_\alpha v^\alpha + u_3 v^3 = u_1 v^1 + u_2 v^2 + u_3 v^3.$$

Les quantités en gras sont des vecteurs, tenseurs et  $\mathbf{e}_i = \mathbf{e}^j$  désignent les vecteurs de la base canonique

$$\hat{v}_i \mathbf{e}^i = \hat{v}_1 \mathbf{e}^1 + \hat{v}_2 \mathbf{e}^2 + \hat{v}_3 \mathbf{e}^3.$$

On note  $\mathcal{E}^3$  l'espace euclidien rapporté à la base canonique  $(\mathbf{e}_1, \mathbf{e}_2, \mathbf{e}_3)$  et à l'origine  $O$ . Étant donné un point  $P \in \mathcal{E}^3$ , on note  $\mathbf{p} = \mathbf{OP}$  son vecteur position.

### Géométrie différentielle

Nous définissons une coque comme une structure tridimensionnelle dont une dimension (l'épaisseur) est négligeable devant ses autres dimensions caractéristiques, de sorte qu'elle est généralement identifiable à une surface. On note  $t > 0$  l'épaisseur de la coque. Un point  $P$  de la coque est défini à l'aide d'un point  $M$  sur la surface moyenne  $\Omega$  et une composante suivant la normale à la surface moyenne.

On suppose que la surface moyenne  $\Omega$  est définie comme l'image d'un domaine bidimensionnel  $\omega \subset \mathbb{R}^2$  par une carte  $\Phi \in C^2(\bar{\omega}, \mathbb{R}^3)$ . On note  $\boldsymbol{\xi} = (\xi^1, \xi^2)$  les coordonnées curvilignes dans  $\omega$  et  $\xi^3$  la composante suivant la fibre normale à la surface moyenne de vecteur normal unitaire  $\mathbf{a}_3$ .

$$\Omega = \{m \in \mathcal{E}^3 \text{ tel que } \mathbf{m} = \Phi(\boldsymbol{\xi}), \boldsymbol{\xi} \in \bar{\omega}\}.$$

On définit la base covariante  $\mathbf{a}_\alpha = \Phi_{,\alpha}$ . La coque est supposée régulière, c'est à dire telle que  $\mathbf{a}_1$  et  $\mathbf{a}_2$  soient linéairement indépendants

$$\sqrt{a} := \|\mathbf{a}_1 \wedge \mathbf{a}_2\| \neq 0.$$

Le vecteur  $\mathbf{a}_3$  est donc naturellement défini comme

$$\mathbf{a}_\alpha \wedge \mathbf{a}_\beta = e_{\alpha\beta} \mathbf{a}_3, \quad e_{\alpha\alpha} = 0 \text{ et } e_{12} = -e_{21} = \sqrt{a}.$$

$e_{\alpha\beta}$  représente les composantes covariantes des symboles de Levi-Civita.

La base contravariante  $\mathbf{a}^\beta$ , duale de  $\mathbf{a}_\alpha$ , est définie par

$$\mathbf{a}_\alpha \cdot \mathbf{a}^\beta = \delta_\alpha^\beta, \quad \mathbf{a}_3 \wedge \mathbf{a}_\alpha = e^{\alpha\beta} \mathbf{a}^\beta \text{ avec } e^{\alpha\alpha} = 0, \text{ et } e^{12} = -e^{21} = a^{-\frac{1}{2}}.$$

On note  $(a_{\alpha\beta})$  le tenseur métrique de calcul de longueur, d'aire et de mesure d'angle

$$a_{\alpha\beta} = \mathbf{a}_\alpha \cdot \mathbf{a}_\beta.$$

Les composantes contravariantes du tenseur métrique sont définies par

$$a^{\alpha\beta} = \mathbf{a}^\alpha \cdot \mathbf{a}^\beta \text{ et } (a^{\alpha\beta}) = (a_{\alpha\beta})^{-1}.$$

Les composantes covariantes  $b_{\alpha\beta}$  du tenseur de courbure sont définies par

$$b_{\alpha\beta} = \mathbf{a}_{\alpha,\beta} \cdot \mathbf{a}_3.$$

Les composantes mixtes sont  $b_\alpha^\beta = a_{,\alpha}^\beta \cdot \mathbf{a}_3 = a^{\beta\lambda} b_{\lambda\alpha}$ .

On peut donc définir le vecteur  $\mathbf{a}_{\alpha,\beta}$  ( resp.  $\mathbf{a}_{,\beta}^\alpha$  ), dérivée de  $\mathbf{a}_\alpha$  ( resp.  $\mathbf{a}^\alpha$  ) par rapport à  $\xi^\beta$ , par

$$\mathbf{a}_{\alpha,\beta} = (\mathbf{a}_{\alpha,\beta} \cdot \mathbf{a}^i) \mathbf{a}_i = \Gamma_{\alpha\beta}^\sigma \mathbf{a}_\sigma + b_{\alpha\beta} \mathbf{a}_3$$

$$\mathbf{a}_{,\beta}^\alpha = (\mathbf{a}_{,\beta}^\alpha \cdot \mathbf{a}_i) \mathbf{a}^i = -\Gamma_{\beta\sigma}^\alpha \mathbf{a}^\sigma + b_{\beta\sigma}^\alpha \mathbf{a}_3.$$

On note  $\Omega_t$  la coque de surface moyenne  $\Omega$  et d'épaisseur  $t$

$$\Omega_t = \{p \in \mathcal{E}^3, \mathbf{p} = \Phi(\boldsymbol{\xi}) + \xi^3 \mathbf{a}_3, (\boldsymbol{\xi}, \xi^3) \in \bar{\omega} \times [-\frac{t}{2}, \frac{t}{2}]\}.$$

Les vecteurs de la base covariante sont définis comme

$$\mathbf{g}_\alpha = \mathbf{a}_\alpha + \xi^3 \mathbf{a}_{3,\alpha} = \mathbf{a}_\alpha - b_\beta^\lambda \mathbf{a}_\lambda = \mu_\alpha^\lambda \mathbf{a}_\lambda, \text{ et } \mathbf{g}_3 = \mathbf{a}_3$$

avec  $\mu_\alpha^\lambda = \delta_\alpha^\lambda - \xi^3 b_\alpha^\lambda$ .

### Hypothèse cinématique

Le modèle de coque de Naghdi se base sur les hypothèses suivantes

- La fibre normale est une ligne droite dans l'état initial et reste une ligne droite après déformation
- La fibre normale peut subir une rotation après déformation (contrairement au modèle de Koiter, avec l'hypothèse de Kirchoff-Love)
- La contrainte est supposée parallèle.

Le déplacement de la coque est donc décrit à l'aide de 5 degrés de liberté : un vecteur déplacement de la surface moyenne de composantes covariantes  $u_i$  et la rotation de la fibre normale de composantes covariantes  $s_\alpha$ . On note  $\mathbf{u} = (u_i)$ ,  $\mathbf{s} = (s_\alpha)$  les vecteurs de composantes covariantes de déplacement et rotation. Les vecteurs cartésiens de déplacement et de rotation sont :

$$\mathbf{u} = u_i \mathbf{a}^i \text{ et } \Psi(\mathbf{u}, \mathbf{s}) = e^{\alpha\beta} s_\alpha \mathbf{a}_\beta + \frac{1}{2} e^{\alpha\beta} u_{\beta|\alpha} \mathbf{a}_3.$$

Où  $u_{\alpha|\beta} = u_{\alpha,\beta} - \Gamma_{\alpha\beta}^\sigma u_\sigma$  désigne la dérivée covariante.

On note respectivement  $\boldsymbol{\epsilon} = \epsilon_{ij}(\mathbf{g}^i \otimes \mathbf{g}^j)$  et  $\boldsymbol{\sigma} = \sigma^{ij}(\mathbf{g}_i \otimes \mathbf{g}_j)$  les tenseurs de déformation et de contrainte associés à la coque. D'après la loi de Hooke, liant le tenseur de déformation au tenseur de contraintes, on a :

$$\boldsymbol{\sigma} = \mathbb{E} : \boldsymbol{\epsilon}, \sigma^{ij} = E^{ijkl} \epsilon_{kl}.$$

Le tenseur  $\mathbb{E}$  satisfait les relations de symmétries majeure et mineure respectivement

$$E^{ijkl} = E^{klij} \text{ et } E^{ijkl} = E^{ijlk}.$$

### Coefficients élastiques

Les coefficients élastiques sont généralement mesurés et définis dans le repère dit matériau, indépendant de la géométrie. On note  $\mathbf{m}_i$  les vecteurs du repère matériau, tels que  $\mathbf{m}_i \cdot \mathbf{m}_j = \delta_{ij}$ . Ainsi donc  $\mathbf{m}^i = \mathbf{m}_i$ . Soit  $A^{pqrs}$  les composantes du tenseur d'élasticité dans le repère matériau; on a  $A_{pqrs} = A^{pqrs}$ . On considère que le matériau est orthotrope. Ceci induit donc les relations suivantes :

$$A^{\alpha\beta 33} = \delta^{\alpha\beta} A^{\alpha\beta 33}, \quad A^{\alpha\beta\lambda 3} = 0, \quad A^{\alpha\beta 12} = (\delta^{\alpha 1} \delta^{\beta 2} + \delta^{\alpha 2} \delta^{\beta 1}) A^{1212}, \quad \text{et} \quad A^{\alpha 3\beta 3} = \delta^{\alpha\beta} A^{\alpha 3\beta 3}.$$

$\delta^{\alpha\beta}$  désigne le symbole de Kronecker  $\delta^{\alpha\beta} = 1$  si  $\alpha = \beta$ , et 0 sinon.

On observe que les composantes contravariantes  $E^{ijkl}$  du tenseur d'élasticité sont

$$E^{ijkl} = G_p^i G_q^j G_r^k G_s^l A^{pqrs}, \quad \text{avec} \quad \mathbf{m}_i = G_i^j \mathbf{a}_j \quad \text{et} \quad G_i^j = \mathbf{m}_i \cdot \mathbf{a}^j.$$

En prenant en compte l'hypothèse de contrainte parallèle  $\sigma^{33} = 0$ , pour un tenseur d'élasticité orthotrope, on a

$$\epsilon_{33} = -\frac{E^{33\lambda\mu}}{E^{3333}} \epsilon_{\lambda\mu}.$$

On observe donc que les contraintes tangentielles sont

$$\sigma^{\alpha\beta} = Q^{\alpha\beta\lambda\mu} \epsilon_{\lambda\mu}, \quad \text{avec} \quad Q^{\alpha\beta\lambda\mu} = E^{\alpha\beta\lambda\mu} - \frac{E^{\alpha\beta 33} E^{33\lambda\mu}}{E^{3333}}.$$

Les composantes covariantes du tenseur de déformation sont définies par

$$\epsilon_{ij} = \frac{1}{2} (\mathbf{U}_{,i} \cdot \mathbf{g}_j + \mathbf{U}_{,j} \cdot \mathbf{g}_i).$$

On peut montrer, après quelques calculs, que les composantes tangentielles et de cisaillement transverse du tenseur de déformation sont:

$$\begin{aligned} \epsilon_{\alpha\beta}(\mathbf{u}, \mathbf{s}) &= \gamma_{\alpha\beta}(\mathbf{u}) + \xi^3 \chi_{\alpha\beta}(\mathbf{u}, \mathbf{s}) \\ \epsilon_{\alpha 3}(\mathbf{u}, \mathbf{s}) &= \gamma_{\alpha 3}(\mathbf{u}, \mathbf{s}) \end{aligned}$$

$\gamma_{\alpha\beta}$  et  $\chi_{\alpha\beta}$  sont respectivement les tenseurs de déformation en membrane et en flexion;  $\gamma_{\alpha 3}$  les composantes de déformation en cisaillement.

L'énergie de déformation  $E_d$  est défini par

$$E_d(\mathbf{u}, \mathbf{s}) = \int_{\Omega_t} t \left\{ Q^{\alpha\beta\lambda\mu} \epsilon_{\lambda\mu}(\mathbf{u}, \mathbf{s}) \epsilon_{\alpha\beta}(\mathbf{u}, \mathbf{s}) + 4E^{\alpha 3\beta 3} \epsilon_{\alpha 3}(\mathbf{u}, \mathbf{s}) \epsilon_{\alpha 3}(\mathbf{u}, \mathbf{s}) \right\} \sqrt{a} dS \, d\xi^3,$$

avec  $dS$  l'élément d'aire dans  $\omega$ .

L'énergie de déformation dans le cas de coques s'obtient en intégrant suivant l'épaisseur. On définit après utilisation du principe des travaux virtuels les deux problèmes bidimensionnels : statique et dynamique (étude de fréquences de vibration).

Nous précisons de manière détaillée dans le chapitre 2 le problème mécanique dans le cas d'un chargement statique et dans le cas d'une étude de fréquences de vibration. Nous terminons en rappelant le résultat d'existence et d'unicité de solution.

## A.3 Jonction de coques de Naghdi et discrétisation non-conformes

Nous définissons dans ce chapitre le modèle mécanique pour les assemblages de coques et nous nous intéressons par la suite à sa discrétisation par la méthode des éléments finis.

Il existe deux principales approches pour la prise en compte des conditions de continuité : la méthode mixte et la méthode directe. Nous implémentons la méthode directe selon le principe de la méthode mortier (joint), qui permet d'intégrer les contraintes de continuité dans l'espace variationnel. Les contraintes de continuité sont définies de manière faible; elles sont satisfaites contre des fonctions test convenablement choisies. L'intérêt d'une telle approche est qu'elle permet de prendre en compte des maillages non-coincidents (non-conformes) et de discrétiser les problèmes associés à chaque coque de manière indépendante.

### A.3.1 Considérations géométriques

On considère une surface moyenne générale  $\Omega$  définie comme

$$\Omega = \bigcup_{k=1}^N \Omega_k.$$

Chaque surface  $\Omega_k$  est supposée régulière, définie comme l'image d'un domaine  $\omega_k \subset \mathbb{R}^2$  par une carte  $\Phi_k \in C^2(\omega_k, \mathbb{R}^3)$ .

Nous supposons que la décomposition géométrique correspondant à  $\Omega$  est conforme dans le sens où l'intersection entre deux surfaces moyennes distinctes est soit vide, un point ou une interface toute entière notée  $\Gamma^l$ .  $\Gamma^l$  représente l'interface physique (une courbe dans l'espace Euclidien), avec  $l \in \{1, \dots, L\}$  l'indice de l'interface

$$\forall l \in \{1, \dots, L\} \exists n(l) \neq m(l) \in \{1, \dots, N\} \text{ such that } \Gamma^l = \bar{\Omega}_{n(l)} \cap \bar{\Omega}_{m(l)}.$$

La notation  $k(l)$  dans l'expression ci-dessus, avec  $k \in \{n, m\}$ , fait référence au fait que la surface  $\Omega_k$  dispose de  $\Gamma^l$  comme interface commune avec une autre surface moyenne. De manière analogue, on pourra écrire  $\Gamma^{l(k)}$  pour désigner l'interface  $\Gamma^l$  vue de la coque  $\Omega_k$ . Soit  $\gamma^{l(k)} \in \partial\omega_k$  l'interface paramétrique associée à l'interface  $\Gamma^{l(k)} := \Phi(\bar{\gamma}^{l(k)})$ . On suppose que les interfaces  $\gamma^{l(k)}$  sont toutes deux définies comme images d'un intervalle  $\gamma^l$  par leurs cartes respectives  $\varphi_{l(k)} = \left( \varphi_{l(k)}^\alpha \right)$ . Ainsi donc les interfaces physiques sont définies comme

$$\gamma^l \xrightarrow{\varphi_{l(k)}} \gamma^{l(k)} \xrightarrow{\Phi_k} \Gamma^{l(k)}.$$

On associe naturellement à chaque coque  $\Omega_k$  sa base covariante (resp. contravariante) dont les vecteurs sont notés  $\mathbf{a}_{i(k)}$  (resp.  $\mathbf{a}^{j(k)}$ ). Une notation similaire est utilisée pour les composantes covariantes (resp. contravariantes) du tenseur métrique  $a_{\alpha\beta(k)}$  (resp.  $a^{\alpha\beta(k)}$ ). Ainsi le vecteur tangent  $\tilde{\mathbf{t}}_{l(k)}$  en un point  $\Phi_k(\varphi_{l(k)}(\eta))$ ,  $\eta \in \gamma^l$  de l'interface  $\Gamma^{l(k)}$ , est défini par

$$\tilde{\mathbf{t}}_{l(k)} = \tilde{t}_{l(k)}^\alpha \mathbf{a}_{\alpha(k)}, \text{ avec } \tilde{t}_{l(k)}^\alpha = \frac{\partial \varphi_{l(k)}^\alpha}{\partial \eta}.$$

Le tangente unitaire  $\mathbf{t}_{l(k)}$  est alors définie par

$$\mathbf{t}_{l(k)} = t_{l(k)}^\alpha \mathbf{a}_{\alpha(k)}, \text{ avec } t_{l(k)}^\alpha = \frac{\tilde{t}_{l(k)}^\alpha}{\sqrt{a_{\alpha\beta(k)} \tilde{t}_{l(k)}^\alpha \tilde{t}_{l(k)}^\beta}}.$$

### A.3.2 Raccordement entre coques

On désigne par  $u_{i(k)}$  et  $s_{\alpha(k)}$  respectivement les composantes covariantes du champ de déplacement de la surface moyenne  $\Omega_k$  et la rotation de la fibre normale de vecteur unitaire  $\mathbf{a}_{3(k)}$ . On introduit l'espace  $\mathbf{H}^1(\boldsymbol{\omega})$

$$\mathbf{H}^1(\boldsymbol{\omega}) = \prod_{i=1}^N H^1(\omega_k) = \left\{ \mathbf{w} = (w^{(k)})_{k=1:N} \text{ tel que } w_k \in H^1(\omega_k) \right\}.$$

Quand  $\mathbf{w}$  représente une composante covariante, on utilise la notation  $w_{(k)}$ . Ainsi on note  $\mathbf{u}_i = (u_{i(k)})$  et  $\mathbf{u} = (\mathbf{u}_1, \mathbf{u}_2, \mathbf{u}_3) \in [\mathbf{H}^1(\boldsymbol{\omega})]^3$ . De manière analogue  $\mathbf{s} = (\mathbf{s}_1, \mathbf{s}_2) \in [\mathbf{H}^1(\boldsymbol{\omega})]^2$ .

Les vecteurs Cartésien de déplacement  $\mathbf{u}^{(k)}$  et de rotation  $\Psi^{(k)}$  sont définis comme

$$\mathbf{u}^{(k)} = u_{i(k)} \mathbf{a}^{i(k)} \text{ et } \Psi^{(k)}(\mathbf{u}, \mathbf{s}) = e^{\alpha\beta(k)} s_{\alpha(k)} \mathbf{a}_{\beta(k)} + \frac{1}{2} e^{\alpha\beta(k)} u_{\beta(k)|\alpha} \mathbf{a}_{3(k)}$$

où  $e^{\alpha\beta(k)}$  sont les composantes contravariantes de symboles de Levi-Civita

$$e^{11(k)} = e^{22(k)} = 0, \quad e^{12(k)} = -e^{21(k)} = \frac{1}{\sqrt{a_k}}.$$

Soit une fonction scalaire  $\mathbf{w} = (w_{(k)})_{k=1:N}$  définie sur  $\boldsymbol{\omega}$ , on note  $w^{l(k)}$  la restriction de  $w_{(k)}$  à l'interface  $\gamma^{l(k)}$ :  $w^{l(k)} := w_{(k)|\gamma^{l(k)}}$ . Pour une fonction vectorielle  $\mathbf{w} = (\mathbf{w}^{(k)})_{k=1:N}$ , la notation  $\mathbf{w}^{l(k)}$  désigne le vecteur composé de restriction de chaque composante cartésienne de  $\mathbf{w}^{(k)} = w_i^{l(k)} \mathbf{a}^i$  à l'interface  $\gamma^{l(k)}$ .

### Conditions de jonctions

Les conditions de jonction de la coque sont

$$\mathbf{u}^{l(n)} = \mathbf{u}^{l(m)} \text{ et } \Psi^{l(n)}(\mathbf{u}, \mathbf{s}) \cdot \mathbf{t}_{l(n)} = \Psi^{l(m)}(\mathbf{u}, \mathbf{s}) \cdot \mathbf{t}_{l(n)}.$$

La première correspond à la continuité du déplacement de la surface moyenne et est une conséquence de la transmission des efforts aux interfaces, sachant que la deuxième correspond à la continuité des composantes tangentielles de rotations et est conséquence de la transmission des moments et de l'hypothèse de moment plan pour les modèles de coques.

Soient  $t_\alpha^{l(k)} = a_{\alpha\beta(k)} t_{l(k)}^\beta$  les composantes covariantes du vecteur tangent unitaire  $\mathbf{t}_{l(k)}$ . Ainsi on a

$$\Psi^{l(k)}(\mathbf{u}, \mathbf{s}) \cdot \mathbf{t}_{l(k)} := \Psi_t^{l(k)}(\mathbf{u}, \mathbf{s}) = \frac{1}{\sqrt{a_k}} (s_{1(k)} t_2^{l(k)} - s_{2(k)} t_1^{l(k)}).$$

En particulier, pour la rotation tangentielle, vue du coté  $\Omega_{m(l)}$ , on a

$$\Psi^{(m)}(\mathbf{u}, \mathbf{s}) \cdot \mathbf{t}_{l(k)} := \Psi_t^{(m)}(\mathbf{u}, \mathbf{s}) = \frac{1}{\sqrt{a_m}} (\mathbf{t}_{l(n)} \cdot \mathbf{t}_{l(m)}) (s_{1(m)} t_2^{l(m)} - s_{2(m)} t_1^{l(m)}).$$

La continuité du déplacement global de la surface  $\Omega$  implique

$$u_{i(n)} = a_{i(n)}^{j(m)} u_{j(m)} \text{ avec } a_{i(n)}^{j(m)} = \mathbf{a}^{j(m)} \cdot \mathbf{a}_{i(n)}.$$

### Problème général

Le problème générale pour l'assemblage de coques est

PROBLEM A.3.1 Trouver  $[\mathbf{u}, \mathbf{s}] \in \mathbf{V}(\omega)$  tel que

$$a([\mathbf{u}, \mathbf{s}], [\mathbf{v}, \mathbf{r}]) = l([\mathbf{v}, \mathbf{r}]) \quad \forall [\mathbf{v}, \mathbf{r}] \in \mathbf{V}(\omega).$$

o La forme bilinéaire  $a(\cdot, \cdot)$  est définie comme

$$a([\mathbf{u}, \mathbf{s}], [\mathbf{v}, \mathbf{r}]) = \sum_{k=1}^N a_{(k)}([\mathbf{u}_{(k)}, \mathbf{s}_{(k)}], [\mathbf{v}_{(k)}, \mathbf{r}_{(k)}])$$

avec  $a_{(k)}(\cdot, \cdot)$  la forme bilinéaire associée à la surface moyenne  $\Omega_k$

$$\begin{aligned} a_{(k)}([\mathbf{u}_{(k)}, \mathbf{s}_{(k)}], [\mathbf{v}_{(k)}, \mathbf{r}_{(k)}]) = & \int_{\omega_k} t \{ Q^{\alpha\beta\lambda\mu(k)} \gamma_{\alpha\beta}(\mathbf{u}_{(k)}) \gamma_{\lambda\mu}(\mathbf{v}_{(k)}) + \\ & \frac{t^2}{12} Q^{\alpha\beta\lambda\mu(k)} \chi_{\alpha\beta}(\mathbf{u}_{(k)}, \mathbf{s}_{(k)}) \chi_{\lambda\mu}(\mathbf{v}_{(k)}, \mathbf{r}_{(k)}) + \\ & E^{\alpha\beta\gamma\delta(k)} \gamma_{\alpha\beta}(\mathbf{u}_{(k)}, \mathbf{s}_{(k)}) \gamma_{\gamma\delta}(\mathbf{v}_{(k)}, \mathbf{r}_{(k)}) \} \sqrt{a_k} dS \end{aligned}$$

où  $dS$  désigne l'élément d'aire sur le domaine (paramétrique) de référence  $\omega$ .

o La forme linéaire  $l(\cdot)$  est définie

$$l([\mathbf{v}, \mathbf{r}]) = \sum_{k=1}^N l_{(k)}([\mathbf{v}, \mathbf{r}])$$

avec  $l_{(k)}(\cdot)$  la forme linéaire associée au travail virtuel des forces appliquées à la coque  $\Omega_k$ .

Nous nous intéressons pour la méthode mortier à ces conditions sous forme faible. La condition sur le déplacement est

$$\int_{\gamma^l} (u_i^{l(n)} s_{l(n)} - a_{i(n)}^{j(m)} u_j^{l(m)} s_{l(m)}) \phi d\eta, \quad \phi \in \mathcal{W}(\gamma^l) \subset \mathbf{L}^2(\gamma^l)$$

et  $\mathcal{W}(\gamma^l)$  étant un espace bien choisi.

On a une relation analogue pour la condition de continuité sur la rotation tangentielle.



### A.3.3 Méthode mortier

Le point essentiel de la méthode mortier réside dans le choix de l'espace  $\mathcal{W}(\gamma^l)$  au niveau de chaque interface. Nous décrivons brièvement le principe de la méthode mortier utilisée dans le chapitre 3.

On considère le problème : Trouver  $\mathbf{w} \in \mathbf{V}(\omega)$  tel que, pour tout  $\mathbf{v} \in \mathbf{V}(\omega)$

$$b(w^{(k)}, v^{(k)}) = l(v^{(k)}).$$

$\mathbf{V}(\omega) \subset \mathbf{H}^1(\omega)$  est le sous-espace dit contraint qui intègre la contrainte de continuité globale du champ  $\mathbf{w}$  d'un sous-domaine à l'autre

$$\mathbf{V}(\omega) = \left\{ \mathbf{w} \in \mathbf{H}^1(\omega) \text{ tel que } w^{l(n)} = w^{l(m)} \forall l \in \{1, \dots, L\} \right\}.$$

On considère  $\omega_{h(k)}$  la triangulation associée au domaine  $\omega_k$ , composée de  $n_k$  éléments

$$\omega_{h(k)} = \bigcup_{i=1}^{n_k} T_i.$$

On note  $X_{h(k)}$  l'espace discret de dimension finie associé au problème local sur le sous-domaine  $\omega_k$ . L'espace  $X_{h(k)}$  est, dans le cas standard, l'ensemble des fonctions continues, polynomiales par morceaux

$$X_{h(k)} = \{v \in C^0(\omega_k) \text{ tel que } v|_T \in P_{d_k}(T) \text{ pour tout } T \in \omega_{h(k)}\}.$$

Où  $d_k$  désigne le degré du polynôme d'interpolation de  $w^{(k)}$  sur  $\omega_{h(k)}$  et  $P_d$  l'ensemble des polynômes de degré  $d \in \mathbb{N}$ . On définit l'espace produit  $\mathbf{X}_h = \prod_{k=1}^N X_{h(k)}$  des fonctions polynomiales par sous-domaines tel que

$$\mathbf{X}_h = \{\mathbf{w} \text{ tel que } w^{(k)} \in X_{h(k)}\}.$$

#### Problème local discret

Soient  $N_k$  le nombre de noeuds du maillage  $\omega_{h(k)}$  et  $\boldsymbol{\xi}_i = (\xi_i^\alpha)$  les coordonnées du  $i$ ème noeud. On note  $p_i^{(k)}$  les fonctions de forme correspondantes. Elles sont indépendantes et vérifient les propriétés usuelles

$$p_i^{(k)}(\boldsymbol{\xi}_j) = \delta_{ij} \text{ et } \sum_{i=1}^{N_k} p_i^{(k)}(\boldsymbol{\xi}) = 1, \forall \boldsymbol{\xi} \in \omega_{h(k)}.$$

L'espace  $X_{h(k)}$  est alors défini comme

$$X_{h(k)} = \text{span} \left\{ (p_i^{(k)})_{i=1:N_k} \right\}.$$

Pour tout  $w^{(k)} \in X_{h(k)}$ , il existe  $w_i^{(k)}$  tel que

$$w^{(k)}(\boldsymbol{\xi}) = \sum_{i=1}^{N_k} w_i^{(k)} p_i^{(k)}(\boldsymbol{\xi}) \text{ avec } w_i^{(k)} = w^{(k)}(\boldsymbol{\xi}_i).$$

Les coefficients  $(w_i^{(k)})$  sont les degrés de liberté. On introduit les notations suivantes relatives aux degrés de liberté et à leurs partitionnements :

### A.3. Jonction de coques de Naghdi et discrétisation non-conformes

- le vecteur de degrés de liberté restreint au sous-domaine  $\omega_k$  est noté  $\underline{w}^{(k)} = (w_i^{(k)})$
- le vecteur de degrés de liberté sur l'ensemble des sous-domaines est noté  $\underline{w} = (\underline{w}^{(1)}, \dots, \underline{w}^{(N)})$
- $S_{l(k)}$  l'ensemble des indices de degrés de liberté sur l'interface paramétrique  $\gamma^{l(k)}$

$$S_{l(k)} = \{i \in \{1, \dots, N_k\} \text{ tel que } \boldsymbol{\xi} \in \gamma^{l(k)}\}$$

- $S_{0(k)}$  le complémentaire de  $(S_{l(k)})_{l=1:L}$ , l'ensemble des indices de degrés de liberté considérés comme intérieur dans le sens où ils ne correspondent pas à des noeuds qui sont sur une interface

$$S_{0(k)} = \{1, \dots, N_k\} \setminus \bigcup_{l=1}^L S_{l(k)}$$

- $\underline{w}^{l(k)} = (w_i^{(k)})_{i \in S_{l(k)}}$  les degrés de liberté restreints à l'interface  $\gamma^{l(k)}$  et  $d_{l(k)} = \text{card}(S_{l(k)})$
- $\underline{w}^{0(k)} = (w_i^{(k)})_{i \in S_{0(k)}}$  l'ensemble des degrés de liberté "intérieurs".

La forme matricielle du problème discret, local au sous-domaine  $\omega_k$ , est: Trouver  $\underline{w}^{(k)} \in \mathbb{R}^{N_k}$  tel que

$$\underline{v}^{(k)\top} \mathbf{B}^{(k)} \underline{w}^{(k)} = \underline{v}^{(k)\top} \mathbf{f}^{(k)}.$$

La matrice  $\mathbf{B}^{(k)}$  et le vecteur  $\mathbf{f}^{(k)}$  de dimensions respectives  $N_k \times N_k$  et  $N_k$ , sont définis par

$$\begin{aligned} \mathbf{B}^{(k)} &= (b_{ij}) \quad \text{avec } b_{ij} = b(p_i^{(k)}, p_j^{(k)}), \quad (i, j) \in \{1, \dots, N_k\}^2 \\ \mathbf{f}^{(k)} &= (f_j^{(k)})_{j=1:N_k} \quad \text{avec } f_j^{(k)} = l(p_j^{(k)}) \end{aligned}$$

Afin de procéder à la discrétisation du problème avec décomposition de domaine, on définit l'espace  $\mathcal{W}(\gamma^l)$  comme l'ensemble des fonctions trace des fonctions test du coté non-mortier, c-à-d du sous-domaine  $\omega_{n(l)}$

$$\mathcal{W}(\gamma^l) = \{f \in C^0(\gamma^l) \text{ tel que } f(\eta) = \sum_{i \in S_{l(n)}} f_j p_j^{(n)}(\boldsymbol{\xi}) \text{ avec } \boldsymbol{\xi} = \varphi_{l(n)}(\eta)\}$$

PROBLEME A.3.2 (Problème global) Trouver  $\mathbf{w} \in \mathbf{H}^1(\boldsymbol{\omega})$  tel que :  $\forall k = 1 : N$  et  $l = 1 : L$

$$\left| \begin{aligned} b(w^{(k)}, v^{(k)}) &= l(v^{(k)}) \\ w^{l(n)} &= w^{l(m)} \end{aligned} \right., \quad \forall \mathbf{v} \in \mathbf{H}^1(\boldsymbol{\omega}) \text{ tel que } v^{l(n)} = v^{l(m)}, \quad (\text{A.1})$$

C'est à dire trouver  $\mathbf{w} \in \mathbf{V}(\boldsymbol{\omega})$  tel que

$$b(w^{(k)}, v^{(k)}) = l(v^{(k)}), \quad \forall \mathbf{v} \in \mathbf{V}(\boldsymbol{\omega}).$$

Notons  $N_d$  le nombre de degrés de liberté sur l'ensemble des sous-domaines  $N_d = \sum_{k=1}^N N_k$ . Le problème discret correspondant dans une formulation standard est alors

PROBLEM A.3.3 (Problème global “discret”) Trouver  $\mathbf{w} \in \mathbf{X}_h$  de vecteur de degrés de liberté associé  $\underline{w} \in \mathbb{R}^{N_d}$  tel que

$$\left| \begin{array}{l} \underline{v}^{(k)} \mathbf{B}^{(k)} \underline{w}^{(k)} = \underline{v}^{(k)\top} \mathbf{f}^{(k)} \\ w^{l(n)} = w^{l(m)} \end{array} \right., \quad \forall \mathbf{v} \in \mathbf{X}_h \text{ tel que } v^{l(n)} = v^{l(m)}, \quad (\text{A.2})$$

avec  $v^{l(k)} : \eta \in \gamma^l \mapsto v^{l(k)}(\eta) = \sum_{i \in S_{l(k)}} v_i^{(k)} p_i^{(k)}(\varphi_{l(k)}(\eta))$ .

Le problème discret avec une formulation de type mortar est:

PROBLEM A.3.4 (Problème global discret avec mortar) Trouver  $\underline{w} \in \mathbb{R}^{N_d}$ , vecteur de degrés de liberté de  $\mathbf{w} \in \mathbf{X}_h$ , tel que

$$\underline{v}^{(k)} \mathbf{B}^{(k)} \underline{w}^{(k)} = \underline{v}^{(k)\top} \mathbf{f}^{(k)}, \quad \forall \mathbf{v} \in \mathbf{V}_h, \quad (\text{A.3})$$

avec

$$\mathbf{V}_h = \left\{ \mathbf{w} \in \mathbf{X}_h \text{ tel que } \int_{\gamma^l} (w^{l(n)} s_{l(n)} - w^{l(m)} s_{l(m)}) p_i^{(n)} d\eta = 0, \text{ pour tout } i \in S_{l(n)} \right\}. \quad (\text{A.4})$$

En définissant la matrice  $\mathbf{M}^{l(k)}$ , de dimension  $d_{l(n)} \times d_{l(k)}$ :

$$M_{\hat{i}\hat{j}}^{l(k)} = \int_{\gamma^l} p_{\hat{i}}^{(n)}(\boldsymbol{\xi}_{(n)}) p_{\hat{j}}^{(k)}(\boldsymbol{\xi}_{(k)}) s_{l(k)}(\eta) d\eta, \quad \hat{i} \in \{1, \dots, d_{l(n)}\}, \hat{j} \in \{1, \dots, d_{l(k)}\}, \quad (\text{A.5})$$

l'intégrale dans l'espace  $\mathbf{V}_h$ , Eq. (A.4), peut s'écrire sous la forme matricielle

$$\mathbf{M}^{l(n)} \underline{w}^{l(n)} = \mathbf{M}^{l(m)} \underline{w}^{l(m)}.$$

Dans l'expression (A.5),  $i$  (resp  $j$ ) sont les indices correspondant à  $\hat{i}$  (resp  $\hat{j}$ ) dans la numérotation globale,  $i \in S_{l(n)}$  (resp.  $j \in S_{l(k)}$ ).

Ainsi, les degrés de liberté  $\underline{w}^{l(n)}$  peuvent alors être définis en fonction des degrés de liberté du coté mortier

$$\underline{w}^{l(n)} = \mathbf{R}^{(l)} \underline{w}^{l(m)} \text{ avec } \mathbf{R}^{(l)} = [\mathbf{M}^{l(n)}]^{-1} \mathbf{M}^{l(m)}. \quad (\text{A.6})$$

Pour la suite,

- on réarrange le vecteur de degrés de liberté  $\underline{w}$  comme suit

$$\underline{w}^\top = (\underline{w}^{0(n)} \quad \underline{w}^{l(n)} \quad \underline{w}^{l(m)} \quad \underline{w}^{0(m)}).$$

- on introduit le vecteur de degrés de liberté indépendants  $\overline{w}$

$$\overline{w} = (\underline{w}^{0(n)} \quad \underline{w}^{l(m)} \quad \underline{w}^{0(m)}).$$

L'ensemble des degrés de liberté sur le domaine  $\omega$  est défini, en fonction des degrés de liberté libres ou indépendants, par la matrice  $\mathbf{M}$ , appelée matrice de raccord

$$\mathbf{M} = \begin{bmatrix} \mathbf{I}_{0(n)} & & & \\ & \mathbf{R}^{(l)} & & \\ & \mathbf{I}_{0(m)}^l & & \\ & & & \mathbf{I}_{0(m)}^0 \end{bmatrix}, \quad (\text{A.7})$$

$\mathbf{I}_{0(k)}$  est la matrice identité associée au degrés de liberté intérieurs d'indices  $S_{0(k)}$ . En particulier pour  $k = m$ , on a  $\mathbf{I}_{0(m)} = \text{diag}(\mathbf{I}_{0(m)}^l, \mathbf{I}_{0(m)}^0)$ ; où  $\mathbf{I}_{0(m)}^l$  (resp.  $\mathbf{I}_{0(m)}^0$ ) est la matrice identité associée aux degrés de liberté d'indice  $S_{l(m)}$  (resp.  $S_{0(m)}$ ).

Le problème discret avec mortier est alors :

PROBLEME A.3.5 (Problème global mortar sous forme matricielle) Trouver  $\bar{\mathbf{w}} \in \mathbb{R}^{N_d - d_{l(n)}}$  tel que

$$\bar{\mathbf{v}}^\top \mathbf{B}_m \bar{\mathbf{w}} = \bar{\mathbf{v}}^\top \mathbf{f}_m.$$

où  $\mathbf{B}_m$  et  $\mathbf{f}_m$  sont respectivement la matrice et le vecteur associés au problème global avec intégration des contraintes de raccord par la méthode de type mortier

$$\mathbf{B}_m = \mathbf{M}^\top \mathbf{B} \mathbf{M}, \quad \mathbf{B} = \text{diag}(B^{(n)}, B^{(m)}); \quad \mathbf{f}_m = \mathbf{M}^\top \mathbf{f}, \quad \mathbf{f}^\top = (\mathbf{f}^{(n)} \quad \mathbf{f}^{(m)}). \quad (\text{A.8})$$

Nous décrivons la méthode dans le chapitre 3 spécifiquement pour les assemblages de coques.

## A.4 Optimisation d'anisotropie et propriétés matériaux

Dans ce chapitre nous nous focalisons sur la définition d'une discrétisation adaptée pour l'optimisation des propriétés matériaux. La motivation pour l'approche que nous proposons provient du fait que la discrétisation des variables dans le processus standard d'optimisation structurale se base sur la résolution par la méthode éléments finis et conduit à un nombre de variables et contraintes d'optimisation (la complexité) qui dépend du nombre des éléments finis.

L'approche que nous proposons repose d'une part sur la représentation du tenseur d'élasticité à l'aide de paramètres polaires et d'autre part à sur la discrétisation de ces paramètres par des fonctions B-splines. Le formalisme polaire permet de définir le tenseur d'élasticité à l'aide d'invariants et d'angles. Il repose sur un changement de variables complexes et présente plusieurs avantages dont notamment le fait que le tenseur d'élasticité dans un repère obtenu par rotation s'obtient simplement par soustraction d'angles. La discrétisation avec des fonctions B-splines permet d'avoir un nombre de variables réduit, des propriétés matériaux régulières et de pouvoir définir un nombre limité de contraintes assurant le respect de contraintes qui doivent être strictement vérifiées en tout point de la structure.

### A.4.1 Formalisme polaire

Les parties plane et hors-plan du tenseur d'élasticité, apparaissant dans la forme bilinéaire associée à l'énergie de déformation, après prise en compte de l'hypothèse de contraintes parallèles, sont respectivement  $Q^{\alpha\beta\lambda\mu}$  et  $E^{\alpha 3\beta 3}$ . Nous les représentons à l'aide du formalisme polaire que nous rappelons ci-dessous.

### Paramètres polaires tenseur plan d'ordre 2

On considère un tenseur symétrique du second ordre  $\mathbf{L} = (L^{\alpha\beta})$ . La représentation correspondante en formalisme polaire est:

$$\begin{aligned} L^{11} &= T + R \cos 2\Phi \\ L^{12} &= R \sin 2\Phi \\ L^{22} &= T - R \cos 2\Phi \end{aligned} .$$

Les paramètres polaires  $T$ ,  $R$  et  $\Phi$  sont définis en fonction des composantes  $L^{\alpha\beta}$  par

$$\begin{aligned} T &= \frac{1}{2} \text{tr}(\mathbf{L}) = \frac{1}{2}(L^{11} + L^{22}) \\ R &= \sqrt{\left(\frac{L^{11} - L^{22}}{2}\right)^2 + (L^{12})^2} \\ \tan 2\Phi &= \frac{2L^{12}}{L^{11} - L^{22}} \end{aligned}$$

### Paramètres polaires tenseur plan d'ordre 4

On considère un tenseur plan d'ordre 4  $\mathbb{E}$ , de matrice représentative

$$\mathbb{E}^p = \begin{pmatrix} E^{1111} & E^{1122} & E^{1112} \\ E^{1122} & E^{2222} & E^{2212} \\ E^{1112} & E^{2212} & E^{1212} \end{pmatrix} .$$

Les coefficients  $E^{\alpha\beta\lambda\mu}$  sont définis en formalisme polaire par

$$\begin{cases} E^{1111} &= T_0 + 2T_1 + R_0 \cos 4\Phi_0 + 4R_1 \cos 2\Phi_1 \\ E^{1112} &= R_0 \sin 4\Phi_0 + 2R_1 \sin 2\Phi_1 \\ E^{1122} &= -T_0 + 2T_1 - R_0 \cos 4\Phi_0 \\ E^{1212} &= T_0 - R_0 \cos 4\Phi_0 \\ E^{1222} &= -R_0 \sin 4\Phi_0 + 2R_1 \sin 2\Phi_1 \\ E^{2222} &= T_0 + 2T_1 + R_0 \cos 4\Phi_0 - 4R_1 \cos 2\Phi_1 \end{cases} . \quad (\text{A.9})$$

En supposant que les coefficients  $E^{\alpha\beta\lambda\mu}$  sont les coefficients dans le repère orthonormé  $(\mathbf{m}_1, \mathbf{m}_2)$ . On note  $(\mathbf{d}_1, \mathbf{d}_2)$  le repère obtenu par rotation d'un angle  $\theta$

$$\begin{aligned} \mathbf{d}_1 &= \cos \theta \mathbf{m}_1 + \sin \theta \mathbf{m}_2 \\ \mathbf{d}_2 &= -\sin \theta \mathbf{m}_1 + \cos \theta \mathbf{m}_2 \end{aligned}$$

Notons  $E^{\alpha\beta\lambda\mu}(\theta)$  les composantes du tenseur d'élasticité dans le repère  $(\mathbf{d}_1, \mathbf{d}_2)$ . Les coefficients  $E^{\alpha\beta\lambda\mu}(\theta)$  sont obtenus en substituant  $\Phi_\sigma \leftarrow \Phi_\sigma - \theta$ , avec  $\sigma \in \{0, 1\}$ .

$T_0$ ,  $T_1$ ,  $R_0$  et  $R_1$  sont des modules et  $\Phi_0$  et  $\Phi_1$  des angles.  $T_0$ ,  $T_1$ ,  $R_0$ ,  $R_1$  et  $\Phi_0 - \Phi_1$  sont des invariants du tenseur  $\mathbb{E}$  :

- $T_0$  et  $T_1$  sont les invariants de la partie sphérique

- $R_0$  et  $R_1$  sont liés à la partie déviatorique (anisotrope).

La différence d'angles est invariante, ainsi seul l'un deux est libre. L'angle  $\Phi_1$  fixe le repère. Un choix usuel consiste à poser  $\Phi_1 = 0$  et correspond à définir la plus forte rigidité suivant le premier axe.

Les symétries élastiques peuvent être définies en fonction des paramètres polaires. On a par exemple :

- pour une symétrie isotrope

$$R_0 = R_1 = 0.$$

- pour une orthotropie ordinaire on a la relation

$$\Phi_0 - \Phi_1 = K \frac{\pi}{4}, \text{ avec } K \in \{0, 1\}.$$

On s'intéresse à des matériaux orthotropes ordinaires. Le coefficient  $K$  définit le type d'orthotropie et joue un rôle important en optimisation. Typiquement, le changement d'une valeur à l'autre change une solution optimale en anti-optimale (vice-versa).

En posant  $\Phi_1 = 0$ ,  $\Phi_0 = K \frac{\pi}{4}$ , on a pour une élasticité ordinaire orthotrope:

$$\begin{cases} E^{1111}(\theta) &= T_0 + 2T_1 + R_0^K \cos 4\theta + 4R_1 \cos 2\theta \\ E^{1112}(\theta) &= -R_0^K \sin 4\theta - 2R_1 \sin 2\theta \\ E^{1122}(\theta) &= -T_0 + 2T_1 - R_0^K \cos 4\theta \\ E^{1212}(\theta) &= T_0 - R_0^K \cos 4\theta \\ E^{1222}(\theta) &= R_0^K \sin 4\theta - 2R_1 \sin 2\theta \\ E^{2222}(\theta) &= T_0 + 2T_1 + R_0^K \cos 4\theta - 4R_1 \cos 2\theta \end{cases} \quad (\text{A.10})$$

avec  $R_0^K = (-1)^K R_0$ .

### Contraintes sur les paramètres polaires

Les contraintes élastiques de définie-positivité de  $\mathbb{E}$  sont :

$$\begin{aligned} T_1[T_0 + R_0^K] &> 2R_1^2 \\ T_0 &> |R_0^K| \\ R_1 &\geq 0 \end{aligned} \quad (\text{A.11})$$

Dans le cas de matériau composite constitué de couches avec des matériaux identiques dont les paramètres polaires sont notés avec un exposant "L", on a

$$\begin{aligned} T_0 &= T_0^L \\ T_1 &= T_1^L \end{aligned} \quad (\text{A.12})$$

Les contraintes de bornes géométriques sont

$$\begin{aligned} 2 \left( \frac{R_1}{R_1^L} \right)^2 - 1 &\leq \frac{R_0^K}{R_0^{KL}} \\ R_0^K &\leq R_0^L \\ R_1 &\leq R_1^L \end{aligned} \quad (\text{A.13})$$

Elles sont plus restrictives que les contraintes élastiques. En effet les composites constituent une classe restreinte de matériaux. Ainsi lors de l'optimisation des composites les contraintes élastiques (A.11) sont remplacées par les contraintes géométriques (A.13). D'autre part, pour les composites dont les couches sont faites d'un même matériau de base, avec les conditions (A.12), le nombre de paramètres polaires à optimiser se réduit à trois :  $R_0^K$ ,  $R_1$  et  $\theta$ .

#### A.4.2 Discrétisation des paramètres polaires

On propose deux types de paramétrage, principalement guidés par la contrainte quadratique figurant parmi les contraintes élastiques ou géométriques :

- le premier, dit conforme, consiste à paramétrer  $R_0^K$  et  $R_1^2$  par des B-splines de mêmes vecteurs de knots et mêmes ordres
- le second, dit direct, revient à paramétrer  $R_1$  et  $R_0^K$  par des B-splines de mêmes vecteurs de knots et mêmes ordres.

Les fonctions B-splines sont définies à l'aide de polynômes B-splines avec des coefficients appelés points de contrôle. On note  $B_d^{ij}$  les polynômes B-splines définis à l'aide de vecteurs de knots  $\Sigma = (\Sigma^\alpha)_{\alpha=1:2}$ .  $\Sigma^\alpha$  représente le vecteur de knots dans la direction paramétrique associée à la coordonnée  $\xi^\alpha$  et est constitué d'une séquence croissante de  $n_\alpha + d_\alpha + 1$  réels appelés knots, avec  $\mathbf{d} = (d_\alpha)$ . Les fonctions  $B_d^{ij}$  sont définies par produit tensoriel de polynômes de base B-splines d'une variable, qui eux mêmes sont définis de manière récursive grâce à la formule de Cox-de-Boor (voir (4.3.1) page 75). Les polynômes de B-splines ainsi définis sont de degrés  $d_\alpha$  suivant la coordonnée  $\xi^\alpha$ .

Les fonctions de B-splines vérifient entre autres les propriétés de positivité

$$0 \leq B_d^{ij}(\boldsymbol{\xi}) \leq 1, \forall \boldsymbol{\xi} \in \omega.$$

En choisissant les vecteurs de knots  $\Sigma^\alpha = (\xi_i^\alpha)_{i=0:n_\alpha+d_\alpha}$  tels que

$$\xi_0^\alpha = \xi_2^\alpha = \dots = \xi_{d_\alpha}^\alpha, \quad \xi_{n_\alpha}^\alpha = \xi_{n_\alpha+2}^\alpha = \dots = \xi_{n_\alpha+d_\alpha}^\alpha,$$

les polynômes de base vérifient la propriété de partition de l'unité

$$\sum_{i,j=0}^{n_1-1, n_2-1} B_d^{ij}(\boldsymbol{\xi}) = 1, \forall \boldsymbol{\xi} \in \omega.$$

Soit  $Sp(\Sigma, \mathbf{d}) \subset C^0(\omega)$  l'espace des fonctions B-splines de degrés  $\mathbf{d}$  définies par  $n_\alpha$  points de contrôle dans la direction paramétrique  $\xi^\alpha$

$$Sp(\Sigma, \mathbf{d}) := \left\{ P : \omega \rightarrow \mathbb{R} \text{ tel que } P(\boldsymbol{\xi}) = \sum_{i,j=1}^{n_1, n_2} p^{ij} B_d^{ij}(\boldsymbol{\xi}) \right\}$$

Dans la définition précédente, les  $p^{ij}$  sont les points de contrôle associés aux polynômes de base  $B_d^{ij}$ .

### A.4.3 Prise en compte de contraintes

On s'intéresse à des contraintes de la forme :

$$C(\boldsymbol{\xi}) := a P(\boldsymbol{\xi}) + b Q(\boldsymbol{\xi}) + c \leq 0.$$

En supposant que  $P, Q \in Sp(\boldsymbol{\Sigma}, \mathbf{d})$  sont tels que les points de début et de fin des vecteurs de knots  $\Sigma^\alpha$  sont de multiplicité complète, c'est-à-dire égale à  $d_\alpha + 1$ . En notant  $p^{ij}$  et  $q^{ij}$  les points de contrôle de  $P$  et  $Q$ , on a

$$\forall (i, j) \in \{0, \dots, n_1 - 1\} \times \{0, \dots, n_2 - 1\} \quad a p^{ij} + b q^{ij} + c \leq 0 \implies C(\boldsymbol{\xi}) \leq 0, \quad \forall \boldsymbol{\xi} \in \omega.$$

Il s'agit de conditions suffisantes mais non nécessaires. Nous discutons plus en détail, au chapitre 4 page 69, les deux paramétrages proposés, leurs avantages et leurs limites propres. La principale limite provient du fait que les contraintes sur les points de contrôle sont fortes, elles peuvent donc restreindre la capacité d'exploration de l'espace de conception. Des résultats numériques sont finalement présentés.

## A.5 Optimisation conjointe de formes et propriétés matériaux

Le modèle mécanique de coque permet de paramétrer le problème mécanique par la forme, ce qui rend possible l'étude de sensibilité de la mécanique par rapport à la forme. On s'intéresse dans un cadre isogéométrique à des fonctions définies par des cartes B-splines. Les variables de conception des propriétés matériaux et de forme sont donc les coordonnées des points de contrôle.

### A.5.1 Géométrie et paramétrage de la forme

On considère que la coque  $\Omega$  est définie à l'aide de cartes B-splines  $\Phi \in C^2(\omega, \mathbb{R}^3) \cap \mathcal{B}_2(\boldsymbol{\Sigma}, \mathbf{d})$ . Dans le cas général d'assemblage de coques, on pose

$$\Omega = \bigcup_{k=1}^N \Omega_k;$$

chaque surface moyenne  $\Omega_k$  étant l'image du domaine paramétrique  $\omega_k = [0, 1]^2$  par sa carte  $\Phi_k = \Phi_{i(k)} \mathbf{e}^i$ . On note  $\mathbf{p}_{i,j(k)}$  les coordonnées des points de contrôle, d'indices  $(i, j)$ , associés à  $\Phi_k \in C^2(\omega_k, \mathbb{R}^3) \cap \mathcal{B}_2(\boldsymbol{\Sigma}^{(k)}, \mathbf{d}_k = (d_{\alpha(k)}))$ , tels que

$$\Phi_k(\boldsymbol{\xi}) = \sum_{i,j=1}^{n_1, n_2} p_{i,j(k)} B_{\mathbf{d}_k}^{i,j(k)}(\boldsymbol{\xi}).$$

$\boldsymbol{\Sigma}^{(k)}$  et  $\mathbf{d}_k$  sont les vecteurs de knots et les ordres des fonctions B-splines associées à  $\Phi_k$ . Pour des raisons de simplicité, et sans perte de généralité, on suppose que

$$\boldsymbol{\Sigma}^{(k)} = \boldsymbol{\Sigma}, \quad d_{\alpha(k)} = d_\alpha \quad \text{et} \quad n_{\alpha(k)} = n_\alpha \quad \text{pour tout } k \in \{1, \dots, N\}.$$

Ainsi on a

$$b_{\mathbf{d}_k}^{ij(k)} = b_{\mathbf{d}}^{ij}, \quad \text{pour tout } (i, j) \in \{1, \dots, n_1\} \times \{1, \dots, n_2\}.$$



### Conditions de continuités (géométrique)

Supposons que l'interface  $\Gamma^l$  entre les deux sous-domaines  $\Omega_{n(l)}$  et  $\Omega_{m(l)}$  correspond respectivement aux coordonnées paramétriques  $\xi_{(n)}^1 = 1$  et  $\xi_{(m)}^1 = 0$ . On suppose d'une part que la décomposition est conforme, c'est-à-dire que l'interface entre deux sous-domaines est soit vide, soit un point, soit une courbe entière; et d'autre part que la paramétrisation est conforme et que les vecteurs de knots associés à  $\Gamma^{l(k)}$  sont identiques et définissent des B-splines de mêmes ordres. Les points de contrôle correspondant à l'interface sont alors :

- du côté "mortier"  $\Gamma^{l(m)}$   $(p_{n,j(m)})_{j=1:n_2}$ .
- du côté "non-mortier"  $\Gamma^{l(n)}$   $(p_{1,j(n)})_{j=1:n_2}$ .

La contrainte de continuité  $C^0$

$$\Phi_m(1, \varphi_{l(m)}^2(\eta)) = \Phi_n(0, \varphi_{l(n)}^2(\eta))$$

se traduit par simple coïncidence ou égalité des points de contrôle:

$$p_{n_1,j(m)} = p_{1,j(n)} := p_j, \quad \forall j \in \{1, \dots, n_2\}. \quad (\text{A.14})$$

D'autre part, la contrainte de continuité  $C^1$  se traduit, en plus des égalités de continuité  $C^0$ , par :

$$\Phi'_m(1, \varphi_{l(m)}^2(\eta)) = \Phi'_n(0, \varphi_{l(n)}^2(\eta)), \quad \text{pour tout } \eta \in \gamma^l.$$

Cette condition implique les relations suivantes sur les points de contrôle:

$$\frac{d_1}{\xi_{n_1+d_1}^1 - \xi_{n_1}^1} (p_{n_1,j(m)} - p_{n_1-1,j(m)}) = \frac{d_1}{\xi_{d_1+2}^1 - \xi_2^1} (p_{2,j(n)} - p_{1,j(n)}).$$

En tenant compte du fait que les vecteurs knots sont encastrés, c-à-d,  $\xi_i^\alpha = 0$ ,  $i \in \{1, \dots, d_1 + 1\}$  et  $\xi_i^\alpha = 1$ ,  $i \in \{n_1 + 1, \dots, n_1 + d_1 + 1\}$ , on a

$$\frac{1}{1 - \xi_{n_1}^1} (p_{n_1,j(m)} - p_{n_1-1,j(m)}) = \frac{1}{\xi_{d_1+2}^1} (p_{2,j(n)} - p_{1,j(n)}).$$

En prenant en compte les relations de continuité, on a

$$\begin{aligned} \frac{1}{1 - \xi_{n_1}^1} (q_{j(l)} - p_{n_1-1,j(m)}) &= \frac{1}{\xi_{d_1+2}^1} (p_{2,j(n)} - q_{j(l)}) \\ \implies p_{2,j(n)} &= q_{j(l)} \left(1 + \frac{\xi_{d_1+2}^1}{1 - \xi_{n_1}^1}\right) - p_{n_1-1,j(m)} \frac{\xi_{d_1+2}^1}{1 - \xi_{n_1}^1}. \end{aligned} \quad (\text{A.15})$$

### Matrice de raccord géométrique

On note que dans le cas d'une continuité  $C^\alpha$ ,  $\alpha \in \{0, 1\}$ , on a  $n_1 \times n_2 + (n_1 - (\alpha + 1)) \times n_2$  points de contrôle indépendants :  $(p_{i,j(m)})_{i=1:n_1}^{j=1:n_2}$ ,  $(p_{i,j(n)})_{i=\alpha+2:n_1}^{j=1:n_2}$ . Plus précisément

## A.5. Optimisation conjointe de formes et propriétés matériaux

- pour une simple continuité  $C^0$  le nombre de points de contrôle indépendants est  $n_1 \times n_2 - n_2$ ,  
 $(p_{i,j(m)})_{i=1:n_1}^{j=1:n_2}, (p_{i,j(n)})_{i=2:n_1}^{j=1:n_2}$
- concernant une continuité  $C^1$ , on  $n_1 \times n_2 - 2 \times n_2$  points de contrôle indépendants,  
 $(p_{i,j(m)})_{i=1:n_1}^{j=1:n_2}, (p_{i,j(n)})_{i=3:n_1}^{j=1:n_2}$ .

On pose  $\mathbf{p} = \left[ (p_{ij(m)})_{i=1:n_1}^{j=1:n_2} \quad (p_{i,j(n)})_{i=1:n_1}^{j=1:n_2} \right]$  et on introduit  $\hat{\mathbf{p}}$  le vecteur de points de contrôle indépendants. Pour des raisons de simplicité, on utilise un mono-indice avec  $\hat{\mathbf{p}} = (\hat{p}_i)_{i=1:n_{12}^\alpha}$

$$\begin{aligned} \hat{p}_{i=1:n_{12}} &= (p_{ij(m)})_{i=1:n_1, j=1:n_2} \\ \hat{p}_{i=n_{12}+1:n_{12}^\alpha} &= (p_{ij(n)})_{i=\alpha+2:n_1}^{j=1:n_2}, \text{ avec } n_{12} = n_1 \times n_2 \text{ et } n_{12}^\alpha = 2 \times n_{12} - (\alpha + 1) \times n_2. \end{aligned}$$

$n_{12}^\alpha$  est le nombre de points de contrôle indépendants pour une régularité  $C^\alpha$ . Au vue de l'équation (A.15), on introduit le coefficient  $c_\beta$

$$c_\beta = \begin{cases} 1 & \text{si } \beta = 0 \\ \left(1 + \frac{\xi_{d_1+2}^1}{1-\xi_{n_1}^1}\right) & \text{si } \beta = 1 \end{cases}.$$

On note  $\mathcal{G}^\alpha$  la matrice de raccord géométrique pour une continuité  $C^\alpha$  exprimant les points de contrôle  $\mathbf{p}$  en fonction des points de contrôle indépendants  $\hat{\mathbf{p}}$

$$\mathbf{p} = \mathcal{G}^\alpha \hat{\mathbf{p}}.$$

Dans le cas d'une continuité  $C^\alpha$ , avec  $\alpha \in \{0, 1\}$ , il s'agit d'une matrice de dimensions  $(2 \times n_{12}, n_{12}^\alpha)$ .

### Coefficients de la matrice $\mathcal{G}^\alpha$

La matrice  $\mathcal{G}^\alpha$  de raccord géométrique pour une régularité  $C^\alpha$ ,

1. Pour les points de contrôle indépendants du côté mortier

$$g_{i,i}^\alpha = 1, \quad i \in \{1, \dots, n_{12}\}.$$

2. Pour les points de contrôle sur l'interface côté non-mortier

$$g_{n(j),c(j)}^\alpha = 1, \quad n(j) = n_{12} + (j-1) \times n_1 + 1 \text{ and } c(j) = j \times n_1, \quad j \in \{1, \dots, n_2\}.$$

3. Pour les points de contrôle indépendants côté non-mortier

$$g_{I(i,j),J(i,j)}^\alpha = 1, \quad i \in \{\alpha + 2, \dots, n_1\}, \quad j \in \{1, \dots, n_2\},$$

avec

$$I(i, j) = ((j-1) \times n_1 + i) + n_{12}, \text{ et } J(i, j) = n_{12} + (j-1) \times (n_1 - (\alpha + 1)) + (i - (\alpha + 1))$$

4. De plus pour une régularité  $C^1$ ,  $\alpha = 1$  on a : pour  $j \in \{1, \dots, n_2\}$  et  $\beta \in \{0, 1\}$

$$g_{I(j), J(n_1 - \beta, j)}^\alpha = c_\beta$$

où le nombre réel  $c_\beta$  est défini par

$$c_\beta = \begin{cases} 1 + \frac{\xi_{d_1+2}^1}{1 - \xi_{n_1}^1} & \text{if } \beta = 0 \\ -\frac{\xi_{d_1+2}^1}{1 - \xi_{n_1}^1} & \text{if } \beta = 1 \end{cases},$$

avec  $I(j)$  et  $J(i, j)$  tels que :

$$I(j) = n_{12} + (j - 1) \times n_1 + 1, \quad J(i, j) = (j - 1) \times n_2 + i.$$

### A.5.2 Optimisation

Les variables d'optimisation de forme sont alors les coordonnées des points de contrôle indépendants  $(\hat{p}_j)_{j=1:n_{12}^\alpha}$ .

Nous considérons comme fonction objectif la compliance dont la fonction coût  $J$  est définie par

$$J(\mathbf{u}) = \mathbf{u}^\top \mathbf{K} \mathbf{u} = \mathbf{f}^\top \mathbf{u}.$$

Soit  $p$  un paramètre de conception (point de contrôle) de forme ou de propriétés matériaux. On trouve aisément, en calculant  $\partial_p \mathbf{u}$  à l'aide de l'équation d'état  $\mathbf{K} \mathbf{u} = \mathbf{f}$ , que

$$\partial_p J(\mathbf{u}) = 2 \partial_p \mathbf{f}^\top \mathbf{u} - \mathbf{u}^\top \mathbf{K} \mathbf{u}.$$

### Gradient pour assemblage de coques

On note  $\partial_{i(k)}^j$  la dérivée par rapport à la  $j$ -ème coordonnée de  $p_{i(k)}$ ,  $i$ -ème point de contrôle définissant la surface moyenne  $\Omega_k$ . On désigne par  $\hat{\partial}_i^j$  la dérivée par rapport à la  $j$ -ème coordonnée du point de contrôle indépendant  $\hat{p}_i$ ,  $i \in \{1, \dots, n_{12}^\alpha\}$  et  $j \in \{1, 2, 3\}$ . On pose  $\nabla^{j(k)}$  le vecteur de dérivées par rapport à la  $j$ -ème coordonnée de la coque  $\Omega_k$

$$\nabla^{j(k)} = \left( \partial_1^{j(k)} \quad \dots \quad \partial_{n_{12}}^{j(k)} \right).$$

On pose  $\nabla^j = [\nabla^{j(m)} \quad \nabla^{j(n)}]$ .  $\nabla^j$  représente le vecteur de dérivées par rapport à la  $j$ -ème coordonnée sans prise en compte de la condition de liaison géométrique. Le vecteur  $\hat{\nabla}^j$  de dérivées par rapport à la  $j$ -ème coordonnée des points de contrôle indépendants  $\hat{\mathbf{p}}$  est défini par

$$\hat{\nabla}^j = [\mathcal{G}^\alpha]^\top \nabla^j.$$

Le gradient par rapport à l'ensemble des coordonnées des points de contrôle indépendants  $\hat{\mathbf{p}}$  est alors  $\hat{\nabla} = [\hat{\nabla}^1 \quad \hat{\nabla}^2 \quad \hat{\nabla}^3]$ .

## Dérivée de la matrice de raccord

Dans le cas d'assemblage de coques, et d'utilisation d'une méthode de gradient, il s'avère nécessaire de calculer la dérivée de la matrice de *raccord mécanique* liée à la contrainte de continuité de déplacement et de la composante tangentielle de rotation, par rapport aux variables de conception liées aux interfaces, dans le présent cadre illustratif  $(p_{n_1, j^{(n)}})_{j=1:n_2}$  et  $(p_{1, j^{(m)}})_{j=1:n_2}$ . En effet, en considérant par exemple l'équation (A.8) page 169, on a

$$\mathbf{B}_m = \mathbf{M}^\top \mathbf{B} \mathbf{M} \implies \partial_p \mathbf{B}_m = \partial_p \mathbf{M}^\top \mathbf{B} \mathbf{M} + \mathbf{M}^\top \partial_p \mathbf{B} \mathbf{M} + \mathbf{M}^\top \mathbf{B} \partial_p \mathbf{M}.$$

On retrouve que

$$\partial_p \mathbf{M} = \begin{bmatrix} \mathbf{0} & & & \\ & \partial_p \mathbf{R}^{(l)} & & \\ & \mathbf{0} & & \\ & & & \mathbf{0} \end{bmatrix}$$

$\mathbf{0}$  étant une matrice nulle de dimensions consistantes avec la définition de  $\mathbf{M}$  (equation (A.7) page 169). De la formule (A.6) page 168, on a

$$\begin{aligned} \partial_p \mathbf{R}^{(l)} &= \partial_p [\mathbf{M}^{l(n)}]^{-1} \mathbf{M}^{l(m)} + [\mathbf{M}^{l(n)}]^{-1} \partial_p \mathbf{M}^{l(m)} \\ &= -[\mathbf{M}^{l(n)}]^{-1} \partial_p \mathbf{M}^{l(n)} + [\mathbf{M}^{l(n)}]^{-1} + [\mathbf{M}^{l(n)}]^{-1} \partial_p \mathbf{M}^{l(m)} \\ &= -[\mathbf{M}^{l(n)}]^{-1} \partial_p \mathbf{M}^{l(n)} \mathbf{R}^{(l)} + [\mathbf{M}^{l(n)}]^{-1} \partial_p \mathbf{M}^{l(m)} \end{aligned} \quad (\text{A.16})$$

On s'intéresse dans le chapitre 5 à l'optimisation de forme et propriétés matériaux dans le cas de coques. On décrit les différents aspects de calcul de gradient pour les assemblages de coques. Ce calcul implique notamment la prise en compte du raccordement mécanique entre les coques et du raccordement géométrique des patches entre eux avec la matrice  $\mathcal{G}^\alpha$ . Le chapitre se termine par des exemples numériques sur l'optimisation de forme et l'optimisation conjointe forme et propriétés matériaux.



# Bibliography

---

- [1] Grégoire Allaire, François Jouve, and Anca-Maria Toader. Structural optimization using sensitivity analysis and a level-set method. *Journal of Computational Physics*, 194(1):363–393, feb 2004. (cited page 7)
- [2] Jasbir S. Arora. Structural design sensitivity analysis: Continuum and discrete approaches. In *Advances in Structural Optimization*, pages 47–70. Springer Netherlands, 1995. (cited page 111)
- [3] K. J. Bathe and H. Saunders. Finite element procedures in engineering analysis. *Journal of Pressure Vessel Technology*, 106(4):421, 1984. (cited page 55)
- [4] Y. Bazilevs, V.M. Calo, J.A. Cottrell, J.A. Evans, T.J.R. Hughes, S. Lipton, M.A. Scott, and T.W. Sederberg. Isogeometric analysis using t-splines. *Computer Methods in Applied Mechanics and Engineering*, 199(5-8):229–263, jan 2010. (cited pages 2 and 158)
- [5] Martin P. Bendsøe. *Optimization of Structural Topology, Shape, and Material*. Springer Berlin Heidelberg, 1995. (cited page 6)
- [6] Martin P. Bendsøe and Ole Sigmund. *Topology Optimization*. Springer Berlin Heidelberg, 2004. (cited page 6)
- [7] Martin Philip Bendsøe and Noboru Kikuchi. Generating optimal topologies in structural design using a homogenization method. *Computer Methods in Applied Mechanics and Engineering*, 71(2):197–224, nov 1988. (cited pages 6 and 10)
- [8] C. Bernardi, Y. Maday, and F. Rapetti. Basics and some applications of the mortar element method. *GAMM-Mitteilungen*, 2005. (cited page 39)
- [9] M. Bernadou. *Méthodes d'éléments finis pour les problèmes de coques minces*. Recherches en Mathématiques Appliquées, 1994. (cited pages 15, 28, 35, and 113)
- [10] M. Bernadou, P. G. Ciarlet, and B. Miara. Existence theorems for two-dimensional linear shell theories. *Journal of Elasticity*, 34(2):111–138, feb 1994. (cited page 28)
- [11] C. Bernardi, Y. Maday, and A. T. Patera. Domain decomposition by the mortar element method. In *Asymptotic and Numerical Methods for Partial Differential Equations with Critical Parameters*, pages 269–286. Springer Netherlands, 1993. (cited page 38)
- [12] S. Beuzit and A. Habbal. Design of an automatic topology/geometry optimization software. In *Integrated Design and Manufacturing in Mechanical Engineering '98*, pages 133–140. Springer Netherlands, 1999. (cited page 7)

## Bibliography

---

- [13] P. Bézier. *Essai de définition numérique des courbes et des surfaces expérimentales: contribution à l'étude des propriétés des courbes et des surfaces paramétriques polynomiales à coefficients vectoriels*. Number vol. 1. 1977. (cited page 103)
- [14] K. U. Bletzinger and E. Ramm. Form finding of shells by structural optimization. *Engineering with Computers*, 9(1):27–35, mar 1993. (cited page 102)
- [15] A. Blouza and H. L. Dret. Existence and uniqueness for the linear koiter model for shells with little regularity. *Quart. Appl. Math.*, 57:317–337, 1999. (cited page 32)
- [16] A. Blouza and H. Le Dret. Nagdhi's shell model: Existence, uniqueness and continuous dependence on the midsurface. *Journal of Elasticity*, 64(2/3):199–216, 2001. (cited page 32)
- [17] Adel Blouza. Une formulation hybride du modèle de coque de naghdi. *Comptes Rendus Mathématique*, 351(7-8):317–321, apr 2013. (cited page 32)
- [18] Adel Blouza, Frédéric Hecht, and Hervé Le Dret. Two finite element approximations of naghdi's shell model in cartesian coordinates. *SIAM Journal on Numerical Analysis*, 44(2):636–654, jan 2006. (cited page 32)
- [19] Ericka Brivadis, Annalisa Buffa, Barbara Wohlmuth, and Linus Wunderlich. Isogeometric mortar methods. *Computer Methods in Applied Mechanics and Engineering*, 284:292–319, feb 2015. (cited page 39)
- [20] A. Catapano, B. Desmorat, and P. Vannucci. Stiffness and strength optimization of the anisotropy distribution for laminated structures. *Journal of Optimization Theory and Applications*, 167(1):118–146, 2015. (cited pages 70 and 71)
- [21] Jean Cea. Conception optimale ou identification de formes, calcul rapide de la dérivée directionnelle de la fonction coût. *ESAIM: Mathematical Modelling and Numerical Analysis*, 20(3):371–402, 1986. (cited page 111)
- [22] Dominique Chapelle and Klaus-Jürgen Bathe. *The Finite Element Analysis of Shells - Fundamentals*. Springer Berlin Heidelberg, 2011. (cited page 16)
- [23] Seonho Cho and Seung-Hyun Ha. Isogeometric shape design optimization: exact geometry and enhanced sensitivity. *Structural and Multidisciplinary Optimization*, 38(1):53–70, may 2008. (cited pages 11, 102, and 159)
- [24] P. G. Ciarlet. *The Finite Element Method for Elliptic Problems*. Classics in Applied Mathematics. 2002. (cited page 51)
- [25] P. G. Ciarlet. *An Introduction to Differential Geometry with Applications to Elasticity*. Springer, Netherlands, 2005. (cited pages 16 and 28)
- [26] P. Jr. Ciarlet and E. Lunéville. *La méthode des éléments finis - De la théorie à la pratique*. 2009. (cited page 51)
- [27] P.G. Ciarlet. *Theory of Shells*. Mathematical Elasticity. Elsevier Science, 2000. (cited pages 15, 20, and 23)

- 
- [28] J. Austin Cottrell, Thomas J. R. Hughes, and Yuri Bazilevs. *Isogeometric Analysis*. John Wiley & Sons, Ltd, aug 2009. (cited pages 2, 11, and 159)
- [29] Charles Dapogny. *Shape optimization, level set methods on unstructured meshes and mesh evolution*. PhD thesis, 2013. Thèse de doctorat dirigée par Allaire, Grégoire et Frey, Pascal Mathématiques Appliquées Paris 6 2013. (cited page 7)
- [30] Philip J. Davis and Philip Rabinowitz. *Methods of Numerical Integration (Computer Science and Applied Mathematics)*. Academic Press, 2014. (cited page 51)
- [31] C. de Boor. *A Practical Guide to Splines*. Applied Mathematical Sciences. Springer, New York, 2001. (cited pages 77 and 80)
- [32] Carl de Boor. On the evaluation of box splines. *Numerical Algorithms*, 5(1):5–23, jan 1993. (cited page 103)
- [33] Gabriel Delgado. *Optimization of composite structures: A shape and topology sensitivity analysis*. PhD thesis, 2014. Thèse de doctorat dirigé par Allaire, Grégoire Mathématiques appliquées Palaiseau, Ecole polytechnique 2014. (cited page 7)
- [34] P. Destuynder. *Sur une justification des modèles de plaques et de coques par les méthodes asymptotiques*. PhD thesis, Université Pierre et Marie Curie, 1980. (cited page 15)
- [35] Paul Du Cazuzé De Nazelle. *Paramétrage de formes surfaciques pour l'optimisation*. PhD thesis, Ecole centrale de Lyon, 2013. Thèse de doctorat dirigée par Jézéquel, Louis et Gillot, Frédéric Mécanique Ecully, Ecole centrale de Lyon 2013. (cited pages xiii, 2, 6, and 159)
- [36] Schnack Eckart. An optimization procedure for stress concentrations by the finite element technique. *International Journal for Numerical Methods in Engineering*, 14(1):115–124, 1979. (cited page 10)
- [37] T.J.R. Hughes, J.A. Cottrell, and Y. Bazilevs. Isogeometric analysis: CAD, finite elements, NURBS, exact geometry and mesh refinement. *Computer Methods in Applied Mechanics and Engineering*, 194(39-41):4135–4195, oct 2005. (cited pages 11 and 102)
- [38] A. Jibawy, B. Desmorat, and A. Vincenti. Structural rigidity optimization of thin laminated shells. *Composite Structures*, 95:35 – 43, 2013. (cited page 70)
- [39] Sarah Julisson. *Shape optimization of thin shell structures for complex geometries*. Theses, Université Paris-Saclay, December 2016. (cited pages 2, 58, and 159)
- [40] Josef M Kiendl. *Isogeometric analysis and shape optimal design of shell structures*. PhD thesis, Shaker, 2011. (cited pages 11 and 159)
- [41] W.T. Koiter. *Foundations and Basic Equations of Shell Theory: A Survey of Recent Progress*. Afdeling der Werktuigbouwkunde: WTHD. Labor. voor Techn. Mechanica, 1968. (cited page 15)
- [42] Vadim Komkov, Kyung K. Choi, and Edward J. Haug. *Design Sensitivity Analysis of Structural Systems*. Elsevier Science, 1986. (cited page 111)



## Bibliography

---

- [43] C. Lacour. Non-conforming domain decomposition method for plate and shell problems. *Contemporary Mathematics*, 218, 1998. (cited page 32)
- [44] S.G. Lekhnitskii. *Theory of elasticity of an anisotropic elastic body*. Holden-Day, Inc, S. Francisco, 1963. (cited page 70)
- [45] J.L. Lions. *Quelques méthodes de résolution des problèmes aux limites non linéaires*. Les Cours de référence. Dunod, 2002. (cited page 111)
- [46] A. Cubier M. Bernadou. Numerical analysis of junctions between thin shells: part 1 - continuous problems. In *Rapport de recherche/INRIA*, page 22. INRIA, 1996. (cited page 32)
- [47] A. Cubier M. Bernadou. Numerical analysis of junctions between thin shells: part 2 - approximation by finite element methods. In *Rapport de recherche/INRIA*, page 36. INRIA, 1996. (cited page 32)
- [48] S. Fayolle M. Bernadou, F. Lene. Numerical analysis of junctions between plates. In *Rapport de recherche INRIA*, page 25. INRIA, 1988. (cited page 32)
- [49] Richard H. Macneal and Robert L. Harder. A proposed standard set of problems to test finite element accuracy. *Finite Elements in Analysis and Design*, 1(1):3–20, apr 1985. (cited page 61)
- [50] M. Montemurro. *Optimal design of advanced engineering modular systems through a new genetic approach*. PhD thesis, Univ. Paris VI, 2012. (cited page 70)
- [51] M. Montemurro and A. Catapano. A new paradigm for the optimum design of variable angle tow laminates. In *Variational analysis and aerospace engineering: mathematical challenges for the aerospace of the future*, volume 116 of *Springer Optimization and Its Applications*. Springer, December (to appear) 2017. (cited page 71)
- [52] M. Montemurro, A. Vincenti, and P. Vannucci. A two-level procedure for the global optimum design of composite modular structures-application to the design of an aircraft wing. part 2: Numerical aspects and examples. *Journal of Optimization Theory and Applications*, 155:24–53, 2012. (cited page 71)
- [53] Marco Montemurro, Paolo Vannucci, and Angela Vincenti. BIANCA, A Genetic Algorithm for Engineering Optimisation - User guide. working paper or preprint, March 2011. (cited page 154)
- [54] F. Murat and J. Simon. Calcul de variation et homogénéisation. In *les méthodes de l'homogénéisation: théorie et application sn physique*, volume 57 of *Coll. Dir. Etudes et Recherches EDF*, pages 319–369. 1985. (cited page 6)
- [55] P.M. Naghdi. *Foundations of Elastic Shell Theory*. North-Holland Publishing CO. - Amsterdam, 1963. (cited page 15)
- [56] Attila P. Nagy, Samuel T. IJsselmuiden, and Mostafa M. Abdalla. Isogeometric design of anisotropic shells: Optimal form and material distribution. *Computer Methods in Applied Mechanics and Engineering*, 264:145–162, sep 2013. (cited pages 11 and 159)

- 
- [57] Kikuchi Noboru, Kyoong Yang Chung, Torigaki Toshikazu, and John E. Taylor. Adaptive finite element methods for shape optimization of linearly elastic structures. *Computer Methods in Applied Mechanics and Engineering*, 57(1):67–89, aug 1986. (cited page 10)
- [58] N. M. Patrikalakis and T. Maekawa. Shape interrogation for computer aided design and manufacturing, 2009. (cited page 80)
- [59] Dr. Wayne Tiller Prof. Dr. Les Piegl. *The NURBS Book*. Springer Berlin Heidelberg, 1997. (cited page 106)
- [60] Xiaoping Qian. Full analytical sensitivities in NURBS based isogeometric shape optimization. *Computer Methods in Applied Mechanics and Engineering*, 199(29-32):2059–2071, jun 2010. (cited page 102)
- [61] Rapetti R. *Approximation des équations de la magnétodynamique en domaine tournant par la méthode des éléments finis joints*. PhD thesis, Université Pierre et Marie Curie, 2000. (cited page 40)
- [62] D. F. Rogers. An introduction to nurbs with historical perspective. Computer Graphics. Morgan Kaufmann publishers, San Francisco, 2001. (cited pages 80, 81, and 103)
- [63] B. Rousselet. Principes d'analyse de sensibilité, utilisation pour la conception optimale. Technical Report RR-0521, INRIA, April 1986. (cited page 111)
- [64] M. B. Rubin. *Cosserat Theories: Shells, Rods and Points*. Springer Netherlands, 2000. (cited page 15)
- [65] P. Vannucci. A special planar orthotropic material. *Journal of Elasticity*, 67:81–96, 2002. (cited page 73)
- [66] P. Vannucci. Plane anisotropy by the polar method. *Meccanica*, 40:437–454, 2005. (cited pages 71, 72, and 73)
- [67] P. Vannucci. Influence of invariant material parameters on the flexural optimal design of thin anisotropic laminates. *International Journal of Mechanical Sciences*, 51:192 – 203, 2009. (cited page 73)
- [68] P. Vannucci. A note on the elastic and geometric bounds for composite laminates. *Journal of Elasticity*, 112:199–215, 2013. (cited pages 70, 71, and 74)
- [69] P. Vannucci and B. Desmorat. Analytical bounds for damage induced planar anisotropy. *International Journal of Solids and Structures*, 60-61:96 – 106, 2015. (cited page 74)
- [70] P. Vannucci and G. Verchery. Stiffness design of laminates using the polar method. *International Journal of Solids and Structures*, 38(50-51):9281 – 9294, 2001. (cited page 73)
- [71] P. Vannucci and G. Verchery. Anisotropy of plane complex elastic bodies. *International Journal of Solids and Structures*, 47:1154 – 1166, 2010. (cited page 71)
- [72] G. Verchery. *Mechanical Behavior of Anisotropic Solids*, chapter Les Invariants des Tenseurs d'Ordre 4 du Type de l'Élasticité, pages 93–104. Editions du CNRS, Paris, 1982. (cited page 71)

## Bibliography

---

- [73] Angela Vincenti, Mohammad Reza Ahmadian, and Paolo Vannucci. Bianca: a genetic algorithm to solve hard combinatorial optimisation problems in engineering. *Journal of Global Optimization*, 48(3):399–421, dec 2009. (cited page 154)
- [74] Barbara I. Wohlmuth. *Discretization Methods and Iterative Solvers Based on Domain Decomposition*. Springer Berlin Heidelberg, 2001. (cited page 39)
- [75] Z. Wu, P. M. Weaver, G. Raju, and B. C. Kim. Buckling analysis and optimisation of variable angle tow composite plates. *Thin-Walled Structures*, 60:163 – 172, 2012. (cited page 71)
- [76] A. T. Patera Y. Maday, C. Marvriplis. Nonconforming mortar element methods: Application to spectral discretizations. *Domain Decomposition Methods, SIAM*, pages 392–418, 1989. (cited page 40)
- [77] M. Zhou, N. Pagalapati, H.L. Thomas, and Y.K. Shyy. An integrated approach to topology, sizing, and shape optimization. *Structural and Multidisciplinary Optimization*, 26(5):308–317, mar 2004. (cited page 7)





